MIT

LARGE-SCALE MODELS OF TRANSIENT UNSATURATED FLOW AND CONTAMINANT TRANSPORT USING STOCHASTIC METHODS

by
ARISTOTELIS MANTOGLOU
and
LYNN W. GELHAR

RALPH M. PARSONS LABORATORY
HYDROLOGY AND WATER RESOURCE SYSTEMS

Report No. 299

January 1985

DEPARTMENT

OF

CIVIL

ENGINEERING

●

R85-2

LARGE-SCALE MODELS OF TRANSIENT UNSATURATED FLOW
AND CONTAMINANT TRANSPORT USING STOCHASTIC METHODS

by

Aristotelis Mantoglou

and

Lynn W. Gelhar

RALPH M. PARSONS LABORATORY

HYDROLOGY AND WATER RESOURCE SYSTEMS

Report Number 299

JANUARY 1985

LARGE-SCALE MODELS OF TRANSIENT UNSATURATED FLOW AND CONTAMINANT TRANSPORT USING STOCHASTIC METHODS

ABSTRACT

A new framework for modeling large-scale unsaturated flow and solute transport systems in spatially variable soils is proposed. The large-scale model structures are derived by averaging the local governing flow and transport equations over the ensemble of realizations of the underlying soil property random fields. The resulting mean representations are in the form of partial differential equations in which averaged or effective model parameters occur. These effective model parameters, i.e., effective hydraulic conductivity, effective specific moisture capacity and effective macro-dispersivity, are evaluated using a quasi-linearized fluctuation equation and a spectral representation of stationary processes. The large-scale model structures consider the large-scale effects of soil variability and have relatively few parameters identifiable from a realistic data set.

The effective parameters are analytically evaluated in particular cases of practical interest, and generic expressions showing explicitly the dependence of the effective parameters on the different flow, transport and soil property characteristics are derived.

General methods for testing the validity of the stochastic theory and application of the large-scale models in practical situations are suggested. The spectral turning bands method developed by Mantoglou and Wilson (1981, 1982) is extended for digital generation of point values or spatial averages of multiple, cross-correlated, stationary random fields. Statistical inference methods are discussed and a new identification method is presented.

The most important findings of this study are that spatial variability of the hydraulic soil properties produces significant large-scale effects. In particular, it was found that the effective hydraulic conductivity, the mean soil moisture content and the effective specific soil moisture capacity show significant hysteresis, and that the effective

2

hydraulic conductivity is anisotropic with a degree of anisotropy depending on the mean flow conditions (wetting or drying). It was also found that in the case of unsaturated flow, the effective macro-dispersivities depend on the soil moisture content, the type of soil stratification and the direction for the mean flow relative to stratification and the direction for the mean flow relative to stratification. The longitudinal macrodispersivity predicted from the stochastic theory is found to be of the same order of magnitude as observed in large-scale field experiments.

The transient unsaturated flow and steady transport results of this study were previously unknown, have important practical implications, and should be considered in field applications such as waste disposal control. The general stochastic modeling framework and the simulation and identification methods developed here are applicable not only to unsaturated flow and transport but also to other distributed parameter systems.

ACKNOWLEDGEMENTS

TABLE OF CONTENTS

LIST OF FIGURES

CHAPTER 1

INTRODUCTION

1.1   Motivation of this Study

Disposal of radioactive wastes in surface or underground storage facilities is now being designed. Uranium mill tailing disposal sites will use unsaturated zone storage. Unsaturated zone storage is also being seriously considered for high level wastes. The possibility of a leak from such waste storage facilities and subsequent contamination of water resources cannot be overlooked. Figures 1.1 and 1.2 illustrate unsaturated zone contamination from a waste storage facility at Hanford, Washington. Figure 1.1 outlines the setting of the waste disposal facility. Figure 1.2 shows measurements of unsaturated zone contamination several years after a contaminant leak from one of the tanks is reported.

Potential contamination of water resources with harmful radioactive wastes imposes serious hazards to the environment. For this reason extensive research activity has been undertaken recently in order to better understand and model the behavior of large-scale unsaturated zone systems. Modeling unsaturated flow and contaminant transport is important for evaluation of the proposed radioactive waste disposal facilities. The importance of unsaturated zone modeling is emphasized by the fact that the Nuclear Regulatory Commission and the National Water Well Association have recently sponsored special symposia on unsaturated flow and contaminant transport. The challenge is to obtain valid and

12
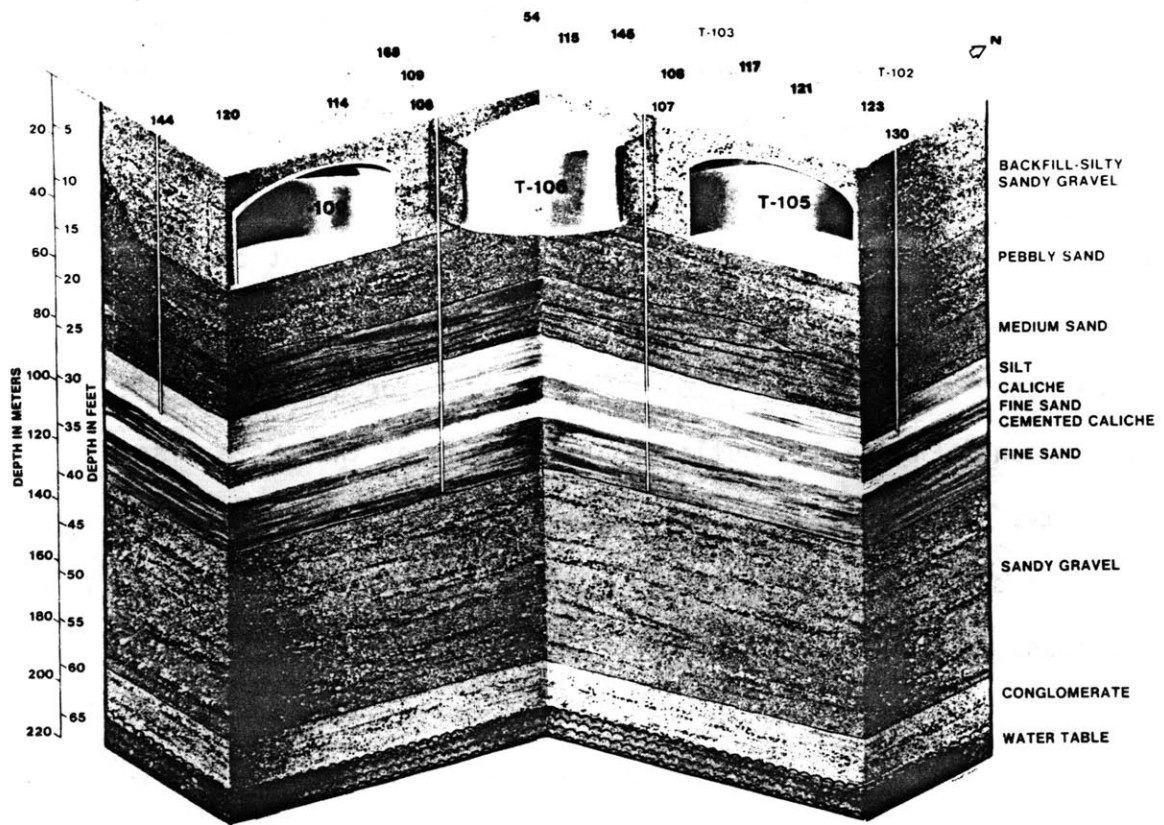
Figure 1.1 Three-dimensional drawing of the distribution of sedimentary lithologies beneath the 241-T-106 tank in Hanford WA. (from Routson et al., 1980).

PLAN VIEW
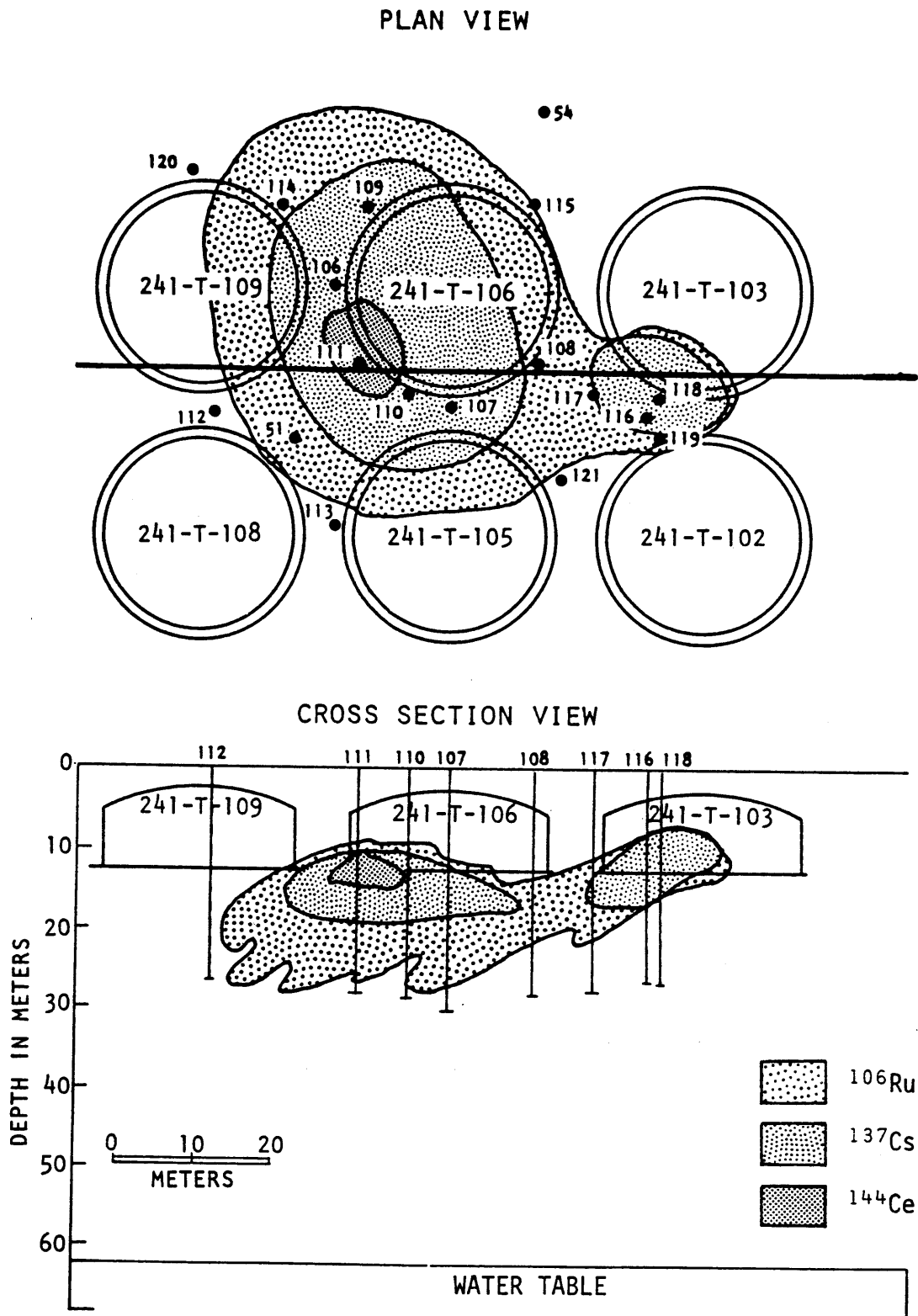
CROSS SECTION VIEW

Figure 1.2   Composite drawing of plan and section views of the 1.0-μCi/ℓ concentrations of ^{144}Ce, ^{137}Cs and ^{106}Ru in 1973 (from Routson et al., 1980).

practical models that realistically portray the complexity of large-scale natural unsaturated flow systems and have relatively few and identifiable parameters that can be estimated from a realistic data set.

Modeling natural large-scale unsaturated flow systems is a very difficult problem. One of the major complications is that natural soil formations exhibit a large degree of spatial variability of their hydraulic soil properties (see Chapter 2). Vapor flow, temperature dependence, etc., may further complicate the large-scale flow problem but these effects are not considered in this study. Predicting soil moisture and contaminant transport in natural soil formations, using numerical solution of the classical governing flow and transport equations, (physical models), requires dense discretization (e.g. a grid consisting of 10^6 nodes) and knowledge of the local details of the soil hydraulic properties. Due to the large degree of spatial soil variability, identifying such local details is, at least today, a formidable task. The data collection process would be extremely expensive and would probably alter the physical characteristics and the waste isolation capabilities of the site.

Waste disposal control applications usually require predictions of the large-scale contamination characteristics rather than local details of contamination. The objective then is to construct an approximate model of the system that: (i) predicts the most important large-scale features of contamination, (ii) has parameters that depend on a few and identifiable characteristics of the soil property variability, and (iii) evaluates the reliability of the approximate model predictions. In the following developments such a model will be called "large-scale model"

and its parameters "effective parameters".

In order to build valid large-scale unsaturated flow and transport models two basic characteristics of the problem should be considered. The first characteristic is that flow and transport in a local scale are generally three-dimensional processes. This is due to the combined effects of gravity and capillary forces and the complex nature of spatial variability of the soil properties. Many field observations illustrate this point (see e.g. Gelhar et al., 1984). The second characteristic of the problem is that the local flow and transport characteristics (e.g. capillary tension head and concentration), depend on the local soil properties in a nonlinear fashion. This can be seen by inspection of the governing local flow and transport equations. As will be seen in later chapters the two characteristics of unsaturated flow and transport discussed above are important and should be considered in a consistent modeling study.

1.2 Past Modeling Approaches

Several approaches have been proposed for modeling unsaturated flow and transport systems with spatially variable soil properties. One approach is to assume that local models are valid on a field scale. The effective parameters of such models are usually interpreted as spatial averages of the local properties (see e.g. Biggar and Nielsen, 1976; Van de Pol et al., 1977). A criticism of this approach is that it does not consider the effects of spatial variability. As was discussed above, the system is parametrically nonlinear and local variability produces important large scale effects.

Another modeling approach visualizes the unsaturated flow system to be composed by a series of one-dimensional, non-interacting columns, and assumes random, but uniform over depth, soil properties (e.g. Dagan and Bresler, 1979, 1983; Bresler and Dagan, 1981, 1983; Milly, 1982). This approach, at least in the applications of our interest, contradicts reality. Numerous field observations show that soil properties are not uniform over depth and lateral flow is often important (see Chapter 4, Section 4.7).

The stochastic approach is a third approach proposed for analysis of the effects of the spatial variability in unsaturated flow. This approach is capable of realistically considering the three-dimensional spatial structure of soil variability and the three-dimensionality of the local flow. Stochastic analysis has been extensively used in the case of saturated flow systems (Freeze, 1975; Bakr et al., 1978; Dagan 1979, 1982; Dettinger and Wilson, 1981; Gelhar and Axness, 1983, etc.). In the unsaturated flow case however, only two applications have been reported. Andersen and Shapiro (1983) examined the case of one-dimensional steady unsaturated flow using a Monte-Carlo simulation and a linearized perturbation method. Their approach is conceptually interesting but it is not applicable in field situations where flow is generally three-dimensional. Yeh et al., (1982), examined the three-dimensional steady unsaturated flow using a stochastic approach and a linearized perturbation method, and found that the effective hydraulic conductivity in stratified unsaturated soils is anisotropic with a degree of anisotropy being dependent on the mean soil moisture content. However, in most practical problems flow is usually unsteady and the steady-state

results of Yeh et al. are not applicable to these situations.

The stochastic literature discussed above investigates the flow problem only. The solute transport problem in heterogeneous unsaturated soils has not been investigated as yet in a realistic way. The models proposed by Dagan and Bresler (1979, 1983) and Bresler and Dagan (1981, 1983) have adopted a simple one-dimensional transport model in which the parameters are treated as spatially constant random variables. Such models may be fitted to field observations but it is doubtful that they can be extrapolated beyond the small scale of observations. The assumption that the parameters are spatially constant is obviously not correct; the key element of natural heterogeneity, its spatial structure, is completely neglected. Jury et al. (1982) proposed a "transfer function" model for modeling solute transport in spatially variable soils. Such a model may be criticized in that it does not use any physics about the processes involved; it is a black box model. Its parameters do not correspond to any physical quantities and must be calibrated based on available data for the particular setting under consideration. Extrapolation of the predictions of such a model to depths, settings or conditions other than the ones from which it was derived is not possible (see discussion in Section 5.3.2).

In the case of saturated flow it is now widely recognized that the dispersion process is strongly affected by scale; field scale dispersivities are found to be several orders of magnitude larger than laboratory parameters. Recent research (Gelhar et al., 1979; Gelhar and Axness, 1983; Dagan, 1982) has established the relationship between aquifer heterogeneity and the large dispersivities observed in the

18

field. In the case of unsaturated flow the possibility of scale
dependence of the dispersion process does not seem to be widely
recognized because large-scale measurements of unsaturated solute
transport are so limited. However, interpretation of some field
measurements (see Section 5.3.2) indicate such scale dependence. Another
question that needs to be answered in the case of dispersion in
unsaturated soils is the possible dependence of the large-scale
dispersion coefficients on the mean soil moisture content. The model of
Wilson (1974) predicts such dependence. Note however, that this work
uses a microscopic statistical pore scale model that cannot consider the
macroscopic soil heterogeneities of a scale larger than the pore scale.
The solute transport problem in unsaturated soils has not been
investigated yet using methods that realistically incorporate the natural
heterogeneity observed in a field scale.

1.3   Scope and Findings of this Study

This study proposes a new modeling framework for treating
large-scale unsaturated flow and transport systems. This framework
suggests using an approximate large-scale model structure in order to
describe the system rather than using the local physical model
structure. The objective is to provide large-scale unsaturated flow and
transport models that consider the heterogeneity of natural soil
formations and have relatively few and identifiable parameters that can
be estimated from a realistic data set.

A stochastic approach is followed. It is assumed that local soil
properties are realizations of three-dimensional random fields. The

local governing flow and transport equations are averaged over the ensemble of realizations of the underlying soil property random fields. The stochastic methodology considers the three-dimensionality of the local flow and transport processes, and the nonlinear dependence of the local outputs on the local soil properties, i.e. it predicts for the large-scale effects of local property variability.

The stochastic approach is developed herein as follows. Chapter 2 discusses the problem of spatial variability of the unsaturated hydraulic soil properties in natural soil formations, and proposes a stochastic representation of such variability in terms of three-dimensional random fields. In Chapter 3 a stochastic methodology is developed for derivation of large-scale models and evaluation of effective parameters of large-scale unsaturated flow and transport. Chapter 4 evaluates the effective unsaturated flow parameters in the case of transient flow in stratified soils. Chapter 5 evaluates effective macrodispersivities in the steady state case. In Chapter 6 a Monte-Carlo simulation method that can be used for testing the validity of the stochastic theory is proposed, a spectral turning bands random field generator is developed, and an identification method that can be used for estimation of large scale parameters is proposed.

The most important finding of this work is that the spatial variability of the hydraulic soil properties produces significant large-scale effects (hysteresis, anisotropy, etc.). These effects were previously unknown and have important implications in practical applications such as waste disposal management.

The general stochastic modeling framework, simulation and

20

identification methods developed here are new and are applicable not only
to unsaturated flow and contaminant transport but also to other
distributed parameter systems (e.g. saturated flow and transport,
geothermal, oil reservoir modeling, etc.).

CHAPTER 2

STOCHASTIC REPRESENTATION OF SPATIAL VARIABILITY

OF UNSATURATED HYDRAULIC SOIL PROPERTIES

2.1 Introduction

Numerous observations of natural soil formations show that soil materials are rather heterogenous. Visual inspection of the slopes of excavations, for example, demonstrate this point. Because of such heterogeneity the hydraulic properties of the soil exhibit a large degree of spatial variability. Figure 2.1 shows observations of the saturated hydraulic conductivity and porosity. These data are based on laboratory analyses of cores collected from deep boreholes in the Mt. Simon aquifer in central Illinois. These data show a large variation of hydraulic conductivity with values ranging over four orders of magnitude. The porosity also shows significant variability but much smaller than that of hydraulic conductivity. Figure 2.1 also shows that the variation of the hydraulic soil properties is not completely disordered in space but a spatial structure (spatial correlation) exists. Many other observations on different geologic formations show similar kinds of spatial variability of the hydraulic soil properties.

Because of the large degree of spatial variability in natural soil formations, it is practically impossible to represent the local soil properties in terms of deterministic functions. If such representation was attempted the number of the required unknown parameters would be extremely large and impossible to estimate from a realistic data set. It is a natural choice then to use a stochastic representation of the local
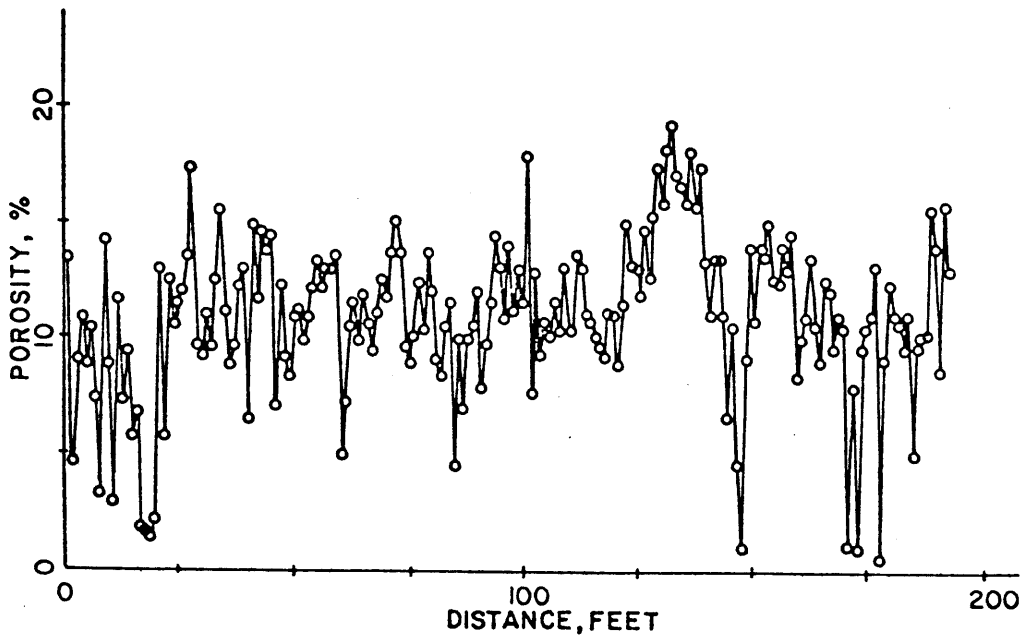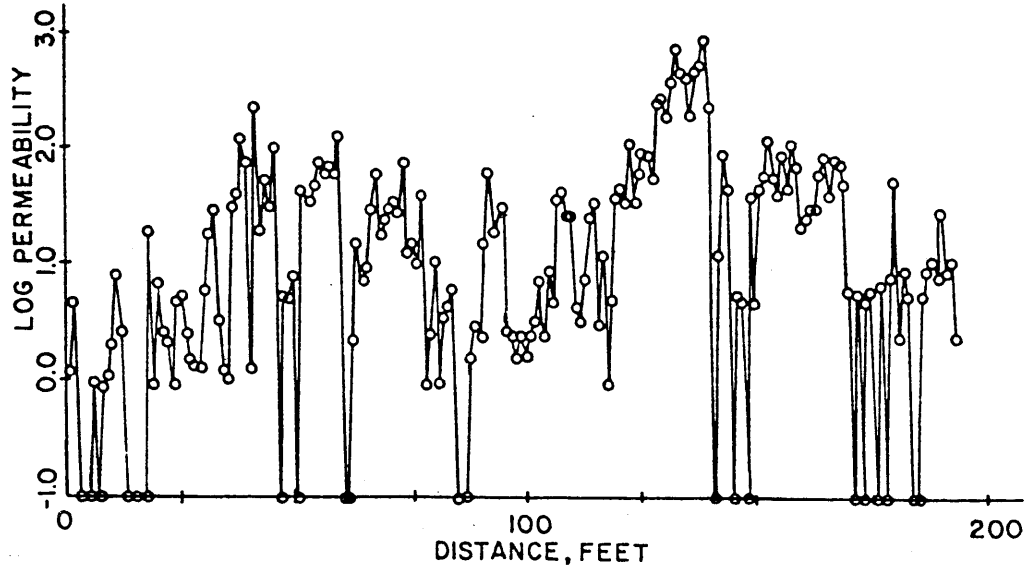
Figure 2.1 Permeability (millidarcy) and porosity space series from laboratory analysis of cores from a borehole in Mt. Simon sandstone aquifer in Illinois (Bakr, 1976).

23

variations of the hydraulic soil properties. It is assumed that the small scale soil property variations are realizations of three-dimensional spatially correlated random fields. The stochastic representation is simply a useful tool of analysis which incorporates the complex spatial variability of actual soil properties through a practical framework requiring only a limited amount of information.

This chapter suggests a representation of the unsaturated hydraulic soil properties in terms of stationary random fields. Section 2.2 discusses some field observations of the local unsaturated hydraulic soil properties and proposes some simple and useful models for parametrization of these properties. Section 2.3 suggests a stochastic representation of these local hydraulic parameters and analyzes some real data for estimation of basic stochastic parameters useful in later applications.

2.2 Unsaturated Hydraulic Soil Properties

The two basic hydraulic properties controlling unsaturated flow are the unsaturated hydraulic conductivity $K(\psi)$ and the moisture retention curve $\theta(\psi)$ describing the dependence of the soil moisture content θ on the capillary tension head ψ (see Chapter 3). In this analysis the unsaturated flow equation is expressed in terms of ψ, so the dependence of K on ψ rather than θ is of interest here.

Figures 2.2 and 2.3 (from Yeh, 1982) show observations of the unsaturated hydraulic conductivity K and its dependence on the capillary tension head ψ in the Panoche silty clay loam (Nielsen et al., 1974) and the Maddock sandy loam (Carvallo et al., 1974). Yeh (1982) discusses in detail the data collection and analysis used for derivation of these

24

curves. For the purposes of this presentation it is sufficient to mention that the different curves shown in Figures 2.2 and 2.3 correspond to the hydraulic conductivity at different spatial locations in the fields under investigation. These figures indicate a large degree of spatial variability of the unsaturated hydraulic conductivity (note the logarithmic scale on the hydraulic conductivity axis).

Figures 2.4 and 2.5 show the dependence of the soil moisture content θ on the capillary tension head ψ in the Panoche silty clay loam soil (Nielsen et al., 1974) and at a site near Socorro, New Mexico (Waldrop at al., 1984) Each of the curves in Figures 2.4 and 2.5 corresponds to a different spatial location in the field under investigation and indicate a spatial dependence of the $\theta(\psi)$ curves. However, the spatial variability of this property is not as large as the spatial variability of the hydraulic conductivity $K(\psi)$ demonstrated by Figures 2.2 and 2.3.

In order to simplify analysis it is convenient to parameterize the two basic hydraulic properties $K(\psi)$ and $\theta(\psi)$ in terms of a small number of parameters. The following parametrization is proposed for the effective hydraulic conductivity:

$$\ln K(\psi) = \ln K_S - \alpha \psi \quad . \tag{2.1}$$

The parameter α may generally depend on ψ but assuming small variations of ψ around a mean value H, it is possible to assume $\alpha(\psi) \approx \alpha(H)$. If local hysteresis exists, $\ln K_S$ and α also depend on the time history of ψ (i.e., wetting or drying conditions). A second important unsaturated hydraulic soil property, is the specific soil moisture capacity $C(\psi)$ defined as $C(\psi) = - \partial\theta/\partial\psi$. Assuming small variations of ψ around a mean value H, it is possible to write approximately
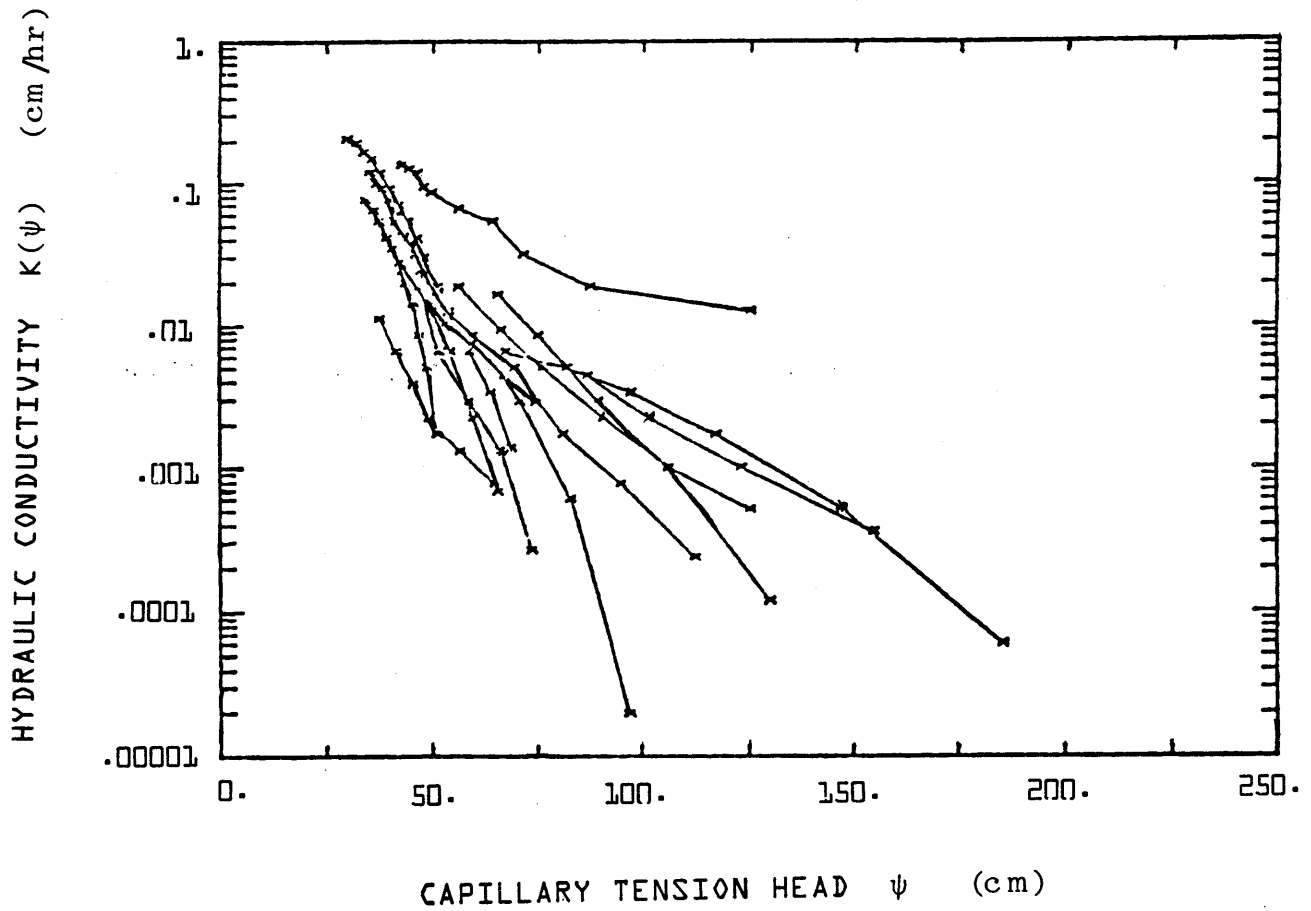
Figure 2.2 Unsaturated hydraulic conductivity versus capillary tension
head for the Maddock sandy loam. Each curve corresponds
to a different spatial location.
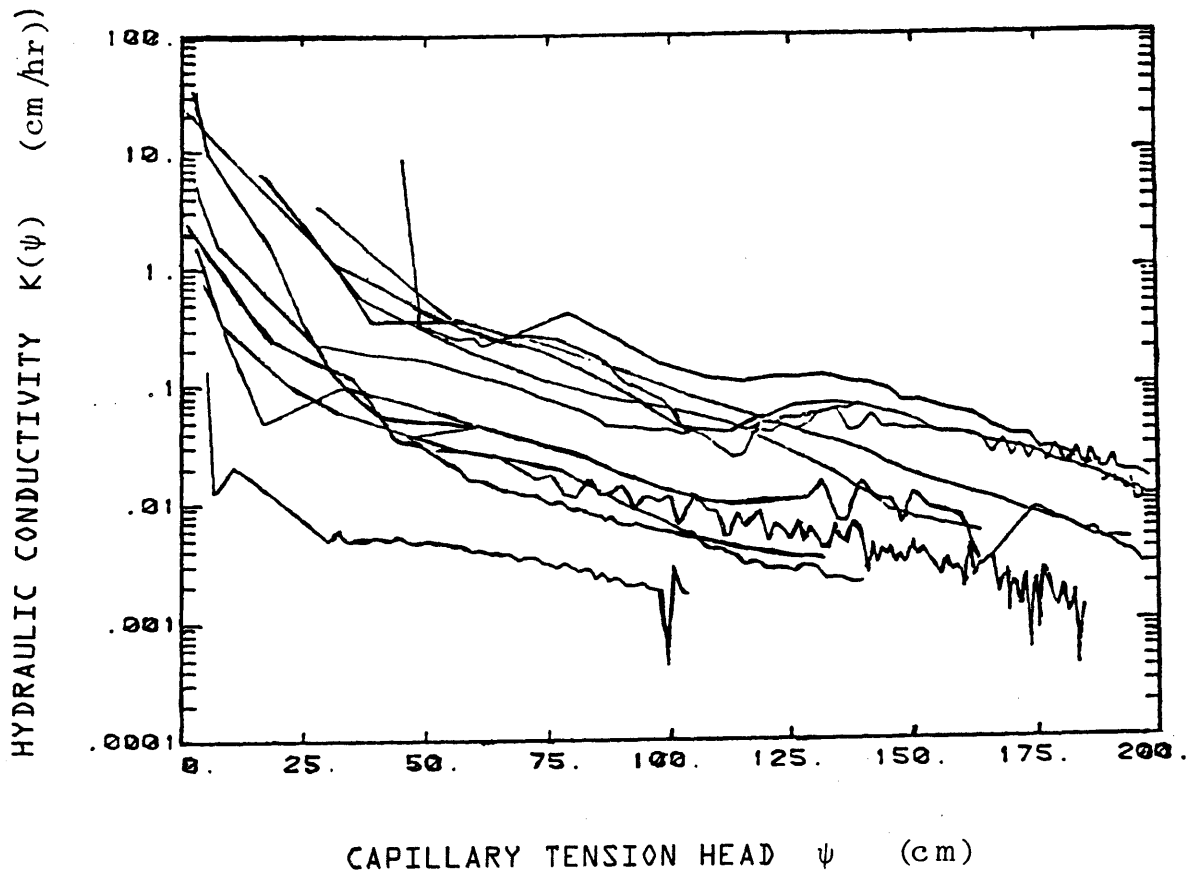
Figure 2.3   Unsaturated hydraulic conductivity K versus capillary tension head ψ for the Panoche silty clay loam. Each curve corresponds to a different spatial location.
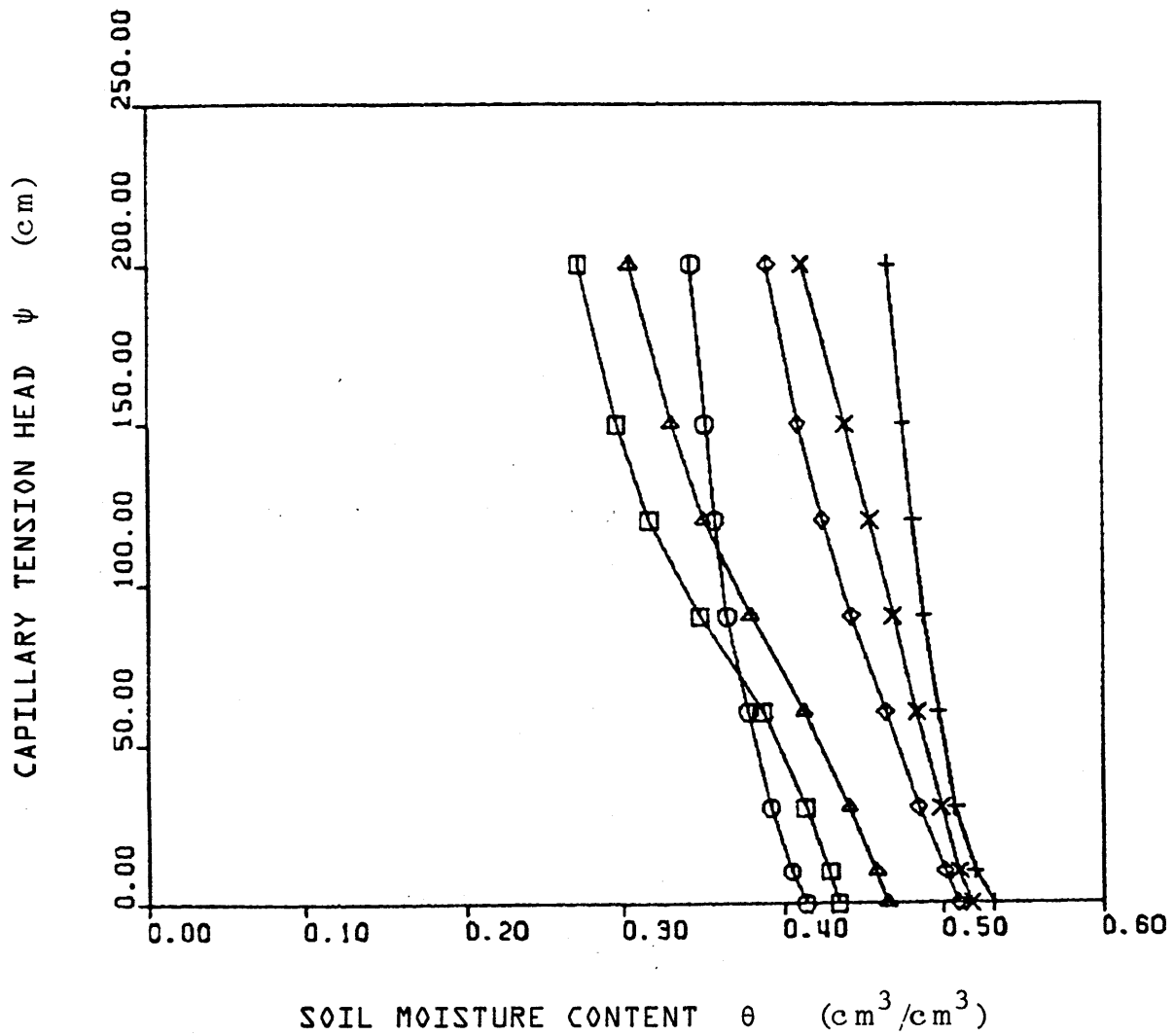
Figure 2.4 Capillary tension head ψ versus soil moisture content θ for
the Panoche silty clay loam. Each curve corresponds to
a different spatial location.
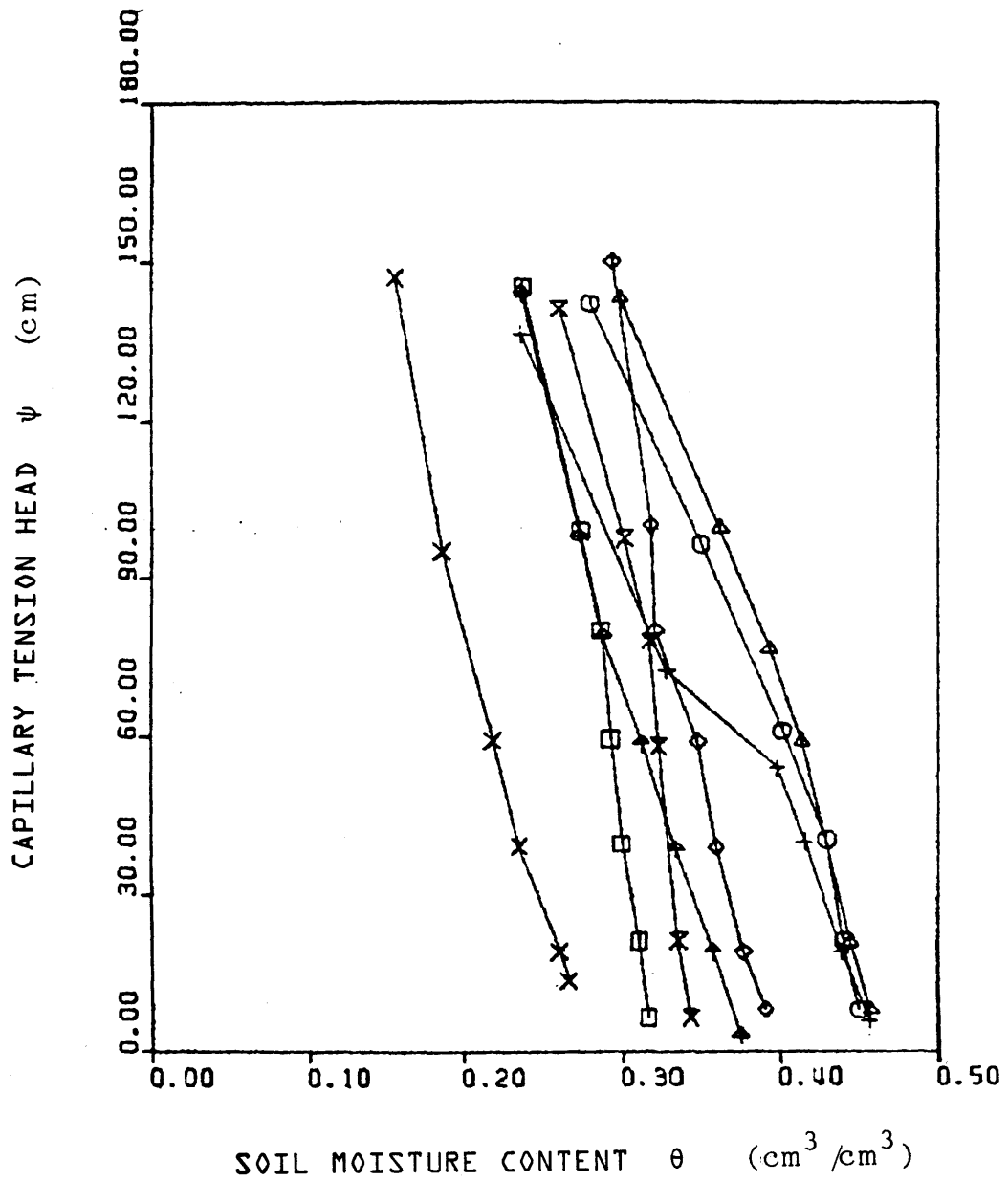
Figure 2.5 Capillary tension head ψ versus soil moisture content θ for
the soil at the New Mexico site. Each curve corresponds to
a different spatial location.

$$\theta(\psi) = \theta(H) + \frac{\partial \theta}{\partial \psi}\bigg|_{\psi=H} (\psi - H).$$

Taking the derivative of this equation with respect to ψ produces

$$\frac{\partial \theta(\psi)}{\partial \psi} \approx \frac{\partial \theta}{\partial \psi}\bigg|_{\psi=H} \quad ,$$

or $C(\psi) \approx C(H)$. Note that if local hysteresis exists $C(H)$ also depends on the time history of H.

For values of H not too small or too large (i.e., not a very wet or very dry soil), and if local hysteresis is relatively small (see discussion in Section 4.1), parameters $\ln K_s$, α and C may be assumed to be independent of H. This assumption is a convenient one when estimating the statistical parameters of $\ln K_s$, α and C from real data, but it is not required in the stochastic methodology developed in later chapters.

The parametrization of the unsaturated hydraulic properties discussed above, seems to describe real observations (e.g., Figures 2.2, 2.3, 2.4, 2.5) quite well and it is conveniently used in the stochastic methodology developed in Chapter 3. Using this parametrization, the unsaturated hydraulic properties have been expressed in terms of a three-dimensional parameter vector $\underline{p}$ with elements $\ln K_s$, α and C. These elements are local soil properties and they depend on the three-dimensional spatial coordinate $\underline{x}$. The next section discusses the representation of these properties in terms of three-dimensional random fields.

2.3 Stochastic Representation of Spatial Variability of the Hydraulic Soil Properties

It was discussed in the Introduction that, because of the large degree of natural spatial variability, it is impossible to represent the local hydraulic soil properties in terms of deterministic functions, and that a stochastic representation seems more appropriate. Following this discussion it is assumed that the local soil properties $\ln K_s(\underline{x})$, $\alpha(\underline{x})$ and $C(\underline{x})$ are composed of two components as follows

$$\ln K_s = F + f$$
$$\alpha = A + a \qquad\qquad (2.2)$$
$$C = \Gamma + \gamma$$

where F, A, Γ are large-scale components and f, a, γ are small scale components of $\ln K_s$, α and C respectively. It is assumed that the large-scale components F, A and Γ are deterministic and slowly varying functions of space and we call them "mean", while the small scale components f, a, γ are realizations of three-dimensional zero mean random fields and we call them "fluctuations".

The stochastic theory developed in the following chapters assumes that the mean properties F, A and Γ are relatively constant compared to the scale of the problem under consideration, while the local fluctuations have a scale of variation much smaller than the scale of the flow domain. This implies that the decomposition suggested by Equation (2.2) depends on the scale of the problem. What is viewed as a mean in a small laboratory scale model for example, may be viewed as a fluctuation in a large field scale problem. A second assumption of the stochastic theory is that fluctuations f, a and γ are realizations of stationary

31

random fields. For simplicity and consistency of the results in the applications presented in Chapters 4 and 5, and since no sufficient information for evaluation of these cross-covariances exists, it is assumed that f, a and γ follow exponential cross-covariance functions with identical correlation lengths. Two particular cases are investigated: (i) f, a, γ being uncorrelated and (ii) f, a, γ being perfectly correlated. Of course, in reality it is expected that f, a, γ are only partially correlated. The above extreme cases of correlation were selected in order to explicitly show the dependence of σ_h^2 on the type of correlation between f, a, γ. It is possible then to express the covariance of u, v (u, v = f, a, γ) as: $C_{uv}(\underline{r}) = \mu C_{ff}(\underline{r})$ where μ depends on u, v and the type of correlation between u, v (see Section 4.3). Assuming an exponential covariance function for f, it holds:

$$C_{ff}(\underline{\xi}) = E[f(\underline{x}) \ f(\underline{\xi}+\underline{x})] = \sigma_f^2 \ \exp[-(\frac{\xi_1^2}{\lambda_1^2} + \frac{\xi_2^2}{\lambda_2^2} + \frac{\xi_3^2}{\lambda_3^2})^{1/2}] \quad (2.3)$$

where $\underline{\xi}$ is the distance vector. Equation (2.3) is expressed in a system of axes oriented in the directions of principal axes of anisotropy of $f(\underline{x})$; λ_1, λ_2, λ_3 are the corresponding correlation lengths and σ_f^2 the variance of $f(\underline{x})$. The spectral density function of $f(\underline{x})$ is defined as the Fourier transform of $C_{ff}(\underline{\xi})$, i.e.

$$S_{ff}(\underline{k}) = \frac{1}{(2\pi)^3} \int\int\int_{-\infty}^{\infty} e^{-j\underline{k}\cdot\underline{\xi}} \ C_{ff}(\underline{\xi}) \ d\underline{\xi} \quad (2.4)$$

where $\underline{k}$ is the wave number vector. Using (2.3), Equation (2.4) yields

$$S_{ff}(\underline{k}) = \frac{\sigma_{ff}^2 \ \lambda_1 \lambda_2 \lambda_3}{\pi^2(1 + \lambda_1^2 k_1^2 + \lambda_2^2 k_2^2 + \lambda_3^2 k_3^2)^2} \quad . \quad (2.5)$$

32

It is desired in later chapters to apply the results of the stochastic methodology to realistic field scale problems. Unfortunately, the current data describing the spatial variability of the soil properties $\ln K_s$, α and C in real field situations, is not sufficient to evaluate the necessary statistical parameters. In the following, some available data on $\ln K_s$, α and C, in the cases of the Panoche clay loam, the Maddock sandy loam and the New Mexico soil, are analyzed.

Using simple least squares curve fitting techniques, the reported data were analyzed and parameters $\ln K_s$, α and C were evaluated. Using simple averaging it was possible to estimate the mean and variance of these parameters. These values are summarized in Table 2.1. Given this limited amount of data it is impossible to estimate reliable correlation lengths for f, a, γ (see discussion in Chapter 6). Using existing information about soil variability in natural soil formations (e.g., Gelhar and Axness, 1983) an approximate correlation length of λ_1 = 100 cm in a direction perpendicular to stratification was assumed.

The parameters shown in Table 2.1, with λ_1 = 100 cm and λ_2, $\lambda_3 \gg \lambda_1$, represent a realistic set of soil property variability parameters and are used in several application examples in Chapters 4 and 5. Note that data on the spatial variability of the specific moisture capacity C are not available in the case of the Maddock soil. However, data on C in other soil types show a relatively small coefficient of variation σ_γ / Γ. Chapter 4 shows that the effect of spatial variability of C, for such small coefficients of variation, is relatively small, at least compared to the effects of spatial variability

33·

TABLE 2.1

STOCHASTIC PARAMETERS OF HYDRAULIC SOIL PROPERTIES

	Panoche	Maddock	New Mexico
A (cm^{-1})	0.0294	0.147	-
Γ (cm^{-1})	0.0052	-	0.00098
σ_f^2	2.48	7.45	-
σ_a^2 (cm^{-2})	0.000067	0.0076	-
σ_γ^2 (cm^{-2})	8.95×10^{-8}	-	$2. \times 10^{-7}$

of $\ln K_s$ and α. Since C is not the most critical parameter, the data on the variability of C for the Panoche soil are also used in the case of the Maddock soil in later examples.

The data basis discussed above is very limited. A large-scale experiment is proposed in the New Mexico desert area (Waldrop et al., 1984). This experiment will collect a large amount of data sufficient for estimation of the parameters required for application of the stochastic theory developed in later chapters. Chapter 6 discusses methods addressing the difficult problem of estimation of such parameters in practical situations.

CHAPTER 3

LARGE SCALE MODELS AND EFFECTIVE PARAMETERS OF UNSATURATED FLOW

AND SOLUTE TRANSPORT: A STOCHASTIC METHODOLOGY

3.1 Introduction

Chapter 1 discussed the need for obtaining large-scale models of unsaturated flow and solute transport. Such models should realistically portray the complexity of large-scale natural unsaturated flow systems and have relatively few and identifiable parameters that can be estimated from a realistic data set.

This chapter develops a general methodology for evaluating large-scale models and effective parameters of unsteady unsaturated flow and steady solute transport using a stochastic approach. Section 3.2 examines the transient unsaturated flow problem while Section 3.3 examines the steady transport problem. The stochastic approach assumes that the local hydraulic soil properties are realizations of three-dimensional, cross-correlated, stationary, random fields and averages the local governing flow and transport equations over the ensemble of soil property realizations in order to derive the large-scale models. The method considers the three-dimensionality of the local flow and transport processes and the nonlinear dependence of the local output on the local soil properties. The stochastic methodology accounts for the large-scale effects of local property variability and is capable of predicting the statistical properties of the model error.

One of the objectives of this study is to provide analytical generic relationships for the dependence of the effective large-scale parameters

on the different soil property and flow characteristics. This is because of the generality, simplicity and insight gained by such results. Numerical (Monte Carlo) evaluations on the other hand are expensive, are valid only for the particular setting considered, and do not offer much insight for the dependence of the effective parameters on the different soil property and flow characteristics. In order to make analytical evaluations possible, several assumptions are required, (e.g., small local property fluctuations, etc.). To keep each step of the stochastic theory developed in this chapter as general as possible, the necessary assumptions are introduced in the steps where they are required and not in previous steps. These assumptions may restrict the validity of the results. However, it is possible that, even in cases where the required assumptions are not strictly valid, the stochastic results may give relatively good quantitative and qualitative approximations of reality. Since large-scale behavior of unsaturated flow and transport processes is presently highly unknown, we believe that even qualitative information about the system behavior is important.

This chapter develops the general methodology for evaluation of large-scale models and effective parameters in a general format without restricting it to any particular applications. This methodology is applied in Chapters 4 and 5 in several cases of practical interest.

3.2 Transient Unsaturated Flow

This section develops a general stochastic methodology for derivation of large-scale unsaturated flow models. These large-scale models are expressed in a partial differential equation form and are capable of predicting the large-scale flow characteristics.

The stochastic method follows three basic steps. In the first step (Section 3.2.1), the form of the large-scale model and its effective parameters are established by averaging the local governing equation over the ensemble of soil property realizations. Evaluation of the effective flow parameters requires evaluation of cross-correlations between local soil properties and output fluctuations. The second step of the stochastic methodology (Section 3.2.2) derives simplified linearized equations relating the output fluctuations to soil property fluctuations. The last step of the analysis, (Section 3.2.3), uses the linearized equations derived in the second step, and some spectral representation properties for evaluation of the large-scale models and the effective model parameters defined in the first step.

3.2.1 Derivation of Large-Scale Models and Effective Parameters

The form of the large-scale unsaturated flow model is derived below by averaging the local governing flow equation over the ensemble of soil property realizations. Ignoring vapor flow and sources or sinks, the law of conservation of mass for soil moisture of constant density moving in in a rigid soil matrix, simplifies to

$$-\frac{\partial \theta}{\partial t} = \frac{\partial q_i}{\partial x_i} \qquad i = 1, 2, 3 \qquad (3.1)$$

where:

θ : the soil moisture content, (cm^3/cm^3)

q_i: the specific discharge in the direction x_i, (cm/sec),

x_1, x_2, x_3 is a Cartesian coordinate system and the standard

Cartesian summation convention of Einstein has been used. Note that

Equation (3.1) is valid on a local scale and θ and q_i correspond to

local quantities. It is further assumed that the local specific

discharge q_i can be expressed by a Darcy equation

$$q_i = K(\psi) \frac{\partial (\psi + z)}{\partial x_i} \qquad (3.2)$$

where

ψ: the capillary tension head (cm)

K: the local unsaturated hydraulic conductivity, (cm/sec)

z: vertical position with z increasing downwards, (cm).

Note that the local hydraulic conductivity is assumed to be isotropic.

Substituting (3.2) into (3.1) yields the standard unsaturated flow equation:

$$-\frac{\partial \theta}{\partial t} = C \frac{\partial \psi}{\partial t} = \frac{\partial}{\partial x_i} \left[K(\psi) \frac{\partial (\psi + z)}{\partial x_i} \right] \qquad (3.3)$$

where $C = -\partial\theta/\partial\psi$ is the specific moisture capacity. The hydraulic soil

properties K and C are local properties, i.e., they depend on the spatial

coordinate $\underline{x} = (x_1, x_2, x_3)$. These properties depend also on ψ.

Further analysis requires a model for the dependence of C and K on ψ.

Assuming small variations of ψ around a mean value H, it is possible,

following the discusssion in Chapter 2, to approximate $C(\psi) \approx C(H)$ and

$$\ln K(\psi) = \ln K_S - \alpha \psi \quad . \tag{3.4}$$

Note that the local parameters α and C may in general depend on H and its time history. For values of H not too small or too large (i.e., not very wet or very dry soils), and if local hysteresis is relatively small, parameters α and C may be assumed to be independent of H (see Chapter 2). This assumption is a convenient one when estimating the statistical parameters of the soil properties from real data, (see Chapter 6), but it is not required in the stochastic methodology developed in this chapter. To simplify notation, possible dependence of α and C on H and its time history will not be explicitly indicated in the following developments. We note, however, that the theory is developed in a general format and will be also valid if local parameters α and C depend on H and if local hysteresis exists (as long as a model for these effects is provided).

It is assumed that the three local hydraulic soil properties $\ln K_S$, α and C are realizations of three-dimensional, cross-correlated, stationary, anisotropic random fields:

$$\ln K_S = F + f$$

$$\alpha = A + a \tag{3.5a}$$

$$C = \Gamma + \gamma$$

where F, A and Γ are the mean values of $\ln K_S$, α and C and f, a, γ the fluctuations around the mean values. The local flow Equation (3.3) can be viewed then as a partial differential equation with stochastic parameters and therefore, stochastic output ψ. It is then possible to express ψ as:

$$\psi = H + h \tag{3.5b}$$

where H is the mean of ψ and h the fluctuations around the mean. It is

assumed that: (i) the fluctuations f, a, γ and h are relatively small and (ii) the scale of variations of the mean values F, A, Γ and H is much larger than the scale of variations of the fluctuations f, a, γ and h.

The large-scale model of transient unsaturated flow is obtained by averaging the local governing Equation (3.1) over the ensemble of possible realizations of stochastic processes f, a, and γ. Taking the expected value of (3.1) with respect to f, a, and γ and using (3.2) and the linearity of the derivative operator, Equation (3.1) yields

$$-\frac{\partial\{E[\theta]\}}{\partial t} = \frac{\partial}{\partial x_i} \left\{ E\left[K \frac{\partial(\psi + z)}{\partial x_i} \right] \right\} \quad . \qquad (3.6)$$

Equation (3.6) is the mean flow equation. In order to derive a more useful form of this equation, the expected values within the brackets should be evaluated and be expressed in terms of the mean soil property and flow characteristics, and the statistical parameters of the soil property variability f, a and γ.

The expected values on the right hand side of Equation (3.6) are evaluated first. Assume that the system of axes (x_1, x_2, x_3) is oriented in the direction of the principal statistical anisotropy axes of f, a and γ. Substituting (3.5) into (3.4) yields:

$$K = K_m e^{f - Ah - Ha - ah} \qquad (3.7)$$

where

$$K_m = e^F e^{-AH} = K_G e^{-AH} \quad . \qquad (3.8)$$

Let:

$$\frac{\partial(\psi + z)}{\partial x_i} = \frac{\partial(H + h + z)}{\partial x_i} = J_i + \frac{\partial h}{\partial x_i} \qquad (3.9)$$

where $J_i = \partial(H + z)/\partial x_i$ is the mean hydraulic gradient. Using (3.7) and (3.9), the expected value in the right hand side of Equation (3.6) is written as:

$$E[q_i] = K_G \; E[e^{f - Ah - Ha - ah} \; (J_i + \frac{\partial h}{\partial x_i})] \quad . \quad (3.10)$$

In order to evaluate this expected value, expand the exponential in a Taylor series

$$e^{f - Ah - Ha - ah} \approx 1 + (f - Ah - Ha - ah) + \frac{1}{2} (f - Ah - Ha - ah)^2 \quad (3.11)$$

where, assuming that fluctuations f, a, γ and h are small, third and higher order terms have been neglected. Substituting (3.11), Equation (3.10) yields:

$$E[q_i] = K_m \; \{J_i(1 + \frac{1}{2} E[(f - Ah - Ha)^2])$$

$$+ E[(f - Ah - Ha) \frac{\partial h}{\partial x_i}]\} \quad (3.12)$$

where the expected values of fluctuation products of third or higher order have been neglected. Note that in the particular case of f, a, γ and h being jointly Gaussian random processes, the expected value in Equation (3.10) can be evaluated without using the Taylor series expansion. This approach uses the joint characteristic function of f, a, γ and h, (see Yeh et al., 1982).

As will be seen later, the expected values of Equation (3.12) depend on the mean flow characteristics H, J_1, J_2, J_3 and $J_t = \partial H/\partial t$ in a complicated and nonlinear manner. The problem of defining an effective hydraulic conductivity tensor $\hat{K}_{ij}$ is now discussed. Such tensor should

42

have the property: $E[q_i] = \hat{K}_{ij}J_j$, where $\hat{K}_{ij}$ is a symmetric tensor. Since $E[q_i]$ depends on the spatial gradients J_j in a nonlinear fashion, in order to determine an effective symmetric hydraulic conductivity tensor $\hat{K}_{ij}$ an additional assumption is required.

Define:

$$\hat{K}_{ii} = \frac{E[q_i]}{J_i} \qquad (3.13)$$

while $\hat{K}_{ij} = 0$ for $i \neq j$, where x_i are the principal statistical anisotropy axes of f, a, γ. Note that since $E[q_i]$ depends on J_j in a a nonlinear fashion, other definitions of an effective hydraulic conductivity tensor are possible as long as the relationship $E[q_i] = \hat{K}_{ij}J_j$ is valid and $\hat{K}_{ij}$ is symmetric. The assumption that $\hat{K}_{ij}$ has as principal axes, the principal statistical anisotropy axes of f, a, γ, was made in order to be consistent with the saturated flow case where a unique effective hydraulic conductivity tensor independent of J_j exists, and having principal axes as defined above (Gelhar and Axness, 1983). The effective hydraulic conductivities $\hat{K}_{ij}$, generally depend on J_1, J_2, J_3, J_t and H, in a nonlinear fashion. As will be seen later, the above definition of $\hat{K}_{ij}$, facilitates expressing the mean flow equation (3.6) in a form similar to the local governing Equation (3.2). Substituting (3.12), Equation (3.13) yields:

43

$$\hat{K}_{ii} = K_m \left[\left(1 + \frac{\sigma_\epsilon^2}{2}\right) + \frac{\tau_i}{J_i} \right] \tag{3.14}$$

where

$$\sigma_\epsilon^2 = E[(f - Ah - Ha)^2] = \sigma_f^2 + A^2 E[h^2] + H^2 \sigma_\alpha^2$$

$$- 2A \, E[fh] - 2H \, E[fa] + 2AH \, E[ah] \tag{3.15a}$$

$$\tau_i = E\left[(f - Ah - Ha)\frac{\partial h}{\partial x_i}\right] = E\left[f \frac{\partial h}{\partial x_i}\right] - H \, E\left[a \frac{\partial h}{\partial x_i}\right] \tag{3.15b}$$

where, assuming that h is stationary, it holds that $2 \, E[h \, \partial h / \partial x_i] = \partial\{E[h^2]\}/\partial x_i = 0$. Evaluation of the effective hydraulic conductivities $\hat{K}_{ii}$ has now been reduced to the evaluation of the expected values $E[h^2]$, $E[fh]$, $E[ah]$, $E[f \, \partial h / \partial x_i]$, and $E[a \, \partial h / \partial x_i]$.

The left hand side of the mean flow Equation (3.6) is now examined. The expected value $E[\theta]$ specifies the mean soil moisture content $\Theta = E[\theta]$. Substituting Θ into Equation (3.6) yields a mean equation of the same form as the local Equation (3.2). The mean soil moisture content Θ is evaluated as follows. For small fluctuations h, it holds: $\theta = \theta(\psi) \simeq \theta(H) - Ch$, where $C = -\partial\theta/\partial\psi\big|_{\psi=H}$. Substituting (3.5) and taking the expected value yields:

$$\Theta = E[\theta(H)] - E[\gamma h] \quad . \tag{3.16}$$

The effective specific moisture capacity is defined by

$$\hat{C} = - \frac{\partial \Theta}{\partial H} \tag{3.17}$$

Evaluation of the mean soil moisture content Θ and the effective specific moisture capacity $\hat{C}$ has been reduced to the evaluation of the expected

value E[γh] where E[θ(H)] is assumed to be a known characteristic of spatial variability of θ(H). In the special case of a linear dependence of θ on ψ, it holds θ = -Cψ + θ₀ and Equation (3.16) reduces to Θ = (- ΓH + E[θo]) - E[γh]. Substituting (3.13) and (3.17) into (3.6) yields the large-scale transient unsaturated flow model:

$$- \frac{\partial \Theta}{\partial t} = \hat{C} \frac{\partial H}{\partial t} = \frac{\partial}{\partial x_i} \left[\hat{K}_{ij} \frac{\partial (H + z)}{\partial x_j} \right] \quad . \tag{3.18}$$

Note that the large-scale transient unsaturated flow model is of the same form as the local governing Equation (3.3). The effective parameters of the mean flow model are given by Equations (3.14), (3.15), (3.16) and (3.17). The remaining problem is to evaluate the cross-correlations between the output fluctuations and the soil property fluctuations f, a, γ in Equations (3.15) and (3.16). Section 3.2.2 derives an approximate linearized expression relating h to f, a, γ. Section 3.2.3 uses this linearized expression for evaluation of the expected values in Equation (3.15) and (3.16) and the corresponding effective parameters $\hat{K}_{ij}$, Θ and $\hat{C}$.

3.2.2 Linearized Fluctuation Equation

This section derives a linearized perturbation equation relating the capillary tension head fluctuations h to the soil property fluctuations f, a and γ using the local flow Equation (3.3). Consider the flow at a point located far away from the boundaries of the flow domain. Substituting (3.4) into (3.3) and expanding derivatives yields

$$\frac{C}{K_s} \exp(\alpha\psi) \frac{\partial \psi}{\partial t} = \frac{\partial (\ell n K_s - \alpha\psi)}{\partial x_i} \frac{\partial (\psi + z)}{\partial x_i} + \nabla^2 \psi \quad . \tag{3.19}$$

45

Substituting (3.5), the left hand side of Equation (3.19) is written as:

$$L = \frac{C}{K_s} \exp(\alpha\psi) \frac{\partial\psi}{\partial t} = (\Gamma + \gamma) e^{AH - F} e^{Ah + Ha - f + ah} \frac{\partial(H + h)}{\partial t} \quad (3.20)$$

A Taylor series expansion of the exponential in (3.20) yields

$$e^{Ah + Ha - f + ah} = 1 + (Ah + Ha - f + ah) + T_H \quad (3.21)$$

where T_H are the remaining higher order terms. Substituting (3.21) into (3.20) produces

$$L = e^{AH - F} [\Gamma \frac{\partial H}{\partial t} + (A\Gamma h + H\Gamma a - \Gamma f + \gamma) \frac{\partial H}{\partial t} + \Gamma \frac{\partial h}{\partial t} +$$

$$+ (\Gamma ah + A\gamma h + H\gamma a - \gamma f + \gamma ah) \frac{\partial H}{\partial t} +$$

$$+ (A\Gamma h + H\Gamma a - \Gamma f + \Gamma ah + \gamma + A\gamma h + H\gamma a - \gamma f + \gamma ah) \frac{\partial h}{\partial t} +$$

$$+ T_H (\Gamma + \gamma) \frac{\partial(H + h)}{\partial t}] \quad . \quad (3.22)$$

The terms inside the brackets of (3.22) have been set in the following order. The first term is independent of the fluctuations f, a, γ, h, (zero order term). The following five terms are linear in the fluctuations, (first order terms). Lastly come the remaining second and higher order terms. To simplify notation Equation (3.22) is written as:

$$L = L_0 + L_1 + L_H \quad (3.23)$$

where L_0, L_1, and L_H are the zero, first and higher order terms respectively.

The first component of the first term in the right hand side of (3.19) is written as follows:

46

$$\frac{\partial(\ell nK_s - \alpha\psi)}{\partial x_i} = \frac{\partial(\ell nK_s - AH - Ah - Ha - ah)}{\partial x_i} =$$

$$= \frac{\partial f}{\partial x_i} - A\frac{\partial H}{\partial x_i} - A\frac{\partial h}{\partial x_i} - a\frac{\partial h}{\partial x_i} - H\frac{\partial a}{\partial x_i} - \frac{\partial(ah)}{\partial x_i} \qquad (3.24)$$

where it is assumed that spatial variation of F and A is slow, and $\partial F/\partial x_i$ and $\partial A/\partial x_i$ are small. Substituting (3.5), and using (3.9), the right hand side of Equation (3.19) is written as:

$$R = \frac{\partial(\ell nK_s - \alpha\psi)}{\partial x_i} \frac{\partial(\psi + z)}{\partial x_i} + \nabla^2\psi =$$

$$= (-J_i A\frac{\partial H}{\partial x_i} + \nabla^2 H) +$$

$$+ (J_i\frac{\partial f}{\partial x_i} - J_i A\frac{\partial h}{\partial x_i} - J_i\frac{\partial H}{\partial x_i}a - J_i H\frac{\partial a}{\partial x_i} - A\frac{\partial H}{\partial x_i}\frac{\partial h}{\partial x_i} + \nabla^2 h) +$$

$$+ [- J_i\frac{\partial(ah)}{\partial x_i} + \frac{\partial f}{\partial x_i}\frac{\partial h}{\partial x_i} - A(\frac{\partial h}{\partial x_i})^2 - \frac{\partial H}{\partial x_i}a\frac{\partial h}{\partial x_i} -$$

$$- H\frac{\partial a}{\partial x_i}\frac{\partial h}{\partial x_i} - \frac{\partial(ah)}{\partial x_i}\frac{\partial h}{\partial x_i}] \qquad (3.25)$$

The terms of (3.25) have been set in the following order. The first two terms are independent of fluctuations, (zero order terms). The following six terms are linear in the fluctuations, (first order terms). Lastly come six higher order terms. To simplify notation (3.25) is written as:

$$R = R_0 + R_1 + R_H \qquad . \qquad (3.26)$$

Equation (3.19) can then be written as:

$$L_0 + L_1 + L_H = R_0 + R_1 + R_H \qquad (3.27)$$

where L_0, L_1, L_H, R_0, R_1, R_H are given by (3.22) and (3.25),
respectively. Taking the expected value of (3.27) with respect to f, a
and γ yields

$$L_0 + E[L_H] = R_0 + E[R_H] \tag{3.28}$$

where the expected value of the linear terms is zero. Subtracting (3.28)
from (3.27) produces

$$L_1 + L_H - E[L_H] = R_1 + R_H - E[R_H] \quad . \tag{3.29}$$

Assuming that fluctuations f, a, γ and h are relatively small, the
higher order terms can be approximated by their expected values, i.e.,
$L_H \approx E[L_H]$ and $R_H \approx E[R_H]$. Equation (3.29) then yields L_1
$\approx R_1$ or

$$e^{AH-F} \left[(A\Gamma h + H\Gamma a - \Gamma f + \gamma) \frac{\partial H}{\partial t} + \Gamma \frac{\partial h}{\partial t} \right] =$$

$$= J_i \frac{\partial f}{\partial x_i} - J_i A \frac{\partial h}{\partial x_i} - J_i \frac{\partial H}{\partial x_i} a - J_i H \frac{\partial a}{\partial x_i} - A \frac{\partial H}{\partial x_i} \frac{\partial h}{\partial x_i} + \nabla^2 h \quad . \tag{3.30}$$

Define:

$$G = \frac{1}{K_m} \frac{\partial H}{\partial t} \tag{3.31}$$

$$L_i = J_i + \frac{\partial H}{\partial x_i} \tag{3.32}$$

where K_m is given by (3.8). Substituting (3.31) and (3.32) into (3.30)
and rearranging terms yields

48

$$\frac{\partial h}{\partial t} + \frac{K_m}{\Gamma} \left(-\nabla^2 h + A\Gamma G\, h + AL_i \frac{\partial h}{\partial x_i} \right) =$$

$$= \frac{K_m}{\Gamma} \left[\left(J_i \frac{\partial f}{\partial x_i} + \Gamma G\, f \right) - \left(J_i H \frac{\partial a}{\partial x_i} + b\, a \right) - G\, \gamma \right] \qquad (3.33)$$

where:

$$b = J_i \frac{\partial H}{\partial x_i} + H\Gamma G \qquad (3.34)$$

Equation (3.33) is a first order approximation describing the capillary tension head fluctuations h in terms of the soil property fluctuations f, a and γ. This equation represents a three-dimensional time varying linear system. The soil property fluctuations f, a, γ are viewed as system inputs while the capillary tension head fluctuations h are viewed as the system output. Equation (3.33) was obtained by linearizing the local governing Equation (3.2) around the mean soil properties F, A, Γ and mean flow characteristics H, J_1, J_2, J_3 and J_t. These mean soil properties and flow characteristics are viewed as system parameters in (3.33). Due to the dependence of the fluctuation equation on the mean flow characteristics, the expected values of Equations (3.15) and (3.16) and the corresponding effective parameters $\hat{K}_{ii}$, Θ and $\hat{C}$ depend on the mean capillary tension head H and its derivatives J_1, J_2, J_3 and J_t. This results in a nonlinear mean flow equation. In addition, because of the dependence of $\hat{K}_{ii}$, Θ, and $\hat{C}$ on $J_t = \partial H/\partial t$, it is expected that these parameters will show hysteresis. Note that although the fluctuation equation was linearized around the mean soil properties and flow characteristics, the mean flow equation, developed in Section 3.2.1, considers the basic nonlinearities

of the local flow equation. In fact, these local model nonlinearities and the existence of local spatial variability are responsible for the large-scale hysteresis effects discussed above.

In order to make further use of the linearized Equation (3.33) possible, assume that the mean soil properties and the mean flow characteristics vary slowly in space, compared to the correlation lengths of the fluctuations f, a, γ and h. It is also assumed that the boundaries of the flow domain are at a relatively large distance compared to the correlation lengths of the fluctuations. It is then possible to assume that f, a, γ and h are realizations of stationary random fields and derive a wave number domain form of the linear fluctuation Equation (3.33). Note that in the transient flow case, the mean flow characteristics (H, etc.) are time varying. This implies that the output h of (3.33) is generally time varying and $\partial h/\partial t \neq 0$. In certain cases, (see Chapter 4), it is possible to ignore term $\partial h/\partial t$. In other cases however, it is not possible to ignore this term. The following analysis considers the general case of $\partial h/\partial t \neq 0$.

The soil property fluctuations f, a, γ were assumed to be realizations of three-dimensional, stationary random fields. They may then be expressed in the wave number domain as follows: (see, e.g., Lumley and Panofsky, 1964)

$$f(\underline{x}) = \int\int\int_{-\infty}^{\infty} e^{j\underline{k}\underline{x}} \, dZ_f(\underline{k})$$

$$a(\underline{x}) = \int\int\int_{-\infty}^{\infty} e^{j\underline{k}\underline{x}} \, dZ_a(\underline{k}) \qquad\qquad (3.35)$$

$$\gamma(\underline{x}) = \int\int\int_{-\infty}^{\infty} e^{j\underline{k}\underline{x}} \, dZ_\gamma(\underline{k})$$

50

where $j = \sqrt{-1}$, $\underline{x}$, the spatial coordinate, $\underline{k}$, the wave number vector, and dZ_f, dZ_a, dZ_γ, the Fourier-Stieltjes spectral amplitudes of f, a and γ. At each time t, the output fluctuations h are stationary in space. It is then possible to view h as a realization of a time varying, but spatially stationary, random field and, using the spectral representation, express h in the following form:

$$h(\underline{x}, t) = \int\!\!\!\int\!\!\!\int_{-\infty}^{\infty} e^{j\underline{k}\underline{x}} \, dZ_h(\underline{k}, t) \qquad (3.36)$$

where the Fourier-Stieltjes amplitudes dZ_h are time dependent. Substituting (3.35) and (3.36) into (3.33) and recalling the uniqueness of the spectral representation

$$\frac{\partial y}{\partial t} + \frac{K_m}{\Gamma} \, (k_1^2 + k_2^2 + k_3^2 + A\Gamma G + jAL_i \, k_i) \, y =$$

$$\frac{K_m}{\Gamma} \left[(jJ_i \, k_i + \Gamma G) \, dZ_f - (jHJ_i \, k_i + b) \, dZ_a - G \, dZ_\gamma \right] \qquad (3.37)$$

where $y = dZ_h(\underline{k}, t)$. Equation (3.37) specifies a set of ordinary differential equations with unknown variable y and parameter $\underline{k}$. In order to evaluate the effective parameters, defined in Section 3.2.1, using spectral respresentations, (3.37) must be solved for y for each value of parameter $\underline{k}$. The general solution of (3.37) is given by:

$$y(\underline{k}, t) = \left[y(\underline{k}, 0) + \int_0^t g(\tau) \, e^{\int_0^\infty g_1(x) \, dx} \, d\tau \right] e^{-\int_0^t g_1(\tau) \, d\tau} \qquad (3.38)$$

where

$$g_1(t) = \frac{K_m}{\Gamma} \, (k_1^2 + k_2^2 + k_3^2 + A\Gamma G + jAL_i \, k_i) \qquad (3.39a)$$

51

$$g(t) = \frac{\dot{K}_m}{\Gamma} \left[(jJ_i k_i + \Gamma G) \, dZ_f \right.$$

$$\left. - (jHJ_i k_i + J_i \frac{\partial H}{\partial x_i} + H\Gamma G) \, dZ_a - G \, dZ_\gamma \right] \quad . \qquad (3.39b)$$

In the transient case, functions g, g_1 depend on t, since the mean flow properties H, etc., depend on t. Function $g(t)$ may be written as:

$$g(t) = g_f(t) \, dZ_f + g_a(t) \, dZ_a + g_\gamma(t) \, dZ_\gamma \qquad (3.40)$$

where functions g_f, g_a and g_γ are defined by comparison to (3.39b).

Equation (3.38) may then be written as:

$$y(\underline{k}, t) = W(\underline{k}) \, y(\underline{k}, 0) + W_f(\underline{k}) \, dZ_f(\underline{k}) + W_a(\underline{k}) \, dZ_a(\underline{k}) + W_\gamma(\underline{k}) \, dZ_\gamma(\underline{k}) \qquad (3.41)$$

where a dependence of W, W_f, W_a, W_γ on t is implied and

$$W(\underline{k}, t) = e^{-\int_0^t g_1(\tau) \, d\tau} \qquad (3.42)$$

$$W_{f,a,\gamma}(\underline{k}, t) = \left[\int_0^t g_{f,a,\gamma}(\tau) \, e^{\int_0^\infty g_1(x) \, dx} \, d\tau \right] e^{-\int_0^t g_1(\tau) \, d\tau} . \qquad (3.43)$$

It seems impossible to derive a general analytical closed form solution of Equation (3.43). This is because of the complicated form of the forcing functions g_1 and $g_{f,a,\gamma}$. In certain cases however, it is possible to derive such solutions. Lets examine, for example, the case of H relatively large (dry soil) and $\partial H/\partial t > 0$ (drying) conditions. Using (3.8) and (3.31), Equation (3.37) simplifies to

$$\frac{\partial y}{\partial t} + AJ_t \, y = (dZ_f - H \, dZ_a - \frac{dZ_\gamma}{\Gamma}) \, J_t \qquad (3.44)$$

52

where $J_t = \partial H / \partial t$. Assume that J_1, J_2, J_3, J_t are practically independent of time t and that H increases as a linear function of t, i.e., $H = H_0 + J_t\, t$. Equation (3.44) can then be written as:

$$\frac{\partial y}{\partial t} + AJ_t\, y = \delta_1 + \delta_2\, t \qquad (3.45)$$

where

$$\delta_1 = J_t\, (dZ_f - H_0\, dZ_a - \frac{dZ_\gamma}{\Gamma})$$

$$\delta_2 = -\, J_t^2\, dZ_a \quad . \qquad\qquad (3.46)$$

Equation (3.45) can be solved analytically (see Appendix A). Its solution is given by

$$y(\underline{k},\ t) = [\frac{dZ_f - H\, dZ_a - \frac{dZ_\gamma}{\Gamma}}{A} + \frac{dZ_a}{A^2}] +$$

$$+ [y(\underline{k},\ 0) - \frac{\delta_1}{AJ_t} - \frac{\delta_2}{(AJ_t)^2}]\ e^{-AJ_t\, t} \quad . \qquad (3.47)$$

At large time t, the term multiplied by $e^{-AJ_t\, t}$, (transient part of the solution), is relatively small and Equation (3.47) simplifies to

$$y(\underline{k}) \approx \frac{dZ_f - H\, dZ_a - \frac{dZ_\gamma}{\Gamma}}{A} + \frac{dZ_a}{A^2} \quad . \qquad (3.48)$$

Note that if derivative $\partial y / \partial t$ was assumed to be zero in Equation (3.44), the estimated y would be given by

$$y(\underline{k}) \approx \frac{dZ_f - H\, dZ_a - \frac{dZ_\gamma}{\Gamma}}{A} \quad . \qquad (3.49)$$

Comparison to (3.48) shows that the error due to assuming $\partial y / \partial t \approx 0$ is dZ_a/A^2. For $AH \gg 1$ (dry soil) term dZ_a/A^2, in (3.48) is insignificant compared to $H \, dZ_a/A$. For a wet soil however, term dZ_a/A^2 may be important and cannot be ignored. Chapter 4 uses a similar but more general procedure for evaluating the solution of Equation (3.37) in the case of a stratified soil. It is shown there that the assumption $\partial y / \partial t \approx 0$ is valid for large H (i.e., relatively dry soils).

In the following developments it is assumed that (3.37) has been solved, (analytically or numerically), and its solution, in the form of (3.41), has been obtained. For simplicity, it is assumed that time t is relatively large and $W(\underline{k}, t)$ in (3.42) is approximately zero. Equation (3.41) then simplifies to:

$$y(\underline{k}) = dZ_h(\underline{k}) = W_f(\underline{k}) \, dZ_f(\underline{k}) + W_a(\underline{k}) \, dZ_a(\underline{k}) + W_\gamma(\underline{k}) \, dZ_\gamma(\underline{k}) \qquad (3.50)$$

where W_f, W_a, W_γ are three-dimensional system response functions, and a time dependence of y, W_f, W_a and W_γ is implied. Equation (3.50) expresses the spectral amplitudes of the capillary tension head fluctuations h as a linear function of the spectral amplitudes of the soil property variations f, a and γ. Section 3.2.3 develops a methodology for evaluating the effective model parameters, defined in Section 3.2.1, using the spectral Equation (3.50) and some properties of spectral representation.

3.2.3 Evaluation of Effective Parameters Using Spectral Representations

This section uses the linearized wave-number domain equation developed in Section 3.3.2 and some spectral representation properties, in order to evaluate the expected values in (3.15) and (3.16). After evaluation of these expected values the effective unsaturated flow parameters $\hat{K}_{ii}$, Θ, $\hat{C}$ are easily assessed from (3.14), (3.16) and (3.17). This section develops the general methodology without restricting it to any particular application. Specific evaluations and applications are given in Chapters 4 and 5.

Some spectral representation properties are now briefly discussed since they are extensively used in this section. Consider two cross-correlated stationary random fields $u(\underline{x})$ and $v(\underline{x})$. If $dZ_u(\underline{k})$, $dZ_v(\underline{k})$ the corresponding random Fourier-Steltjes amplitudes of $u(\underline{x})$ and $v(\underline{x})$, the following property holds: (Lumley and Panofsky, 1964)

$$E[dZ_u(\underline{k}_1) \, dZ_v^*(\underline{k}_2)] = \begin{cases} S_{uv}(\underline{k}) \, d\underline{k} \; ; \; \text{if} \; \underline{k}_1 = \underline{k}_2 = \underline{k} \\ 0 \quad ; \; \text{otherwise} \end{cases} \tag{3.51}$$

where $S_{uv}(\underline{k})$ is the cross-spectral density function of u and v. The expected value of $E[u(\underline{x}) \, v(\underline{x})]$ can be evaluated as follows:

$$E[uv] = E[\iiint_{-\infty}^{\infty} e^{j\underline{k}\cdot\underline{x}} \, dZ_u(\underline{k}) \iiint_{-\infty}^{\infty} e^{-j\underline{k}\cdot\underline{x}} \, dZ_v^*(\underline{k})] =$$

$$= \iiint_{-\infty}^{\infty} S_{uv}(\underline{k}) \, d\underline{k} \qquad . \tag{3.52}$$

Evaluation of the effective parameters $\hat{K}_{ii}$, Θ and $\hat{C}$ requires evaluation of the expected values: $E[h^2]$, $E[fh]$, $E[ah]$, $E[f \, \partial h/\partial x_i]$,

55

$E[a\ \partial h/\partial x_i]$ and $E[\gamma h]$ using the general linearized Equation (3.50), relating dZ_h to dZ_f, dZ_a, dZ_γ, and the spectral representation properties (3.51), (3.52). If the cross-spectral density functions of soil property fluctuations are known, these evaluations reduce to computation of several quite complicated three-dimensional integrals. Analytical evaluation of the resulting integrals is not possible in general. In certain cases however, (see e.g., Chapter 4), it is possible to analytically evaluate these integrals and derive closed form expressions for the effective parameters.

$\underline{E[h^2]}$

The variance of h, σ_h^2, is given by (3.52) as

$$E[h^2] = \sigma_h^2 = \iiint\limits_{-\infty}^{\infty} S_{hh}(\underline{k})\ d\underline{k} \qquad . \qquad (3.53)$$

Using (3.50) and (3.51) the spectral density function S_{hh} is given by

$$S_{hh}(\underline{k}) = \frac{1}{d\underline{k}} E[(W_f\ dZ_f + W_a\ dZ_a + W_\gamma\ dZ_\gamma)(W_f\ dZ_f + W_a\ dZ_a + W_\gamma\ dZ_\gamma)^*] =$$

$$= |W_f|^2\ S_{ff} + |W_a|^2\ S_{aa} + |W_\gamma|^2\ S_{\gamma\gamma} +$$

$$+ W_f\ W_a^*\ S_{fa} + W_f\ W_\gamma^*\ S_{f\gamma} + W_a\ W_f^*\ S_{af} +$$

$$+ W_a\ W_\gamma^*\ S_{a\gamma} + W_\gamma\ W_f^*\ S_{\gamma f} + W_\gamma\ W_a^*\ S_{\gamma a} \qquad (3.54)$$

where it is assumed that the cross-spectral density functions of the soil property random fields f, a and γ are known.

The variance σ_h^2 can then be evaluated from the three-dimensional integral (3.53).

E[fh]

Term E[fh] is given by

$$E[fh] = E[hf] = \iiint\limits_{-\infty}^{\infty} S_{hf}(\underline{k}) \, d\underline{k} \tag{3.55}$$

where S_{hf} is given by

$$
\begin{aligned}
S_{hf} &= \frac{1}{d\underline{k}} \, E\left[(W_f \, dZ_f + W_a \, dZ_a + W_\gamma dZ_\gamma) \, dZ_f^* \right] \\
&= W_f \, S_{ff} + W_a \, S_{af} + W_\gamma \, S_{\gamma f} \qquad .
\end{aligned} \tag{3.56}
$$

Evaluation of $E[fh]$ has been reduced to evaluation of the three-dimensional integral (3.55), where it is assumed that the cross-spectral density functions of f, a, and γ are known.

E[ah]

It holds:

$$E[ah] = E[ha] = \iiint\limits_{-\infty}^{\infty} S_{ha}(\underline{k}) \, d\underline{k} \tag{3.57}$$

where S_{ha} is given by

$$
\begin{aligned}
S_{ha} &= \frac{1}{d\underline{k}} \, E\left[(W_f \, dZ_f + W_a \, dZ_a + W_\gamma \, dZ_\gamma) \, dZ_a^* \right] = \\
&= W_f \, S_{fa} + W_a \, S_{aa} + W_\gamma \, S_{\gamma a} \qquad .
\end{aligned} \tag{3.58}
$$

$$\underline{E[f \frac{\partial h}{\partial x_i}]}$$

It holds:

$$\frac{\partial h}{\partial x_i} = \frac{\partial}{\partial x_i} [\iiint_{-\infty}^{\infty} e^{j\underline{k}\underline{x}} dZ_h(\underline{k})] = \iiint_{-\infty}^{\infty} e^{j\underline{k}\underline{x}} (jk_i) dZ_h(\underline{k}) \qquad (3.59)$$

and $E[f \, \partial h / \partial x_i]$ can be evaluated by

$$E[f \frac{\partial h}{\partial x_i}] = E[\frac{\partial h}{\partial x_i} f] = \iiint_{-\infty}^{\infty} (jk_i) S_{hf}(\underline{k}) d\underline{k} \qquad (3.60)$$

where S_{hf} is given by (3.56).

$$\underline{E[a \frac{\partial h}{\partial x_i}]}$$

Similarly as above it holds:

$$E[a \frac{\partial h}{\partial x_i}] = \iiint_{-\infty}^{\infty} (jk_i) S_{ha}(\underline{k}) d\underline{k} \qquad (3.61)$$

where S_{ha} is given by (3.58).

$$\underline{E[\gamma h]}$$

Term $E[\gamma h]$ is given by

$$E[\gamma h] = \iiint_{-\infty}^{\infty} S_{h\gamma}(\underline{k}) d\underline{k} \qquad (3.62)$$

where

$$S_{h\gamma} = \frac{1}{dk} E[W_f \, dZ_f + W_a \, dZ_a + W_\gamma \, dZ_\gamma) \, dZ_\gamma^*]$$

$$= W_f \, S_{f\gamma} + W_a \, S_{a\gamma} + W_\gamma \, S_{\gamma\gamma} \qquad . \qquad (3.63)$$

The effective properties $\hat{K}_{ii}$, Θ and $\hat{C}$ can now be evaluated using (3.14), (3.15), (3.16) and (3.17). Note that W_f, W_a, W_γ depend on the mean soil properties F, A and Γ and the mean flow characteristics J_1, J_2, J_3 and $J_t = \partial H/\partial t$. Evaluation of the effective parameters requires knowledge of the mean soil properties F, A, Γ and the cross-spectral density functions of f, a and γ. The dependence of the effective parameters on the mean flow characteristics suggests a nonlinear large-scale flow model. In addition, it is expected that the effective flow parameters $\hat{K}_{ii}$, Θ and $\hat{C}$ will show hysteresis. This is because these parameters depend on the time history of the capillary tension head through the time derivative $J_t = \partial H/\partial t$.

59

3.3 Steady Solute Transport

This section develops a general stochastic method for derivation of
large-scale unsaturated solute transport models. Similarly to the
unsaturated flow case, the method follows three basic steps. In the first
step (Section 3.3.1), the form of the large-scale transport model and its
effective parameters (macrodispersion coefficients) are derived by
averaging the local governing transport equation over the ensemble of
soil property realizations. Evaluation of the effective transport
parameters requires evaluations of the cross-correlations between
concentration and specific discharge fluctuations. The second step of
the stochastic methodology (Section 3.3.2) derives simplified linearized
equations, relating concentration fluctuations to specific discharge
fluctuations and the specific discharge fluctuations to soil property
fluctuations. The last step of the analysis (Section 3.3.3) uses the
linearized equations derived in the second step and some spectral
representation properties for the evaluation of the large-scale transport
models and the effective macrodispersion coefficients defined in Section
3.3.1.

3.3.1 Derivation of Large-Scale Models and Macrodispersion Coefficients

This section derives the form of the large-scale transport model by
averaging the local governing transport equation over the ensemble of
soil property realizations. The analysis of this section closely follows
the analysis of Gelhar and Axness (1983) which was developed for the
saturated flow case. The general equation describing transport of an
ideal nonreactive conservative solute by unsaturated flow is given by:

$$\frac{\partial(\theta c)}{\partial t} = \frac{\partial}{\partial x_i} \left[E_{ij} \frac{\partial c}{\partial x_j} - cq_i \right] \qquad i, j = 1, 2, 3 \qquad (3.64)$$

where it is assumed that soil moisture is homogeneous (constant density and viscosity) and

c : concentration of transported solute

θ : soil moisture content

E_{ij}: local bulk dispersion coefficient, equal to θD_{ij}

D_{ij}: dispersion coefficient tensor (including hydrodynamic dispersion and molecular diffusion).

Assuming steady state, Equation (3.64) simplifies to

$$\frac{\partial(cq_i)}{\partial x_i} = \frac{\partial}{\partial x_i} \left[E_{ij} \frac{\partial c}{\partial x_j} \right] \qquad . \qquad (3.65)$$

It is assumed that the local coefficient of bulk dispersion E_{ij} is constant. As will be seen in Chapter 5, in several cases of interest the results are not very sensitive to parameter E_{ij}.

Consider the concentration c as the output of (3.65). Due to spatial variability of parameters f and a the local specific discharge q_i is spatially variable resulting in a spatially variable concentration c. Similarly to Section 3.2.1, it is assumed that parameters f and a are realizations of three-dimensional stationary random fields. The local specific discharge q_i and the concentration c are considered to be realizations of stationary random fields as well.

Let:

$$q_i = \bar{q}_i + q_i' \qquad i = 1, 2, 3$$
$$\bar{c} = \bar{c} + c' \qquad (3.66)$$

61

where $\bar{q}_i$, $\bar{c}$ are the mean of q_i, c and q_i', c' the corresponding fluctuations around the mean.

The large-scale model of steady solute transport in unsaturated soils is derived by averaging the local governing Equation (3.65) over the ensemble of realizations of the random fields f and a. Taking the expected value of (3.65) with respect to f and a, yields

$$\frac{\partial\{E[cq_i]\}}{\partial x_i} = \frac{\partial}{\partial x_i}\left\{E_{ij}\frac{\partial E[c]}{\partial x_j}\right\} \qquad . \qquad (3.67)$$

The expected value in the right hand side of (3.67) represents the mean $\bar{c}$. Substituting (3.66), the expected value in the left hand side of (3.67) is written as

$$E[cq_i] = \bar{c}\,\bar{q}_i + E[c'q_i'] \qquad . \qquad (3.68)$$

Term $\bar{c}\,\bar{q}_i$ represents the convective flux associated with the mean flow while term $E[c'q_i']$ is a macroscopic dispersive flux due to the spatial variation of q_i.

Assuming that the macroscopic dispersive flux can be expressed in a Fickian form, we may write

$$E[q_i'\,c'] = -\hat{E}_{ij}\frac{\partial\bar{c}}{\partial x_j} \qquad (3.69)$$

where E_{ij} is an effective bulk macrodispersion coefficient tensor. Define a macrodispersivity tensor

$$A_{ij} = \frac{\hat{E}_{ij}}{q} \qquad (3.70)$$

where generally A_{ij} may depend on q. Equation (3.67) may then be

62

written as

$$\frac{\partial(\bar{c}\,\bar{q}_i)}{\partial x_i} = \frac{\partial}{\partial x_i}\left[(E_{ij} + \hat{A}_{ij}\,q)\frac{\partial \bar{c}}{\partial x_j}\right] \quad . \qquad (3.71)$$

This is the large-scale transport equation and it is of a similar form as the local transport Equation (3.65). Note that the total large-scale dispersion coefficient is: $E_{ij} + A_{ij}\,q$, where the bulk macrodispersion coefficient $\hat{E}_{ij} = A_{ij}\,q$ accounts for the additional dispersion due to the spatial variability of q_i.

Evaluation of the macrodispersivity A_{ij} and the bulk macrodispersion coefficient $\hat{E}_{ij}$ requires evaluation of the expected value $E[q_i'\,c']$ in (3.69). Section 3.3.2 derives linearized expressions relating q_i' and c' to f and a. These expressions are used in Section 3.3.3 for the evaluation of the expected value of (3.69) and the corresponding $\hat{E}_{ij}$ and A_{ij}. Note that the analysis in Section 3.3.3 will establish directly that the Fickian form assumed above, (3.69), is correct.

3.3.2 Linearized Fluctuation Equations

This section derives linearized equations relating the specific discharge and the concentration fluctuations to soil property fluctuations. First, a linearized perturbation equation, relating c' to q_i' is derived using the local governing equation of steady transport (3.65). Following Gelhar and Axness, (1983), substituting (3.66) into (3.65) and expanding products, yields.

$$\frac{\partial}{\partial x_i}\left[\bar{q}_i\,\bar{c} + \bar{q}_i\,c' + q_i'\,\bar{c} + q_i'\,c'\right] = E_{ij}\frac{\partial^2(\bar{c} + c')}{\partial x_i\,\partial x_j} \qquad (3.72)$$

63

where E_{ij} is assumed to be a constant. Taking the expected value of (3.72) produces the mean equation

$$\frac{\partial}{\partial x_i} \{\bar{q} \ \bar{c} + E[q_i' \ c']\} = E_{ij} \frac{\partial^2 \bar{c}}{\partial x_i \ \partial x_j} \qquad . \qquad (3.73)$$

Subtracting the mean Equation (3.73) from the local Equation (3.72) produces

$$\frac{\partial}{\partial x_i} \{\bar{q}_i \ c' + q_i' \ \bar{c} + q_i' \ c' - E[q_i' \ c']\} = E_{ij} \frac{\partial^2 \bar{c}}{\partial x_i \ \partial x_j} \qquad . \qquad (3.74)$$

Assuming that q_i' and c' are small, the second order term $q_i'c' - E[q_i'c']$ may be neglected. The first order approximation describing the concentration fluctuations c' in terms of specific discharge fluctuations q_i' is then

$$\frac{\partial}{\partial x_i} (q_i' \ \bar{c} + \bar{q}_i \ c') = E_{ij} \frac{\partial^2 c'}{\partial x_i \ \partial x_j} \qquad . \qquad (3.75)$$

It is assumed for convenience that the coordinate axis x_1 is aligned in the direction of the mean fluid flow so that $q_1 = q$ and $q_2 = q_3 = 0$, (see Figure 3.1). Note that this orientation of axes is different than the one in the flow case; the system of axes x_1, x_2, x_3 is now not aligned in the principal statistical anisotropy directions. The local dispersion tensor may than be approximated in the form, (Naff 1978)

$$[E_{ij}] = \begin{bmatrix} \alpha_L q & 0 & 0 \\ 0 & \alpha_T q & 0 \\ 0 & 0 & \alpha_T q \end{bmatrix} \qquad (3.76)$$

where α_L and α_T are the local longitudinal and transverse dispersivities. Expanding the left term of (3.75) and utilizing (3.76),

64
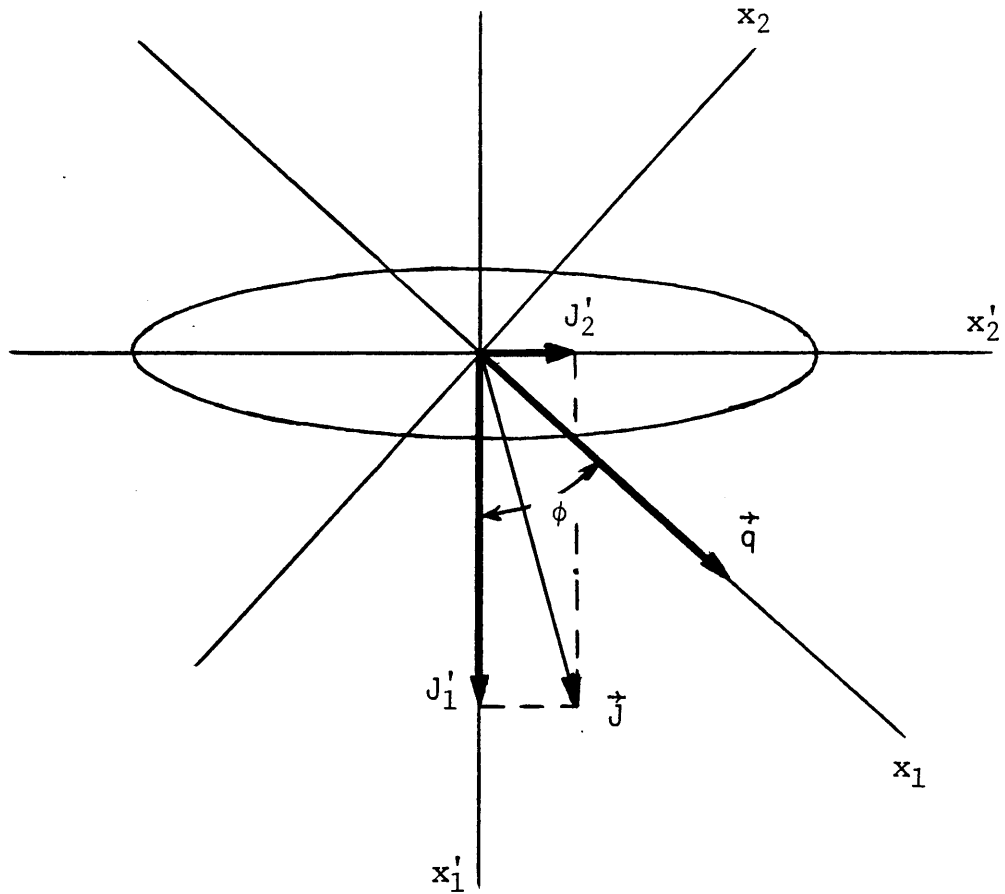
Figure 3.1 Coordinate system x_1', x_2', x_3' corresponds to the
principal anisotropy axes of f, a, γ. The ellipse
represents an equal covariance level. Axis x_1 of
coordinate system x_1, x_2, x_3 is oriented in the
direction of the mean specific discharge $\vec{q}$. Note that
the direction of the mean specific discharge is different
than the direction of the mean head gradient $\vec{J}$

65

(3.75) reduces to:

$$q_i' \frac{\partial \bar{c}}{\partial x_i} + q \frac{\partial c'}{\partial x_i} = q \left[\alpha_L \frac{\partial^2 c'}{\partial x_1^2} + \alpha_T \left(\frac{\partial^2 c'}{\partial x_2^2} + \frac{\partial^2 c'}{\partial x_3^2} \right) \right] \qquad (3.77)$$

where the conservation of mass equation $\partial q_i/\partial x_i = 0$ has been used.
Equation (3.77) is an approximate linearized partial differential
equation relating concentration fluctuations c' produced as a result of
specific discharge fluctuations q_i'. The mean specific discharge q is
a parameter to this equation.

Assuming that q_i' and c' are realizations of three-dimensional
stationary random fields, it is possible to express q_i', c' in the wave
number domain as follows:

$$q_i' = \int\!\!\int\!\!\int_{-\infty}^{\infty} e^{j\underline{k}\underline{x}} \, dZ_{q_i}(\underline{k})$$

$$c' = \int\!\!\int\!\!\int_{-\infty}^{\infty} e^{j\underline{k}\underline{x}} \, dZ_c(\underline{k}) \qquad (3.78)$$

Substituting into (3.77) and recalling the uniqueness of the spectral
representation gives

$$dZ_c = - \frac{\frac{\partial \bar{c}}{\partial x_j} \, dZ_{q_j}}{q \left[jk_1 + \alpha_L k_1^2 + \alpha_T (k_2^2 + k_3^2) \right]} \qquad (3.79)$$

where index j corresponds to repeated summation.

Next, a linearized equation relating q_i' to f and a is derived.
The specific discharge is given by

66

$$q_i = K(\psi) \frac{\partial(\psi + z)}{\partial x_i} = K(\psi) \left[J_i + \frac{\partial h}{\partial x_i} \right] \qquad (3.80)$$

where from (3.7)

$$K(\psi) = K_m e^{f - Ah - Ha - ha} \qquad (3.81)$$

with K_m given by (3.8). Expanding the exponential and assuming products of fluctuations are small, (3.81) gives

$$K(\psi) \approx K_m (1 + f - Ah - Ha) \qquad . \qquad (3.82)$$

Using (3.82), (3.80) gives

$$q_i = K_m \left(J_i + J_i f - J_i A h - J_i H a + \frac{\partial h}{\partial x_i} + f \frac{\partial h}{\partial x_i} - Ah \frac{\partial h}{\partial x_i} - Ha \frac{\partial h}{\partial x_i} \right) . \qquad (3.83)$$

Taking the expected value of (3.83), subtracting the mean equation from (3.83), and assuming products of fluctuations are equal to their mean values, yields the following linearized equation

$$q_i' = q_i - E[q_i] = K_m \left[\left(\frac{\partial h}{\partial x_i} - J_i A h \right) + J_i (f - Ha) \right] . \qquad (3.84)$$

Equation (3.84) relates the specific discharge fluctuations to the capillary tension head and soil property fluctuations. Using spectral representations, (3.84) yields

$$dZ_{q_i} = K_m \left[(jk_i - A J_i) dZ_h + J_i (dZ_f - H dZ_a) \right] . \qquad (3.85)$$

The Fourier-Stieltjes amplitudes dZ_h are related to dZ_f and dZ_a by (3.37). In the steady state case $\partial H / \partial t$ and G are zero and (3.37) simplifies to

$$dZ_h = \frac{j(dZ_f - H dZ_a) J_j k_j - \left(J_j \frac{\partial H}{\partial x_j} \right) dZ_a}{k^2 + jAL_i k_i} \qquad . \qquad (3.86)$$

67

Substituting (3.86) into (3.85) gives:

$$dZ_{q_i} = W_i \, dZ_f + V_i \, dZ_a \qquad (3.87)$$

where

$$W_i = K_m \frac{J_j (\delta_{ij} k^2 - k_i k_j) + jAJ_i (L_j - J_j) k_j}{k^2 + jAL_j k_j} \qquad (3.88)$$

$$V_i = K_m$$

$$\frac{-HJ_j (\delta_{ij} k^2 - k_i k_j) - jAHJ_i (L_j - J_j) k_j - (j k_i - AJ_j) (J_j \frac{\partial H}{\partial x_j})}{k^2 + jAL_j k_j} \cdot \qquad (3.89)$$

Equations (3.79) and (3.87) relate fluctuations c' and q_i' to soil property fluctuations f and a. These equations are used in Section 3.3.3 for evaluation of $E[c'q_i]$ and the corresponding A_{ij}.

3.3.3 Evaluation of Effective Macrodispersion Coefficients Using Spectral Representations

A methodology for evaluation of $E[c'q_i']$ and the macrodispersivities A_{ij} is developed in this section. The methodology utilizes the steady-state linearized equations derived in Section 3.3.2. Using the spectral representation theorem, term $E[c'q_i']$ is given by

$$E[c'q_i'] = \int\!\!\!\int\!\!\!\int_{-\infty}^{\infty} S_{cq_i}(\underline{k}) \, d\underline{k} = - A_{ij} \, q \, \frac{\partial \bar{c}}{\partial x_j} \qquad (3.90)$$

where from (3.79) and $S_{cq_i} = E[dZ_c \, dZ_{q_i}{}^*]$

68

$$S_{cq_i}(\underline{k}) = -\frac{S_{q_j q_i} \frac{\partial \bar{c}}{\partial x_j}}{q \left[jk_1 + \alpha_L k_1^2 + \alpha_T (k_2^2 + k_3^2) \right]} \quad . \quad (3.91)$$

From (3.91) in (3.90) it is evident that the macrodispersive flux is Fickian, i.e. proportional to the mean concentration gradient; the resulting macrodispersivity is then

$$A_{ij} = \frac{1}{q^2} \iiint\limits_{-\infty}^{\infty} \frac{S_{q_j q_i}(\underline{k}) \, d\underline{k}}{\left[j k_1 + \alpha_L k_1^2 + \alpha_T (k_2^2 + k_3^2) \right]}$$

$$= \frac{1}{q^2} \iiint\limits_{-\infty}^{\infty} \frac{S_{q_j q_i}(\underline{k}) \left[-j k_1 + \alpha_L k_1^2 + \alpha_T (k_2^2 + k_3^2) \right]}{k_1^2 + \left[\alpha_L k_1^2 + \alpha_T (k_2^2 + k_3^2) \right]^2} \, d\underline{k} \quad (3.92)$$

Note that (3.92) is identical to the result for the saturated flow case (Gelhar and Axness, 1983, Eq. 28'). However, the mean specific discharge and the spectrum of the specific discharge fluctuations is different in the unsaturated flow case as discussed below.

Using (3.87) and (3.51) the cross-spectral density function $S_{q_j q_i}$ is given by:

$$S_{q_j q_i} = \frac{1}{d\underline{k}} E\left[(W_j \, dZ_f + V_j \, dZ_a)(W_i \, dZ_f + V_i \, dZ_a)^* \right]$$

$$= W_j W_i^* S_{ff} + V_j V_i^* S_{aa} +$$

$$+ W_j V_i^* S_{fa} + V_j W_i^* S_{af} \quad . \quad (3.93)$$

Note that the spectral density function in (3.93) should be expressed in coordinate system k_1, k_2, k_3, (see Figure 3.1), which is generally different than system k_1', k_2', k_3' aligned in the direction of

the principal anisotropy axes. Let $S(k_1', k_2', k_3')$ be the expressions for the spectral density functions in (3.93) in the system of principal anisotropy axes k_1', k_2', k_3'. The corresponding spectral density function in an arbitrary system of axes k_1, k_2, k_3 is given by $S(a_{1j} k_j, a_{2j} k_j, a_{3j} k_j)$, where a_{ij} are the directional cosines $a_{ij} = \cos(x_i', x_j)$ and $k_i' = a_{ij} k_j$, (see, Gelhar and Axness, 1983).

The mean flow model (3.18) is capable of predicting the mean capillary tension head H and its spatial derivatives J_1', J_2', J_3' in the principal anisotropy directions x_1', x_2', x_3', (see Figure 3.1). In order to be able to evaluate A_{ij} from (3.92) and use the large-scale dispersion model (3.71), the mean specific discharge $\vec{q}$, the directional cosines a_{ij}, and the components of the gradient $\vec{J}$ on the x_1, x_2, x_3 axes, must be evaluated as a function of H and J_1', J_2', J_3'. Note that in the general anisotropic case the direction of the mean specific discharge $E[\vec{q}] = (\bar{q}_1, \bar{q}_2, \bar{q}_3)$ is in general different than the direction of the mean gradient $\vec{J} = (J_1', J_2', J_3')$, (see Figure 3.1). It is thus necessary to evaluate both the magnitude and direction of $\vec{q}$ for a given set of H, J_1', J_2', J_3' values. Assume for simplicity that $\lambda_2 = \lambda_3$ and, without loss of generality, that $J_3 = 0$. The mean specific discharge q_3 in the principal anisotropy direction x_3' then is zero. The specific discharge q_i in the directions x_1' and x_2' is given by (3.13) where $\hat{K}_{ij}$ are given by (3.14) and (3.15). The magnitude of $E[\vec{q}]$ is then given by

$$q = \sqrt{(\hat{K}_{11}J_1')^2 + (\hat{K}_{22}J_2')^2} \qquad (3.94)$$

and the direction of $E[\vec{q}]$ is given by

$$\phi = \text{arctg} \left(\frac{\hat{K}_{22}J_2'}{\hat{K}_{11}J_1'} \right) \qquad (3.95)$$

where ϕ defines the direction of the axes x_1, x_2, x_3 with respect

to axes x_1', x_2', x_3', (see Figure 3.1). The directional cosines

a_{ij}, $(k_i' = a_{ij} k_j)$, are then given by

$$[a_{ij}] = \begin{vmatrix} \cos\phi & -\sin\phi & 0 \\ \sin\phi & \cos\phi & 0 \\ 0 & 0 & 1 \end{vmatrix} \qquad . \qquad (3.96)$$

The effective hydraulic conductivities $\hat{K}_{11}$, $\hat{K}_{22}$ can be evaluated as a

special case of the general theory developed in Section 3.2 for $\partial H/\partial t =$

0. The components of the gradient $\vec{J}$ on axes x_1, x_2, x_3 are

evaluated from (3.93), (3.94), (3.95), and (3.96). Assuming that the

cross-spectral density functions of the soil property fluctuations f and

a are known, the macrodispersivities A_{ij} can be evaluated from (3.92).

Note that the integral in (3.92) is of a very complicated form which in

general, will require numerical evaluation. In certain cases,(see

Chapter 5), it is possible to analytically evaluate this integral and

derive relatively simple closed form expressions for the

macrodispersivities A_{ij}.

3.4 Summary and Discussion

This chapter developed a general methodology for derivation of large-scale models of transient unsaturated flow and steady contaminant transport, and evaluation of the effective model parameters. Section 3.2 examined the transient unsaturated flow problem while Section 3.3 examined the steady transport problem. A stochastic methodology that accounts for the local soil property variability and the basic nonlinearities of the local governing equations was developed. It was assumed that the local soil properties are realizations of three-dimensional stationary random fields with known means and cross-spectral density functions. The stochastic approach followed three steps. In the first step, (Sections, 3.2.1, 3.3.1), the form of the large-scale models and the effective model parameters were derived. The second step, (Section 3.2.2, 3.3.2), related the output fluctuations h, q_i' and c' to the soil property fluctuations f, a and γ, through three-dimensional, linearized, partial differential equations. The third step, (Section 3.2.3, 3.3.3), evaluated the effective parameters, defined in the first step, using the linearized equations derived in the second step and some spectral representation properties.

The large-scale models derived in this chapter are expressed in a partial differential equation form and are capable of predicting the large-scale flow and transport characteristics (mean behavior) rather than local details. The effective parameters of the large-scale models do not depend on the actual realization of the local soil properties but they rather depend on a few parameters describing the statistics of local variability, (e.g. mean, variances, correlation scales, etc.). As it is

72

discussed in Chapter 6, these parameters can be estimated from a finite data set and/or prior information about soil property variability. Note that since the large-scale model predicts large-scale characteristics of flow and transport, rather than local details, a prediction error (model error) is introduced. The stochastic methodology is capable of evaluating the statistical properties of this error which provides a measure of reliability of model predictions. The effective parameters also depend on the mean flow parameters H, J_1, J_2, J_3 and J_t.

The purpose of this chapter was to present the general methodology without focusing on specific evaluations and applications. Thus the conclusions are of qualitative rather than quantitative nature. It was found, that in the unsaturated flow case, a unique effective hydraulic conductivity tensor does not generally exist and that the effective parameters $\hat{K}_{ij}$, Θ, and $\hat{C}$ depend on the mean flow parameters H, J_1, J_2, J_3 and $\partial H/\partial t$. The dependence of the effective parameters on the model output suggests a nonlinear mean flow model, while the dependence on the time history of H (through $\partial H/\partial t$) suggests a hysteresis of the effective parameters. The effective macrodispersivities A_{ij} depend on the mean capillary tension head H and on the specific discharge q. These effects are due to local spatial variability and the parametric nonlinearity of the local governing equations. Note that these effects are not predicted by traditional models since these models do not realistically consider the spatial variability of the local soil properties, the three-dimensionality of the flow and transport processes and the parametric nonlinearity of the local governing flow and transport equations.

Application of the general methodology developed in this chapter generally requires numerical evaluations. In some cases of practical interest however, analytical evaluations are possible. Analytical results are highly attractive because of their simplicity, flexibility and the insight they provide. Chapters 4 and 5 derive analytical generic expressions for the effective parameters in such cases. Chapter 4 examines unsteady flow in stratified formations, while Chapter 5 examines steady transport in statistically isotropic or stratified formations.

CHAPTER 4

TRANSIENT UNSATURATED FLOW IN STRATIFIED SOILS

4.1 Introduction

In order to evaluate the effective flow parameters using the general stochastic theory developed in Chapter 3, several three-dimensional integrals must be evaluated. These integrals are quite complex and are not generally analytically tractable. Natural soil formations are often stratified. The hydraulic soil properties of stratified soil formations may be visualized as realizations of three-dimensional, statistically anisotropic random fields with correlation lengths in directions parallel to stratification being significantly larger than the correlation length in the direction perpendicular to stratification. This chapter examines the case of transient unsaturated flow in such stratified soil formations. The stratified soil assumption allows analytical evaluation of the three-dimensional integrals of Section 3.2.3 and allows derivation of relatively simple generic expressions for the effective large-scale model parameters and the variance of model errors. These expressions are useful since they explicitly indicate the dependence of the effective parameters on the various soil property and flow characteristics.

The outline of this chapter is as follows. Section 4.2 derives a simplified expression relating the capillary tension head fluctuations to the soil property fluctuations using the disparity of the correlation scales in a stratified soil. Sections 4.3, 4.4 and 4.5 derive closed form expressions for the effective parameters and the variance of the model errors. Simple asymptotic expressions which are valid in particu-

lar ranges of the soil property and the mean flow characteristics, are also derived. In addition, several examples investigating the dependence of the variance of the model errors and the effective large-scale model parameters on the mean flow properties are given for the cases of a Panoche clay loam and a Maddock sandy loam soil.

The most important findings of Sections 4.3, 4.4 and 4.5 are:

(i) The effective hydraulic conductivities, the mean soil moisture content and the effective specific moisture capacity show significant hysteresis.

(ii) The effective hydraulic conductivity is anisotropic with a degree of anisotropy depending on the mean flow conditions (wetting, drying).

These effects are due to the spatial variability of the local soil properties and they are not due to local hysteresis and anisotropy.

Section 4.6 shows that the quasi-steady assumptions introduced in Section 4.2 are valid if the soil matrix remains relativey dry. If the soil is wet and the water addition is rapid, unsaturated flow may not be governed by diffusion type laws. Section 4.7 gives a physical interpretation of the large-scale hysteresis and anisotropy, compares the results of the stochastic theory to a series of field observations, and discusses the implications of these results on waste disposal applications.

4.2 Stratified Soil Simplifications

This section derives a simplified spectral equation relating the capillary tension head fluctuations to the soil property fluctuations using the disparity of the correlation scales in a stratified soil.

The general linearized spectral Equation (3.37) is simplified as follows. The solution of (3.37) is given by (3.38) where functions $g_1(t)$, $g(t)$ depend on $\underline{k}$ and are given by (3.39). Using the transformation $u_1 = \lambda_1 k_1$, $u_2 = \lambda_2 k_2$, $u_3 = \lambda_3 u_3$, where λ_1, λ_2, λ_3 the correlation lengths with λ_2, $\lambda_3 \gg \lambda_1$, Equations (3.39) are written as:

$$g_1(t) = \frac{K_m}{\Gamma} \left[\frac{1}{\lambda_1^2} (u_1^2 + \delta_2^2 u_2^2 + \delta_3^2 u_3^2) + A\Gamma G + \right.$$
$$\left. + \frac{jA}{\lambda_1} (L_1 u_1 + \delta_2 L_2 u_2 + \delta_3 L_3 u_3) \right] \tag{4.1}$$

$$g(t) = \frac{K_m}{\Gamma} \left\{ \left[\frac{j}{\lambda_1} (J_1 u_1 + \delta_2 J_2 u_2 + \delta_3 J_3 u_3) + \Gamma G \right] dZ_f \right.$$
$$- \left[\frac{jH}{\lambda_1} (J_1 u_1 + \delta_2 \cdot J_2 u_2 + \delta_3 J_3 u_3 + J_i \frac{\partial H}{\partial x_i} + H\Gamma G) \right] dZ_a -$$
$$- G \, dZ_\gamma \tag{4.2}$$

where $\delta_2 = \lambda_1/\lambda_2$, $\delta_3 = \lambda_1/\lambda_3$. For a stratified soil with stratification parallel to x_2, x_3, δ_2, $\delta_3 \approx 0$. Functions g_1 and g are well behaved functions of u_1, u_2, u_3. Taking the limit of (3.38) for δ_2, $\delta_3 \rightarrow 0$, gives

$$y(\underline{k}, t) = \left[y(\underline{k}, o) + \int_o^\tau g'(\tau) e^{\int_o^t g_1'(x)\, dx}\, d\tau\right] e^{-\int_o^\tau g_1'(\tau)\, d\tau} \quad (4.3)$$

where g_1', g_1' are the limit expressions of $g(t)$, $g_1(t)$ for δ_2, $\delta_3 \to 0$, i.e.,

$$g_1'(t) = \lim_{\delta_2, \delta_3 \to o} [g_1(t)] = \frac{K_m}{\Gamma}[k_1^2 + A\Gamma G + jAk_1] \quad (4.4)$$

$$g'(t) = \lim_{\delta_2, \delta_3 \to o} [g(t)] = \frac{K_m}{\Gamma}[(jJ_1 k_1 + \Gamma G)dZ_f -$$

$$- (jH J_1 k_1 + J_i \frac{\partial H}{\partial x_i} + H\Gamma G)\, dZ_a - G\, dZ_\gamma] \quad . \quad (4.5)$$

Substituting (4.4) and (4.5) into (4.3), it is easy to see that (4.3) is the solution of the following ordinary differential equation.

$$\frac{\partial y}{\partial t} + \frac{K_m}{\Gamma}(k_1^2 + A\Gamma G + jAL_1 k_1)\, y =$$

$$\frac{K_m}{\Gamma}[(jJ_1 k_1 + \Gamma G)\, dZ_f - (jH J_1 k_1 + b)dZ_a - G\, dZ_\gamma] \quad (4.6)$$

where $b = J_i\, \partial H/\partial x_i + H\Gamma G$. Let

$$g'(t) = g_f'(t)\, dZ_f + g_a'(t)\, dZ_a + g_\gamma'\, dZ_\gamma \quad (4.7)$$

where g_f', g_a', g_γ' are functions of k_1 and they are independent of k_2, k_3 and are given by comparison of (4.7) to (4.5). Assuming that time t is relatively large and the effect of the initial conditions

78

$y(\underline{k}, 0)$ in (4.3) is relatively small, Equation (4.3) can be written as

$$y(\underline{k}) = dZ_h(\underline{k}) = W_f'(k_1)\ dZ_f(\underline{k}) + W_a'(k_1)\ dZ_a(\underline{k}) + W_\gamma'(k_1)\ dZ_\gamma(\underline{k}) \qquad (4.8)$$

where a time dependence of $\underline{y}(\underline{k})$, $dZ_h(\underline{k})$, W_f', W_a', W_γ' is implied and W_f', W_a', W_γ' are given by

$$W'_{f,a,\gamma}(k_1, t) = \left[\int_0^t g'_{f,a,\gamma}\ e^{\int_0^\tau g_1'(x)dx}\ d\tau\right] e^{-\int_0^t g_1'(\tau)d\tau} . \qquad (4.9)$$

The conclusion of the above analysis is that in the case of a stratified soil the spectral amplitudes of the capillary tension head fluctuations can be evaluated from Equation (4.6). The solution of (4.6) is in the form of (4.8), where W_f', W_a', W_γ' are functions of k_1 and are independent of k_2, k_3.

As will be seen in Sections 4.3, 4.4 and 4.5, because functions W_f', W_a', W_γ' in Equation (4.8) are independent of k_2 and k_3, the integrals in Section 3.2.3 can be integrated with respect to k_2 and k_3 and are thus reduced to one-dimensional integrals. In order to perform the remaining integrations with respect to k_1, functions W_f', W_a', W_γ' of (4.8) must be determined. Since functions g_1' and $g_{f,a,\gamma}$ of (4.9) are of a complex form, it seems impossible to derive simple and general closed form solutions for W_f', W_a', W_γ'. Since our objective is to obtain analytical results, we must seek an approximate solution to (4.9). To obtain such an approximate solution, assume that $\partial y/\partial t$ in (4.6) is very small compared to the other terms. Equation (4.6) then yields

$$y = dZ_h = \frac{j\, J_1\, k_1 + \Gamma G}{k_1^2 + A\Gamma G + j\, A\, L_1\, k_1}\, dZ_f - \frac{j\, H\, J_1\, k_1 + b}{k_1^2 + A\Gamma G + j\, A\, L_1\, k_1}\, dZ_a -$$

$$- \frac{G}{k_1^2 + A\Gamma G + j\, A\, L_1\, k_1}\, dZ_\gamma \qquad . \qquad (4.10)$$

Sections 4.3, 4.4, and 4.5 evaluate the variance of the capillary tension head and the effective parameters of the large-scale unsaturated flow model using the general theory developed in Chapter 3 and the simplified spectral Equation (4.10).

Note that the assumption of $\partial y/\partial t$ being small introduces some error. The significance of this error is evaluated in Section 4.5. It is found there that in the transient case and at large mean capillary tension head H (relatively dry soils), the assumption $\partial y/\partial t \approx 0$ is justified. For H small however, (relatively wet soils), the assumption $\partial y/\partial t \approx 0$ may not be appropriate. It is discussed in Section 4.5 that flow in such cases is usually rapid and highly unpredictable (particularly in coarser soil layers) and it may not be governed by diffusion type laws. It is possible that the whole idea of using a diffusion type mean flow model (such as Equation 3.18) may not be suitable in such cases. In view of this discussion the results of the next sections should be taken as strictly valid only in the cases when the soil is relatively dry, (i.e. H is large). Note that the case of flow in dry soils is of practical significance in many applications, such as waste disposal in arid environments.

80

4.3 Variance of the Capillary Tension Head Fluctuations

This section evaluates the variance of the capillary tension head fluctuations h in the case of a stratified soil using the general theory developed in Chapter 3, and the simplifications discussed in Section 4.2 Section 4.3.1 evaluates the variance σ_h^2 analytically. The derived expressions however, are of a quite complex form. Section 4.3.2 derives some simplified asymptotic expressions for σ_h^2, valid at particular ranges of the mean flow characteristics. These asymptotic expressions are quite simple and they explicitly indicate the dependence of the variance on the different soil property and flow characteristics. Section 4.3.3 applies the results of the stochastic theory to the Panoche silty clay loam and the Maddock sandy loam soils.

Note that the fluctuations h are defined as the difference between the local capillary tension head ψ and the predictions of the large-scale model H. Thus the variance of h gives an estimate of the reliability of the large-scale model predictions.

4.3.1 Evaluation of the Capillary Tension Head Variance

The variance σ_h^2 is given by (3.53) where $S_{hh}(\underline{k})$ is given by (3.54). In the case of a stratified soil the spectral amplitudes dZ_h are approximately given by (4.8), where the response functions W_f', W_a', W_γ' depend on k_1 and are independent of k_2 and k_3. Replacing W_f, W_a, W_γ in (3.54) by W_f', W_a', W_γ' substituting (3.54) into (3.53) and integrating the resulting equation with respect to k_2 and k_3 gives

$$\sigma_h^2 = \int_{-\infty}^{\infty} S_{hh}'(k_1) \, dk_1 \qquad (4.11)$$

where

$$S'_{hh} = \left|W'_f\right|^2 S'_{ff} + \left|W'_a\right|^2 S'_{aa} + \left|W'_\gamma\right|^2 S'_{\gamma\gamma} +$$

$$+ W'_f W'^*_a S'_{fa} + W'_f W'^*_\gamma S'_{f\gamma} + W_a W'^*_f S'_{af} + \qquad (4.12)$$

$$+ W'_a W'^*_\gamma S'_{a\gamma} + W'_\gamma W'^*_f S'_{\gamma f} + W'_\gamma W'^*_a S'_{\gamma a} \quad .$$

The primed functions S'_{uv} $(u,v = f,a,\gamma)$ in (4.12) are given by

$$S'_{uv}(k_1) = \int\int\limits_{-\infty}^{\infty} S_{uv}(\underline{k})\, dk_2\, dk_3 \qquad (4.13)$$

for u and v following an exponential cross-covariance function, (4.13) simplifies to

$$S'_{uv}(k_1) = \int\int\limits_{-\infty}^{\infty} \frac{\sigma^2_{uv}\, \lambda_1\, \lambda_2\, \lambda_3}{\pi^2\left(1 + \lambda_1^2 k_1^2 + \lambda_2^2 k_2^2 + \lambda_3^2 k_3^2\right)^2}\, dk_2\, dk_3$$

$$= \frac{\sigma^2_{uv}\, \lambda_1}{\pi\left(1 + \lambda_1^2 k_1^2\right)} \qquad . \qquad (4.14)$$

Evaluation of σ^2_h, using Equations (4.11), (4.12) and (4.13), re-quires knowledge of the cross-covariance functions of the soil property fluctuations f, a and γ. Since no sufficient information about the form of these cross-covariances presently exists, it is assumed that f, a and γ follow exponential cross-covariance functions with identical correlation lengths. Two particular cases are investigated: (i) f, a, γ being uncorrelated and (ii) f, a, γ being perfectly correlated. In reality, of course, it is expected that f, a, γ are only partially correlated. The

82

above extreme cases were selected in order to better illustrate the dependence of σ_h^2 on the type of correlation between f, a, γ. Let ζ^2, η^2 be the ratios of the variances of a and γ to the variance of f, i.e.,

$$\zeta^2 = \frac{\sigma_a^2}{\sigma_f^2}$$

$$\eta^2 = \frac{\sigma_\gamma^2}{\sigma_f^2} \qquad .$$

(4.15)

The cross-spectral density functions of f, a, γ are then related to the spectral density function of f by

(i) f, a, γ uncorrelated

$$S_{aa} = \zeta^2 \, S_{ff}$$

$$S_{\gamma\gamma} = \eta^2 \, S_{ff}$$

$$S_{fa} = 0$$

(4.16)

$$S_{a\gamma} = 0$$

$$S_{\gamma a} = 0$$

(ii) f, a, γ perfectly correlated

$$S_{aa} = \zeta^2 \, S_{ff}$$

$$S_{\gamma\gamma} = \eta^2 \, S_{ff}$$

$$S_{fa} = \zeta \, S_{ff}$$

(4.17)

$$S_{a\gamma} = \zeta\eta \, S_{ff}$$

$$S_{\gamma f} = \eta \, S_{ff}$$

83

i.e., in general it holds: $S_{uv}(\underline{k}) = \mu\, S_{ff}(\underline{k})$, where $\mu = \zeta^2$, η^2,

0, ζ, $\zeta\eta$, or η depending on u, v and the type of correlation between f,

a, γ. Substituting into (4.13) and assuming an exponential covariance

for f, (4.13) and (4.14) yield

$$S'_{uv}(k_1) = \mu\, S'_{ff}(k_1) = \mu\, \frac{\sigma_f^2\, \lambda_1}{\pi(1 + \lambda_1^2\, k_1^2)} \qquad (4.18)$$

where μ are given from (4.16) or (4.17).

Using (4.12), (4.16) or (4.17) and (4.18), the variance σ_h^2 may be

evaluated from the one-dimensional integral (4.11). In order to deter-

mine S_{hh}' in (4.12), knowledge of functions W_f', W_a', W_γ' is

required. As it was discussed in Section 4.2, it is impossible to obtain

simple analytical expressions for W_f', W_a', W_γ' in the general

case. In certain cases however, (see Section 4.5), it is possible to

neglect term $\partial y/\partial t$ in (4.6) and obtain relatively simple expressions for

W_f', W_a', W_γ' given by (4.10). It will be seen below that for

these cases it is possible to analytically evaluate the variance.

Substituting the values of W_f', W_a' and W_γ' given by (4.10)

into (4.12) and using (4.16), (4.17) and (4.18), (4.12) yields:

    (i) f, a, γ uncorrelated

$$S'_{hh}(k_1) = \frac{(1 + \zeta\, H^2)\, J_1^2\, k_1^2 + [(\Gamma^2 + \eta^2)\, G^2 + \zeta^2\, b^2}{(k_1^2 + A\Gamma G)^2 + A^2\, L_1^2\, k_1^2}\; \frac{\sigma_f^2\, \lambda_1}{\pi(1 + \lambda_1^2\, k_1^2)} \qquad (4.19)$$

(ii) f, a, γ perfectly correlated

$$S_{hh}'(k_1) = \frac{(1 - \zeta H)^2 \, J_1^2 \, k_1^2 + (\Gamma G - \zeta b - \eta G)^2}{(k_1^2 + A\Gamma G)^2 + A^2 \, L_1^2 \, k_1^2} \; \frac{\sigma_f^2 \, \lambda_1}{\pi(1 + \lambda_1^2 \, k_1^2)} \; . \quad (4.20)$$

Note that (4.19) and (4.20) are of the following general form.

$$S_{hh}'(k_1) = \frac{\sigma_f^2 \, \lambda_1}{\pi} \; \frac{a_1 \, k_1^2 + a_2}{k_1^4 + a_3 \, k_1^2 + a_4} \; \frac{1}{1 + a_5 k_1^2} \quad (4.21)$$

where

$$a_3 = 2A\Gamma G + A^2 \, L_1^2$$

$$a_4 = A^2 \, \Gamma^2 \, G^2 \quad (4.22)$$

$$a_5 = \lambda_1^2$$

and a_1, a_1 are given by

   (i)   f, a, γ uncorrelated

$$a_1 = (1 + \zeta^2 \, H^2) \, J_1^2$$

$$a_2 = (\Gamma^2 + \eta^2) \, G^2 + \zeta^2 \, b^2 \quad (4.23)$$

   (ii)   f, a, γ perfectly correlated

$$a_1 = (1 - \zeta \, H^2) \, J_1^2$$

$$a_2 = (\Gamma G - \zeta b - \eta G) \quad . \quad (4.24)$$

85

Substituting (4.21) into (4.11), the variance σ_h^2 is given by

$$\sigma_h^2 = 2 \frac{\sigma_f^2 \lambda_1}{\pi} I_1 \tag{4.26}$$

where

$$I_1 = \int_0^\infty \frac{a_1 k_1^2 + a_2}{k_1^2 + a_3 k_1^2 + a_4} \frac{1}{1 + a_5 k_1^2} dk_1 \quad . \tag{4.27}$$

Integral I_1 is evaluated in Appendix C for positive or negative values of the determinate $\Delta = a_3^2 - 4a_4 = A^2 L_1^2 + 4A\Gamma G$. Substituting I_1 (4.26) yields, for $\Delta > 0$

$$\sigma_h^2 = \sigma_f^2 \lambda_1 \left[\frac{a_1\sqrt{a_4} + a_1 a_4 a_5 - \sqrt{a_4} a_2 a_5 + a_2 - a_2 a_3 a_5}{(A\Gamma G)\sqrt{4A\Gamma G + A^2 L_1^2} \left(1 + a_4 a_5^2 - a_3 a_5\right)} \right.$$

$$\left. - a_5 \frac{a_1 - a_2 a_5}{\left(1 + a_4 a_5^2 - a_3 a_5\right)\lambda_1} \right] \tag{4.28}$$

while for $\Delta < 0$

$$\sigma_h^2 = \sigma_f^2 \lambda_1 \left[\frac{-a_1 \sqrt{a_4} - a_1 a_4 a_5 + \sqrt{a_4} a_2 a_5 - a_2 + a_2 a_3 a_5}{(A\Gamma G)(A L_1)\left(1 + a_4 a_5^2 - a_3 a_5\right)} \right.$$

$$\left. - a_5 \frac{a_1 - a_2 a_5}{\left(1 + a_4 a_5^2 - a_3 a_5\right)\lambda_1} \right] \tag{4.29}$$

where a_1, a_2 are given by (4.23) or (4.24) and a_3, a_4, a_5 are

86

given by (4.22).

The linearized equations relating h to f, a, γ were derived in Chapter 3 using linearization around the mean soil properties and the mean flow characteristics. In response, this produces functions W_f', W_a', W_γ' which depend on the mean characteristics F, A, Γ, J_1, J_2 J_3, and J_t ($J_t = \partial H/\partial t$). The variance σ_h^2 determined above depends on these characteristics but it also depends on the statistical parameters of local soil property variability i.e., the variances σ_f^2, σ_a^2, σ_γ^2 and the correlation length λ_1 in the direction perpendicular to stratification. We may then write:

$$\sigma_h^2 = \sigma_h^2 \left(F,\ A,\ \Gamma,\ \sigma_f^2,\ \sigma_a^2,\ \sigma_\gamma^2\ ,\ \lambda_1;\ H,\ J_1,\ J_2,\ J_3,\ J_t \right)\ . \qquad (4.30)$$

Section 4.3.3 gives some examples illustrating the dependence of σ_h^2 on several of these parameters.

Note that although the expressions for the variance (4.28), (4.29) are of a closed form, it is difficult, because of the complex form of these expressions, to visualize the dependence of σ_h^2 on each of the parameters of Equation (4.30). Next section derives some asymptotic expressions for σ_h^2 that are valid at particular ranges of the flow conditions H and $\partial H/\partial t$. These expressions are very simple and explicitly indicate the dependence of σ_h^2 on the different parameters of (4.30).

4.3.2 Asymptotic Expressions

This section derives some simplified asymptotic expressions for the variance σ_h^2. These expressions are derived by examining the magnitude of variable G in (4.28) and (4.29). Variable G is defined by (3.31). Substituting K_m from (3.8), (3.31) gives

$$G = e^{-F} e^{AH} \frac{\partial H}{\partial t} \qquad . \qquad (4.31)$$

Note that G is proportional to the exponential e^{AH} and the time derivative $\partial H / \partial t$. In the transient case $\partial H / \partial t \neq 0$ and when H is large, (relatively dry soil), e^{AH} tends to $+\infty$ and parameter G tends to $\pm \infty$, depending on the sign of $\partial H / \partial t$. In the case of $\partial H / \partial t > 0$ (drying conditions) $G \to +\infty$, while in the case of $\partial H / \partial t < 0$ (wetting conditions) $G \to -\infty$. In the steady state case or in the case of H small (wet soil) and $\partial H / \partial t$ small (almost steady state) parameter $G \to 0$. In other words, for transient flow in a dry soil $G \to \pm\infty$, while in the steady case or transient flow in a relatively wet soil $G \to 0$. Since these cases are of interest in practical situations, it is important to investigate the form of the variance σ_h^2 for $G \to \pm\infty$ and $G \to 0$.

For $G \to +\infty$ the determinate $\Delta = A^2 L_1^2 + 4A\Gamma G$ is positive and the variance σ_h^2 is given by (4.28), where a_1, a_2 are given by (4.23) or (4.24) and a_3, a_4, a_5 are given by (4.22). Substituting a_1, a_2, a_3, a_4, a_5 into (4.28) and taking the limit $G \to +\infty$ yields

(i) f, a, γ uncorrelated

$$\sigma_h^2 = \sigma_f^2 \frac{\Gamma^2(1 + \zeta^2 H^2) + \eta^2}{A^2 \Gamma^2} \qquad (4.32)$$

(ii) f, a, γ perfectly correlated

$$\sigma_h^2 = \sigma_f^2 \; \frac{\Gamma^2 \left(1 + \zeta^2 H^2\right) + n^2 - 2n \, \Gamma}{A^2 \, \Gamma^2} \qquad . \qquad (4.33)$$

For $G \to 0$, $\Delta > 0$ and (4.28) yields:

(i) f, a, γ uncorrelated

$$\sigma_h^2 = \frac{\sigma_f^2 \, \lambda_1}{A \, L_1 (1 + A \, L_1 \, \lambda_1)} \; [J_1^2 \left(1 + \zeta^2 H^2\right) + \zeta^2 (J_i \, \frac{\partial H}{\partial x_i})^2 \lambda_1^2) +$$

$$+ \; \frac{\zeta^2 (J_i \, \frac{\partial H}{\partial x_i})^2 \, (1 + A \, L_1 \, \lambda_1)}{|A\Gamma G|} \;] \qquad\qquad (4.34)$$

(ii) f, a, γ perfectly correlated

$$\sigma_h^2 = \frac{\sigma_f^2 \, \lambda_1}{A \, L_1 (1 + A \, L_1 \, \lambda_1)} \; [J_1^2 \left(1 - \zeta H\right)^2 + \zeta^2 (J_i \, \frac{\partial H}{\partial x_i})^2 \lambda_1^2 \; +$$

$$+ \; \frac{\zeta^2 (J_i \, \frac{\partial H}{\partial x_i})^2 \, (1 + A \, L_1 \, \lambda_1)}{|A\Gamma G|} \;] \qquad . \qquad (4.35)$$

Equations (4.34), (4.35) suggest that the variance σ_h^2 tends to infinity as $G \to 0$. Note however, that $J_i \, \partial H/\partial x_i$ generally depends on $\partial H/\partial t$, i.e., it depends on G. For a soil moisture plume moving in a stratified soil for example, the condition $G \to 0$ (or $\partial H/\partial t \to 0$) corresponds to the central part (core) of the plume. Near the core of the plume it is expected that the spatial gradients of the capillary tension head H are

89

relatively small so that $J_i \, \partial H/\partial x_i \approx 0$. In the cases when the
square $(J_i \, \partial H/\partial x_i)^2$ tends to zero faster than $|\partial H/\partial t|$, (4.34) and
(4.35) simplify to

(i)   f, a, γ uncorrelated

$$\sigma_h^2 = \frac{\sigma_f^2 \, \lambda_1 \, J_1^2 \, (1 + \zeta^2 \, H^2)}{A \, L_1 \, (1 + A \, L_1 \lambda_1)} \qquad (4.36)$$

(ii) f, a, γ perfectly correlated

$$\sigma_h^2 = \frac{\sigma_f^2 \, \lambda_1 \, J_1^2 \, (1 - \zeta H)^2}{A \, L_1 \, (1 + A \, L_1 \lambda_1)} \qquad . \qquad (4.37)$$

Note also that it is possible to avoid the infinite variance for $G \to 0$,
by selecting a different spectrum for f, a, γ which does not include
certain large-scale spectral components. For $G \to -\infty$, $\Delta < 0$ and (4.29)
gives:

(i)   f, a, γ uncorrelated

$$\sigma_h^2 = \sigma_f^2 \, \frac{\Gamma^2(1 + \zeta^2 \, H^2) + n^2}{A^2 \, \Gamma^2} \left[1 + \frac{1}{A \, L_1 \, \lambda_1} \right] \qquad (4.38)$$

(ii) f, a, γ perfectly correlated

$$\sigma_h^2 = \sigma_f^2 \, \frac{\Gamma^2(1 + \zeta^2 \, H^2) + n^2 - 2n\Gamma}{A^2 \, \Gamma^2} \left[1 + \frac{1}{A \, L_1 \, \lambda_1} \right] \, . \quad (4.39)$$

Note that the variance for $G \to -\infty$ is equal to the variance for $G \to +\infty$
multiplied by the factor $1 + 1/A \, L_1 \, \lambda_1$. Note also that the expres-

90

sions (4.36) and (4.37), obtained here as a particular case of the general transient results for $G \rightarrow 0$, were also obtained by Yeh et al., (1982), using a less general steady state analysis.

Let us now discuss the implications of the above results. The condition $G \rightarrow +\infty$ occurs when $\partial H/\partial t$ is positive and large (drying), A and/or H are large (coarse and/or dry soil) and F is small (small K_G). For $G \rightarrow +\infty$ the variance is given by (4.32) and (4.33). Note that in these cases σ_h^2 is independent of the mean soil property F, the correlation length λ_1, the flow gradients J_1, J_2, J_3 and the magnitude of $\partial H/\partial t$. If it is further assumed that σ_γ^2/Γ^2 is small, (which is usually the case, see Chapter 2) and ζH is relatively large, (dry soil), (4.32) and (4.33) simplify to

$$\sigma_h^2 \simeq \sigma_f^2 \frac{\zeta^2 H^2}{A^2} = \frac{\sigma_a^2 H^2}{A^2} \qquad . \qquad (4.40)$$

We conclude that in this particular case σ_h^2 is also independent of Γ, σ_γ^2 and on the type of correlation between f, a and γ. The variance σ_h^2 depends on A^2, σ_a^2 and H^2 only, through (4.40). Note that for a given soil (σ_a^2 and A constant) σ_h^2 increases as H^2 so that the coefficient of variation of ψ is constant under these conditions.

The condition $G \rightarrow 0$ occurs when $\partial H/\partial t$ is small (steady state), A and/or H are relatively small (fine textured and wet soil) and/or f is large (large K_G). For $G \rightarrow 0$ and $(J_i \ \partial H/\partial x_i)^2 \rightarrow 0$ faster than G, the variance σ_h^2 is given by (4.36) or (4.37). Note that in this case σ_h^2 is independent of F, Γ, σ_γ^2, J_2, J_3 and the magnitude of $\partial H/\partial t$.

If it is further assumed that ζH is large (dry soil), Equations (4.36), (4.37) simplify to

$$\sigma_h^2 = \sigma_f^2 \frac{\lambda_1 J_1^2 \zeta^2 H^2}{A L_1 (1 + A L_1 \lambda_1)} \qquad (4.41a)$$

while for ζH small (wet soil) (4.36) and (4.37) simplify to

$$\sigma_h^2 = \sigma_f^2 \frac{\lambda_1 J_1^2}{A L_1 (1 + A L_1 \lambda_1)} \qquad . \qquad (4.41b)$$

The condition $G \rightarrow -\infty$ occurs when $\partial H/\partial t$ is negative and has a relatively large magnitude, (wetting), A and/or H are large, (coarse and/or dry soil), and F is small, (small K_G). For $G \rightarrow -\infty$ the variance σ_h^2 is given by (4.38), (4.39). Note that in these cases σ_h^2 is independent of F, J_2, J_3 and the magnitude of $\partial H/\partial t$. Contrary to the $G \rightarrow +\infty$ case σ_h^2 for $G \rightarrow -\infty$ depends on the gradient J_1 and the correlation length λ_1. If we further assume that σ_γ^2 is small and ζH relatively large, Equations (4.38) and (4.39) simplify to

$$\sigma_h^2 \approx \frac{\sigma_a^2 H^2}{A^2} \left[1 + \frac{1}{A L_1 \lambda_1} \right] \qquad . \qquad (4.42)$$

In this particular case, σ_h^2 is independent of Γ, σ_γ^2 and of the type of correlation between f, a, γ.

The asymptotic expressions developed in this section are very useful because they offer valuable insight about the dependence of σ_h^2 on the 11 parameters F, A, Γ, σ_f^2, σ_a^2, σ_γ^2, λ_1, J_1, J_2, J_3, J_t and

on the type of correlation of f, a, γ. This is important since evalua-

tion of the dependence of σ_h^2 on each of these parameters would require

sensitivity analysis with respect to 11 different variables. The asymp-

totic results derived in this section show that the variance of h is

generally larger in the case of wetting conditions than it is in the case

of drying conditions. Because of this, the vertical hydraulic conductiv-

ity is smaller in the case of wetting than it is in the case of drying,

(see, Sections 4.4 and 4.7.1).

The next section shows that these asymptotic expressions are very

close to the exact results at the appropriate ranges of H and $\partial H/\partial t$.

4.3.3 Application and Discussion

This section gives several examples for the dependence of the vari-

ance on different soil and flow characteristics and compares the values

derived using the approximate expressions of Section 4.3.2 to the exact

values. Since σ_h^2 depends on a large number of variables, (12 varia-

bles), only a particular set of parameter values is considered. In order

for these examples to be as realistic as possible, we have chosen to use

combinations of soil parameters that have been observed in the field,

instead of using arbitrary parameter values. Two types of soil were

selected for illustration: the Panoche clay loam and the Maddock sandy

loam soils (see, Chapter 2). It is assumed that parameters F, A, Γ,

σ_f^2, σ_a^2, σ_γ^2 and λ_1 are independent of H and they do not show

hysteresis. For illustration, only the case of f, a, γ being

uncorrelated is examined.

Following the discussion in Section 4.3.2 the most important flow

characteristics that affect the variance, particularly at large H (dry soils), are H and J_t. For this reason, the dependence of σ_h^2 on H and J_t is investigated. The values of the spatial derivatives are fixed to $J_1 = 1$, $J_2 = J_3 = 0$. These conditions are approximately valid near the central part (core) of a soil moisture plume moving in a horizontally stratified formation. The dependence of σ_h^2 on H and J_t is shown in Figures 4.1, 4.2, 4.3 and 4.4. Figures 4.1 and 4.2 correspond to drying and wetting in the Panoche soil while Figures 4.3, 4.4 correspond to drying and wetting in the Maddock soil respectively. These figures plot σ_h^2 as a function of H for a set of discrete values of J_t. The values of σ_h^2 predicted using the asymptotic expressions of Section 4.3.2, for $G \to \pm\infty$ and $G \to 0$ are also plotted for comparison. Note that the asymptotic curves depend on H and the sign of J_t but they are independent of the magnitude of J_t.

Examination of Figures 4.1, 4.2, 4.3, 4.4 shows that σ_h^2 depends on H and J_t (especially its sign). For H and/or J_t small σ_h^2 follows closely the asymptotic curve predicted for $G \to 0$. This curve is practically independent of the magnitude and sign of J_t but it depends on H. As H increases however, the value of σ_h^2 diverges from the $G \to 0$ asymptote. The variance σ_h^2 then depends on both the magnitude and the sign of J_t. For a fixed H, σ_h^2 increases as $\left| \partial H / \partial t \right|$ increases. In addition σ_h^2 tends to be larger for $\partial H / \partial t < 0$. As H continues to increase, σ_h^2 approaches the $G \to +\infty$ or $G \to -\infty$ asymptotes, depending on the sign of J_t. These asymptotes are independent of the magnitude of J_t but they depend on the sign of J_t. The variance for $\partial H / \partial t < 0$ is $1 + 1/AL_1 \lambda_1$ times the variance for $\partial H / \partial t > 0$. Note that the value

94
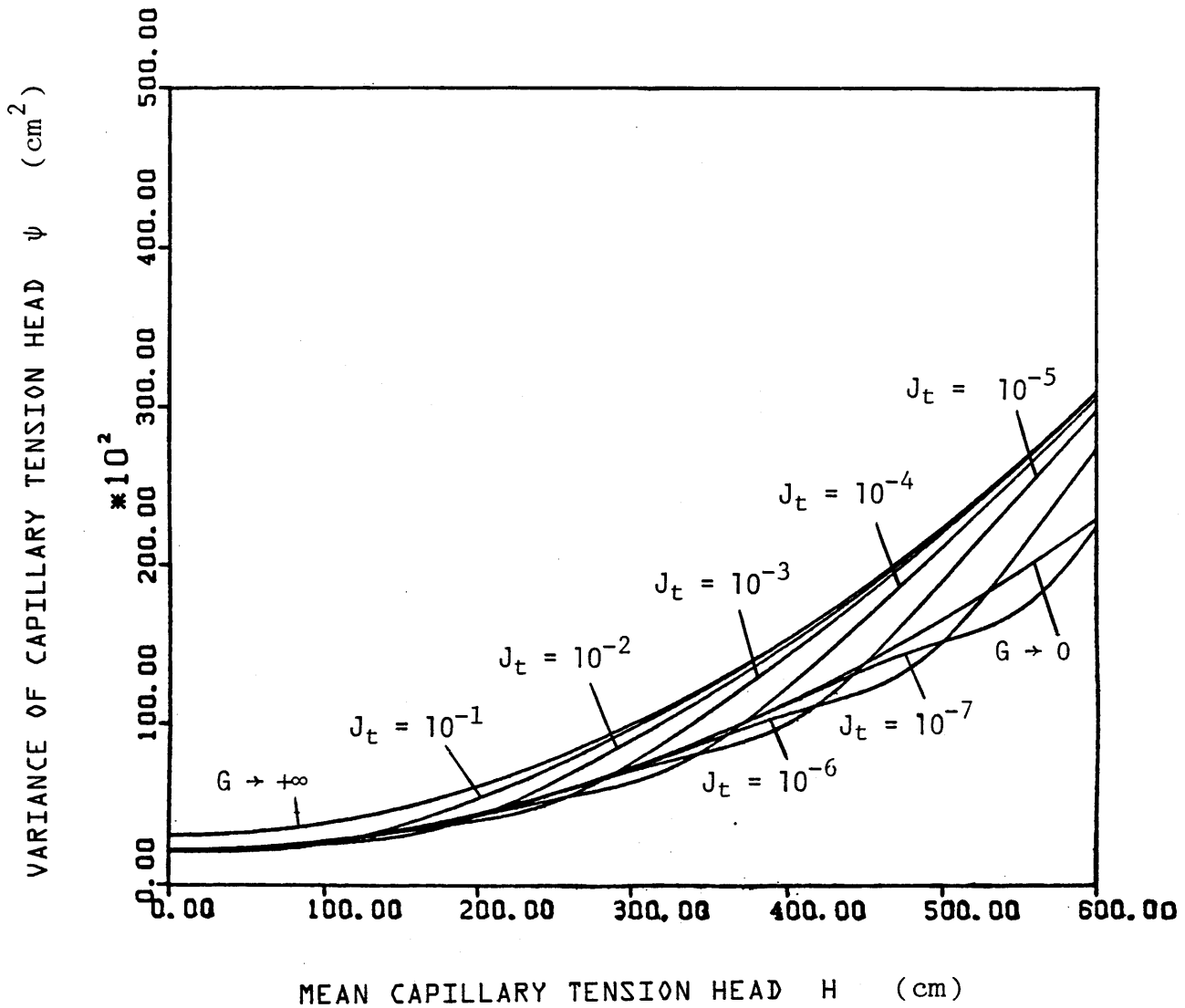
Figure 4.1 Variance of the capillary tension head σ_h^2 versus the mean capillary tension H for the Panoche silty clay loam soil in the case of drying. The curves correspond to different values of J_t in cm/sec. The asymptotic curves for $G \to 0$ and $G \to +\infty$ are also shown.
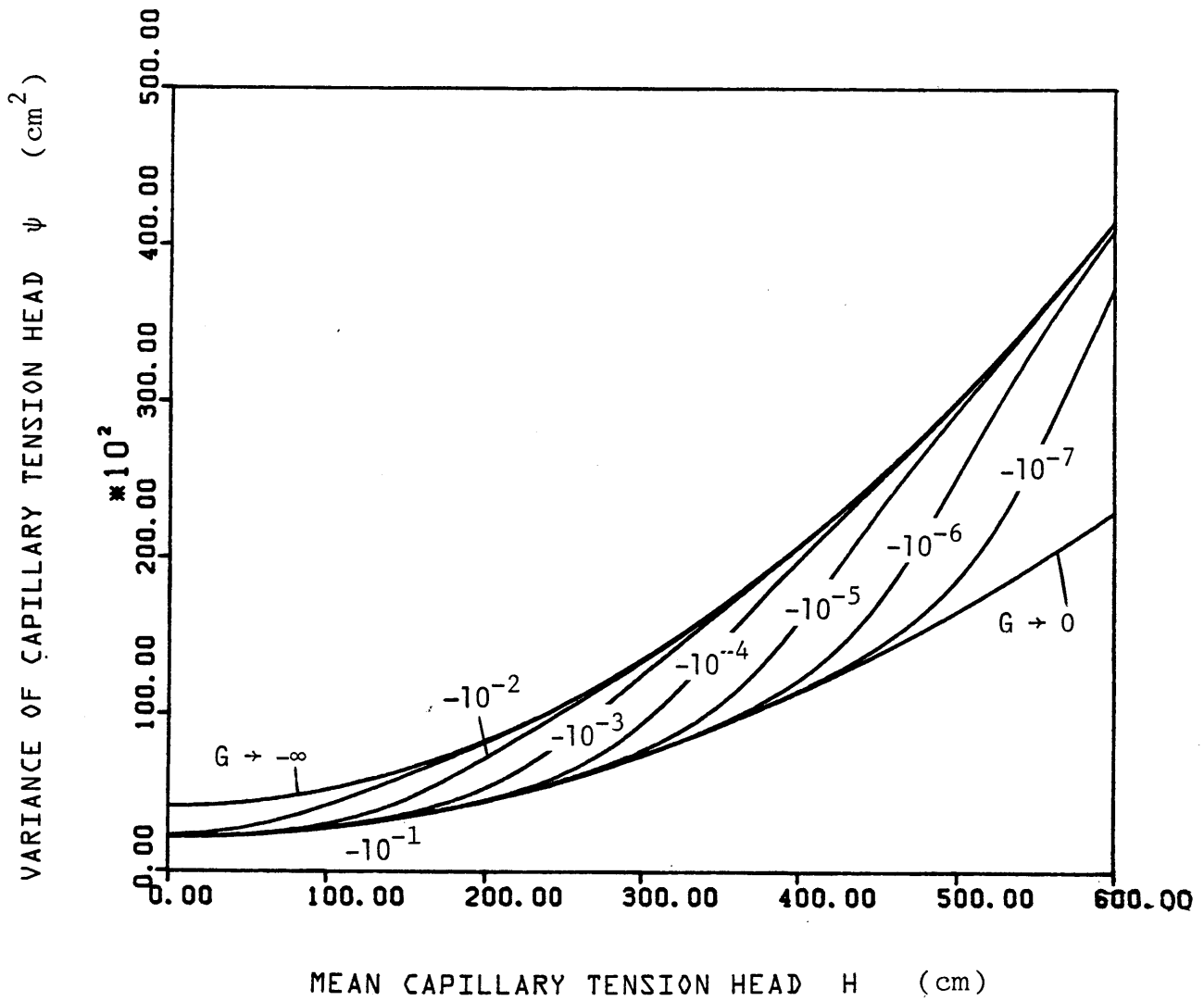
Figure 4.2 Variance of the capillary tension head σ_h^2 versus the mean capillary tension head H for the Panoche silty clay loam soil in the case of wetting. The curves correspond to different values of J_t. The asymptotic curves for $G \to 0$ and $G \to -\infty$ are also shown.

Figure 4.3   Variance of the capillary tension   head $\sigma_h{}^2$ versus the
mean capillary tension head H for the Maddock sandy loam
soil in the case of drying. The curves correspond to
different values of J_t. The asymptotic curves for $G \to 0$
and $G \to +\infty$ are also shown.
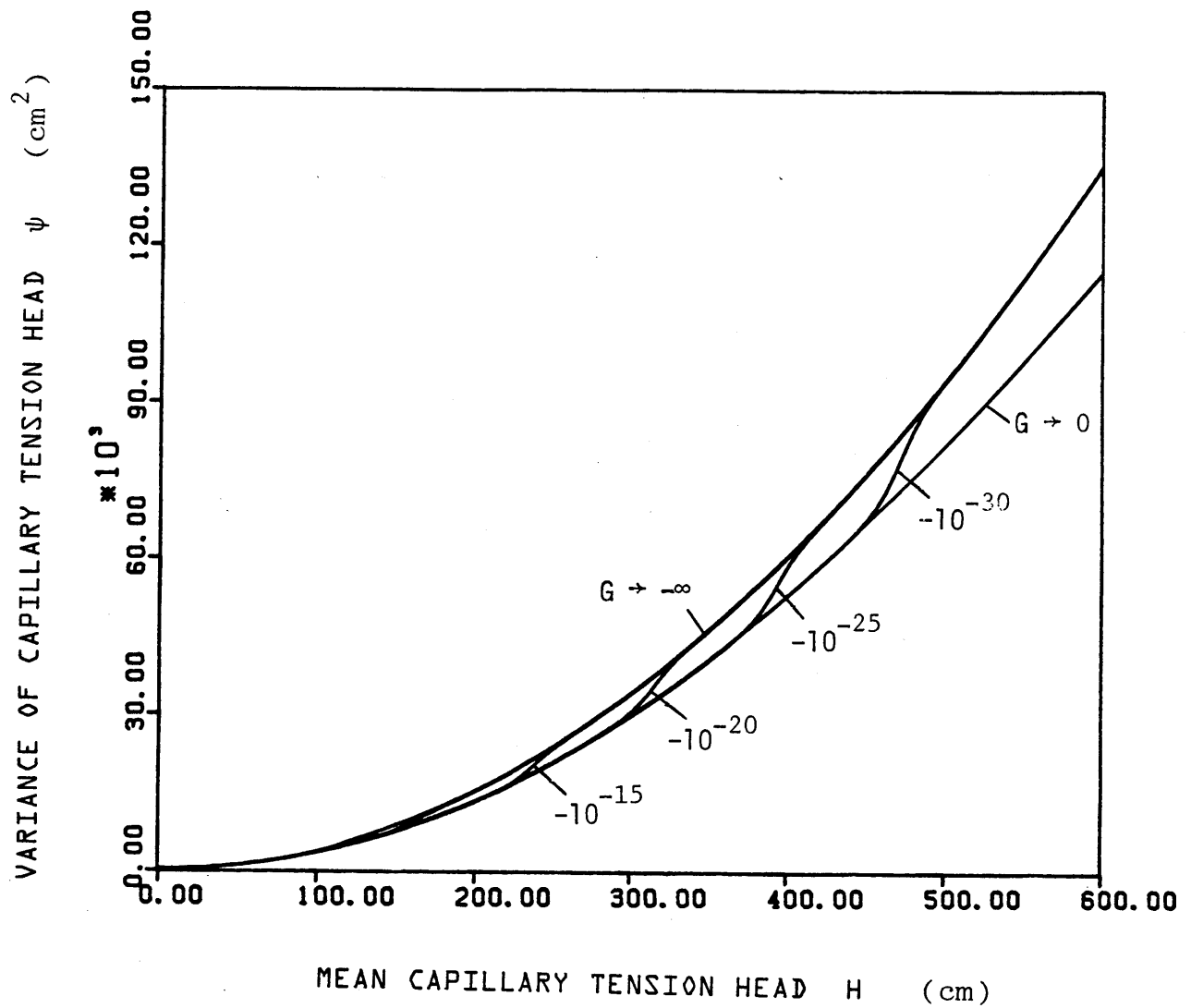
Figure 4.4   Variance of the capillary tension head σ_h^2 versus the
mean capillary tension head H for the Maddock sandy loam
soil in the case of wetting. The curves correspond to
different values of J_t. The asymptotic curves for G → 0
and G → −∞ are also shown.

of H where σ_h^2 diverges from the G → 0 asymptote and converges to the G → ±∞ asymptotes increases with decreasing $|\partial H/\partial t|$.

Comparing Figures 4.1 and 4.2 to 4.3. and 4.4 shows that σ_h^2 is much larger for the Maddock soil than it is for the Panoche soil. This may be explained by the fact that the Maddock soil has a larger variety of textures than the Panoche soil (larger σ_a^2). Note also that the G → +∞, G → 0 and the G → −∞ asymptotes lie close to each other in the Maddock than they do in the Panoche soil. This is in accordance with the asymptotic Equations (4.32), (4.36) and (4.38) since in the case of a Maddock soil parameter A is relatively large and $AL_1 \lambda_1 \approx 1 + AL_1 \lambda_1$. Parameter A is larger and $AL_1 \lambda_1 + 1$ is closer to $AL_1 \lambda_1$ in the Maddock than it is in the Panoche soil.

4.4 Effective Hydraulic Conductivities

This section evaluates the effective hydraulic conductivities in the case of a stratified soil in directions perpendicular to stratification (x_1) and parallel to stratification (x_2, x_3). The general theory developed in Chapter 3 and the simplifications discussed in Section 4.2 are used. Section 4.4.1 analytically evaluates the expected values of (3.15) and the effective hydraulic conductivities $\hat{K}_{ii}$; $i = 1, 2, 3$ given by (3.14). The expressions derived for $\hat{K}_{ii}$ are of a quite complex form. Section 4.4.2 derives asymptotic relationships for $\hat{K}_{ii}$ when $G \rightarrow \pm\infty$ and $G \rightarrow 0$. These expressions are of a simple form and show the dependence of the hydraulic conductivity on the different soil property and flow characteristics. Section 4.4.3 applies the results of the stochastic theory to the Panoche silty clay loam and the Maddock sandy loam soils.

4.4.1 Evaluation of the Effective Hydraulic Conductivities

Similarly to Section 4.3 it is assumed that f, a, γ follow exponential cross-covariance functions with identical correlation lengths. The two cases of (i) f, a, γ being uncorrelated and (ii) f, a, γ being perfectly correlated are investigated. The cross-spectral density functions of f, a, γ are then related to the spectral density function of f through (4.16) or (4.17), where parameters ζ^2 and n^2 are defined by (4.15). In order to evaluate the effective hydraulic conductivites, using (3.14) and (3.15), the expected values E[fh], E[fa], E[ah], $E[f\,\partial h/\partial x_i]$ and $E[a\,\partial h/\partial x_i]$ are evaluated as follows.

$E[fh]$

Using the approximations discussed in Section 4.2 for a stratified soil, the spectral amplitudes dZ_h are given by Equation (4.8), where the response functions W'_f, W'_a, W'_γ depend on k_1 and are independent of k_2, k_3. Replacing W_f, W_a, W_γ in Equation (3.56) by W'_f, W'_a, W'_γ, substituting (3.56) into (3.55), and integrating the resulting equation with respect to k_2 and k_3 gives:

$$E[fh] = \int_{-\infty}^{\infty} S'_{hf}(k_1) \, d k_1 \qquad (4.44)$$

where

$$S'_{hf} = W'_f \, S'_{ff} + W'_a \, S'_{af} + W'_\gamma \, S'_{\gamma f} \qquad (4.45)$$

The primed functions S'_{uv} ($u = f, a, \gamma$; $v = f, a, \gamma$) in (4.45) are given by (4.13). Substituting the expressions for W'_f, W'_a, W'_γ given by (4.10) into (4.45,) and using (4.16), (4.17) and (4.18), (4.45) yields

    (i)   f, a, γ uncorrelated

$$S'_{hf}(k_1) = \frac{j \, J_1 \, k_1}{k_1^2 + A\Gamma G + j \, AL_1 \, k_1} \cdot S'_{ff}(k_1)$$

$$= \left[\frac{(\Gamma G + AL_1 \, J_1) \, k_1^2 + A\Gamma^2 G^2}{(k_1^2 + A\Gamma G)^2 + A^2 L_1^2 k_1^2} + j \, k_1 \frac{J_1 \, k_1^2 - A\Gamma G(L_1 - J_1)}{(k_1^2 + A\Gamma G)^2 + A^2 L_1^2 k_1^2} \right] S'_{ff}(k_1) \quad (4.46)$$

    (ii) f, a, γ perfectly correlated

$$S'_{hf}(k_1) = \frac{j(1 - \zeta H) \, J_1 \, k_1 + b_1}{(k_1^2 + A\Gamma G) + j \, A \, L_1 \, k_1} \, S'_{ff}(k_1) =$$

$$= \left\{ \frac{[b_1 + AL_1 \, J_1(1 - \zeta H)] k_1^2 + b_1 \, A\Gamma G}{(k_1^2 + A\Gamma G)^2 + A^2 L_1^2 \, k_1^2} + \right.$$

(4.47)

$$\left. + j \, k_1 \, \frac{J_1(1 - \zeta H) \, k_1^2 + [A\Gamma G \, (1 - \zeta H) \, J_1 - AL_1 \, b_1]}{(k_1^2 + A\Gamma G)^2 + A^2 L_1^2 \, k_1^2} \right\} \, S'_{ff}(k_1)$$

where

$$b_1 = \Gamma G - \zeta \left(J_i \, \frac{\partial H}{\partial x_i} + H\Gamma G \right) - \eta G = (\Gamma - \eta) \, G - \zeta b \qquad (4.48)$$

and for f, a, γ following an exponential covariance function S_{ff}' is given by (4.18). Substituting (4.47), (4.48) into (4.44) and because the integral of the term multiplying $j \, k_1$ is zero (odd term), (4.44) is written in the following general form

$$E[fh] = \frac{2 \, \sigma_f^2 \, \lambda_1}{\pi} \int_0^\infty \frac{a_1 \, k_1^2 + a_2}{k_1^4 + a_3 \, k_1^2 + a_4} \, \frac{1}{1 + a_5 \, k_1^2} \, dk_1 \qquad (4.49)$$

where a_3, a_4, a_5 are given by (4.22) and a_1, a_2 are given by

    (i) f, a, γ uncorrelated

$$a_1 = \Gamma G + AL_1 \, J_1 \qquad (4.50)$$

$$a_2 = A\Gamma^2 \, G^2$$

    (ii) f, a, γ perfectly correlated

$$a_1 = \Gamma G - \zeta(J_i\, \partial H/\partial x_i + H\Gamma G) - \eta G + AL_1\, J_1\, (1 - \zeta H) \qquad (4.51)$$

$$a_2 = [\Gamma G - \zeta(J_i\, \partial H/\partial x_i + H\Gamma G) - \eta G]A\Gamma G \ .$$

Equation (4.49) is written as follows:

$$E[fh] = \frac{2\, \sigma_f^2\, \lambda_1}{\pi}\, I_1 \qquad . \qquad (4.52)$$

Integral I_1 is evaluated in Appendix C for positive or negative values of the determinate $\Delta = a_3^2 - 4a_4 = A^2\, L_1^2 + 4A\Gamma G$. Substituting I_1, (4.52) yields, for $\Delta > 0$

$$E[fh] = \sigma_f^2\, \lambda_1\, \left[\frac{a_1\sqrt{a_4} + a_1\, a_4\, a_5 - \sqrt{a_4}\, a_2\, a_5 + a_2 - a_2\, a_3\, a_5}{(A\Gamma G)\, \sqrt{4A\Gamma G + A^2 L_1^2}\, (1 + a_4\, a_5^2 - a_3\, a_5)} - \right.$$

$$\left. - a_5\, \frac{a_1 - a_2\, a_5}{(1 + a_4\, a_5^2 - a_3\, a_5)\lambda_1}\, \right] \qquad (4.53)$$

while for $\Delta < 0$

$$E[fh] = \sigma_f^2\, \lambda_1\, \left[\frac{-a_1\sqrt{a_4} + a_1\, a_4\, a_5 + \sqrt{a_4}\, a_2\, a_5 - a_2 + a_2\, a_3\, a_5}{(A\Gamma G)\, (AL_1)\, (1 + a_4\, a_5^2 - a_3\, a_5)} - \right.$$

$$\left. - a_5\, \frac{a_1 - a_2\, a_5}{(1 + a_4\, a_5^2 - a_3\, a_5)\lambda_1}\, \right] \qquad (4.54)$$

where a_1, a_2 are given by (4.50) or (4.51) and a_3, a_4, a_5 are given by (4.22).

<u>E[ah]</u>

Similarly as above, substituting (3.58) into (3.57) and integrating the resulting equation with respect to k_2, k_3, yields

$$E[ah] = \int_{-\infty}^{\infty} S'_{ha}(k_1)\, dk_1 \qquad (4.55)$$

where

$$S'_{ha} = W'_f\, S'_{fa} + W'_a\, S'_{aa} + W'_\gamma\, S'_{\gamma a} \qquad . \qquad (4.56)$$

Substituting W_f', W_a' W_γ' given by (4.10) and using (4.16), (4.17), and (4.18), (4.56) yields

(i) f, a, γ uncorrelated

$$S'_{ah}(k_1) = -\zeta^2\, \frac{j\,H\,J_1\,k_1 + b}{(k_1^2 + A\Gamma G) + j\,AL_1\,k_1}\,]\, S'_{ff}(k_1) =$$

$$= -\zeta^2[\frac{(b + AL_1\,J_1\,H)\,k_1^2 + b\,A\Gamma G}{(k_1^2 + A\Gamma G)^2 + A^2\,L_1^2\,k_1^2}$$

$$+ j\,k_1\,\frac{H_1J_1\,k_1^2 + (H\,J_1\,A\Gamma G - AL_1\,b)}{(k_1^2 + A\Gamma G)^2 + A^2L_1^2\,k_1^2}\, S'_{ff}(k_1) \qquad (4.57)$$

(ii) f, a, γ perfectly correlated

$$S'_{ha}(k_1) = \zeta\, S'_{hf}(k_1) \qquad (4.58)$$

where $S_{hf}'(k_1)$ is given by (4.46) or (4.47). Substituting (4.57), (4.58) and (4.18) into (4.55) and because the integral of the the multi-

plying $j k_1$ is zero, (4.55) is written as:

$$E[ah] = \frac{2 \sigma_f^2 \lambda_1}{\pi} \int_0^\infty \frac{a_1 k_1^2 + a_2}{k_1^4 + a_3 k_1^2 + a_4} \frac{1}{1 + a_5 k_1^2} \, dk_1 \qquad (4.59)$$

where a_3, a_4, a_5 are as in (4.22) and a_1, a_2 are given by

(i) f, a, γ uncorrelated

$$a_1 = -\zeta^2 (b + AL_1 J_1 H) \qquad (4.60)$$

$$a_2 = -\zeta^2 b A\Gamma G$$

(ii) f, a, γ perfectly correlated

$$a_1 = \zeta[b + AL_1 J_1 (1 - \zeta H)] \qquad (4.61)$$

$$a_2 = \zeta b A\Gamma G \qquad \cdot \quad .$$

Equation (4.59) can be written as follows

$$E[ah] = \frac{2 \sigma_f^2 \lambda_1}{\pi} I_1 \qquad (4.62)$$

where integral I_1 is evaluated in Appendix C. For $\Delta > 0$, $E[ah]$ is given by

$$E[ah] = \sigma_f^2 \lambda_1 \left[\frac{a_1 \sqrt{a_4} + a_1 a_4 a_5 - \sqrt{a_4} a_2 a_4 + a_2 - a_2 a_3 a_5}{(A\Gamma G) \sqrt{4A\Gamma G + A^2 L_1^2} (1 + a_4 a_5^2 - a_3 a_5)} \right.$$

$$\left. - a_5 \frac{a_1 - a_2 a_5}{(1 + a_4 a_5^2 - a_3 a_5)\lambda_1} \right] \qquad (4.63)$$

while for $\Delta < 0$

105

$$E[ah] = \sigma_f^2 \lambda_1 \left[\frac{-a_1 \sqrt{a_4} - a_1 a_4 a_5 + \sqrt{a_4} a_2 a_5 - a_2 + a_2 a_3 a_5}{(A\Gamma G)(A L_1)(1 + a_4 a_5^2 - a_3 a_5)} - \right.$$

$$\left. - a_5 \frac{a_1 - a_2 a_5}{(1 + a_4 a_5^2 - a_3 a_5)\lambda_1} \right. \tag{4.64}$$

where a_1, a_2 are now given by (4.60) or (4.61) and a_3, a_4, a_5 are given by (4.22)

$$\underline{E\left[f \frac{\partial h}{\partial x_i} \right]}$$

For a stratified soil, (3.60) simplifies to

$$E\left[f \frac{\partial h}{\partial x_i} \right] = \int_{-\infty}^{\infty} (j k_i) S'_{hf}(k_1) \, dk_1 \tag{4.65}$$

where S_{hf}' is given by (4.46) or (4.47). It holds:

   (i) f, a, γ uncorrelated

$$(j k_i) S'_{hf}(k_1) = \left[- k_1 k_i \frac{J_1 k_1^2 - A\Gamma G(L_1 - J_1)}{(k_1^2 + A\Gamma G)^2 + A^2 L_1^2 k_1^2} + \right.$$

$$\left. + j k_i \frac{(\Gamma G + AL_1 J_1) k_1^2 + A\Gamma^2 G^2}{(k_1^2 + A\Gamma G)^2 + A^2 L_1^2 k_1^2} \right] S'_{ff}(k_1) \tag{4.66}$$

   (ii) f, a, γ perfectly correlated

$$(j\,k_i)\,S'_{hf}(k_1) = [-\,k_1\,k_i\,\frac{J_1(1 - \zeta H)\,k_1^2 + [A\Gamma G(1 - \zeta H)\,J_1 - AL_1\,b_1}{(k_1^2 + A\Gamma G)^2 + A^2 L_1^2\,k_1^2} +$$

$$+\,j\,k_i\,\frac{[b_1 + AL_1 J_1\,(1 - \zeta H)]\,k_1^2 + b_1 A\Gamma G}{(k_1^2 + A\Gamma G)^2 + A^2 L_1^2\,k_1^2}\,]\,S'_{ff}(k_1) \qquad (4.67)$$

Substituting (4.66), (4.67) and (4.18) into (4.65) and dropping integrals of odd terms, (4.65) gives for $i = 1$,

$$E[f\,\frac{\partial h}{\partial x_1}] = \frac{2\,\sigma_f^2\,\lambda_1}{\pi}\,\int_0^\infty\,\frac{(a_1\,k_1^2 + a_2)\,k_1^2}{k_1^4 + a_3\,k_1^2 + a_5}\,\frac{1}{1 + a_5\,k_1^2}\,dk_1 \qquad (4.68)$$

where a_3, a_4, a_5 are as in (4.22) and a_1, a_2 are given by

(i) f, a, γ uncorrelated

$$a_1 = -J_1 \qquad (4.69)$$

$$a_2 = A\Gamma G\,(L_1 - J_1)$$

(ii) f, a, γ perfectly correlated

$$a_1 = -J_1\,(1 - \zeta H) \qquad (4.70)$$

$$a_2 = -[A\Gamma G\,(1 - \zeta H)J_1 - AL_1\,b_1] \quad .$$

Equation (4.68) is written as

$$E[f\,\frac{\partial h}{\partial x_1}] = \frac{2\,\sigma_f^2\,\lambda_1}{\pi}\,I_2 \qquad (4.71)$$

where integral I_2 is evaluated in Appendix D. For $\Delta > 0$, (4.71) gives

$$E\left[f \frac{\partial h}{\partial x_1}\right] =$$

$$\sigma_f^2 \lambda_1 \left[\frac{a_2 \sqrt{a_4} + a_2 a_4 a_5 + a_1 a_4 a_5 \sqrt{a_4} - a_1 a_3 \sqrt{a_4} - a_1 a_4}{(\mathrm{ArG}) \sqrt{4\mathrm{ArG} + A^2 L_1^2} \, (1 + a_4 a_5^2 - a_3 a_5)} + \right.$$

$$\left. + \frac{a_1 - a_2 a_5}{(1 + a_4 a_5^2 - a_3 a_5) \lambda_1} \right] \qquad (4.72)$$

while for $\Delta < 0$

$$E\left[f \frac{\partial h}{\partial x_1}\right] =$$

$$\sigma_f^2 \lambda_1 \left[\frac{-a_2 \sqrt{a_4} - a_2 a_4 a_5 - a_1 a_4 a_5 \sqrt{a_4} + a_1 a_3 \sqrt{a_4} + a_1 a_4}{(\mathrm{ArG}) (AL_1) \, (1 + a_4 a_5^2 - a_3 a_5)} + \right.$$

$$\left. + \frac{a_1 - a_2 a_5}{(1 + a_4 a_5^2 - a_3 a_5) \lambda_1} \right] \qquad (4.73)$$

where a_1, a_2 are now given by (4.69) or (4.70) and a_3, a_4, a_5 are given by (4.22).

For $i = 2, 3$, substituting $(j k_i) S_{hf}'(k_1)$ into (4.65) yields

$$E\left[f \frac{\partial h}{\partial x_i}\right] = 0 \qquad (4.74)$$

$$E[a \frac{\partial h}{\partial x_i}]$$
___

For a stratified soil (3.61) simplifies to

$$E[a \frac{\partial h}{\partial x_i}] = \int_{-\infty}^{\infty} (j \ k_i) \ S'_{ha}(k_1) \ dk_1 \qquad (4.75)$$

where S_{ha}' is given by (4.57) or (4.58). It holds

    (i)   f, a, γ uncorrelated

$$(j \ k_i) \ S'_{ha}(k_1) = -\zeta^2 \Big[-k_1 \ k_i \ \frac{H \ J_1 \ k_1^2 + (H \ J_1 \ A\Gamma G - AL_1 \ b)}{(k_1^2 + A\Gamma G)^2 + A^2 \ L_1^2 \ k_1^2} +$$

$$+ \ j \ k_i \ \frac{(b + AL_1 \ J_1 \ H) \ k_1^2 + b \ A\Gamma G}{(k_i^2 + A\Gamma G)^2 + A^2 L_1^2 \ k_1^2} \Big] \ S'_{ff}(k_1) \qquad (4.76)$$

    (ii)   f, a, γ perfectly correlated

$$(j \ k_i) \ S'_{ha}(k_1) = \zeta (j \ k_i) \ S'_{hf}(k_1) \qquad . \qquad (4.77)$$

Substituting (4.76), (4.77) and (4.18) into (4.75) and dropping integrals of odd terms, (4.75) gives for i = 1,

$$E[a \frac{\partial h}{\partial x_1}] = \frac{2 \ \sigma_f^2 \ \lambda_1}{\pi} \int_0^{\infty} \frac{(a_1 \ k_1^2 + a_2) \ k_1^2}{k_1^4 + a_3 \ k_1^2 + a_4} \ \frac{1}{1 + a_5 \ k_1^2} \ dk_1 \qquad (4.78)$$

where a_3, a_4, a_5 are as in (4.22) and a_1, a_2 are given by

    (i)   f, a, γ uncorrelated

$$a_1 = J_1 \ \zeta^2 \ H$$

$$A_2 = \zeta^2 (H \ J_1 \ A\Gamma G - AL_1 \ b) \qquad (4.79)$$

(ii) f, a, γ perfectly correlated

$$a_1 = -\zeta J_1(1 - \zeta H)$$

$$a_2 = -\zeta\left[\text{A}\Gamma\text{G }(1 - \zeta H)J_1 - \text{AL}_1 b_1\right] \quad . \tag{4.80}$$

Equation (4.78) is written as

$$E\left[a\,\frac{\partial h}{\partial x_1}\right] = \frac{2\,\sigma_f^2\,\lambda_1}{\pi}\,I_2 \tag{4.81}$$

where integral I_2 is evaluated in Appendix D. For $\Delta > 0$, (4.81) gives

$$E\left[a\,\frac{\partial h}{\partial x_1}\right] =$$

$$\sigma_f^2\,\lambda_1\left[\frac{a_2\sqrt{a_4} + a_2 a_4 a_5 + a_1 a_4 a_5 \sqrt{a_4} - a_1 a_3 \sqrt{a_4} - a_1 a_4}{(\text{A}\Gamma\text{G})\sqrt{4\text{A}\Gamma\text{G} + \text{A}^2\text{L}_1^2}\,(1 + a_4 a_5^2 - a_3 a_5)} + \right.$$

$$\left. + \frac{a_1 - a_2 a_5}{(1 + a_4 a_5^2 - a_3 a_5)\,\lambda_1}\right] \tag{4.82}$$

while for $\Delta < 0$

$$E\left[a\,\frac{\partial h}{\partial x_1}\right] =$$

$$\sigma_f^2\,\lambda_1\left[\frac{-a_2\sqrt{a_4} - a_2 a_4 a_5 - a_1 a_4 a_5 \sqrt{a_4} + a_1 a_3 \sqrt{a_4} + a_1 a_4}{(\text{A}\Gamma\text{G})\,(\text{A L}_1)\,(1 + a_4 a_5^2 - a_3 a_5)} + \right.$$

$$\left. + \frac{a_1 - a_2 a_5}{(1 + a_4 a_5^2 - a_2 a_5)\,\lambda_1}\right] \tag{4.83}$$

where a_1, a_2 are now given by (4.79) or (4.80) and a_3, a_4, a_5 are given by (4.18)

For $i = 2$, 3 (4.75) yields

$$E\left[a \frac{\partial h}{\partial x_i}\right] = 0 \tag{4.84}$$

Given the expressions for $E[fh]$, $E[ah]$, $E[f \partial h/\partial x_i]$ and $E[a \partial h/\partial x_i]$ evaluated above, and the expressions for the variance $E[h^2]$ evaluated in Section 4.3.1, terms σ_ϵ^2 and τ_i of (3.16) can be evaluated. The effective hydraulic conductivities $\hat{K}_{ii}$ can then determined from (3.14).

Similarly to the variance, the effective hydraulic conductivities $\hat{K}_{ii}$ depend on the following soil property and mean flow characteristics:

$$\hat{K}_{ii} = \hat{K}_{ii} \left(F, A, \Gamma, \sigma_f^2, \sigma_a^2, \sigma_\gamma^2, \lambda_1; H, J_1, J_2, J_3, J_t\right). \tag{4.85}$$

Section 4.4.3 gives illustrative examples for the dependence of $\hat{K}_{ii}$ on some of these parameters. Note that although a closed form expression, has been derived for $\hat{K}_{ii}$ because of the complex form of this expression it is difficult to visualize the dependence of $\hat{K}_{ii}$ on each of these parameters. The next section derives some asymptotic expressions for $\hat{K}_{ii}$ that are valid at particular ranges of H and $\partial H/\partial t$. These expressions are very simple and explictly show the dependence of $\hat{K}_{ii}$ on each of the parameters of Equation (4.85). In addition, these expressions suggest a modification of the effective hydraulic

conductivities evaluated using (3.14).

4.4.2 Asymptotic Expressions, Modification of the Effective Hydraulic Conductivities

This section derives some simplified asymptotic expressions for

$G \rightarrow \pm\infty$ and $G \rightarrow 0$. These expressions explicitly show the dependence of

K_{ii} on the different variables of (4.85). Because of their simplicity,

these asymptotic expressions make analyses, comparisons, etc., very

easy. In fact, as will be seen later in this section, the asymptotic

results show that the effective hydraulic conductivities evaluated, using

the approximate (4.14), are a first order approximation of the exact

results. This suggests a modification of (3.14) (exponential

generalization), in order to account for the error due to neglecting

higher order terms. Since the evaluations are quite lengthy for economy

of space, only the case of f, a, γ being uncorrelated is examined.

Similar results can be easily obtained for f, a, γ being perfectly

correlated.

Similarly to Section 4.3.2, simplified asymptotic expressions for

K_{ii} are derived by letting variable G, given by (3.31) tend to $\pm\infty$ or 0,

(see discussion in Section 4.3.2). This requires evaluating asymptotic

expressions for $E[fh]$, $E[ah]$, $E[f\ \partial h/\partial x_i]$ and $E[a\ \partial h/\partial x_i]$ $G \rightarrow \pm\infty$ for

$G \rightarrow 0$.

$E[fh]$

Asymptotic expressions for $E[fh]$ are derived first. For $G \rightarrow +\infty$,

$\Delta = A^2 L_1^2 + 4A\Gamma G$ is positive and $E[fh]$ is given by (4.53) where a_1,

112

a_2 are given by (4.50) and a_3, a_4, a_5 are given by (4.22). Substituting a_1, a_2, a_3, a_4, a_5 into (4.53) and taking the limit for $G \rightarrow +\infty$ yields

$$E[fh] = \frac{\sigma_f^2}{A} \qquad . \qquad (4.86)$$

For $G \rightarrow 0$, (4.53) yields

$$E[fh] = \frac{\sigma_f^2 \, J_1 \, \lambda_1}{1 + AL_1 \, \lambda_1} \qquad . \qquad (4.87)$$

For $G \rightarrow -\infty$, Δ is negative and (4.54) yields

$$E[fh] = \frac{\sigma_f^2}{A} \qquad . \qquad (4.88)$$

<u>E[ah]</u>

Asymptotic expressions for E[ah] are now derived. For $G \rightarrow +\infty$, Δ is positive and E[ah] is given by (4.63) where a_1, a_2, a_3, a_4, a_5 are given by (4.60) and (4.22). Substituting a_1, a_2, a_3, a_4, a_5 into (4.63) and taking the limit for $G \rightarrow +\infty$ yields

$$E[ah] = -\sigma_f^2 \frac{\varsigma^2 H}{A} \qquad . \qquad (4.89)$$

For $G \rightarrow 0$, (4.63) gives

$$E[ah] = -\frac{\sigma_f^2 \, \varsigma^2}{AL_1} \left[\frac{\lambda_1 (J_i \frac{\partial H}{\partial x_i} + AL_1 \, J_1 \, H)}{1 + AL_1 \, \lambda_1} + \left(J_i \frac{\partial H}{\partial x_i} \right) \right] \qquad . \qquad (4.90)$$

113

For the case of $J_i \, \partial H/\partial x_i \approx 0$, which is expected to be valid near the core of a soil moisture plume, (see discussion in Section 4.3.2), Equation (4.90) simplifies to

$$E[ah] = - \frac{\sigma_f^2 \, J_1 \, \lambda_1 \, \zeta^2 \, H}{1 + AL_1 \lambda_1} \quad . \qquad (4.91)$$

For $G \rightarrow -\infty$, Δ is negative and (4.64) yields

$$E[ah] = -\sigma_f^2 \, \frac{\zeta^2 H}{A} \quad . \qquad (4.92)$$

$$\frac{E[f \, \frac{\partial h}{\partial x_1}]}{\rule{3cm}{0.4pt}}$$

Similar asymptotic expressions are derived for $[f \, \partial h/\partial x_1]$. For $G \rightarrow +\infty$, Δ is positive and $E[f \, \partial h/\partial x_1]$ is given by (4.72) where a_1, a_2, a_3, a_4, a_5 are given by (4.69) and (4.22). Substituting a_1, a_2, a_3, a_4, a_5 into (4.72) and taking the limit for $G \rightarrow +\infty$ gives

$$E[f \, \frac{\partial h}{\partial x_1}] = 0 \quad . \qquad (4.93)$$

For $G \rightarrow 0$, (4.72) gives

$$E[f \, \frac{\partial h}{\partial x_1}] = - \frac{\sigma_f^2 \, J_1}{1 + AL_1 \, \lambda_1} \quad . \qquad (4.94)$$

For $G \rightarrow -\infty$, Δ is negative and (4.73) gives

114

$$E\left[f \frac{\partial h}{\partial x_1}\right] = -\frac{\sigma_f^2}{A \lambda_1} \qquad . \qquad (4.95)$$

As was discussed in Section 4.4.1 the expected values $E\left[f \partial h/\partial x_i\right]$; $i = 2, 3$ is always zero.

$$\underline{E\left[a \frac{\partial h}{\partial x_1}\right]}$$

Asymptotic expressions for the term $E\left[a \partial h/\partial x_1\right]$ are now derived. For $G \to +\infty$, Δ is positive and $E\left[a \partial h/\partial x_1\right]$ is given by (4.82), where a_1, a_2, a_3, a_4, a_5 are given by (4.79) and (4.22). Substituting a_1, a_2, a_3, a_4, a_5 into (4.82) and taking the limit for $G \to +\infty$ produces

$$E\left[a \frac{\partial h}{\partial x_1}\right] = 0 \qquad . \qquad (4.96)$$

For $G \to 0$, (4.82) gives

$$E\left[a \frac{\partial h}{\partial x_1}\right] = \frac{\sigma_f^2 \zeta^2}{1 + AL_1 \lambda_1} \left[J_1 H - \lambda_1 \left(J_i \frac{\partial H}{\partial x_i}\right)\right] \qquad . \qquad (4.97)$$

For $J_i \partial H/\partial x_i \approx 0$, this equation simplifies to

$$E\left[a \frac{\partial h}{\partial x_1}\right] = \frac{\sigma_f^2 \zeta^2 H}{1 + AL_1 \lambda_1} \qquad . \qquad (4.98)$$

For $G \to -\infty$, Δ is negative (4.83) gives

115

$$E\left[a\,\frac{\partial h}{\partial x_1}\right] = \frac{\sigma_f^2\,\zeta^2\,H}{A\,\lambda_1} \qquad . \qquad (4.99)$$

As was discussed in Section 4.4.1, the expected value $E\left[a\,\partial h/\partial x_i\right]$; $i = 2, 3$, is always zero.

Using the above asymptotic results, simplified expressions for $\hat{K}_{ii}$ are derived. The case of $J_i\,\partial H/\partial x_i \approx 0$ is examined for illustration. The term σ_ϵ^2, given by (3.15a), is evaluated first. Substituting for $E[h^2]$, $E[fh]$, and $E[ah]$, (3.15a) yields, for $G \to +\infty$

$$\sigma_\epsilon^2 = \sigma_f^2\,\frac{n^2}{r^2} \qquad . \qquad (4.100)$$

For $G \to 0$ (Case of $\partial H/\partial x_i \approx 0$)

$$\sigma_\epsilon^2 = \frac{\sigma_f^2\,(1 + \zeta^2\,H^2)}{1 + AL_1\,\lambda_1} \qquad (4.101)$$

while for $G \to -\infty$

$$\sigma_\epsilon^2 = \sigma_f^2\left[\frac{1 + \zeta^2\,H^2}{A\,L_1\,\lambda_1} + \frac{n^2}{r^2}\left(\frac{1}{1 + AL_1\,\lambda_1}\right)\right] \qquad . \qquad (4.102)$$

Term τ_i, given by (3.15b), is now evaluated. Substituting $E[f\,\partial h/\partial x_i]$, $E\left[a\,\partial h/\partial x_i\right]$, (3.15b) gives, for $G \to +\infty$

$$\tau_1 = 0 \qquad . \qquad (4.103)$$

For $G \to 0$

116

$$\tau_1 = - \frac{\sigma_f^2 \, J_1}{1 + AL_1 \, \lambda_1} \, (1 + \zeta^2 \, H^2) \tag{4.104}$$

while for $G \rightarrow -\infty$

$$\tau_1 = - \frac{\sigma_f^2 \, J_1}{AL_1 \, \lambda_1} \, (1 + \zeta^2 \, H^2) \qquad . \tag{4.105}$$

The variables τ_2, τ_3 are always zero.

Substituting the above expressions for σ_ϵ^2, τ_i into (3.14), the following asymptotic expressions for the effective hydraulic conductivities are obtained, for $G \rightarrow +\infty$

$$\hat{K}_{11} = K_m \left[1 + \frac{\sigma_f^2 \, \eta^2}{2\Gamma^2} \right]$$

$$\tag{4.106}$$

$$\hat{K}_{22} = K_m \left[1 + \frac{\sigma_f^2 \, \eta^2}{2\Gamma^2} \right] \qquad .$$

For $G \rightarrow 0$

$$\hat{K}_{11} = K_m \left[1 - \frac{\sigma_f^2}{2} \frac{1 + \zeta^2 \, H^2}{1 + AL_1 \, \lambda_1} \right]$$

$$\tag{4.107}$$

$$\hat{K}_{22} = K_m \left[1 + \frac{\sigma_f^2}{2} \frac{1 + \zeta^2 \, H^2}{1 + AL_1 \, \lambda_1} \right]$$

while for $G \rightarrow -\infty$

117

$$\hat{K}_{11} = K_m\left[1 - \frac{\sigma_f^2}{2} \frac{1 + \zeta^2 H^2}{AL_1 \lambda_1} + \frac{\sigma_f^2 \eta^2}{2\Gamma^2}\left(1 + \frac{1}{1 + AL_1 \lambda_1}\right)\right]$$

(4.108)

$$\hat{K}_{22} = K_m\left[1 + \frac{\sigma_f^2}{2} \frac{1 + \zeta^2 H^2}{AL_1 \lambda_1} + \frac{\sigma_f^2 \eta^2}{2\Gamma^2}\left(1 + \frac{1}{1 + AL_1 \lambda_1}\right)\right] \quad .$$

Note that for $\partial H/\partial x_i \approx 0$, the lateral hydraulic conductivity $\hat{K}_{33}$ is equal to $\hat{K}_{22}$.

The coefficient of variation of the specific moisture capacity $C = \Gamma + \gamma$ is usually small, i.e., $\sigma_\gamma^2/\Gamma^2 = \sigma_f^2 \eta^2/\Gamma^2 \ll 1$. Equations (4.106) are then further simplified to

$$\hat{K}_{11} = K_m$$

(4.109)

$$\hat{K}_{22} = K_m$$

while (4.108) simplifies to:

$$\hat{K}_{11} = K_m\left[1 - \frac{\sigma_f^2}{2} \frac{1 + \zeta^2 H^2}{AL_1 \lambda_1}\right]$$

(4.110)

$$\hat{K}_{11} = K_m\left[1 + \frac{\sigma_f^2}{2} \frac{1 + \zeta^2 H^2}{AL_1 \lambda_1}\right] \quad .$$

These simplified asymptotic expressions for $\hat{K}_{ii}$ have been derived for G absolutely large or G small. A physical interpretation of this assumption is given in Section 4.3.2. As a reminder, it is mentioned that $G \to +\infty$ corresponds to drying in relatively dry soils, $G \to -\infty$ corresponds to wetting in relatively dry soils, and $G \to 0$ corresponds to the steady

state case. Note that the expressions (4.107), derived here as a particular case of the general transient results for G → 0, were also obtained by Yeh, et al., (1982) using a less general steady state analysis. Note also that for $AL_1 \lambda_1$ large, the hydraulic conductivities in the case of wetting, given by (4.110), tend to the steady state hydraulic conductivites (4.107).

The above expressions for the effective hydraulic conductivities were derived using (3.14). This equation was obtained by expanding (3.10) in a Taylor series and retaining only the first and second order terms. Note that the exponents in (3.10) and (3.11) depend on the mean capillary tension head H. For H relatively small, it is expected that (3.11) is approximately valid. For H large, however, the higher order terms, in (3.11) could be important since they depend on powers of H (H^3, H^4, ...). It is thus expected that the expressions derived previously for the effective hydraulic conductivities, using (3.14), will be valid only for H relatively small while for H relatively large these expressions will not be valid. In the case of a perfectly stratified formation and if f, a, γ are assumed to follow normal probability density functions and J_2, $J_3 \approx 0$, the effective hydraulic conductivities can be directly evaluated with no need to expand the exponential in (3.10). Such expressions are derived below and are compared to the effective hydraulic conductivity expressions derived previously.

For J_2, $J_3 \approx 0$, assume that the flux of water parallel to stratification is small. The specific discharge in a direction perpendicular to stratification is given by

$$q_1 = K(\psi) \frac{\partial(\psi + z)}{\partial x_1} \quad . \qquad (4.111)$$

Because the lateral flux is small, the law of conservation of mass suggests that q_1 is approximately constant over x_1. Dividing (4.111) by $K(\psi)$ and taking the expected value of the resulting equation yields

$$E[q_1 \, K^{-1}(\psi)] = \frac{\partial(H + z)}{\partial x_1} = J_1 \quad . \qquad (4.112)$$

For q_1 constant, using Equation (3.13) we get

$$\hat{K}_{11} = q_1 / J_1 = \frac{1}{E[K^{-1}(\psi)]} \qquad (4.113)$$

i.e., the effective hydraulic conductivity $\hat{K}_{11}$ is equal to the harmonic mean of the unsaturated hydraulic conductivity. Substituting (3.5), the expected value $E[K^{-1}(\psi)]$ is given by

$$E[K^{-1}(\psi)] = \frac{1}{K_m} E[e^{f - Ha - Ah - ah}] \approx \frac{1}{K_m} e^{\frac{\sigma_\varepsilon^2}{2}} \qquad (4.114)$$

where K_m is given by (3.8), σ_ε^2 is the variance of $\varepsilon = f - Ha - Ah$ given by (3.15a), fluctuation products of an order higher than second are ignored and the relationship $E[e^\varepsilon] = e^{\sigma_\varepsilon^2/2}$ (Gaussian ε) is used. Substituting (4.114) into (4.113) yields the effective hydraulic conductivity $\hat{K}_{11}$

$$\hat{K}_{11} = K_m \, e^{-\frac{\sigma_\varepsilon^2}{2}} \qquad (4.115)$$

where σ_ε^2 is given by (3.15a).

The lateral effective hydraulic conductivity $\hat{K}_{22}$ is now evaluated. For $J_2 \approx 0$, it can be assumed that $\partial(H + h)/\partial x_2 \approx \partial H/\partial x_2$. Then

$$E[q_2] = E\left[K(\psi)\frac{\partial(\psi + z)}{\partial x_2}\right] \approx E[K(\psi)] J_2 \qquad (4.116)$$

$$\hat{K}_{22} = \frac{E[q_2]}{J_2} = E[K(\psi)] \qquad (4.117)$$

i.e., the lateral hydraulic conductivity is equal to the arithmetic mean of the unsaturated hydraulic conductivity. Substituting (3.5) and taking the expected value, Equation (4.117) gives

$$\hat{K}_{22} = K_m \, e^{\frac{\sigma_\varepsilon^2}{2}} \qquad (4.118)$$

where σ_ε^2 is as defined above. For $J_3 \approx 0$ the lateral effective hydraulic conductivity $\hat{K}_{33}$ is also given by (4.118).

Asymptotic expressions for the effective hydraulic conductivities predicted by the second approach are now derived for $G \to \pm\infty$ and $G \to 0$. Substituting the previously derived expressions for σ_ε^2, given by (4.100), (4.101) and (4.102), into (4.115), (4.118) and assuming that $\sigma_\gamma^2/\Gamma^2 \ll 1$ yields, for $G \to +\infty$

121

$$\hat{K}_{11} = K_m \exp\left[-\frac{\sigma_f^2 \, n^2}{2\Gamma^2}\right] \approx K_m$$

$$\hat{K}_{22} = K_m \exp\left[\frac{\sigma_f^2 \, n^2}{2\Gamma^2}\right] \approx K_m \qquad .$$

(4.119)

For $G \to 0$

$$\hat{K}_{11} = K_m \exp\left[-\frac{\sigma_f^2}{2} \, \frac{1 + \zeta^2 H^2}{1 + AL_1 \lambda_1}\right]$$

$$\hat{K}_{22} = K_m \exp\left[\frac{\sigma_f^2}{2} \, \frac{1 + \zeta^2 H^2}{1 + AL_1 \lambda_1}\right]$$

(4.120)

while for $G \to -\infty$

$$\hat{K}_{11} = K_m \exp\left[-\frac{\sigma_f^2}{2} \, \frac{1 + \zeta^2 H^2}{AL_1 \lambda_1}\right]$$

$$\hat{K}_{22} = K_m \exp\left[\frac{\sigma_f^2}{2} \, \frac{1 + \zeta^2 H^2}{AL_1 \lambda_1}\right] \qquad .$$

(4.121)

Comparing the above equations to (4.109), (4.107) and (4.110), we see that (4.109), (4.107) and (4.110) are equal to the first two terms of a Taylor series expansion of the exponential in (4.119), (4.120) and (4.121). Note that for σ_f^2 and ζH relatively small, the two sets of equations approach each other. For σ_f^2 and /or ζH large however, the discrepancy between the two sets of equations is significant.

Equations (4.115) and (4.118) and the corresponding asymptotic

expressions (4.119), (4.120) and (4.121) were obtained without expanding the exponential in (3.10). It is thus expected that these equations are closer to reality, at least in the particular case of a stratified soil, than the corresponding results (3.14) and (4.109), (4.107), (4.110), obtained using a Taylor series expansion in (3.10). For this reason (4.115), (4.118) and their asymptotic expressions (4.119), (4.120) and (4.121) are used in further analysis. Note that the variance σ_ϵ^2 is evaluated from (3.15a) and the results of Section 3.4.1.

The effective hydraulic conductivities $\hat{K}_{ii}$ are generally given by some quite complicated expressions (see Section 4.4.1). The asymptotic expressions (4.119), (4.120) and (4.121) are useful since they are very simple and they explicitly show the dependence of $\hat{K}_{ii}$ on the different soil property and flow characteristics at different ranges of H an $\partial H/\partial t$.

The implications of the asymptotic results are now discussed. The condition $G \rightarrow +\infty$ occurs when $\partial H/\partial t$ is positive and relatively large (drying), A and/or H are large (coarse and/or dry soil) and F is small (small K_G). For $G \rightarrow +\infty$ the effective hydraulic conductivities are given by (4.119). Note that if $\sigma_\gamma^2/\Gamma^2 \ll 1$, it holds $\hat{K}_{11} \approx \hat{K}_{22} \approx K_m$, where $K_m = e^F e^{AH}$. This implies that, in this case, the effective hydraulic conductivities can be evaluated by an expression similar to the local hydraulic conductivities. The "effective" saturated hydraulic conductivity $K_G = e^F$, is equal to the geometric mean of the local saturated hydraulic conductivity K_s and the "effective" pore size distribution parameter A is equal to the arithmetic mean of the local pore size distribution parameter α. Note that $\hat{K}_{ii}$, in this case, is independent of Γ^2, σ_f^2, σ_a^2, σ_γ^2, λ_1, J_1, J_2, J_3 and J_t and

depends only on F, A, and H.

The condition $G \to -\infty$ occurs when $\partial H/\partial t$ is negative and has a relatively large magnitude (wetting), A and/or H are large, (coarse and/or dry soil), and F is small, (small K_G). For $G \to -\infty$ and $\sigma_\gamma^2/\Gamma^2 \ll 1$, the effective hydraulic conductivities are given by (4.121). Note that in this case $\hat{K}_{ii}$ is different than the corresponding $\hat{K}_{ii}$ in the drying case. Here $\hat{K}_{ii}$ is given by a product of K_m by an exponential term. This term is due to local soil property variability and is predicted by the stochastic theory since this theory takes into account the existence of local variability. Traditional approaches do not predict this term and the necessary adjustments of $\hat{K}_{ii}$ in the case of wetting. This is because these approaches do not realistically account for the existence of variability of the local soil properties. Note that in the case of wetting and large H (dry soil) $\hat{K}_{ii}$ depends on F, A, σ_f^2, σ_a^2, λ_1, H and J_1 and it is independent of Γ^2, σ_γ^2, J_2, J_3 and J_t. It is further observed that, in this case, $\hat{K}_{ii}$ is anisotropic with a degree of anisotropy given by

$$\frac{\hat{K}_{22}}{\hat{K}_{11}} = \exp\left[\sigma_f^2 \frac{1 + \zeta^2 H^2}{AL_1 \lambda_1}\right] = \exp\left[\frac{\sigma_f^2 + \sigma_a^2 H^2}{AL_1 \lambda_1}\right] \quad . \quad (4.122)$$

The degree of anisotropy increases as σ_f^2 and σ_a^2 increase and $AL_1 \lambda_1$ decreases. The degree of anisotropy depends on the mean capillary tension head H and it increases as H increases (dry soil). A physical explanation of this effect is given in Section 4.7.

Note that in the above case, the effective hydraulic conductivities

124

depend on the mean flow gradient J_1 perpendicular to stratification. Because $\hat{K}_{ii}$ depends on J_1, it is generally impossible to define an effective hydraulic conductivity tensor independent of J_1. If J_1 does not vary significantly around a constant value $\bar{J}_1$ (e.g., $\bar{J}_1 \approx 1$) however, it is possible to approximate $\hat{K}_{ii}(J_1)$ with the value of $\hat{K}_{ii}$ at $\bar{J}_1$. To see this, expand $\hat{K}_{ii}$ in a Taylor series as follows:

$$\hat{K}_{ii}(J_1) \approx \hat{K}_{ii}(\bar{J}_1) + \frac{\partial \hat{K}_{ii}}{\partial J_1}\Big|_{J = \bar{J}_1} (J_1 - \bar{J}_1) =$$

$$\hat{K}_{ii}(\bar{J}_1)[1 \pm \sigma_f^2 \frac{1 + \zeta^2 H^2}{A \lambda_1 (2\bar{J}_1 - 1)^2} (J_1 - \bar{J}_1)]$$

where it is assumed that soil is horizontally stratified i.e.,

$$L_1 = J_1 + \partial H/\partial x_1 = 2 J_1 - 1.$$

This equation shows that if J_1 does not vary significantly around $\bar{J}_1$ and/or σ_f^2 is small, λ_1 large (i.e., soil tends to be homogeneous) and A is large (coarse soil), it is possible to write $\hat{K}_{ii} \approx \hat{K}_{ii}(\bar{J}_1)$. Since $\hat{K}_{ii}$ is independent of spatial gradients J_1, J_2, J_3, we may conclude that, in this particular case, an effective hydraulic conductivity tensor independent of spatial gradients, exists.

The condition $G \to 0$ occurs when $\partial H/\partial t$ is small (steady state), A and/or H are small (fine textured and/or wet soil), and/or F is large (large K_G). For $G \to 0$ the effective hydraulic conductivites are given by (4.120). Here $\hat{K}_{ii}$ is given by a product of K_m by an exponential term as well. As was discussed in the $G \to -\infty$ case, this term is due to

125

the existence of local variability and it is not predicted by traditional approaches. Similarly to the wetting case, $\hat{K}_{ii}$ depend on F, A, σ_f^2, σ_a^2, λ_1, H and J_1, but are independent of Γ, σ_γ, J_2, J_3 and J_t. Note that for $AL_1 \lambda_1$ large (coarse and/or spatially smoothly varying soil) these hydraulic conductivities tend to the hydraulic conductivities (4.121) corresponding to the wetting case. The effective hydraulic conductivities are anisotropic in this case as well. The degree of anisotropy is given by

$$\frac{\hat{K}_{22}}{\hat{K}_{11}} = \exp\left[\sigma_f^2 \frac{1 + \zeta^2 H^2}{AL_1 \lambda_1}\right] = \exp\left[\frac{\sigma_f^2 + \sigma_a^2 H^2}{AL_1 \lambda_1}\right] . \qquad (4.123)$$

The degree of anisotropy also increases as H increases (drying), but it is smaller than that in the wetting case, particularly for small AL_1 λ_1 (i.e., fine and of small scale variable soil). Equation (4.122), derived here as a particular case of the general transient results for $G \to 0$, was also obtained by Yeh, et al., (1982), using a steady state analysis.

Similarly to the wetting case, the effective hydraulic conductivities $\hat{K}_{ii}$ depend on L_1 in the case of $G \to 0$ as well. It is thus generally impossible to define an effective hydraulic conductivity tensor which is independent of J_i. If $J_1 \approx \bar{J}_1$, however, it is possible to approximate $\hat{K}_{ii}(J_1) \approx \hat{K}_{ii}(\bar{J}_1)$. In this particular case, such an approximate hydraulic conductivity tensor exists.

The simplified asymptotic expressions developed in this section proved very useful. Using these expressions, it was possible to compare

the approximate effective hydraulic conductivities for a stratified soil

obtained using the expansion of the exponential in (3.10), to the exact

effective hydraulic conductivities. In addition, the simplified asymp

totic expressions offered valuable insight about the dependence of $\hat{K}_{ii}$

on parameters F, A, Γ, $\hat{\sigma}_f^2$, $\hat{\sigma}_a^2$, λ_1, H, J_1, J_2, J_3 and J_t.

This is important since evaluation of the dependence of K_{ii} on each of

the above parameters would require sensitivity analysis with respect to

12 variables. The asymptotic results derived in this section show that

the effective hydraulic conductivities depend on the flow conditions

(wetting, drying), which suggests a hysteresis of the effective hydraulic

conductivities. In addition, the anisotropy ratio of the effective

hydraulic conductivities depends on the flow conditions (wetting, drying)

and on the mean capillary tension head.

Section 4.4.3 applies the results of Section 4.4.1 and 4.4.2 to the

Panoche clay loam and the Maddock sandy loam soils.

4.4.3 Applications and Discussion

This section gives several examples for the dependence of the effec-

tive hydraulic conductivities on the different soil and flow characteris-

tics, and compares the values derived using the approximate expressions

of Section 4.4.2 to the exact values. Since the effective conductivities

depend on a large number of variables (12 variables), only a particular

set of parameter values is considered. In order for these examples to be

as realistic as possible, we have choosen to use combinations of soil

parameters that have been observed in the field, instead of using

arbitrary parameter values. The Panoche clay loam and the Maddock sandy

loam soils are selected for illustration. It is assumed that parameters F, A, Γ, σ_f^2, σ_a^2, σ_γ^2 and λ_1 are independent of H. For illustration only the case of f, a, γ being uncorrelated is examined. Note that $\hat{K}_{ii}$ generally depends on the mean flow characteristics H, J_1, J_2, J_3, J_t. Because of the dependence of $\hat{K}_{ii}$ on the term G $\propto e^{AH} J_t$, the dependence of $\hat{K}_{ii}$ on H and J_t is stronger and more important than the dependence on J_1, J_2, J_3, particularly at large H (dry soils). For this reason, this section investigates the dependence of $\hat{K}_{ii}$ on H and J_t. The values of the spatial derivatives are fixed to $J_1 = 1$, $J_2 = J_3 = 0$. This is approximately valid near the central part (core) of a soil moisture plume, moving in a horizontally stratified formation. Evaluation of $\hat{K}_{ii}$ for other soil parameters or mean flow conditions is straightforward, using the general equations developed in Section 4.4.1.

Following the discussion in Section 4.4.2, the effective hydraulic conductivities $\hat{K}_{11}$, $\hat{K}_{22}$ are given by (4.115) and (4.118) where σ_ϵ^2 is given by (3.15a), and the expected values of (3.15a) are evaluated in Section 4.4.1. Since $\hat{K}_{11}$, $\hat{K}_{22}$ are both directly related to σ_ϵ^2 the variance σ_ϵ^2 is evaluated first. The dependence of σ_ϵ^2 on H and J_t is shown in Figures 4.5 and 4.6. Figure 4.5 corresponds to the Panoche soil,while Figure 4.6 corresponds to the Maddock soil. These figures plot σ_ϵ^2 as a function of H for a set of discrete values of J_t. The values of σ_ϵ^2 predicted, using the asymptotic expressions of Section 4.4.2, for G $\to$ $\pm\infty$, G $\to$ 0, are also plotted for comparison. Note that these curves depend on H and the sign of J_t but they are independent of the magnitude of J_t.

Examination of Figures 4.5 and 4.6 shows that σ_ϵ^2 generally

depends on H and J_t, (especially its sign). For H and/or $|J_t|$ small σ_ϵ^2 follows closely the asymptotic curve predicted for $G \to 0$. This curve is practically independent of the magnitude and sign of J_t but it depends on H. As H increases however, σ_ϵ^2 diverges from the $G \to 0$ asymptote. The variance σ_ϵ^2 then depends on both the magnitude and the sign of J_t. For $J_t < 0$, σ_ϵ^2 tends to be larger than the $G \to 0$ asymptote. For a fixed H, σ_ϵ^2 decreases with increasing J_t. As H continues to increase σ_ϵ^2 approaches the $G \to -\infty$ asymptote, depending on the sign of J_t. Note that the value of H where σ_h^2 diverges from the $G \to 0$ asymptote and convergences to the $G \to \pm\infty$ asymptotes increase with increasing $|\partial H/\partial t|$. Note also that for $J_t < 0$, σ_ϵ^2 generally increases for increasing H, while for $J_t > 0$, σ_ϵ^2 reaches a maximum and then starts to decrease to the $G \to +\infty$ asymptote which is independent of J_t and H.

Comparing Figure 4.5 to Figure 4.6 shows that σ_ϵ^2 is much larger for the Maddock soil than it is for Panoche soil. This may be explained by the fact that the Maddock soil has a larger variety of textures than the Panoche soil. Note also that the $G \to -\infty$ and $G \to 0$ asymptotes lie closer to each other in the Maddock than in the Panoche soil. In fact, in the Maddock soil σ_ϵ^2 is practically independent of J_t for $J_t \leq 0$. This is in accordance to the asymptotic Equations (4.120), (4.121) since in the Maddock soil case parameter A is relatively large and $AL_1 \lambda_1 \approx 1 + AL_1 \lambda_1$. In the case of the Panoche soil however, $AL_1 \lambda_1$ is relatively small and the two asymptotes are significantly different. Note also, that the asymptotic value of σ_ϵ^2 for $G \to +\infty$, given by $\sigma_\epsilon^2 = \sigma_a^2/\Gamma^2$, is relatively small, particularly in the Maddock soil case. This justifies the approximation $\hat{K}_{11} \approx \hat{K}_{22} \approx K_m$ (see 4.126, 4.127).

Given the values of σ_ϵ^2 evaluated above, the natural logarithms of
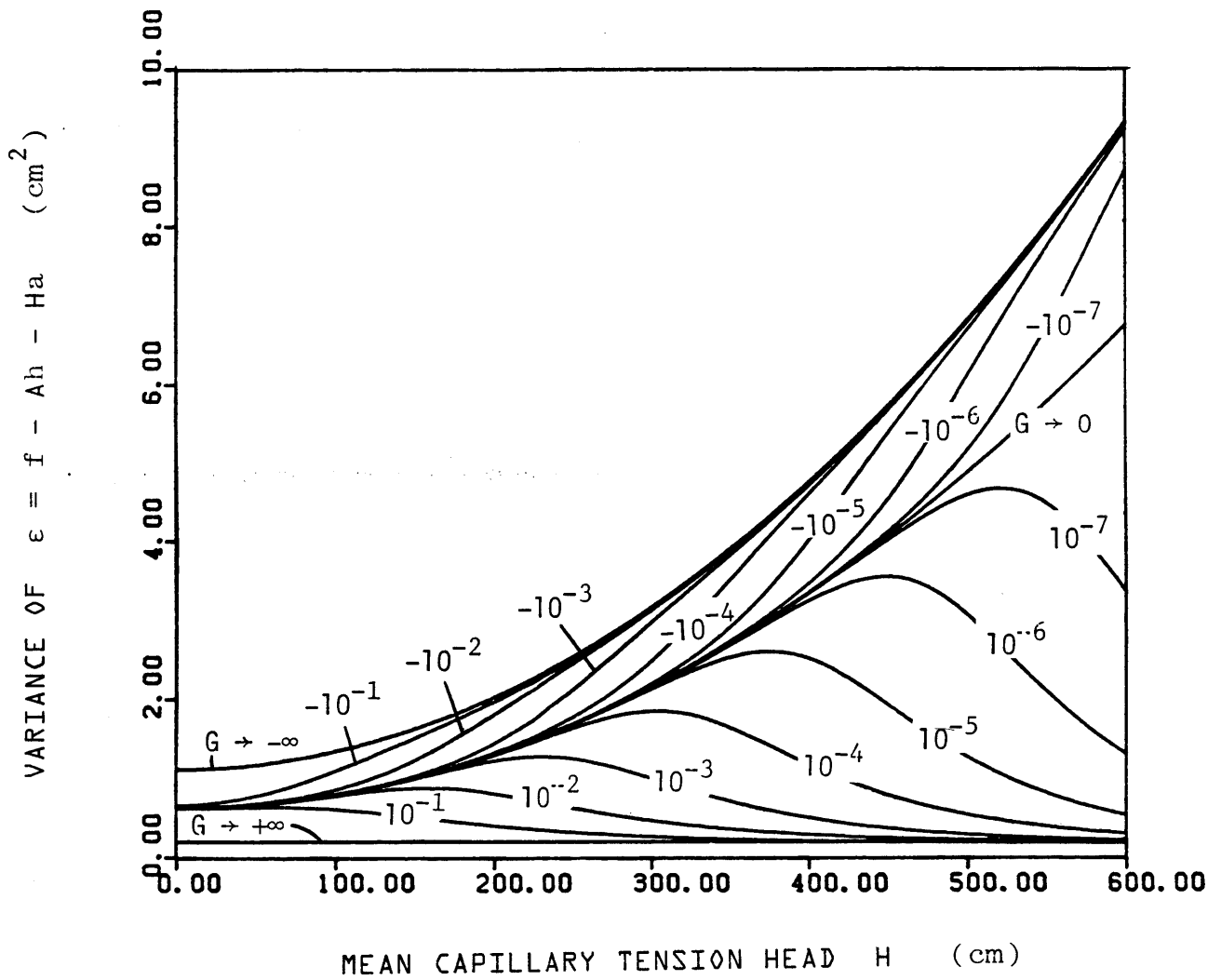
Figure 4.5   Variance of $\varepsilon = f - Ah - Ha$ versus the mean capillary ten-
sion head H for the Panoche soil. The curves correspond to
different values of J_t. The asymptotic curves for $G \to 0$,
$G \to +\infty$, and $G \to -\infty$ are also shown.
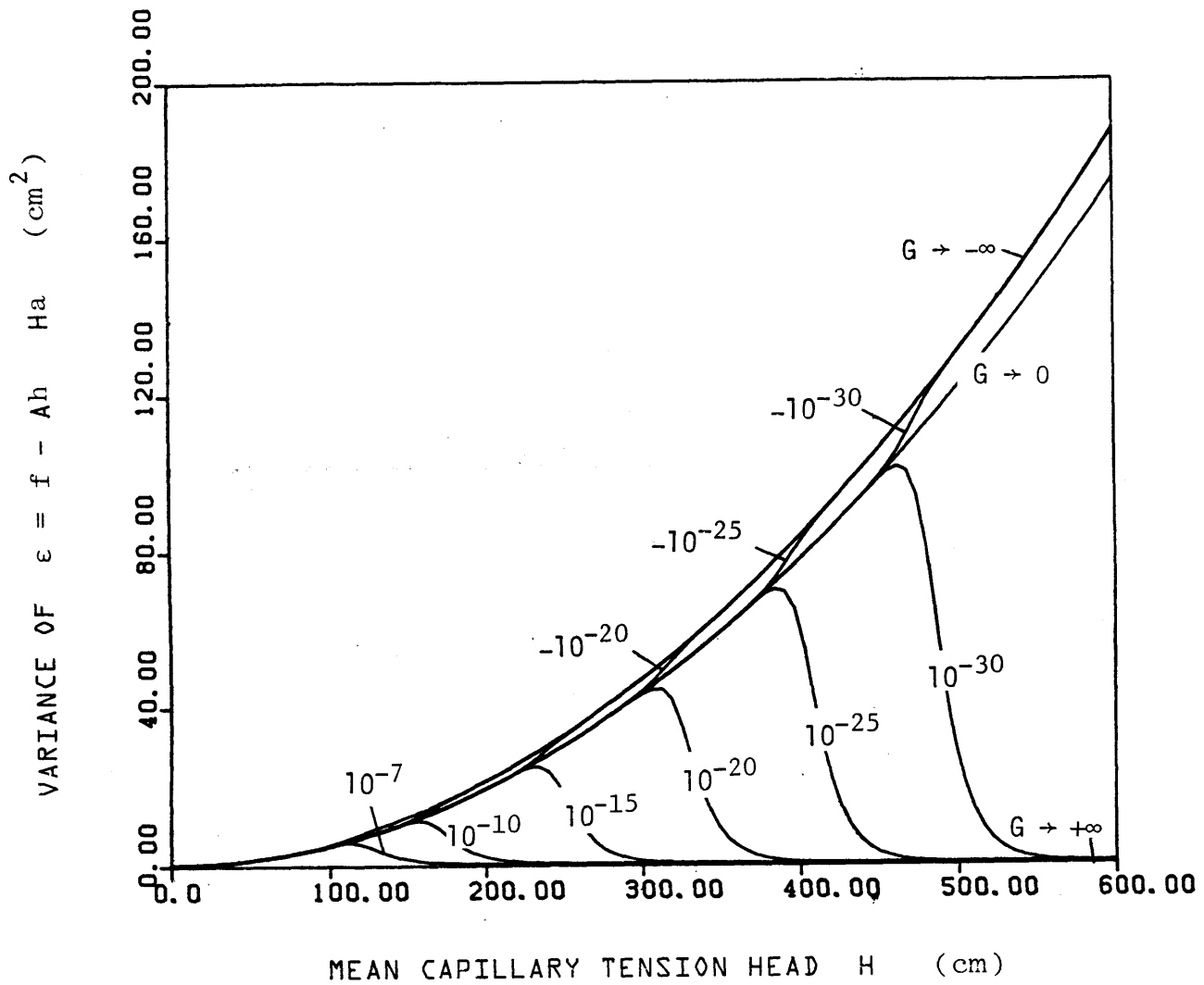
Figure 4.6   Variance of e = h - Ah - Ha versus the mean capillary ten-
sion head H for the Maddock soil. The curves correspond to
different values of J_t. The asymptotic curves for G → 0,
G → +∞, and G → -∞ are also shown.

131

the corresponding effective hydraulic conductivities $\hat{K}_{11}$, $\hat{K}_{22}$ can be evaluated using (4.115) and (4.116). Substituting K_m from (3.8), (3.118) and (3.119) yield

$$\ln\hat{K}_{11} = F - AH - \frac{\sigma_\varepsilon^2}{2}$$

$$\ln\hat{K}_{22} = F - AH + \frac{\sigma_\varepsilon^2}{2} \quad .$$

(4.123)$'$

Using (4.123)$'$ $\ln\hat{K}_{11}$, $\ln\hat{K}_{22}$ are evaluated and they are plotted in Figures 4.7 and 4.8. Figure 4.7 corresponds to the Panoche soil while Figure 4.8 corresponds to the Maddock soil. Since $\ln\hat{K}_{11}$ and $\ln\hat{K}_{22}$ are directly proportional to σ_ε^2 the previous discussion for the dependence of σ_ε^2 on H and J_t provides useful information for the dependence of $\ln\hat{K}_{11}$, $\ln\hat{K}_{22}$ on H and J_t. Figures 4.7, 4.8 show that $\hat{K}_{11}$, $\hat{K}_{22}$ depend on H but they also depend on J_t and particularly on the sign of J_t (i.e., wetting or drying conditions). The dependence of $\hat{K}_{ii}$ on J_t suggests a hysteresis of the effective hydraulic conductivities. Figures 4.7, 4.8 also show that $\hat{K}_{22}$ is generally larger than $\hat{K}_{11}$, particularly in the case or wetting ($J_t \leq 0$). In the case of drying, $\hat{K}_{22} \approx \hat{K}_{11} \approx K_m$.

In order to better illustrate the hysteresis and anisotropy of the effective hydraulic conductivities, $\ln\hat{K}_{11}$ and $\ln\hat{K}_{22}$ are plotted as a function of H for $J_t = \pm 0.01$ cm/sec in Figures 4.9, 4.10. These figures show that $\hat{K}_{11}$, $\hat{K}_{22}$ generally depend on the sign of J_t, (i.e., wetting or drying conditions). The effective hydraulic conductivity perpendicular to stratification $\hat{K}_{11}$, is smaller for decreasing H
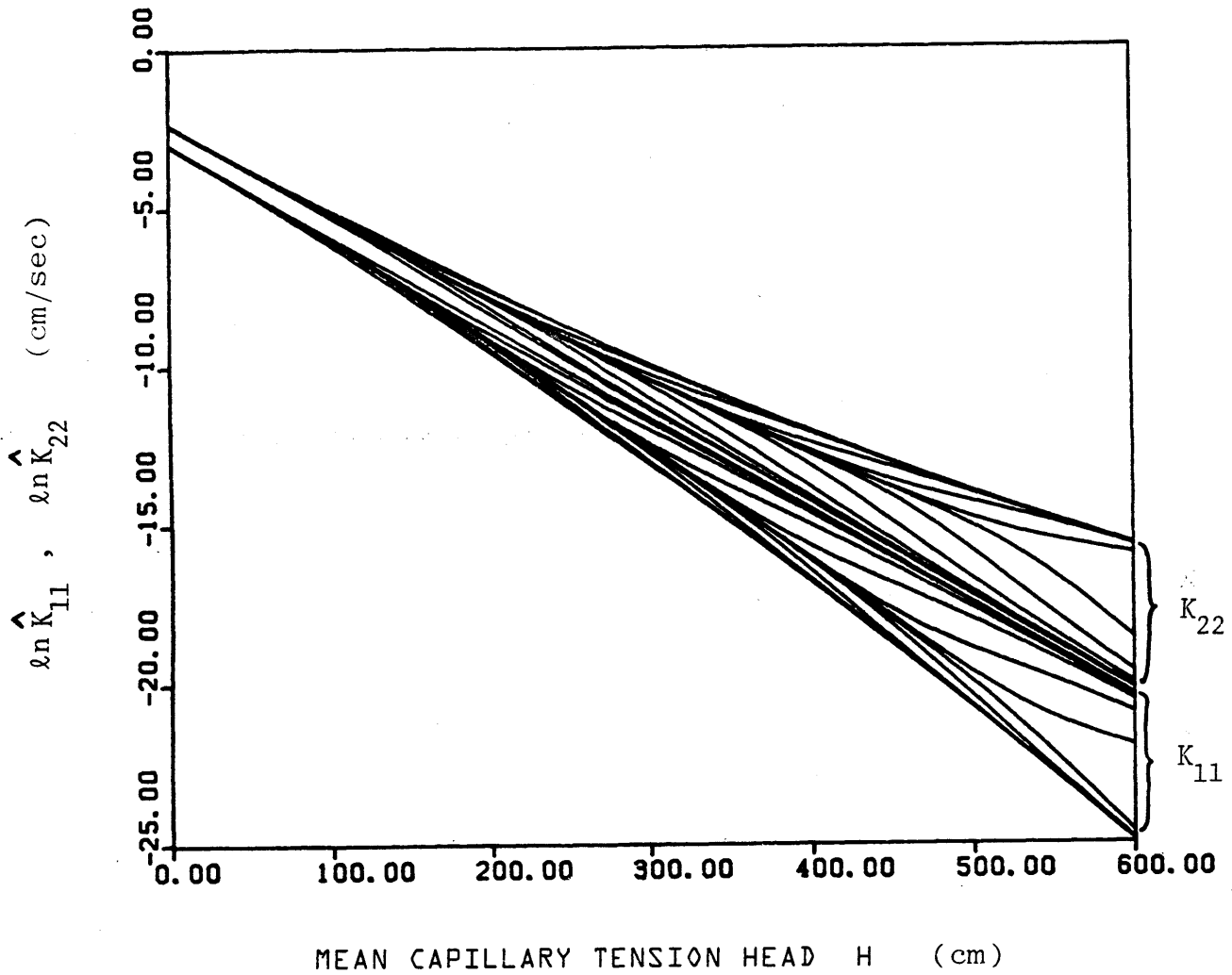
Figure 4.7   Vertical and lateral effective hydraulic conductivities
versus the mean capillary tension head H for the Panoche
soil. The curves correspond to the values of J_t shown
in Figure 4.5.
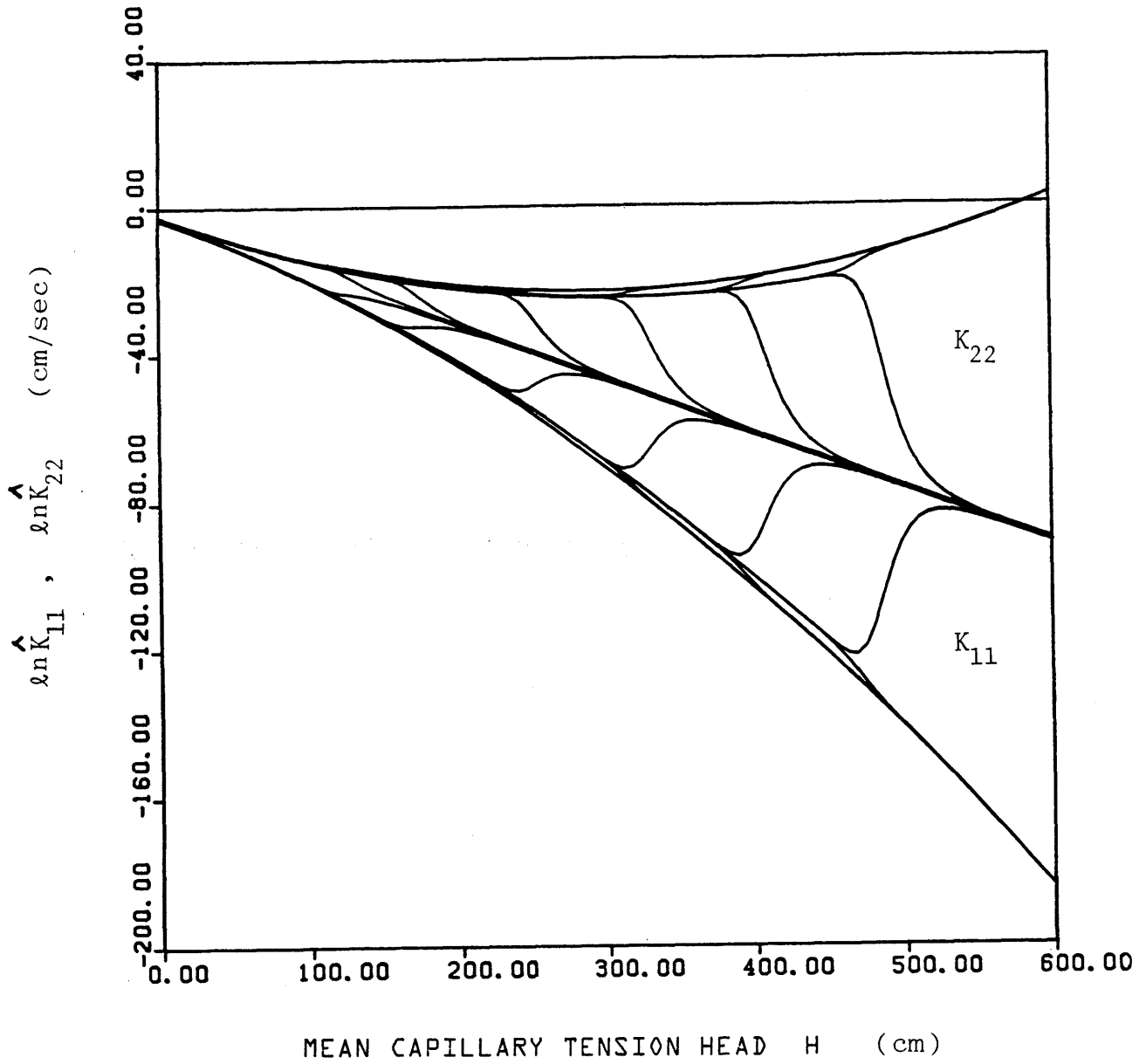
Figure 4.8   Vertical and lateral effective hydraulic conductivities
versus the mean capillary tension head H for the Maddock
soil. The curves correspond to the values of J_t shown
in Figure 4.6.
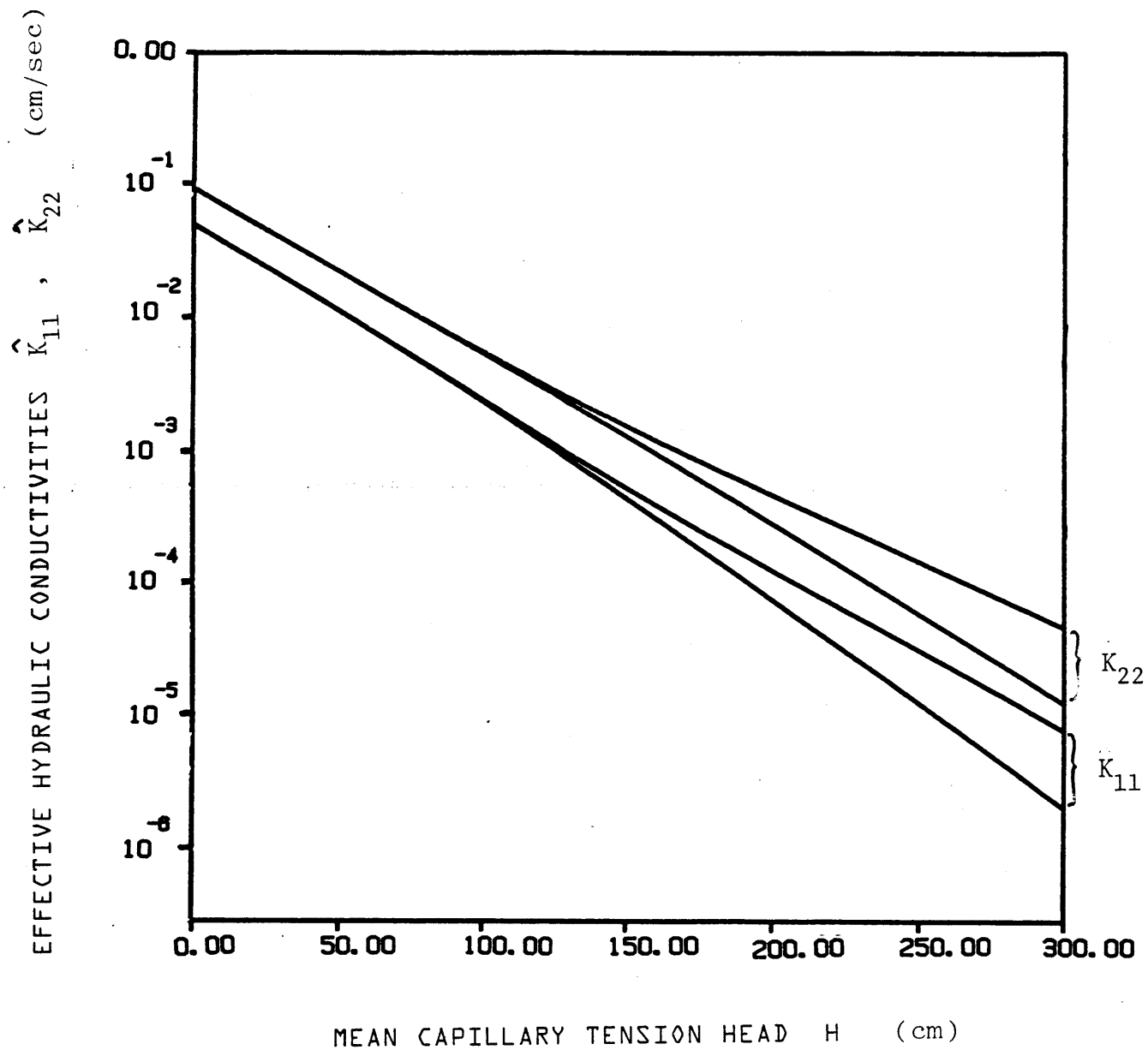
Figure 4.9   Vertical and lateral effective hydraulic conductivities
versus the mean capillary tension head H for the Panoche
soil, with J_t = + 0.01 cm/sec, illustrating hysteresis
and anisotropy of the effective hydraulic conductivities.

135
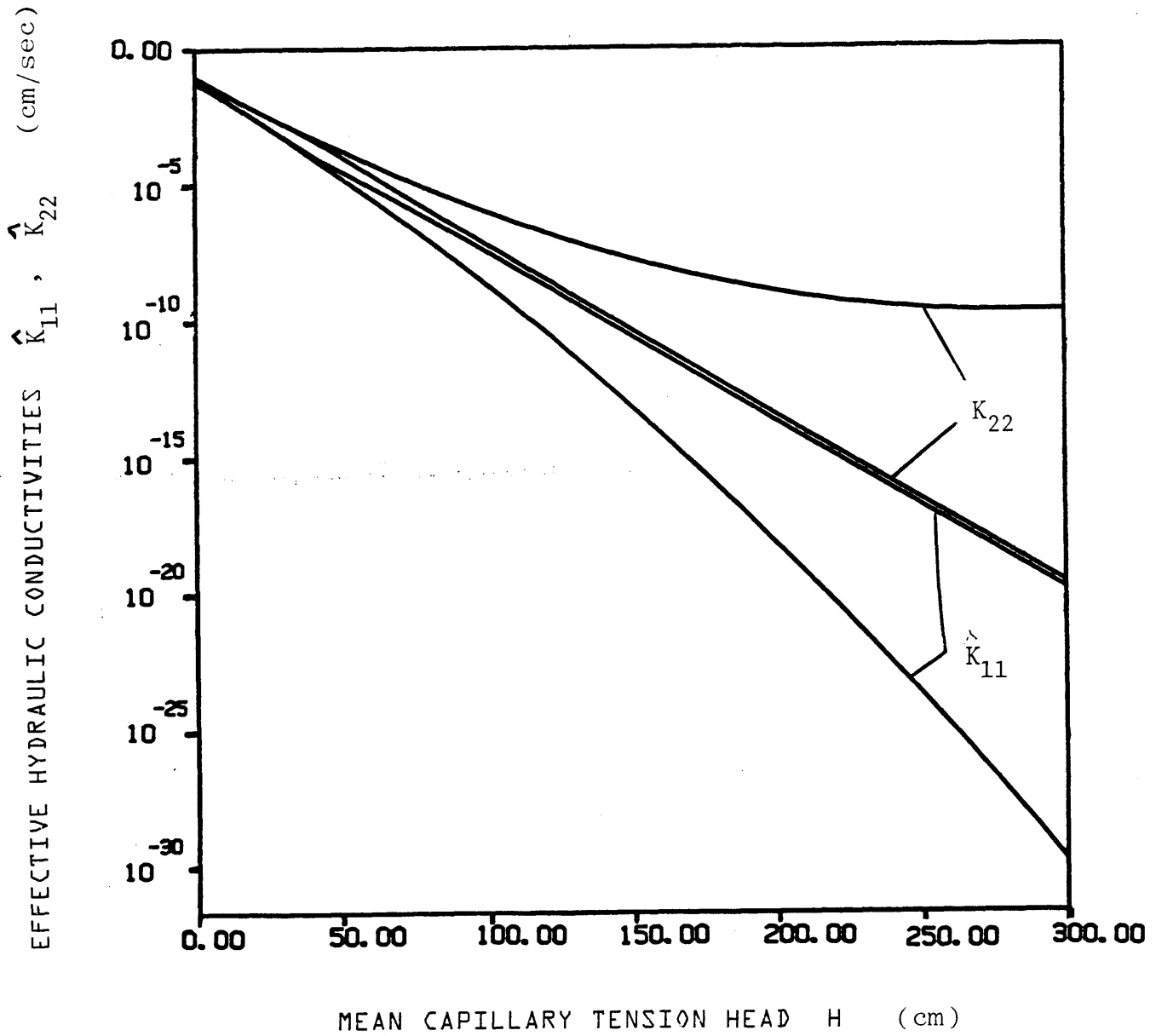
Figure 4.10 Vertical and lateral hydraulic conductivities versus the
mean capillary tension head H for the Maddock soil with
J_t = $\pm$ 0.01 cm/sec, illustrating hysteresis and
anisotropy of the effective hydraulic conductivities.

(wetting), than it is for increasing H (drying). The lateral effective

hydraulic conductivity $\hat{K}_{22}$ however, is larger for decreasing H

(wetting) than it is for increasing H (drying). It is further observed

that $\hat{K}_{22}$ is generally larger than $\hat{K}_{11}$. The anisotropy ratio

$\hat{K}_{22}/\hat{K}_{11}$, in the case of wetting, is relatively large, particularly at

large H (dry soil). In the case of drying however, $\hat{K}_{22}$ is

approximately equal to $\hat{K}_{11}$ ($\hat{K}_{22} \approx \hat{K}_{11} \approx K_m$) which implies that

the soil dries out isotropically.

The effective hydraulic conductivities $\hat{K}_{ii}$, in the above examples,

were evaluated and plotted for different sets of values of H and J_t.

These values were selected for illustration purposes and they do not

correspond to any particular real problem. In order to further

illustrate the hysteresis and anisotropy of the effective hydraulic

conductivities, it is desired to evaluate $\hat{K}_{ii}$ for a set of H and J_t

values corresponding to a real problem. In a real situation, H, J_t,

etc., should be determined by iterative solution of the governing

large-scale (mean) flow equation, given the initial and boundary

conditions of the specific problem. This requires numerical solution of

the large-scale equation and it is out of the scope of the present work.

In some cases however, it is possible to obtain simple approximate

analytical solutions of the mean flow equation.

Let us consider, for example, the case of a water input pulse at the

soil surface. It is assumed that the initial mean capillary tension head

in the soil matrix is uniform with depth. It is also assumed that the

flow is approximately vertical, and the vertical hydraulic conductivity

is $\hat{K}_{11} \approx K_m$, independent of the flow conditions. It is then possible

to analytically evaluate H and J_t, using the approximate perturbation method described in Wilson (1974), (see Appendix D).

The case of a Maddock soil with f, a, γ being uncorrelated is considered for illustration. Two different water pulse depths at the soil surface are examined, i.e., water depths of 50 cm and 30 cm. The mean flow parameters H and J_t are evaluated as a function of time at a depth of 10 m. The initial capillary tension head is assumed to be H_0 = 300 cm. Figures 4.11 and 4.12 plot H as a function of time as the soil moisture plume passes the 10 m depth. Given the calculated values of H and J_t and Equations (4.123), the corresponding effective hydraulic conductivities are determined and are plotted in Figures 4.13 and 4.14 as a function of H at the depth of 10 m as the soil moisture pulse moves past this depth. The sign of J_t is also illustrated by the directional arrows in these figures. For the 50 cm water input depth, H decreases from H_0 = 300 cm to a relatively small value where the effective hydraulic conductivities approach the limiting curve G → 0, independent of the sign of J_t, (see Figure 4.13). However, for the lower water input depth, the minimum value of H is relatively large and the effective hydraulic conductivities do not approach the asymptote G → 0. As a matter of fact, for the range of H, values in this case e^{AH} is always relatively large and $\hat{K}_{11}$, $\hat{K}_{22}$ remain close to the G → +∞ or G → −∞ curves, depending on the sign of J_t. Since for H large these curves are far from each other, the values of $\hat{K}_{11}$, $\hat{K}_{22}$ jump for the G → −∞ to the G → +∞ curve as H reaches its minimum value and J_t changes sign (see Figure 4.14). Figures 4.13 and 4.14 show similar hysteresis and anisotropy effects as Figures 4.9, 4.10. Note that the effective

138
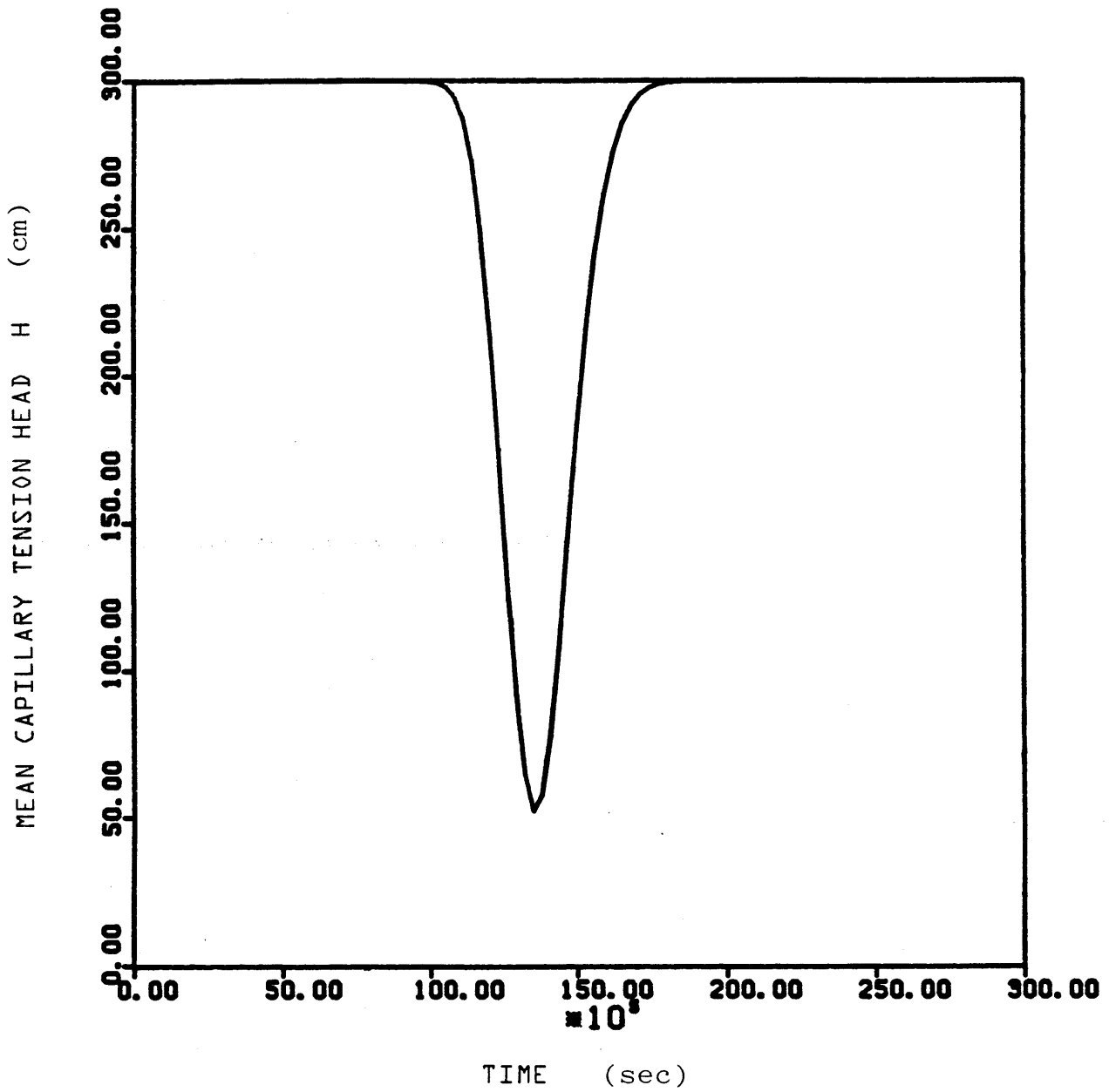
Figure 4.11   Mean capillary tension head versus time at a depth of 10 m
for a water pulse of 50 cm at the soil surface.
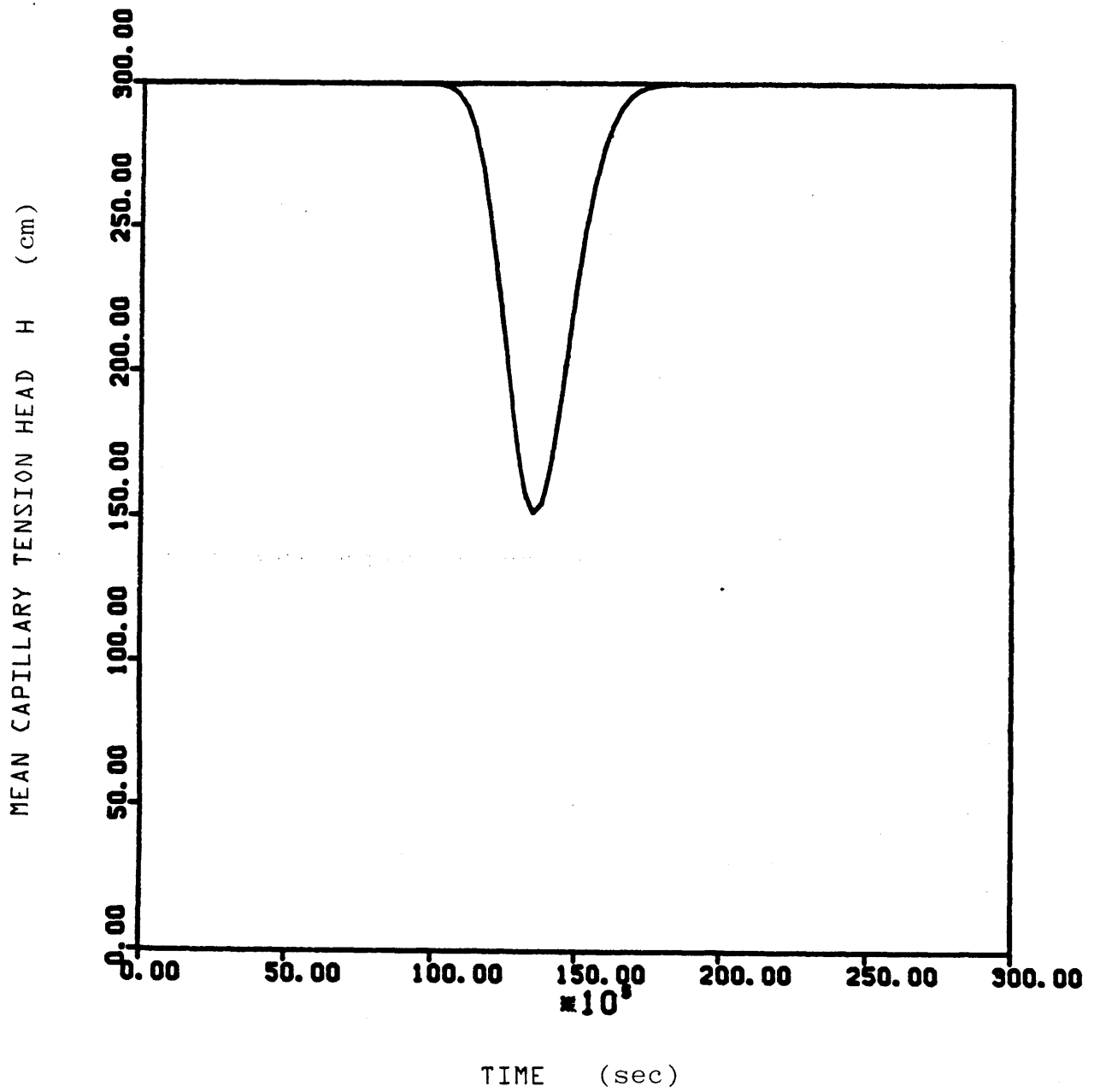
Figure 4.12   Mean capillary tension head versus time at a depth of 10 m
             for a water pulse of 30 cm at the soil surface.
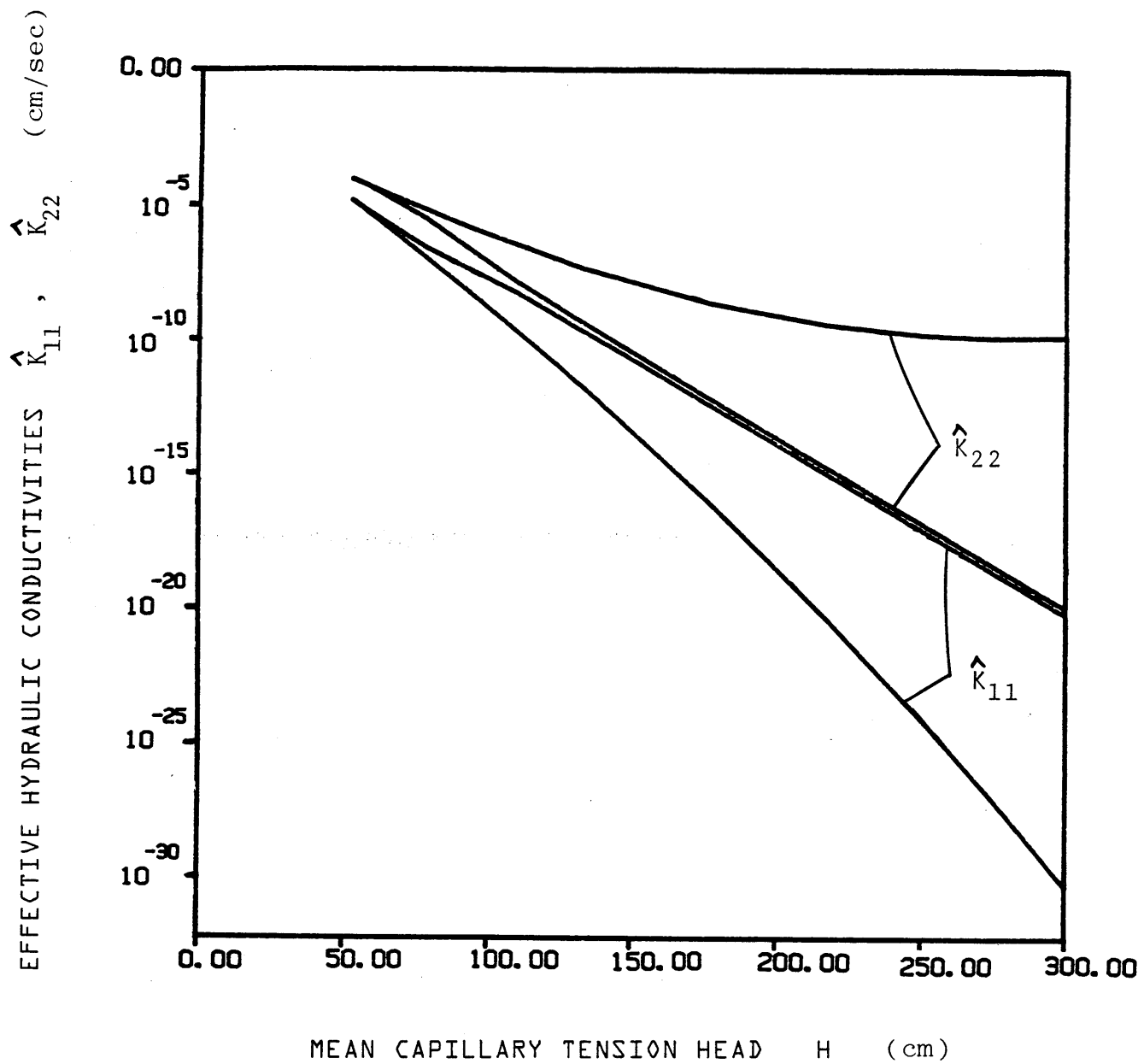
Figure 4.13   Vertical and lateral effective hydraulic conductivities versus mean capillary tension head at a depth of 10 m for a water pulse of 50 cm at the soil surface (Maddock soil).

141
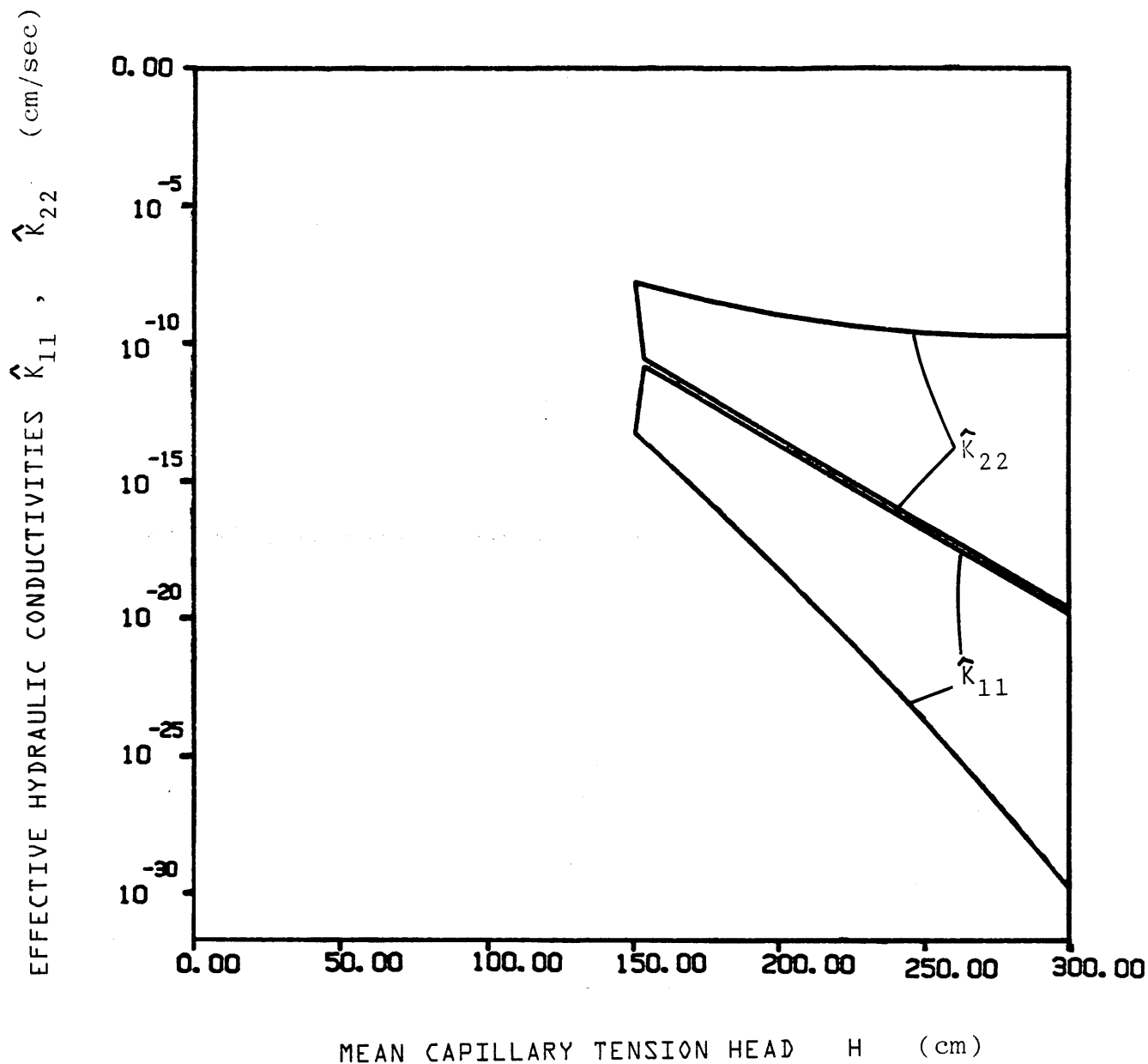
Figure 4.14 Vertical and lateral effective hydraulic conductivities
versus mean capillary tension head at a depth of 10 m for a
water pulse of 30 cm at the soil surface (Maddock soil).

hydraulic conductivity at the wetting front of the soil moisture plume is generally smaller than the one in the drying front. Since the approximate perturbation method assumes equal values of the effective hydraulic conductivity at both fronts, the estimated values of H and J_t may not be very realistic. In order to obtain more realistic estimates of H, J_t, the mean flow equation should take into account the hysteresis of $\hat{K}_{11}$. Nevertheless, even approximated, the above example shows similar hysteresis and anisotropy effects for the effective hydraulic conductivities, as did the examples in Figures 4.11, 4.12.

It is of interest to note that the local soil properties were assumed to be nonhysteretic and isotropic. This implies that the hysteresis and anisotropy of the large-scale effective hydraulic conductivities are not due to local hysteresis and anisotropy but they are due to the the spatial variability of the local soil properties. The fact that spatial variability on soil properties introduces hysteresis of the effective hydraulic conductivities is a previously unkown and important result since it cannot be predicted by traditional models. Section 4.7 gives an interpretation of the large-scale hysteresis and anisotropy, predicted by the stochastic theory, and discusses a series of field observations showing agreement with these results.

4.5 Mean Soil Moisture Content and Effective Specific Moisture Capacity

This section evaluates the mean soil moisture content and the effective specific moisture capacity in the case of a stratified soil using the general theory developed in Chapter 3 and the simplifications discussed in Section 4.2. Section 4.5.1 analytically evaluates the expected value $E[\gamma h]$ in (3.16) and the corresponding mean soil moisture content Θ and the specific moisture capacity $\hat{C}$, using Equations (3.16) and (3.17). The expressions for Θ and $\hat{C}$, derived in Section 4.5.1, are of a quite complex form. Section 4.5.2 derives asymptotic relationships for Θ and $\hat{C}$ when $G \rightarrow \pm\infty$ and $G \rightarrow 0$. These expressions are quite simple and they explicitly indicate the dependence of Θ and $\hat{C}$ on the different soil property and flow characteristics. Section 4.5.3 gives examples applying the results of the stochastic theory.

4.5.1 Evaluation of the Mean Soil Moisture Content and the Effective Specific Moisture Capacity

The mean soil moisture Θ and the effective specific moisture capacity $\hat{C}$ require evaluation of the expected value $E[\gamma h]$. Similarly to Sections 4.3 and 4.4 it is assumed that f, a, γ follow exponential cross-covariance functions with identical correlation lengths. The two cases of (i) f, a, γ uncorrelated and (ii) f, a, γ perfectly correlated are investigated. The cross-spectral density functions of f, a, γ are then related to the spectral density function of f through (4.16) or (4.17), where parameters ζ^2 and η^2 are given by (4.15).

Using the approximations for a stratified soil discussed in Section 4.2, the spectral amplitudes dZ_h are given by (4.8), where the

144

response functions W_f', W_a', W_γ' depend on k_1 and are independent of k_2, k_3. Replacing W_f, W_a, W_γ in (3.63) by W_f', W_a', W_γ', substituting (3.63) into (3.62) and integrating the resulting equation with respect to k_2, k_3 yields

$$E[\gamma h] = \int_\infty^\infty S_{h\gamma}'(k_1)\,dk_1 \qquad (4.124)$$

where

$$S_{h\gamma}' = W_f'\,S_{f\gamma}' + W_a'\,S_{a\gamma}' + W_\gamma'\,S_{\gamma\gamma}' \qquad (4.125)$$

The primed functions S_{uv}' (u, $v = f$, a, γ) in (4.125) are given by (4.13). Substituting the expressions for W_f', W_a', W_γ' given by (4.10) into (4.125) and using (4.16), (4.17) and (4.18), (4.125) yields

(i) f, a, γ uncorrelated

$$S_{h\gamma}'(k_1) = -\frac{n^2 G}{(k_1^2 + A\Gamma G) + jAL_1 k_1}\ S_{ff}'(k_1) =$$

$$= \left[\frac{-n^2 G k_1^2 - n^2 A\Gamma G^2}{(k_1^2 + A\Gamma G)^2 + A^2 L_1^2 k_1^2} + j\frac{n^2 G\, AL_1 k_1}{(k_1^2 + A\Gamma G)^2 + A^2 L_1^2 k_1^2}\right] S_{ff}'(k_1) \qquad (4.126)$$

(ii) f, a γ perfectly correlated

$$S_{h\gamma}'(k_1) = n\,S_{hf}'(k_1) \qquad (4.127)$$

145

where $S_{hf'}$ is given by (4.47) and for f, a, γ following exponential covariance functions, $S_{ff'}$ is given by (4.18). Substituting (4.126), (4.127) into (4.124) and because the integral of the term multiplying jk_1 is zero (odd term), (4.124) can be written in the following general form

$$E[\gamma h] = \frac{2\sigma_f^2 \lambda_1}{\pi} \int_0^\infty \frac{a_1 k_1^2 + a_2}{k_1^4 + a_3 k_1^2 + a_4} \frac{1}{1 + a_5 k_1^2} dk_1 \qquad (4.128)$$

where a_3, a_4, a_5 are given by (4.22) and a_1, a_2 are given by

(i)   f, a, γ uncorrelated

$$a_1 = -\eta^2 G$$

$$(4.129)$$

$$a_2 = -\eta^2 A \Gamma G^2$$

(ii)   f, a, γ perfectly correlated

$$a_1 = \eta \left[\Gamma G - \zeta (J_i \frac{\partial H}{i \partial x_i} + H \Gamma G) - \eta G + A L_1 J_1 (1 - \zeta H) \right]$$

$$(4.130)$$

$$a_2 = \eta \left[\Gamma G - \zeta (J_i \frac{\partial H}{i \partial x_i} + H \Gamma G) - \eta G \right] A \Gamma G$$

Equation (4.128) is written as follows

$$E[\gamma h] = \frac{2\sigma_f^2 \lambda_1}{\pi} I_1 \qquad (4.131)$$

Integral I_1 is evaluated in Appendix C. For $\Delta = a_3^2 - 4a_4 > 0$,
$E[\gamma h]$ is given by

$$E[\gamma h] = \sigma_f^2 \lambda_1 \left[\frac{a_1\sqrt{a_4} + a_1 a_4 a_5 - \sqrt{a_4}\, a_2 a_5 + a_2 - a_2 a_3 a_5}{(A\Gamma G)\sqrt{4A\Gamma G + A^2 L_1^2}\,(1 + a_4 a_5^2 - a_3 a_5)} \right.$$

$$\left. - a_5 \frac{a_1 - a_2 a_5}{(1 + a_4 a_5^2 - a_3 a_5)\lambda_1} \right] \qquad (4.132)$$

while for $\Delta < 0$

$$E[\gamma h] = \sigma_f^2 \lambda_1 \left[\frac{-a_1\sqrt{a_4} - a_1 a_4 a_5 + \sqrt{a_4}\, a_2 a_5 - a_2 + a_2 a_3 a_5}{(A\Gamma G)\,(AL_1)\,(1 + a_4 a_5^2 - a_3 a_5)} \right.$$

$$\left. - a_5 \frac{a_1 - a_2 a_5}{(1 + a_4 a_5^2 - a_3 a_5)\lambda_1} \right] \qquad (4.133)$$

where a_1, a_2, are given by (4.129) or (4.130) and a_3, a_4, a_5
are given by (4.22).

Given $E[\gamma h]$, the mean soil moisture content Θ can be evaluated from
(3.16) where it is assumed that the soil characteristic $E[\theta(H)]$ is
known. The expected value $E[\gamma h]$ depends on the same soil property and
mean flow characteristics as the effective hydraulic conductivity.
Equation (3.16) then gives

$$\Theta = E[\theta(H)] - g(F, A, \Gamma, \sigma_f^2, \sigma_a^2, \sigma_\gamma^2, \lambda_1; H, J_1, J_2, J_3, J_t) \qquad (4.134)$$

where $g = E[\gamma h]$. Given the above expression for the mean soil moisture
content, the effective specific moisture capacity $\hat{C}$ can be evaluated from

$$\hat{C} = -\frac{\partial \Theta}{\partial H} \ . \tag{4.135}$$

In the special case of θ being linearly dependent on ψ (3.16) reduces to $\Theta = \left(-\Gamma H + E[\theta_0] \right) - E[\gamma h]$ and $\hat{C}$ reduces to $\hat{C} = \Gamma + \partial (E[\gamma h])/\partial H$, where θ_0 the soil moisture content at saturation.

Section 4.5.2 derives asymptotic expressions for Θ and $\hat{C}$ when $G \to \pm\infty$ and $G \to 0$. These expressions are very simple and they explicitly indicate the dependence of Θ and $\hat{C}$ on the different parameters of (4.134). Section 4.5.3 gives examples for the dependence of Θ and $\hat{C}$ on H and J_t.

4.5.2 Asymptotic Expressions

This section derives asymptotic expressions for $E[\gamma h]$, Θ and $\hat{C}$ when parameter $G \to \pm\infty$ or $G \to 0$. For discussion on the meaning of these limits of parameter G see Sections 4.3.2 and 4.4.2. The cases of f, a, γ being uncorrelated or perfectly correlated are considered.

Asymptotic expressions for $E[\gamma h]$ are derived first. For $G \to \pm\infty$, $\Delta = a_3^2 - 4a_4 > 0$ and $E[\gamma h]$ is given by (4.132). Substituting a_1, a_2, a_3, a_4 and a_5, given by (4.129) or (4.130) and (4.22), into (4.132) and taking the limit for $G \to \pm\infty$ gives

(i)   f, a, γ uncorrelated

$$E[\gamma h] = -\frac{\sigma_f^2 \eta^2}{A\Gamma} \tag{4.136}$$

148

(ii)   f, a, γ perfectly correlated

$$E[\gamma h] = \frac{\sigma_f^2}{A\Gamma} \left[n\Gamma(1-\zeta H) - n^2 \right] \qquad (4.137)$$

For $G \to 0$ Equation (4.132) yields

(i)   f, a, γ uncorrelated

$$E[\gamma h] = 0 \qquad (4.138)$$

(ii)   f, a, γ perfectly correlated

$$E[\gamma h] = \frac{\sigma_f^2 \lambda_1 J_1 n(1-\zeta H)}{1+AL_1\lambda_1} \qquad (4.139)$$

For $G \to -\infty$, Δ is negative and $E[\gamma h]$ is given by (4.133). Substituting a_1, a_2, a_3, a_4 and a_5 and taking the limit for $G \to -\infty$, (4.133) produces.

(i)   f, a, γ uncorrelated

$$E[\gamma h] = -\frac{\sigma_f^2 n^2}{A\Gamma} \qquad (4.140)$$

(ii)   f, a, γ perfectly correlated

$$E[\gamma h] = \frac{\sigma_f^2}{A\Gamma} \left[n\Gamma(1-\zeta H) - n^2 \right] \qquad (4.141)$$

149

Asymptotic expressions for Θ and $\hat{C}$ are easily obtained by substitution of the asymptotic expressions for $E[\gamma h]$ derived above, into (4.134) and (4.135). Asymptotic expressions for $\hat{C}$ for example, are given as follows, for $G \rightarrow \underline{+\infty}$

(I) f, a, γ uncorrelated

$$\hat{C} = \frac{\partial(E[\theta(H)])}{\partial H} \tag{4.142}$$

(ii) f, a, γ perfectly correlated

$$\hat{C} = \frac{\partial(E[\theta(H)])}{\partial H} - \frac{\sigma_f^2 \eta \zeta}{A} \tag{4.143}$$

while for $G \rightarrow 0$

(i) f, a, γ uncorrelated

$$\hat{C} = \frac{\partial(E[\theta(H)])}{\partial H} \tag{4.144}$$

(ii) f, a, γ perfectly correlated

$$\hat{C} = - \frac{\partial(E[\theta(H)])}{\partial H} - \frac{\sigma_f^2 \lambda_1 J_1 \eta \zeta}{1 + AL_1 \lambda_1} \tag{4.145}$$

In the special case of θ being linearly dependent on ψ it holds

$$-\partial(E[\theta(H)])/\partial H = \Gamma \quad .$$

Asymptotic expressions for Θ can be easily obtained using (4.134) and (4.136)-(4.141). Note that for f, a, γ uncorrelated and $\sigma_\gamma^2/A\Gamma<<1$, $E[\gamma h]\approx0$ and $\Theta=E[\theta(H)]$ for $G\to\pm\infty$ or $G\to0$. In this case the effects of spatial variability on the mean soil moisture content and the effective specific moisture capacity $\hat{C}$ are small. In the case of f, a, γ being perfectly correlated however, $E[\gamma h]$ depends on H and $E[\gamma h]$ can be significant. Spatial variability in this case can have a significant effect on Θ and $\hat{C}$. Since f, a, γ are expected to be, at least partially, correlated, we may infer that spatial variability produces a large-scale effect on parameters Θ and $\hat{C}$.

The above simplified asymptotic expressions are useful since they show the type of dependence of Θ and $\hat{C}$ on each of the following parameters F, A, Γ, σ_f^2, σ_a^2, σ_γ^2, λ_1, H, J_1, J_2, J_3, J_t and $E[\theta(H)]$.

4.5.3 Applications and Discussion

This section gives examples for the dependence of the mean soil moisture content Θ on the mean capillary tension head H, in the Maddock soil. Section 4.5.1, showed that Θ not only depends on H, but it also depends on its time derivative J_t, i.e. Θ depends on the flow conditions (wetting or drying). Because of this dependence it is expected that Θ will show hysteresis similarly to the effective hydraulic conductivity. In order to demonstrate this effect, Θ should be evaluated for a set of pairs of values of H and J_t that correspond to a real problem. As was discussed in Section 4.4.3, obtaining H and J_t for a

151

real problem requires a solution of the large-scale flow equation subject to the initial and boundary conditions of the problem. This is a difficult problem of numerical analysis and its solution is out of the scope of this work. Nevertheless, it is possible to select a realistic time history for H and J_t based on physical arguments, past field observations, etc. This approach is followed here.

Consider the case of a leak from a waste disposal tank at a time later than the time when the leak ended. The soil moisture plume generated from the leak tends to move vertically due to gravity forces and diffuses in all directions due to capillary forces. Because there is an asymmetry in the directions of the gravity and capillary forces in the wetting and drying fronts of the plume, (gravity and capillary forces act in the same direction in the wetting front, but they act in opposing directions in the drying front), it is expected that the magnitude of the time gradient of H in the wetting front will be larger than that in the drying front. Although in typical cases J_t depends on H as well, assume for simplicity that J_t depends only on the wetting or drying conditions. Taking into account the above discussion a value of $J_t = -10^{-2}$cm/sec was selected for the wetting front while a value of $J_t = 10^{-15}$cm/sec was selected for the drying front.

The mean soil moisture content Θ is evaluated in the case of f, a, γ being perfectly correlated and is plotted as a function of H in Figure 4.15. This figure also plots the mean soil moisture content that would have been predicted by a simple model which assumes $\hat{C} = \Gamma$. Figure 4.15

152
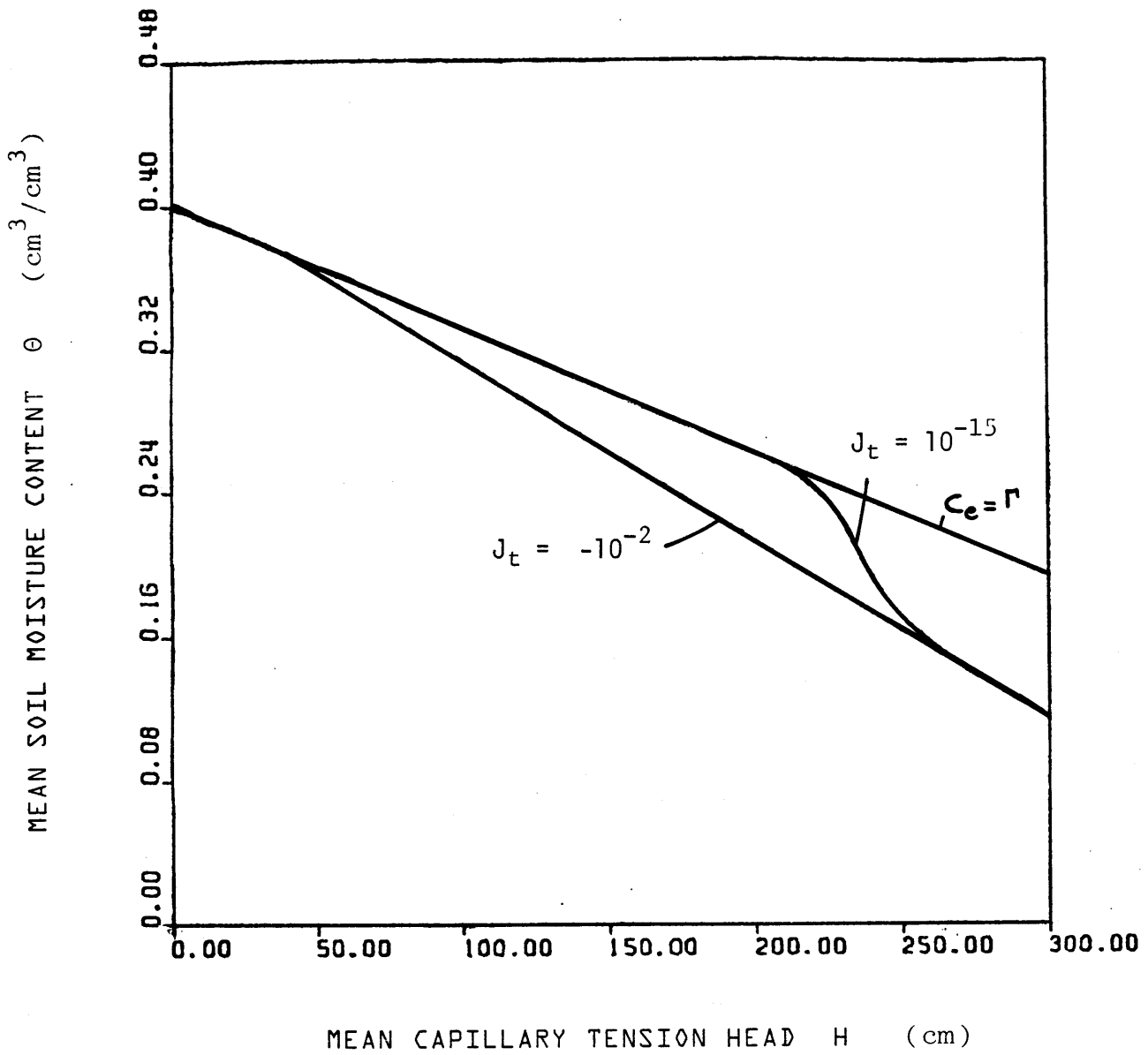
Figure 4.15 Mean soil moisture content versus mean capillary tension head for the Maddock soil for $J_t = 10^{-15}$ cm/sec and $J_t = -10^{-2}$ cm/sec, illustrating hysteresis of the mean soil moisture content.

153

shows that Θ is generally smaller than what it is predicted by deterministic models and that Θ and $\hat{C}$ depend on H but they also depend on J_t, i.e., they show a hysteresis effect. In the case of wetting Θ is smaller than the corresponding Θ in the case of drying. If f, a, γ are partially correlated a smaller hysteresis is expected.

It is of interest to note that the local parameters were assumed to be nonhysteretic. This suggests that the hysteresis of the mean soil moisture content Θ and the effective specific moisture capacity $\hat{C}$, are not due to local hysteresis but they are due to spatial variability of the local soil properties. The fact that spatial variability introduces hysteresis on Θ and $\hat{C}$ was previously unknown since it cannot be predicted by traditional models. Section 4.7 gives a possible physical interpretation of such hysteresis.

4.6 Evaluation of Assumption $\partial h/\partial t \approx 0$

One objective of this report is to provide simple generic expressions for the large-scale effective parameters. In order to make analytical evaluations feasible several assumptions were necessary in the different steps of the analysis (see Chapter 3). The effective parameters evaluated in previous sections assumed that $\partial h/\partial t$ in (4.6) is small (see Section 4.2). The conditions when the assumption $\partial h/\partial t$ is appropriate are now investigated. A trial and error procedure is used. It is first assumed that the true value of dZ_h is approximately given by (4.10). Using (4.10) an estimate of the variance of $\partial h/\partial t$ is obtained. If this estimate is relatively small it is expected that $\partial h/\partial t \approx 0$ and (4.10) is a good approximation of dZ_h. If the variance of $\partial h/\partial t$ is relatively large however, it is not possible to assume $\partial h/\partial t \approx 0$ and (4.10) is not a good approximation of dZ_h.

Section 4.5.1 evaluates the variance of $\partial h/\partial t$ and investigates its relative magnitude. Section 4.6.2 derives some simplified asymptotic expressions and investigates the conditions when the expressions developed in previous sections are appropriate.

4.6.1 Evaluation of the Variance of $\partial h/\partial t$

Let $y_1 = dZ_{h_1}$ the value of dZ_h estimated from Equation (4.10). Assume that dZ_{h_1} is approximately equal to the true value of dZ_h. Taking the derivative of (4.10) with respect to time, (see Appendix E), assuming that second order derivatives of H and the squares $(\partial H/\partial t)^2$ and $[\exp(-AH)]^2$ are relatively small, the derivative $\partial y/\partial t$ simplifies to

155

$$\frac{\partial y}{\partial t} = \frac{\partial (dZ_h)}{\partial t} = -\frac{j\,J_1 A\,k_1}{k_1^2 + A\Gamma G + jAL_1 k_1}\left(\frac{\partial H}{\partial t}\right) dZ_f -$$

$$= -\frac{jJ_1(1-HA)k_1 - A\left(J_i \frac{\partial H}{\partial x_i}\right) + \Gamma G}{k_1^2 + A\Gamma G + j\,AL_1 k_1}\left(\frac{\partial H}{\partial t}\right) dZ_a \qquad (4.146)$$

or

$$\frac{\partial y}{\partial t} = V_f'\, dZ_f + V_a'\, dZ_a \qquad (4.147)$$

where V_f' and V_a' are defined by comparison to (4.146). Let h correspond to $y = dZ_h$. It holds

$$h = \iiint\limits_{-\infty}^{\infty} e^{j\,\underline{k}\cdot\underline{x}}\, dZ_h \qquad (4.148)$$

and taking the derivative of h with respect to t yields

$$\frac{\partial h}{\partial t} = \iiint\limits_{-\infty}^{\infty} e^{j\,\underline{k}\cdot\underline{x}}\, \frac{\partial(dZ_h)}{\partial t} \qquad . \qquad (4.149)$$

Taking the complex conjugate of (4.149), multiplying by (4.149) and using the spectral representation property (3.51), gives the variance of $\partial h/\partial t$

$$E\left[\left(\frac{\partial h}{\partial t}\right)^2\right] = \iiint\limits_{-\infty}^{\infty} S_{dd}(\underline{k}) d\underline{k} \qquad (4.150)$$

where

156

$$S_{dd}(\underline{k}) = \frac{1}{d\underline{k}} E\left[\left(\frac{\partial(dZ_h)}{\partial t}\right)\left(\frac{\partial(dZ_h)}{\partial t}\right)^*\right] =$$

$$= \left|V_f'\right|^2 S_{ff} + \left|V_a'\right|^2 S_{aa} + V_f' V_a^* S_{fa} + V_f' V_a' S_{af} \quad . \tag{4.151}$$

Similarly to Sections 4.3, 4.4, 4.5 it is assumed that f, a, γ follow exponential covariance functions with identical correlation lengths. The two cases of (i) f, a, γ being uncorrelated and (ii) f, a, γ being perfectly correlated are investigated. The cross-spectral density functions of f, a, γ are then related to the spectral density function of f through Equations (4.16) or (4.17), where parameters ζ^2 and η^2 are defined in (4.15).

Substituting (4.151) into (4.150) and integrating with respect to k_2, k_3 yields

$$E\left[\left(\frac{\partial h}{\partial t}\right)^2\right] = \iiint_{-\infty}^{\infty} S_{dd}'(k_1)\, dk_1 \tag{4.152}$$

where

$$S_{dd}' = \left|V_f'\right|^2 S_{ff}' + \left|V_a'\right|^2 S_{aa}' + V_f' V_a^* S_{fa}' + V_f^* V_a' S_{af}' \quad . \tag{4.153}$$

The primed functions S_{uv}' (u'v = f, a, γ) in (4.153) are given by (4.13). Substituting the expressions for V_f', V_a' given by (4.146) into (4.153) and using (4.16), (4.17) and (4.18), (4.153) yields

(i) f, a, γ uncorrelated

$$S_{dd}'(k_1) = \frac{\left[J_1^2 A^2 + \zeta^2 J_1^2 (1-HA)^2\right] k_1^2 + \zeta^2 \left[A(J_i \frac{\partial H}{\partial x_i}) - \Gamma G\right]^2}{(k_1^2 + A\Gamma G)^2 + A^2 L_1^2 k_1^2} \left(\frac{\partial H}{\partial t}\right)^2 S_{ff}'(k_1)$$

(4.154)

(ii) f, a, γ perfectly correlated

$$S_{dd}'(k_1) = \frac{\left[J_1 A + \zeta J_1(1-HA)\right]^2 k_1^2 + \zeta^2 \left[A(J_i \frac{\partial H}{\partial x_i}) - \Gamma G\right]^2}{(k_1^2 + A\Gamma G)^2 + A^2 L_1^2 k_1^2} \left(\frac{\partial H}{\partial t}\right)^2 S_{ff}'(k_1)$$

(4.155)

For f, a, γ following exponential covariance functions, S_{ff}' is given
by (4.18). Substituting (4.154), (4.155) into (4.152), gives

$$E\left[\left(\frac{\partial h}{\partial t}\right)^2\right] = \frac{2\sigma_f^2 \lambda_1}{\pi} \left(\frac{\partial H}{\partial t}\right)^2 \int_0^\infty \frac{a_1 k_1^2 + a_2}{k_1^4 + a_3 k_1^2 + a_4} \frac{1}{1 + a_5 k_1^2} \, dk_1$$

(4.156)

where a_1, a_4, a_5 are given by (4.22) and a_1, a_2 are given by

(i) f, a, γ uncorrelated

$$a_1 = J_1^2 A^2 + \zeta^2 J_1^2 (1-HA)^2$$

(4.157)

$$a_2 = \zeta^2 \left[A(J_i \frac{\partial H}{\partial x_i}) - \Gamma G\right]^2$$

(ii) f, a, γ perfectly correlated

$$a_1 = \left[J_1 A + \zeta J_1 (1-HA) \right]^2$$

$$a_2 = \zeta^2 \left[A(J_i \frac{\partial H}{\partial x_i}) - \Gamma G \right]^2 \tag{4.158}$$

Equation (4.156) is written as follows

$$E\left[(\frac{\partial h}{\partial t})^2 \right] = \frac{2\sigma_f^2 \lambda_1}{\pi} (\frac{\partial H}{\partial t})^2 I_1 \qquad . \tag{4.159}$$

Integral I_1 is evaluated in Appendix C as a function of a_1, a_2, a_3, a_4, a_5.

Let us now examine the relative magnitude of term $\partial h/\partial t$, compared to the term $K_m AGh = A(\partial H/\partial t) h$ at the left hand side of (3.33). We have chosen to compare $\partial h/\partial t$ to this term because this term has certain things in common to $\partial h/\partial t$, i.e. it is independent of spatial derivatives and it is proportional to $\partial H/\partial t$ as is $\partial h/\partial t$ (see Equations 4.149, 4.146). The relative significance of each of these terms depends on the ratio of their variances given by

$$\rho^2 = \frac{E\left[(\frac{\partial h}{\partial t})^2 \right]}{A^2 (\frac{\partial H}{\partial t})^2 E[h^2]} \tag{4.160}$$

and using (4.159) and (4.26) yields

$$\rho^2 = \frac{\cdot I_1'}{A^2 I_1} \tag{4.161}$$

159

where I_1' is evaluated for the a_1, a_2 given by (4.157), (4.158), while I_1 is evaluated for a_1, a_2 given by (4.23), (4.24). If $\rho^2 \ll 1$, it may be assumed that term $\partial h/\partial t$ is not important and can be ignored compared to the other terms of (3.33). If ρ^2 is significant however, it is not possible to ignore this term.

Next section derives simplified asymptotic expressions for ρ^2, and discusses the implications of these results.

4.6.2 Asymptotic Expressions, Comparisons and Discussion

This section derives some simplified expressions for the ratio ρ^2, examines the magnitude of ρ^2 relative to one and discusses the implications of the results.

Asymptotic results for ρ^2 are derived when parameter $G \to \pm\infty$ or $G \to 0$. For $G \to \pm\infty$, $\Delta = a_3^2 - 4a_4 > 0$ and $E[(\partial h/\partial t)^2]$ is given by

$$E\left[\left(\frac{\partial h}{\partial t}\right)^2\right] = \sigma_f^2 \lambda_1 \left[\frac{a_1\sqrt{a_4} + a_1 a_4 a_5 - \sqrt{a_4}\, a_5 + a_2 - a_2 a_3 a_5}{(A\Gamma G)\sqrt{4 A\Gamma G + A^2 L_1^2}\,(1 + a_4 a_5^2 - a_3 a_5)} \right.$$

$$\left. - a_5 \frac{a_1 - a_2 a_5}{(1 + a_4 a_5^2 - a_3 a_5)\lambda_1} \right] \left(\frac{\partial H}{\partial t}\right)^2 \quad . \tag{4.162}$$

Substituting a_1, a_2, a_3, a_4 and a_5 given by (4.157) or (4.158) and (4.22) into (4.162) and taking the limit for $G \to +\infty$ yields

(i) f, a, γ uncorrelated

$$E[(\frac{\partial h}{\partial t})^2] = \frac{\sigma_f^2 \zeta^2}{A^2} (\frac{\partial H}{\partial t})^2 \qquad (4.163)$$

(ii) f, a, γ perfectly correlated

$$E[(\frac{\partial h}{\partial t})^2] = \frac{\sigma_f^2 \zeta^2}{A^2} (\frac{\partial H}{\partial t})^2 \qquad . \qquad (4.164)$$

For G→0 Equation (4.162) yields (in the case of $J_i \frac{\partial H}{\partial x_i} \approx 0$).

(i) f, a, γ uncorrelated

$$E[(\frac{\partial h}{\partial t})^2] = \frac{\sigma_f^2 \lambda_1 [J_1^2 A^2 + \zeta^2 J_1^2 (1-HA)^2]}{AL_1(1+AL_1\lambda_1)} (\frac{\partial H}{\partial t})^2 \qquad (4.165)$$

(ii) f, a, γ perfectly correlated

$$E[(\frac{\partial h}{\partial t})^2] = \frac{\sigma_f^2 \lambda_1 [J_1 A + \zeta J_1 (1-HA)]^2}{AL_1 (1 + AL_1\lambda_1)} (\frac{\partial H}{\partial t})^2 \qquad . \qquad (4.166)$$

For G → −∞, Δ is negative and $E[(\partial h/\partial t)^2]$ is given by

$$E[(\frac{\partial h}{\partial t})^2] = \sigma_f^2 \lambda_1 [\frac{-a_1\sqrt{a_4} - a_1 a_4 a_5 + \sqrt{a_4} a_2 a_5 -a_2 + a_2 a_3 a_5}{(A \Gamma G)(AL_1)(1 + a_4 a_5^2 - a_3 a_5)} -$$

$$-a_5 \frac{a_1 - a_2 a_5}{(1 + a_4 a_5^2 - a_3 a_5)\lambda_1}] (\frac{\partial H}{\partial t})^2 \quad . \tag{4.167}$$

Substituting a_1, a_2, a_3, a_4, a_5 and taking the limit for $G \to 0$, (4.167) produces

    (i) f, a, γ uncorrelated

$$E[(\frac{\partial h}{\partial t})^2] = \frac{\sigma_f^2 \zeta^2}{A^2} [1 + \frac{1}{A L_1 \lambda_1}] (\frac{\partial H}{\partial t})^2 \tag{4.168}$$

    (ii) f, a, γ perfectly correlated

$$E[(\frac{\partial h}{\partial t})^2] = \frac{\sigma_f^2 \zeta^2}{A^2} [1 + \frac{1}{A L_1 \lambda_1}] (\frac{\partial H}{\partial t})^2 \quad . \tag{4.169}$$

Using (4.160) and the asymptotic expressions for $E[h^2]$ derived in Section 4.2.2, produces the following asymptotic expressions for ρ^2, for $G \to +\infty$

    (i) f, a, γ uncorrelated

$$\rho^2 = \frac{\zeta^2 \Gamma^2}{A^2[\Gamma^2(1 + \zeta^2 H^2) + \eta^2]} \quad . \tag{4.170}$$

    (ii) f, a, γ perfectly correlated

$$\rho^2 = \frac{\zeta^2 \Gamma^2}{A^2[\Gamma^2(1 + \zeta^2 H^2) + \eta^2 - 2\eta\Gamma]} \quad . \tag{4.171}$$

For $G \to 0$

(i) f, a, γ uncorrelated

$$\rho^2 = \frac{A^2 + \zeta^2(1 - HA)^2}{A^2(1 + \zeta^2 H^2)}$$

(4.172)

(ii) f, a, γ perfectly correlated

$$\rho^2 = \frac{\lfloor A + \zeta(1 - HA) \rfloor^2}{A^2(1 - \zeta H)^2}$$

(4.173)

while for G → -∞

(i) f, a, γ uncorrelated

$$\rho^2 = \frac{\zeta^2 \Gamma^2}{A^2 \lfloor \Gamma^2(1 + \zeta^2 H^2) + \eta^2 \rfloor}$$

(4.174)

(ii) f, a, γ perfectly correlated

$$\rho^2 = \frac{\zeta^2 \Gamma^2}{A^2 \lfloor \Gamma^2(1 + \zeta^2 H^2) + \eta^2 - 2\eta\Gamma \rfloor}$$

(4.175)

Let us now discuss the implications of the above results. First note that for J_t → 0 we have steady state conditions and it is thus expected that $\partial h/\partial t$ in (3.33) tends to zero. For $J_t \neq 0$ (transient conditions) Equations (4.170) - (4.175) show that ρ^2 depends in general on H. For $J_t \neq 0$ and H large (dry soil), it holds G → ±∞ and ρ^2 is given by (4.170), (4.171), (4.174), (4.175). Note that in this case ρ^2 is independent of the magnitude and sign of J_t, but it depends on H. For large H, (4.170), (4.171), (4.174) and (4.175) simplify even further

163

$$\rho^2 \approx \frac{1}{A^2 H^2} \qquad\qquad (4.176)$$

and since H is large $\rho^2 \ll 1$. For a Maddock soil, for example, and H>100 cm, then $\rho^2 < 0.0046 \ll 1$. This implies that for H relatively large (dry soils) term $\partial h/\partial t$ is much smaller than term K_m AGh in Equation (3.33) and it can be ignored. For small H, (wet soils), G is relatively small. In this case ρ^2 is given by (4.172), (4.173). For H small, these terms are of the order of one. This implies that in the transient case and small H (wet soils) term $\partial h/\partial t$ is of the same order of magnitude as term K_mAGh in Equation (3.33), i.e. $\partial h/\partial t$ is important and cannot be ignored in this case.

The above results have a reasonable physical interpretation. In the transient case in a relatively wet soil, a soil moisture plume tends to move rapidly, especially in the coarser soil layers, due to gravity forces. Because of such rapid movement, the local values of the capillary tension head ψ and its fluctuations $h = \psi - H$ tend to change rapidly with time and $\partial h/\partial t$ is generally not zero. In order to develop models in the case of a relatively wet soil, term $\partial h/\partial t$ must be considered in (4.6). It is possible however, that in such cases of rapid water movement, the whole idea of using a large scale diffusion type mean flow model, similar to the one in (3.18) is not possible. Field observations show that flow in such cases is highly unpredictable and it is possible that even approximate predictive models do not exist in these cases. Nevertheless, most waste disposal situations involve dry soil formations, significant depths to the water table and small rates of leakage. In these cases, it is expected that the vadose zone remains

relatively dry and the movement of the soil moisture plume can be predicted using a diffusion type mean flow model similar to (3.18). The effective parameters of such a model are evaluated in Sections 4.4, 4.5.

4.7 Interpretation of Results

The stochastic theory of transient unsaturated flow in stratified soils produced the following results: (i) the large-scale effective hydraulic conductivities $\hat{K}_{ii}$, the mean soil moisture content θ, and the large-scale effective moisture capacity $\hat{C}$ show significant hysteresis, i.e. their values depend on the mean flow conditions (wetting, drying) and (ii) the effective hydraulic conductivity $\hat{K}_{ii}$ is anisotropic with a degree of anisotropy being dependent on the mean flow conditions.

This section discusses the origin and implications of these results and reviews several field observations for comparison. Section 4.7.1 gives a physical interpretation of the hysteresis and anisotropy of the large-scale parameters. Section 4.7.2 discusses a series of pertinent field observations and compares them to the stochastic theory predictions. Section 4.7.3 discusses the implications of the results of the stochastic theory on practical waste disposal control applications.

4.7.1 Interpretation of Hysteresis and Anisotropy of Large-Scale Unsaturated Flow Parameters

The stochastic theory developed in Chapters 3 and 4 and the expressions derived in Section 4.4 and 4.5 predict that the effective large-scale parameters show hysteresis and anisotropy effects. These large-scale effects were obtained using nonhysteretic and isotropic local parameters. This implies that the predicted large-scale hysteresis and anisotropy are not due to hysteresis and anisotropy of the local parameters but they are due to the existence of spatial variability of

166

the local soil properties. Note that the stochastic theory developed in Chapter 3 can take into account hysteresis and anisotropy of local parameters if such hysteresis and anisotropy exist and can be described mathematically. However, Chapter 4 did not consider such local effects for three reasons: (i) existing mathematical models of local hysteresis are often oversimplified and of unknown reliability, (ii) if local hysteresis and anisotropy were assumed it would be impossible to know whether the predicted large-scale hysteresis and anisotropy are due to spatial variability of soil properties, or to local hysteresis and anisotropy. Also the relative significance of each factor, i.e. local hysteresis and anisotropy and spatial variability, would be unknown and (iii) the soils in the experiments where typical observations of hysteresis and anisotropy are obtained, usually show spatial variability, (e.g. stratification of sand due to gravity forces). Since spatial variability produces hysteresis and anisotropy, it is possible that the hysteresis and anisotropy observed in these experiments are (at least partly) due to spatial soil variability within the experimental apparatus and may not be due to hysteresis and anisotropy of the local parameters (generated from pore scale effects).

The hysteresis and anisotropy results were predicted using the local governing flow equation and a realistic representation of the spatial variability of a stratified soil in terms of three-dimensional statistically anisotropic random fields. A possible physical interpretation of the large-scale hysteresis and anisotropy is given below. Although *highly qualitative*, such physical interpretation is useful since it gives a physical justification and a useful intuitive

interpretation of the mathematical results of the stochastic theory.

Visualize the soil matrix as being composed of many discrete soil layers (i.e. silt, clay, sand, gravel, etc.). The hydraulic soil properties of such a medium vary discretely with depth. This is an approximation to the continuous variability assumption used by the stochastic theory. Consider the movement of the soil moisture plume, generated from a leak from a waste disposal tank (see, e.g. Figures 1.1, 1.2), at times after the leak stops. Assume that the initial soil moisture content is relatively low (high H) and that the leak rate is relatively small, so that it does not saturate the soil matrix. Under the effect of gravity forces the soil moisture plume tends to move vertically, while under the effect of the capillary forces, depending on the capillary tension head gradients, the soil moisture tends to diffuse in all directions. Note that as the plume moves vertically, wetting conditions ($\partial H / \partial t < 0$) prevail at the front part of the soil moisture plume while drying conditions ($\partial H / \partial t > 0$) prevail at the top part of the plume. As will be discussed below such a stratified soil can show a large-scale hysteresis and anisotropy.

The hysteresis and anisotropy of the effective hydraulic conductivities is discussed first. Let us examine the movement of the wetting front of the plume. As the wetting front moves vertically, it encounters a series of dry coarse soil layers. Water meets a relatively large resistance in entering these dry coarse soil layers because at high capillary tensions heads H (dry soils) the unsaturated hydraulic conductivity of coarse layers is very small (see, Figure 4.16). As a result, even when significant vertical gravity and capillary forces

168
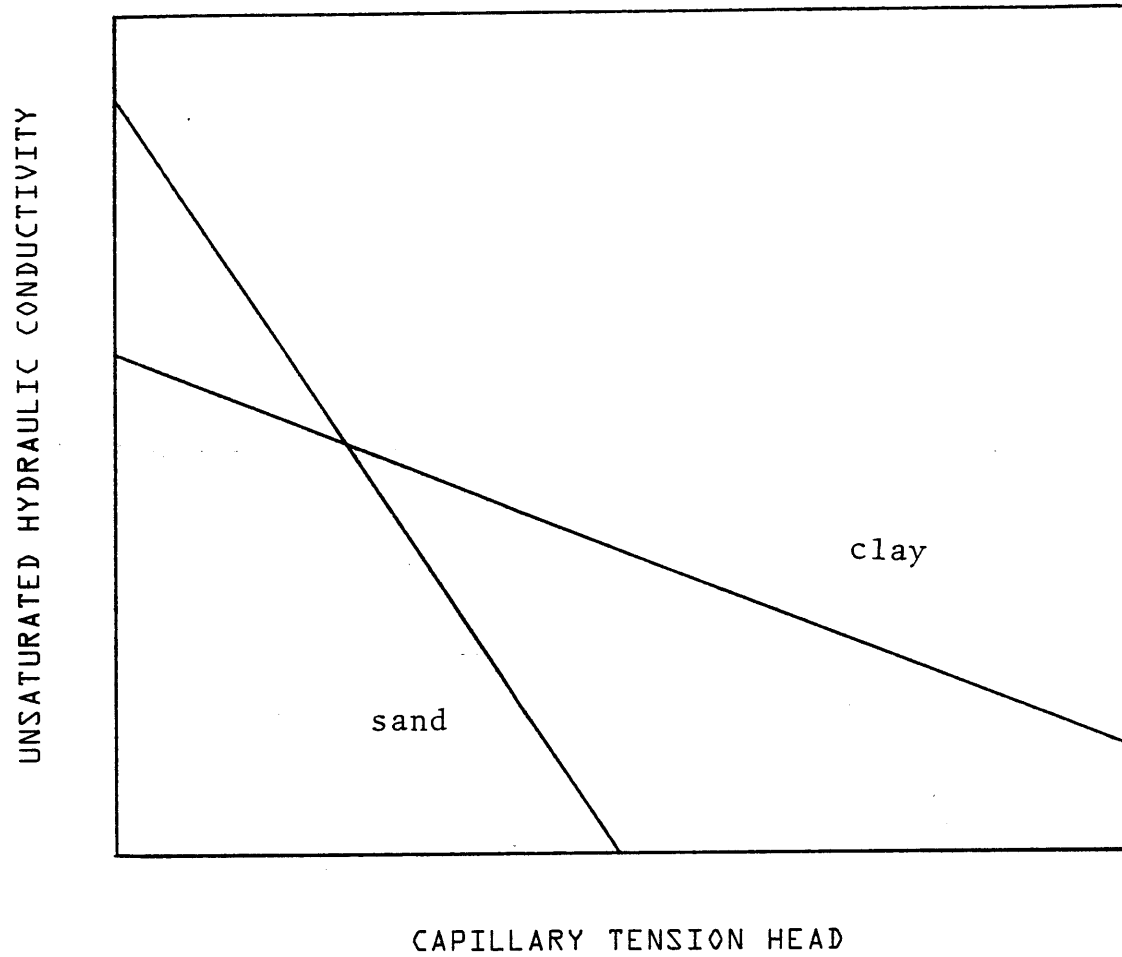
Figure 4.16   Schematic graph showing the dependence of the unsaturated
hydraulic conductivity $K(\psi)$ on the capillary tension head ψ
for a sandy and clayey soil.

exist, the coarse soil layers inhibit the vertical movement of the plume. Because of inhibition of the vertical movement, the soil moisture content in the plume front increases and produces high lateral gradients. Water then tends to spread laterally in the fine soil layers since the unsaturated hydraulic conductivity of fine layers is relatively large even at high H (dry soils), (Figure 4.16). Looking at the overall mean behavior of the system we may conclude that vertical movement is generally inhibited while lateral movement is pronounced at the wetting front of a soil moisture plume. This implies that at the wetting front $(\partial H/\partial t < 0)$, the vertical effective hydraulic conductivity $\hat{K}_{11}$ is small while the lateral effective hydraulic conductivity $\hat{K}_{22}$ is large.

Let us now examine the movement of the drying part of the plume. As the drying part of the plume moves vertically, the coarse layers it encounters are not as dry as in the wetting front (at a given mean capillary tension head), but they are rather wet since the core (i.e. the wettest part) of the plume was previously there. It is expected that these layers do not inhibit vertical movement in this case and water moves with ease vertically through the soil matrix. In addition, since vertical flow is not inhibited, no concentration of the soil moisture, producing large lateral gradients, is expected in the drying part of the plume. Looking at the overall mean behavior of the system we may conclude that water moves with ease vertically and there is no reason for pronounced lateral movement at the drying part of a soil moisture plume. This suggests that in the drying part of the plume, the vertical effective hydraulic conductivity is large while the lateral effective

170

hydraulic conductivity is relatively small.

The above discussion implies that the effective hydraulic conductivities of a stratified soil do not only depend on the capillary tension head but they also depend on the wetting or drying conditions, i.e. they show hysteresis. In addition the effective hydraulic conductivity is anisotropic with a degree of anisotropy depending on the mean flow conditions (wetting or drying). In the case of wetting, the degree of anisotropy is large while in the case of drying, the degree of anisotropy is small. This behavior of the hydraulic conductivities of a stratified soil is in agreement with the stochastic theory results (see, Figures 4.9, 4.10).

A physical interpretation of the hysteresis of the mean soil moisture content and the effective specific soil moisture capacity is now given. It was discussed earlier that the large-scale hysteresis is due to local soil variability and is not due to pore scale effects. It is possible however, to explain this large scale hysteresis by analogy to the ink bottle effect occurring in a pore scale. Figure 4.17 shows an analogy of the large-scale stratified system to a pore having diameters of variable size. As water in the wetting front of the soil moisture plume moves vertically, it encounters difficulty in entering the coarse soil layers, or, by analogy, the large diameter part of the pore model. As a result, the soil moisture content at the wetting front of the plume is relatively small for a given H. In the drying part of the plume however, as water moves vertically it tends to stay in the finer soil layers, or, by analogy, in the small diameter parts of the pore model, and requires additional tension in order to leave these finer soil

171

Stratified Soil   Pore Model

```
─────────────────────  loam
            │
─────────────────────  gravel
            │
─────────────────────  clay
            ↓
─────────────────────  loam

─────────────────────  sand

─────────────────────  clay
```
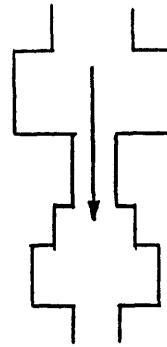
Figure 4.17   An example of a discretely stratified soil and a
              corresponding pore model analog.

layers. This results in a relatively large soil moisture content at the drying part of the plume for a given H. The above discussion suggests that, because of soil property variability, the $\Theta(H)$ curve shows hysteresis. Such large-scale hysteresis and the direction of the hysteresis loop are in agreement with the predictions of the stochastic theory (see Figure 4.15).

The above discussion may provide a physical justification of the stochastic theory. Another point illustrating the existence of large-scale hysteresis is now discussed. The hysteresis observed in a local scale is usually attributed to pore size variations (e.g. ink bottle effect, etc., see, e.g. Bear, 1972, 1979). These variations are a form of microscopic scale spatial variability. Since these microscopic scale variations produce hysteresis of local parameters, it is reasonable to expect that soil property variations in a larger scale also produce a large-scale hysteresis. Since spatial variability is the rule rather than the exception, it is expected that such large-scale hysteresis could be important. It is also possible that the hysteresis observed in the laboratory or in the field, or at least a major part of it, is due to spatial variability of local properties and it is not due to pore scale effects. If this is the case, the stochastic model provides a physically and mathematically justified model for predicting hysteresis. This is important since past models of hysteresis are, to a large degree, arbitrary.

4.7.2 Discussion of Field Observations of Unsaturated Flow

Section 4.7.1 gave a physical interpretation of the large-scale

hysteresis and anisotropy. In order to further investigate the validity of the stochastic theory predictions it is of interest to examine some pertinent large-scale (field) observations. Unfortunately, only few and incomplete field scale observations of unsaturated flow exist. It is thus impossible to quantitatively compare the results of the stochastic theory to real field observations. It is possible however, to perform qualitative comparisons. This section discusses a series of field observations which are qualitatively in agreement with the predictions of the stochastic theory. A large experiment is proposed in the New Mexico desert in order to collect data for validation of the stochastic theory results (see, Waldrop, 1984).

An important result of the stochastic theory is that in stratified soils the vertical effective hydraulic conductivity is small while the lateral effective hydraulic conductivity is large in the wetting front. The degree 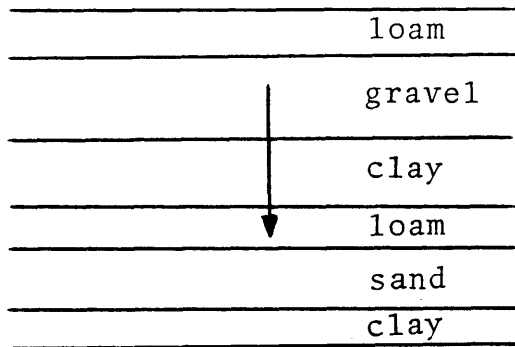of anisotropy of the effective hydraulic conductivities increases as the capillary tension head increases (i.e. the soil dries out). This result has important implications in waste disposal control applications since it implies a relatively small vertical movement and a large lateral spread of contamination. A series of field observations discussed below are in agreement with this result.

Routson, et al., (1979) investigated the time history of leakage beneath a radioactive waste storage tank at Hanford, Washington. The soil formation consists of glaciofluvial deposits with principal units consisting of pebbly and medium sand. The deposits are bedded, and sharp boundaries often exist between sediment types. Bedding consists of thin, nearly horizontal, discontinuous laminations and cross-stratified

174

sedimentary units. The climate where the tank is located is arid and the sediments have a low soil moisture content. In 1973, a leak from a storage tank was observed. Measurements of unsaturated zone contamination, using gamma radiation logs in wells around the tank, indicated significant lateral movement of wastes in the sediment layers, at least at the initial stages of the leak (between 1973-1974). At later stages of the leak, flow is so slow that lateral movement cannot be detected, given that the radioactive decay of tracers is relatively rapid (^{106}Ru has a half life of approximately one year). Plotted isopleths of ^{106}Ru (the main radioactive component of the waste liquid) also show lateral movement. Lateral spread is much larger than the diameter of the tank, while vertical movement is restricted to on the order of ten meters (see Figure 12). The report assumed that the lateral spread is due to unsaturated flow and sediment layering but no physical explanation that leads to such phenomenon was given. Lateral movement is probably due to the relatively high tensions occurring in such dry soil materials. Horizontal stratification enhances such movement, since at high tension hydraulic conductivities of fine textured materials are relatively high and water may prefer to spread laterally in fine beds than to move vertically through coarser ones. These observations are in accordance with the result of the stochastic theory that in dry soils (large H) the lateral hydraulic conductivity is much larger than the vertical effective hydraulic conductivity.

The papers of Crosby et al., (1968, 1971) discussed observations of soil moisture and pollutants below a septic tank drain field area in the Spokane Valley in Washington. The sediments below the drain field

175

consist of glacial outwash deposits and are probably highly stratified.
The environment is also arid. Moisture data in the unsaturated zone
below the drain field indicated unexpectedly high tension conditions
below a depth of 7-10 m. Under such high tensions, gravitational
movement of water cannot be expected. Since water is continuously added
in the drain field the law of conservation of mass requires an accounting
for the lost moisture. The authors assumed that water must be moving
laterally away from the drain field and be removed to the atmosphere by
evapotranspiration. If the assumption about lateral flow is correct,
these field observations also suggest a large lateral effective hydraulic
conductivity compared to the vertical, at high moisture tensions.

Price et al., (1979) reported on the movement of wastes in the
unsaturated zone below a waste disposal crib at Hanford, Washington. The
sedimentary units below the crib are stratified and consist of layers of
medium to very fine sand, pebbly very coarse to medium sand and sandy
silt. The crib is located in an arid environment and the initial soil
moisture of the sediments is relatively low. Sediment samples were
analyzed for radioactivity and isopleths of Pu and Am were plotted.
These data show a lateral movement of wastes in the unsaturated zone
below the crib extending to a width of 10m, encompassing the crib
perimeter. The waste liquid was more prone to spread laterally in the
medium to very fine sand unit than to move deeper into the pebbly very
coarse to medium sand unit. This observation also shows that at
relatively dry stratified soils a high lateral and small vertical
hydraulic conductivity is to be expected.

Knoll and Nelson (1962), described soil moisture movement beneath a

six inch square crib. The soil of the study area consisted of a relatively homogeneous fine sand, except for some thin irregularly placed lenses of a material of slightly different porosity. The soil matrix was initially relatively dry. Water application was controlled so that ponding was always maintained in the crib. The lateral spread of soil moisture was quite significant and was more pronounced at the 2m depth. The authors suggested that this is probably due to the existence of a lens of a slightly more permeable material at this depth. This experiment indicated that for initially relatively dry soil and small size of application area, relative to the observed depth of the unsaturated zone, dry soil conditions below the soil surface enhance the lateral spread of soil moisture. This indicates a large lateral effective hydraulic conductivity at high moisture tensions.

Prill (1977), discussed moisture movement in the unsaturated zone below four artificial groundwater recharge ponds. The alluvial deposits below the ponds consisted of layers of sand and gravel interbedded with clay, silty clay and loam layers. The ponds are circular with 15 m diameters. Before the start of ponding, the soil moisture content in the sediments below the pond was relatively high (with a 70 percent degree of saturation). Measurements of soil moisture content beneath and around the pond (to a depth of 10 m) indicated vertical movement of the moisture front but no significant lateral spread. Wetting front patterns suggested that a major part of the applied water (estimated to be around 90 percent) moved downward beneath the pond. Lateral movement was very slow and was restricted to a short distance even in the finer texture layers. This is probably due to the fact that at high soil moisture

177

contents, gravitational forces may be more important than capillarity forces. This experiment suggests that when the initial soil moisture is high, the water application rate is rapid and the application area is large, relative to the depth of observed unsaturated zone the soil moisture content below the application surface can be large and lateral spread may not be important even in stratified soils. This observation is in agreement with the stochastic theory since for increasing soil moisture content the effective hydraulic conductivity anisotropy ratio is expected to decrease.

The observations by Trautwein and Daniel (1983) are particularly interesting since they sample a very large unsaturated flow system which extends to a depth of 120m below the ground surface. The leakage of waste water in the unsaturated zone beneath a waste disposal evaporation pond was studied. The soil formation consists of alternating layers of sand and clay. Borings in the vicinity of the pond revealed that 20 years after pond construction pond water moved to a depth of 94 m. The authors attempted to model unsaturated flow beneath the pond using a one-dimensional finite element unsaturated flow mode. Functional relationships were assumed for soil moisture characteristic curves and hydraulic conductivity curves at each soil layer, depending on the soil type. These relationships were adjusted so that the results of the model would fit the mean soil moisture data well. Comparing the adjusted model values of saturated hydraulic conductivity K_s to measured laboratory values shows a large discrepancy. Field values are one or two orders of magnitude larger than laboratory values. This suggests that seepage from the pond occurred at a much faster rate than would have been predicted

178

using the laboratory measurements of K_s. Using the laboratory measurements, the model would have predicted that the contaminant front would have moved only a few feet in 20 years, while in actuality the front moved approximately 100m. The large differences between laboratory and field values of K_s are probably due to macroscopic features and natural soil heterogeneity not accounted for in laboratory experiments.

The authors have based their one-dimensional flow assumption on the fact that the dimensions of the pond (500 m x 100 m) are much greater than the thickness of the unsaturated zone (approximately 100 m). However, field investigations of the site (Kent, et al., 1982), show an extremely large lateral spread of water in the unsaturated zone. The contamination plume extends laterally to a distance of about 2000 m around the pond! Some of the lateral spreading at this site may be due to the formation of saturated perched water zones above the water table. Obviously, the one-dimensional assumption does not seem justified. A three-dimensional model is required for a more realistic treatment of the flow in the unsaturated zone of this setting.

In order to complete this discussion some pertinent laboratory experiments are reviewed. Crosby et al. (1968), reported a series of laboratory experiments performed in order to investigate the conditions for lateral movement in stratified soils. Fine, medium and coarse sands were bedded in a sand box model. Water was added to a square inch surface area. Under high water application rates, water essentially moved as saturated masses or ribbons to the bottom of the model. This is in accordance with the observations of Prill et al., (1977), discussed above. Under low water application rates however, capillary dispersion

of water in the finest layers was able to keep in pace with water additions before the lateral boundaries of the laboratory model affected the flow. These observations are also in accordance with the stochastic result of an increasing effective hydraulic conductivity ratio with increasing soil moisture tension H.

Palmquist, et al. (1962), described a laboratory experiment which contains some pertinent observations. A tank model was filled with glass beads forming a porous matrix. Water was applied through a small crib at the upper surface of the porous matrix. A first model consisted of initially dry glass beads of 0.47 mm diameter (corresponding to medium sand size). After water application started the wetted area was confined to a relatively narrow vertical column. A second model consisted of three layers of 0.036 mm diameter glass beads (silt size) separated by two layers of 0.47 mm beads. After water application started, water in the small diameter bead layer initially moved away from the crib at nearby equal vertical and horizontal velocities, until it reached the top of the higher diameter bead layer. Water then tended to move laterally in the fine bead layer instead of moving into the coarser layer. After pressure built up, water eventually moved in the coarser layer. These observations show that soil stratification enhances lateral flow.

The field observations discussed above are in agreement with the predictions of the stochastic theory for anisotropic effective hydraulic conductivities in the case of wetting, with a degree of anisotropy increasing as the mean capillary tension head increases (i.e. soil dries out). These field observations correspond to relatively short times of observations and the movement of the drying part of the soil moisture

180

plume is not observed. It is thus impossible to compare the hysteresis predicted by the stochastic theory to these field observations. Comparison of the hysteresis predicted by the stochastic theory to the hysteresis observed in small field scale and laboratory experiments (see, e.g. Bear, 1979), shows that the hysteresis loops for the vertical hydraulic conductivity and the mean soil moisture content have the same direction as observed ones. Note that hysteresis in such experiments is usually attributed to pore scale effects. Since spatial variability is the rule rather than the exception it is possible that the observed hysteresis, or at least part of it, is due to spatial variability (e.g. sand stratification).

The fact that the hysteresis loops predicted from the stochastic theory are similar to observed ones, strengthens the validity of the stochastic theory and it may suggest that hysteresis observed in experiments may, at least partly, be due to spatial variability and not due to pore scale effects which it is now attributed to (see, e.g. Bear, 1972, 1979).

It was suggested in Section 4.6 that flow in the case of a relatively wet soil can be very rapid and it may not be possible to describe it by a diffusion type equation. Some field observations seem to indicate such behavior. Starr, et al. (1972) provided experimental evidence for the existence of fast flow moving in discrete fingers in a coarse layer of a stratified soil. The soil consisted of a 60 cm layer of sandy loam over a layer of coarse sand. Two experiments were performed. In the first experiment, a steel cylinder 1.8 m in diameter was driven into the soil to a depth of 3.6 m. A depth of 45 cm

of water containing a green dye was infiltrated into the column. After infiltration ended, successive layers of soil were removed from the cylinder and the dye pattern of each newly exposed surface was photographed. In layers near the soil surface a general green hue was observed. Over the cross-sectional areas below 1 m, 12 discrete fingers of flow were observed. The fingers ranged from 5 to 20 cm in diameter and occupied only 5 percent of the total cross-sectional area of the cylinder. These observations suggest that in the case of ponding in this layered, fine over coarse soil, water moves in discrete three-dimensional fingers in the coarse subsoil, rather than as a one-dimensional front. The locations of such fingers may be controlled by natural heterogeneities of the soil, i.e., they may tend to occur in the coarser regions which offer less resistance to flow under wet conditions. Simple calculations show that the flow in such fingers is very rapid. In a second experiment the solute movement under four 4.6 by 6.1 m ponded plots adjacent to the first experiment, was studied. It was observed that several salt pulses reached depths of 120 cm and 180 cm very soon after they had reached the 60 cm depth. Such rapid movement may be due to fast flow in the coarse layer in discrete fingers of flow similar to the ones observed in the first experiment. The paper concludes that water moving through layered field soils may move rapidly in fingers of rapid flow through coarse subsoils. The assumption of a one-dimensional front type flow under these field conditions may lead to gross errors if it is used to estimate the time the solutes arrive at the water table. A similar type of flow moving in discrete fingers in coarse layers of stratified soils were observed in the laboratory experiments

182

discussed in Palmquist, et al. (1982).

Quisenberry and Phillips (1976) studied percolation of rapidly surface-applied water in field soils with strong structure. Several 2.13 by 2.13 m plots were established in two types of soil, Maury silty loam and Huntington silty clay loam. The experiments show that water movement through the profile is characterized by an initial rapid movement of water into the soil and subsequent movement to a depth depending, to a large extent, on the initial water content. The relative increase of water content throughout the profile corresponds very well with the increase in chloride concentration. This suggests that water moved through the profile without displacing much of the initial water. It was assumed that water moved primarily in soil structures called macropores. The amount of displacement that occurs depends on the rate of water movement on the macropores as compared to the soil matrix.

Johnston, et al. (1983) reported preferential flow in pipe-like channels associated with root channels, in lateritic profiles in Western Australia. A 4.4 m by 2.3 m plot was established, and a tracer solution containing Rhodamine and NaCl replaced natural rainfall in the plot. The soil profile underlying the plot consisted of a humus-rich sandy topsoil grading into sandy gravels that, in turn, overlay a weathering profile, developed on both granite and doleritic parent rocks, granitic on the west and doleritic on the east side of the plot. Granite saprolite was coarser grained than the dolerite, and included deep descending roots. Bright Rhodamine WT staining was found around the root channels of the granite saprolite, indicating preferential flow of water in these channels. The tracer solution also moved deeper in the coarser grained

183

granite saprolite, but lateral dispersion was more pronounced in the finer grained dolerite. The lack of evidence of vertical flow in the dolerite is most likely associated with its finer texture. Large continuous voids observed in the dolerite saprolite probably do not conduct water, since these voids would only transmit water if their uppermost extension intersects a saturated layer. The paper concluded that the physical and hydraulic properties of both the clay rich matrix and the more permeable inclusions, the areal frequency of preferential flow paths and their connection with an overlying source of free water, are of paramount importance to their role as structures bypassing the relatively impermeable unsaturated clays.

Thomas and Phillips (1979) also discussed the significance of water movement in macropores. They concluded that water movement in macropores is influenced by the rate of water addition, soil structure, relative sizes of pores, clay orientation, soil water content and tillage. They further discussed the most important consequences of water movement in such macropores. They suggested that recharge of groundwater can begin long before soil reaches field capacity. Also some of the salts in the surface of a soil will be moved to a much greater depth by rain or irrigation, and because of this it is not likely that water will carry a surge of contaminants to groundwater at some time predictable by Darcian flow theory.

Buma (1981) and Beven and German (1982) provided further discussion and evidence of the significance of macropores in vadose zone flow and transport. These papers suggest that rapid flow through macropores depends on moisture content and rate of water application. Large

184

continuous voids will be filled and conduct water only at suctions close to zero (i.e., near saturation). In low moisture conditions these voids are empty and do not contribute to water flow.

The above papers show that when soil is well structured, (i.e., large σ_a^2) and relatively wet, fast gravity flow may be significant. As was discussed in Section 4.6, flow in these cases is probably not characterized by diffusion type laws and it may be impossible to model it using a mean equation of the form of 3.18.

4.7.3 Implications of the Stochastic Theory Results on Waste Disposal Applications

Harmful wastes are presently disposed in facilities near the surface of dry stratified soil formations (see, e.g., Figures 1.1, 1.2). The possibility of leakage from such facilities cannot be overlooked since a high risk to the environment is involved. For a risk assessment evaluation, it is necessary to be able to predict the movement of a contaminant plume if such a leak occurs. Sections 4.7.1 and 4.7.2 discussed the general movement of a soil moisture plume, produced by a leak from a waste disposal tank, as would have been predicted by the stochastic theory developed in this section. Such movement is now compared to the movement that would have been predicted by a classical deterministic model that uses a simple average of local properties as effective parameters.

Consider for example, the waste disposal tank of Figure 4.18. It is assumed that the stratified soil matrix below the tank is initially dry. It is also assumed that the leak rate is relatively small so it

185

does not saturate the soil matrix, and that the rainfall rate is insignificant. The leak generates a soil moisture plume that moves vertically and laterally under the influence of gravity and capillary forces.

At the initial stages of the leak the soil moisture content, in the soil matrix, increases, particularly at the front part of the plume. This implies wetting conditions and a negative $\partial H/\partial t$. Under wetting conditions the stochastic theory predicts a small vertical and a large lateral effective hydraulic conductivity, particularly at a large H (dry soils). It is expected that the vertical movement of the soil moisture plume is relatively small and that the plume spreads laterally at considerable distances. A traditional deterministic model, using as effective hydraulic conductivities an average of the local properties, on the other hand, would have predicted a significant vertical movement (under gravity forces) and a relatively small lateral movement. This situation is depicted in Figure 4.18. This figure shows the shape of the central part (core) of the plume at times t_1, t_2 ($t_1 < t_2$) as predicted by the stochastic theory and as predicted by a simple deterministic model.

Let us now examine the movement of the plume at times after the leak stops. Assume that the soil moisture front has not yet arrived at the water table by the time the leak stops. Under the influence of gravitational forces the soil moisture plume tends to continue moving vertically. At locations at the front part of the plume, soil moisture content tends to increase with time, as the core moves vertically. This suggests wetting conditions ($\partial H/\partial t < 0$) at the front. At locations at

Waste Disposal Tank

t_2 t_1

t_1

t_2

Stratified Sediments

Water Table
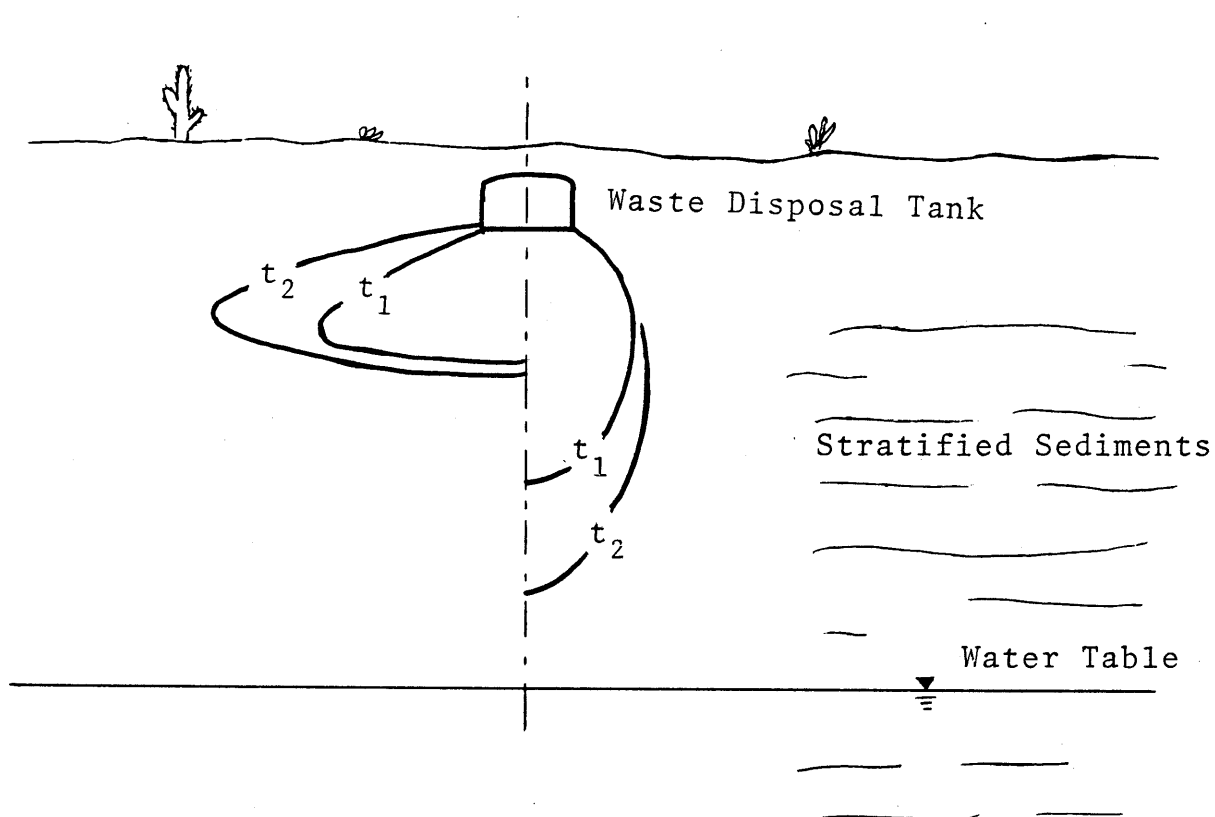
Figure 4.18   Schematic graph showing the movement of a moisture plume
              generated from a leak from a waste storage tank as would
              have been predicted by the stochastic theory developed in
              this chapter and a classical deterministic theory. The
              curves correspond to equal soil moisture levels near the
              core part of the plume and time t_2 is larger than t_1.

187

the top part of the plume however, soil moisture content is expected to decrease with time as the core moves vertically. This suggests drying conditions $(J_t > 0)$. At the central part of the plume, soil moisture content remains relatively constant which implies steady-state conditions. Since wetting conditions prevail at the front part of the plume, it is expected, based on the results of the stochastic theory, that vertical movement of this front is still slow and the plume continues to spread laterally. In the drying part of the plume however, vertical hydraulic conductivities are large. It is thus expected that the top part of the plume (particularly the one near the core where capillary diffusion towards the soil surface is relatively small) moves faster than the wetting part. This situation is depicted in Figure 4.19. This figure shows the movement of the central part (core) of the plume at times t_3, t_4 ($t_3 < t_4$) after the leak has stopped, as would have been predicted by the stochastic theory and by a classical model.

Note that the vertical flow gradient is smaller in the drying part of the plume than it is in the wetting part of the plume. This is because the capillary tension forces oppose gravity forces. Because of the capillary forces, acting in an opposite direction to the direction of flow, part of the soil moisture in the drying part of the plume does not move with the core of the plume but lags behind. This situation is depicted in Figure 4.20. This results in a gradient of J_t being absolutely larger in the wetting front than it is in the drying front (see also discussion in Section 4.5.3).

The general movement of a soil moisture plume described above, based
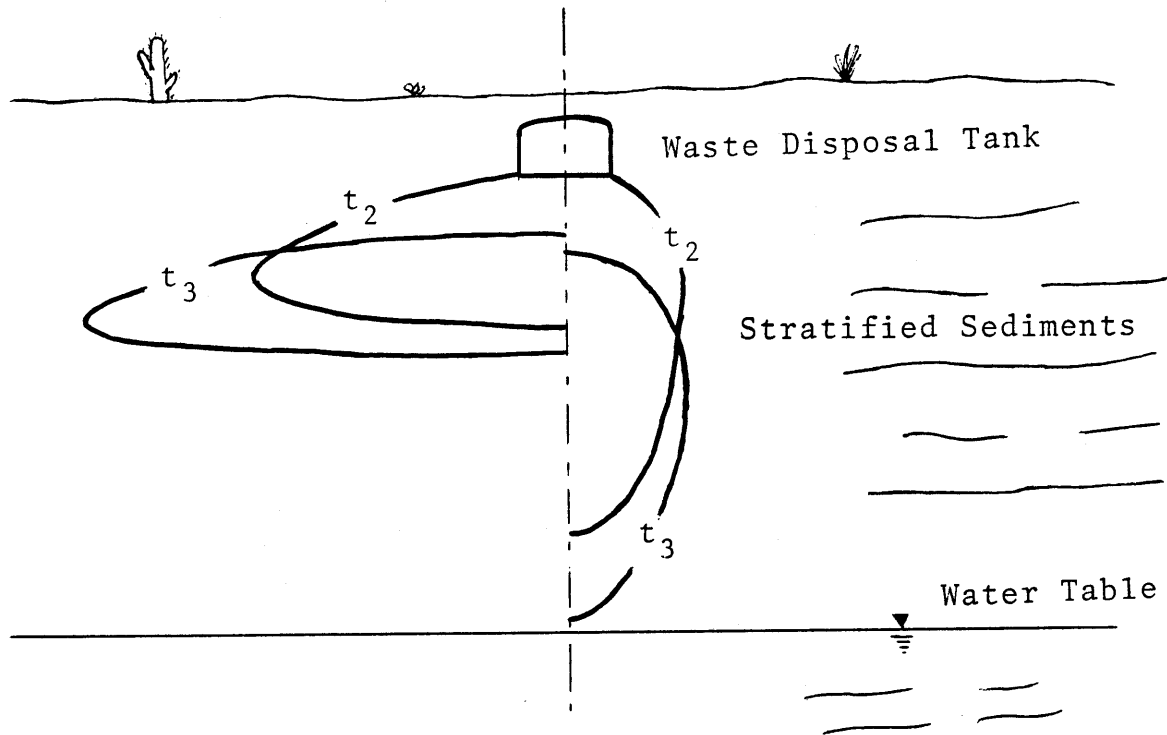
Figure 4.19   Schematic graph showing the movement of the soil moisture
              plume after the leak stops, as would have been predicted by
              the stochastic theory and a classical deterministic theory.
              The curves correspond to equal soil moisture levels near the
              core part of the plume and time $t_3 > t_2$.

Waste Disposal Tank

H = 200 cm

H = 100 cm
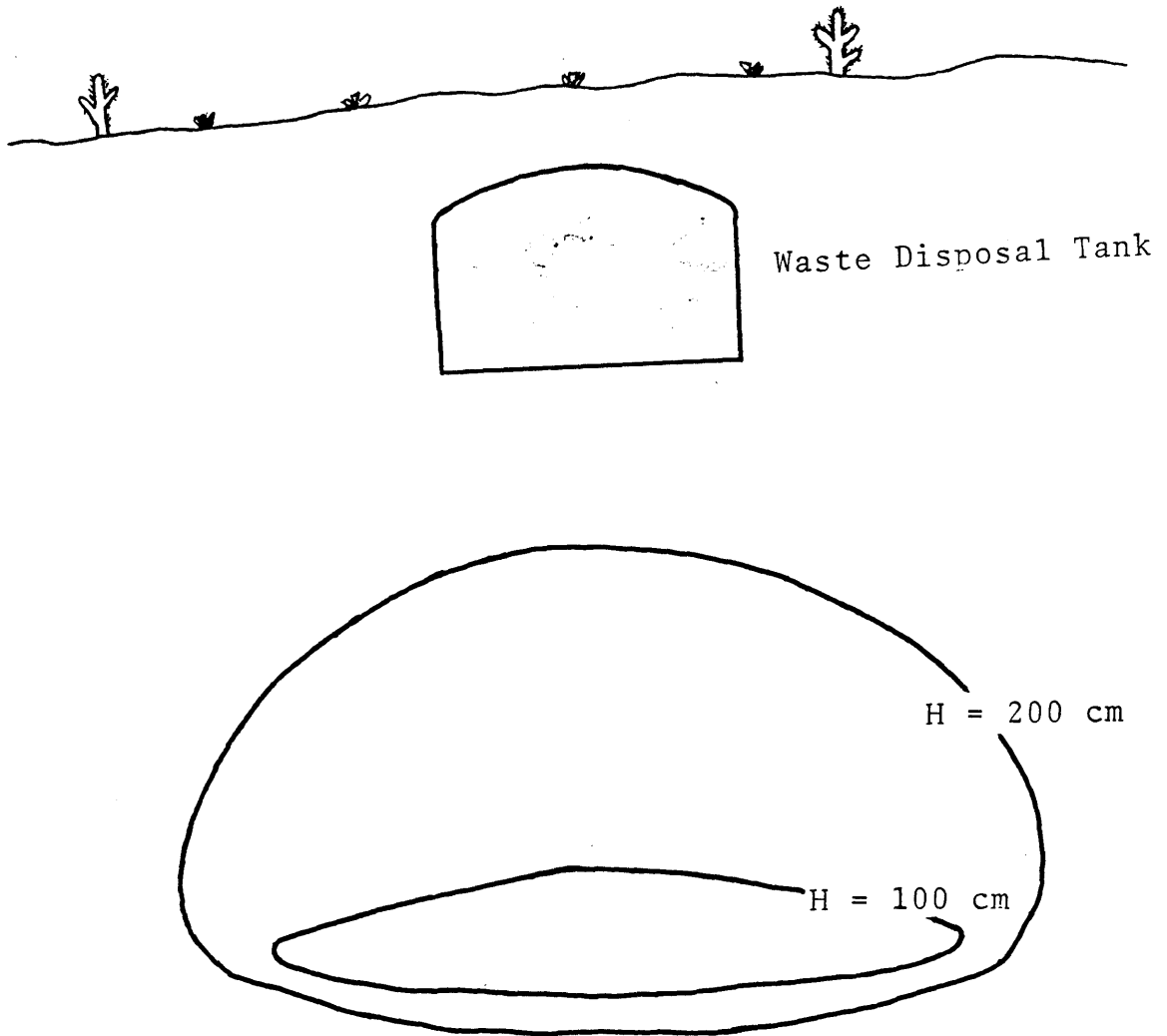
Figure 4.20   Schematic graph showing equal soil moisture levels of the
             soil moisture plume after the leak stops as would have been
             predicted by the stochastic theory.

on the results of the stochastic theory, seems plausible based on physical and intuitive arguments (see, Section 4.7.2). We may conclude that a contamination leak in such arid stratified sediments spreads laterally while vertical movement is relatively slow. As a result, contamination may arrive at the water table much later than what would have been predicted by a classical one-dimensional model and areally extensive contamination may occur. Since evaporation rates in arid climates can be high, it is possible that the contaminated water is removed to the atmosphere by evaporation before reaching the water table. The field data discussed in Section 4.7.2 (e.g., Corsby et al., 1969) suggest such a possibility.

4.8 Summary and Conclusion

This chapter derived effective parameters of large-scale transient unsaturated flow in stratified soils and evaluated the variance of the large-scale model predictions. Such models are required for modeling the unsaturated flow in waste disposal and other applications in the fields of hydrology, agriculture, etc.

The theory of the chapter is developed by six sections. Section 4.2 derived a simplified expression relating the capillary tension head fluctuations to the soil property fluctuations, using the disparity of the correlation scales in stratified soils. Sections 4.3, 4.4 and 4.5 derived closed form expressions for the effective parameters and the variance. Several simplified asymptotic expressions were also derived which are valid at particular ranges of the soil property and the mean flow characteristics. These expressions are useful since they explicitly

191

illustrate the dependence of the effective parameters and the variance on the different soil properties and the mean flow characteristics. Sections 4.3, 4.4 and 4.5 also give several examples for the dependence of the effective parameters and the variance on the mean capillary tension head and its time derivative for two types of soil: the Panoche silty clay loam and the Maddock sandy loam soil. The main findings of Sections 4.3, 4.4 and 4.5 are :

(i)   the effective hydraulic conductivity, the mean soil moisture content and the effective specific soil moisture capacity show significant hysteresis. The hysteresis loops of the vertical and the lateral hydraulic conductivities have opposite directions The vertical hydraulic conductivity is smaller for wetting than it is for drying conditions. However,the lateral hydraulic conductivity, is larger for wetting than it is for drying conditions. The mean soil moisture content is smaller for wetting than it is for drying conditions.

(ii) The effective hydraulic conductivity is anisotropic with a degree of anisotropy depending on the mean capillary tension head and the mean flow conditions. In the case of wetting the degree of anisotropy is large and increases as the mean capillary tension head increases. In the case of drying however, the degree of anisotropy is relatively small (i.e. soil dries out isotropically).

Note that the local parameters used in the stochastic theory are assumed to be nonhysteretic and isotropic. This implies that the predicted hysteresis and anisotropy are due to spatial variability of the local soil properties and they are not due to pore scale effects.

Section 4.6 evaluated the errors due to neglecting term $\partial h/\partial t$ in Section 4.2. It was found that in the transient flow case, term $\partial h/\partial t$ is small when the soil is relatively dry. In the case of a wet soil however, this term cannot be ignored. Since hazardous wastes are usually disposed in relatively dry soils we may infer that the stochastic theory, based on the assumption that $\partial h/\partial t$ is small, is appropriate in these cases. However, in the cases of a relatively wet soil it may be impossible to model the mean flow by a diffusion type mean flow model. Flow in such cases can be very rapid and highly unpredictable (especially in the coarser layers) and may not be governed by a gradient transport relationship. Several field observations suggest such a possibility.

Section 4.7 gave a possible physical interpretation of the large-scale hysteresis and anisotropy, examined a series of field observations showing agreement with the results of the stochastic theory, and discussed the implication of these results on waste disposal control applications. This section showed that the large-scale hysteresis and anisotropy, predicted by the stochastic theory, are physically and intuitively plausible and are in agreement with field observations.

Hysteresis is usually attributed to microscopic pore scale variability (i.e. ink bottle effect, etc.). This chapter has shown that soil property variability also produces hysteresis of the large-scale parameters. The hysteresis loops for the vertical hydraulic conductivity and the soil moisture content observed in experiments, have the same direction as the hysteresis loops predicted from the stochastic theory. The fact that large-scale hysteresis is physically and intuitively plausible might suggest that the hysteresis observed in experiments is at

least partly due to soil variability and not due to pore scale effects. This effect could be anticipated since spatial variability exists even in small scale experiments. If the above implication is true, the stochastic theory provides a mathematically and physically justified model for predicting hysteresis. This is important since models of hysteresis are, to a large degree, arbitrary.

The results of the stochastic theory have important implications on waste disposal control. For example, the stochastic theory predicts that in dry soils a contamination plume tends to spread laterally while vertical movement is slow. As a result, contamination may arrive at the water table much later than is predicted by classical one-dimensional models, and areally extensive contamination could occur.

The large-scale hysteresis and anisotropy results of this chapter are new and were previously unknown in the field. They have important practical implications and they should be considered in the numerical modeling of large-scale unsaturated flow systems.

CHAPTER 5

MACRODISPERSION IN UNSATURATED SOILS

5.1 Introduction

This chapter evaluates effective macrodispersivities in unsaturated soils in the steady state case, using the general theory developed in Chapter 3 and certain simplifications that allow analytical evaluation of the corresponding three-dimensional integrals. Section 5.2 derives some relatively simple expressions for the macrodispersivities in terms of the local dispersivities, the soil property and the mean flow characteristics. The cases of a statistically isotropic or statistically anisotropic soil are examined. Section 5.3 applies the results of the stochastic theory for evaluation of the macrodispersivities corresponding to the Panoche clay loam and the Maddock sandy loam soils, and discusses the implications of the results. Several field observations are also analyzed and are compared to the predictions of the stochastic theory.

5.2 Evaluation of Macrodispersivities

This section evaluates the macrodispersivities A_{ij} in three cases of interest. Section 5.2.1 examines macrodispersion in the case of one dimensional steady vertical infiltration in a statistically isotropic soil, Section 5.2.2 examines macrodispersion in a horizontally stratified soil when the mean flow is perpendicular to stratification while Section 5.2.3 discusses the more general case when a lateral flow gradient exists. These sections provide generic analytical expressions for the macrodispersivities A_{ij}. Analytical evaluation was possible using the fact that the local longitudinal and transverse dispersivities α_L and α_T are relatively small compared to the correlation lengths of the soil properties. The disparity of the correlation scales is also used in the analysis of a stratified soil (Section 5.2.2) to simplify the evaluations.

5.2.1 Statistically Isotropic Soil

This section evaluates the macrodispersivities A_{ij} in the case of a statistically isotropic soil formation, i.e. $\lambda_1 = \lambda_2 = \lambda_3 = \lambda$, using the general theory developed in Chapter 3. Note that the expression for A_{ij} in (3.92) was derived assuming that the coordinate axis x_1 is oriented towards the direction of the mean flow vector $\vec{q}$. The mean flow equation (3.17) predicts the components J_1', J_2', J_3' of the head gradient $\vec{J}$ in a spatially fixed set of axes x_1', x_2', x_3'. In order to evaluate A_{ij} and be able to use the mean transport model (3.71), the magnitude and direction of $\vec{q}$ must be determined as a function of J_1', J_2', J_3'. In the case of a one-dimensional steady

vertical infiltration, $\partial H/\partial x_j$ is relatively small. The assumption $\partial H/\partial x_j \approx 0$ implies small lateral mean gradients. In a statistically isotropic formation, it is expected that under small lateral gradients, lateral flow is relatively small. (This is not true for a statistically anisotropic soil; see Section 5.2.3.) This implies that vector $\vec{q}$ is oriented in the vertical direction, i.e. axis x_1 is oriented towards the vertical direction and that J_1 is approximately equal to the magnitude of $\vec{J}$ which is known.

For $\partial H/\partial x_j$ small it holds $L_j \approx J_j$ and $J_j \partial H/\partial x_j \approx 0$. Equations (3.87), (3.88) and (3.89) then simplify to

$$dZ_{q_i} = K_m \frac{J_1(\delta_{i1} k^2 - k_i k_1)}{k^2 + jAL_1 k_1} \quad (dZf - H \, dZa) \quad . \quad (5.1)$$

Using the spectral representation property (3.51), the cross-spectral density function $S_{q_j q_i}$ is given by

$$S_{q_j q_i} = \frac{1}{d\underline{k}} E\lfloor dZ_{q_j} dZ_{q_i} \rfloor =$$

$$= K_m^2 \frac{J_1^2(\delta_{i1}k^2 - k_i k_1)(\delta_{j1} k^2 - k_j k_1)}{k^4 + A^2 L_1^2 k_1^2} \beta^2 S_{ff}(\underline{k}) \quad (5.2)$$

where an exponential cross-covariance function for f and a, with identical correlation length, is assumed. Parameter β^2 is given by (see discussion in Section 4.3),

(i) f, a uncorrelated

$$\beta^2 = 1 + \zeta^2 H^2 \qquad (5.3a)$$

(ii) f, a perfectly correlated

$$\beta^2 = (1-\zeta H)^2 \qquad (5.3b)$$

where $\zeta^2 = \sigma_a^2/\sigma_f^2$. Substituting (5.2) into (3.92) gives

$$A_{ij} = -\frac{K_m^2 J_1^2 \beta^2}{q^2} \iiint\limits_{-\infty}^{\infty} \frac{(\delta_{i1}k^2 - k_i k_1)(\delta_{j1}k^2 - k_j k_1)}{k^4 + A^2 L^2 k^2}$$

$$\cdot \frac{[-jk_1 + \alpha_L k_1^2 + \alpha_T(k_2^2 + k_3^2)]}{k_1^2 + [\alpha_L k_1^2 + \alpha_T(k_2^2 + k_3^2)]^2} S_{ff}(\underline{k}) \, d\underline{k} \ . \qquad (5.4)$$

The product in the numerator of the first term is expanded to

$\delta_{i1}\delta_{j1}k^4 - \delta_{i1}k^2 k_j k_1 - \delta_{j1}k^2 k_i k_1 + k_i k_j k_1^2$.

Since S_{ff} is an even function of $\underline{k}$, the terms multiplying jk_1, in

(5.4) are odd in k_1, k_2 or k_3 and produce a zero contribution to

the integral. Note also that for $i \neq j$ term $\delta_{i1}\delta_{j1}k^4 = 0$, while

terms $\delta_{i1}k^2 k_j k_1$, $\delta_{j1}k^2 k_i k_1$ and $k_i k_j k_1^2$ are

either zero or odd in k_1, k_2 or k_3. This implies that $A_{ij} = 0$

for $i \neq j$, i.e. in the isotropic case one of the principal axes of the

macrodispersivity tensor is oriented in the direction of the mean flow.

The longitudinal macrodispersivity A_{11} is given by

$$A_{11} = \frac{1}{\gamma^2} \iiint\limits_{-\infty}^{\infty} \frac{(k_2^2 + k_3^2)^2}{k^4 + A^2 L_1^2 k_1^2} \frac{\alpha_L k_1^2 + \alpha_T(k_2^2 + k_3^2)}{k_1^2 + [\alpha_L k_1^2 + \alpha_T(k_2^2 + k_3^2)]^2} S_{ff}(\underline{k}) \, d\underline{k} \qquad (5.5)$$

198

where parameter γ^2 is given by

$$\gamma^2 = \frac{q^2}{K_m^2 J_1^2 \beta^2} \qquad (5.6)$$

and is evaluated later. Using the transformation $u_i = \lambda k_i$ this equation gives

$$A_{11} = \frac{1}{\gamma^2 \lambda^2} \int\int\int_{-\infty}^{\infty} \frac{(u_2^2 + u_3^2)^2}{u^4 + A^2 L_1^2 \lambda^2 u_1^2} \frac{\varepsilon[u_1^2 + \mu(u_2^2 + u_3^2)]}{u_1^2 + \varepsilon^2[u_1^2 + \mu(u_2^2 + u_3^2)]^2}$$

$$\cdot S_{ff}(u_1, u_2, u_3) \, du_1 \, du_2 \, du_3 \qquad (5.7)$$

where $\varepsilon = \alpha_L/\lambda$ and $\mu = \alpha_T/\alpha_L$. An exact analytical evaluation of this integral does not seem possible. However, it is possible to obtain an approximate solution using the fact that $\varepsilon \ll 1$ (see the discussion in Gelhar and Axness, 1983). Note that for $u_1^2 \neq 0$ the integrand in (5.7) is proportional to ε and for $\varepsilon \ll 1$ it has a negligible contribution. The main contribution to the integral comes from $u_1 \approx 0$. Letting $u_1 = \varepsilon v$, (5.7) is then written as

$$A_{11} = \frac{1}{\gamma^2 \lambda^2} \int\int\int_{-\infty}^{\infty} \frac{(u_2^2 + u_3^2)^2}{[(\varepsilon^2 v^2 + u_2^2 + u_3^2)^2 + A^2 L_1^2 \alpha_L^2 v^2]} \frac{\varepsilon^2 v^2 + \mu(u_2^2 + u_3^2)}{\{v^2 + [\varepsilon^2 v^2 + \mu(u_2^2 + u_3^2)]^2\}}$$

$$\cdot S_{ff}(\varepsilon v, u_2, u_3) \, dv \, du_2 \, du_3 \qquad \cdot \qquad (5.8)$$

Taking the limit for $\varepsilon \rightarrow 0$ produces

$$A_{11} = \frac{1}{\gamma^2 \lambda^2} \int\int\int_{-\infty}^{\infty} \frac{(u_2^2 + u_3^2)^2}{(u_2^2 + u_3^2)^2 + A^2 L_1^2 \alpha_L^2 v^2}$$

$$\cdot \frac{\mu(u_2^2 + u_3^2)}{v^2 + \mu(u_2^2 + u_3^2)^2} S_{ff}(0, u_2, u_3) \, dv \, du_2 \, du_3 \, . \qquad (5.9)$$

Substituting for S_{ff} corresponding to an exponential covariance function gives

$$A_{11} = \frac{\sigma_f^2 \lambda \mu}{\pi^2 \gamma^2} \int\int\int_{-\infty}^{\infty} \frac{(u_2^2 + u_3^2)^3}{(u_2^2 + u_3^2)^2 + A^2 L_1^2 \alpha_L^2 v^2}$$

$$\cdot \frac{1}{v^2 + \mu(u_2^2 + u_3^2)^2} \frac{1}{(1 + u_2^2 + u_3^2)^2} \, dv \, du_2 du_3. \qquad (5.10)$$

This integral is evaluated in Appendix G. The longitudinal macrodispersivity A_{11} is given by

$$A_{11} = \frac{\sigma_f^2 \lambda}{\gamma^2} \frac{1}{1 + A L_1 \alpha_T} \, . \qquad (5.11)$$

Note that for $A \alpha_T \rightarrow 0$ this equation is of the same form as Equation (33) of Gelhar and Axness (1983). In this case A_{11} is proportional to λ, i.e. it is connectively controlled.

The longitudinal macrodispersivity A_{22} is given by

200

$$A_{22} = \frac{1}{\gamma^2} \int\int\int_{-\infty}^{\infty} \frac{k_1^2 k_2^2}{k^4 + A^2 L_1^2 k_1^2}$$

$$\cdot \frac{\alpha_L k_1^2 + \alpha_T (k_2^2 + k_3^2)}{k_1^2 + [\alpha_L k_1^2 + \alpha_T (k_2^2 + k_3^2)]^2} \; S_{ff}(\underline{k}) \; d\underline{k} \qquad (5.12)$$

and using $u_i = \lambda k_i$, $\varepsilon = \alpha_L/\lambda$ and $\mu = \alpha_T/\alpha_L$ gives

$$A_{22} = \frac{\alpha_L}{\gamma^2 \lambda^3} \int\int\int_{-\infty}^{\infty} \frac{u_1^2 u_2^2}{u^4 + A^2 L_1^2 \lambda^2 u_1^2}$$

$$\cdot \frac{u_1^2 + \mu(u_2^2 + u_3^2)}{u_1^2 + \varepsilon^2 [u_1^2 + \mu(u_2^2 + u_3^2)]^2} \; S_f(u_1, u_2, u_3) \; du_1 du_2 du_3 \; . \qquad (5.13)$$

Taking the limit for $\varepsilon \to 0$, and substituting for S_{ff} gives

$$A_{22} = \frac{\sigma_f^2 \alpha_L}{\pi^2 \gamma^2} \int\int\int_{-\infty}^{\infty} \frac{u_2^2 [u_1^2 + \mu(u_2^2 + u_3^2)]}{u^4 + A^2 L_1^2 \lambda^2 u_1^2} \; \frac{1}{(1+u^2)^2} \; du_1 du_2 du_3. \qquad (5.14)$$

This integral is analytically evaluated in Appendix H. The resulting transverse macrodispersivity A_{22} is given by

$$A_{22} = \frac{\sigma_f^2 \alpha_L}{\gamma^2} \left(g_1 + g_2 \frac{\alpha_T}{\alpha_L}\right) \qquad (5.15)$$

where g_1, g_2 are functions of $AL_1\lambda$ and they are given by

$$g_1(x) = \frac{1}{x} - \frac{4}{x^2} - \frac{6}{x^3} + \frac{12}{x^4} + \left(-\frac{12}{x^5} + \frac{8}{x^3}\right) \ln(1+x)$$

$$g_2(x) = -\frac{5}{x} + \frac{12}{x^2} + \frac{6}{x^3} - \frac{12}{x^4} + \left(\frac{12}{x^5} - \frac{16}{x^3} + \frac{4}{x}\right) \ln(1+x)$$

(5.16)

where $x = AL_1\lambda$. Functions g_1 and g_2 are plotted in Figure 5.1. Note that for $x \to 0$, g_1, g_2 tend to $g_1 = 1/15$, $g_2 = 4/15$. In this case (5.15) is of the same form as equation (36) of Gelhar and Axness (1983). Note that A_{22} depends on the local dispersivities α_L, α_T but it is independent of the correlation length λ. We conclude that the transverse macrodispersivity in this case is not convection controlled but it is controlled by local dispersion.

In order to be able to evaluate A_{ii}, parameter γ^2, given by (5.6), must be determined. Using (3.13), (5.6) gives

$$\gamma = \frac{\hat{K}_{11}}{K_m \beta}$$

(5.17)

where $\hat{K}_{11}$ the effective vertical hydraulic conductivity given by (3.14) and (3.15). Using Equation (3.5.13) of Yeh (1982) and taking into account variability of the pore side distribution parameter α, gives

$$\hat{K}_{11} = K_m \left[1 + g \, \sigma_f^2 \, \beta^2\right] \quad .$$

(5.18)

where

$$g(x) = \frac{\ln(1+x)}{x} - \frac{1}{2(1+x)} + \frac{3}{x^2} - \frac{1}{x} - \frac{4\ln(1+x)}{x^3} + \frac{1}{x^2(1+x)}$$

(5.19)
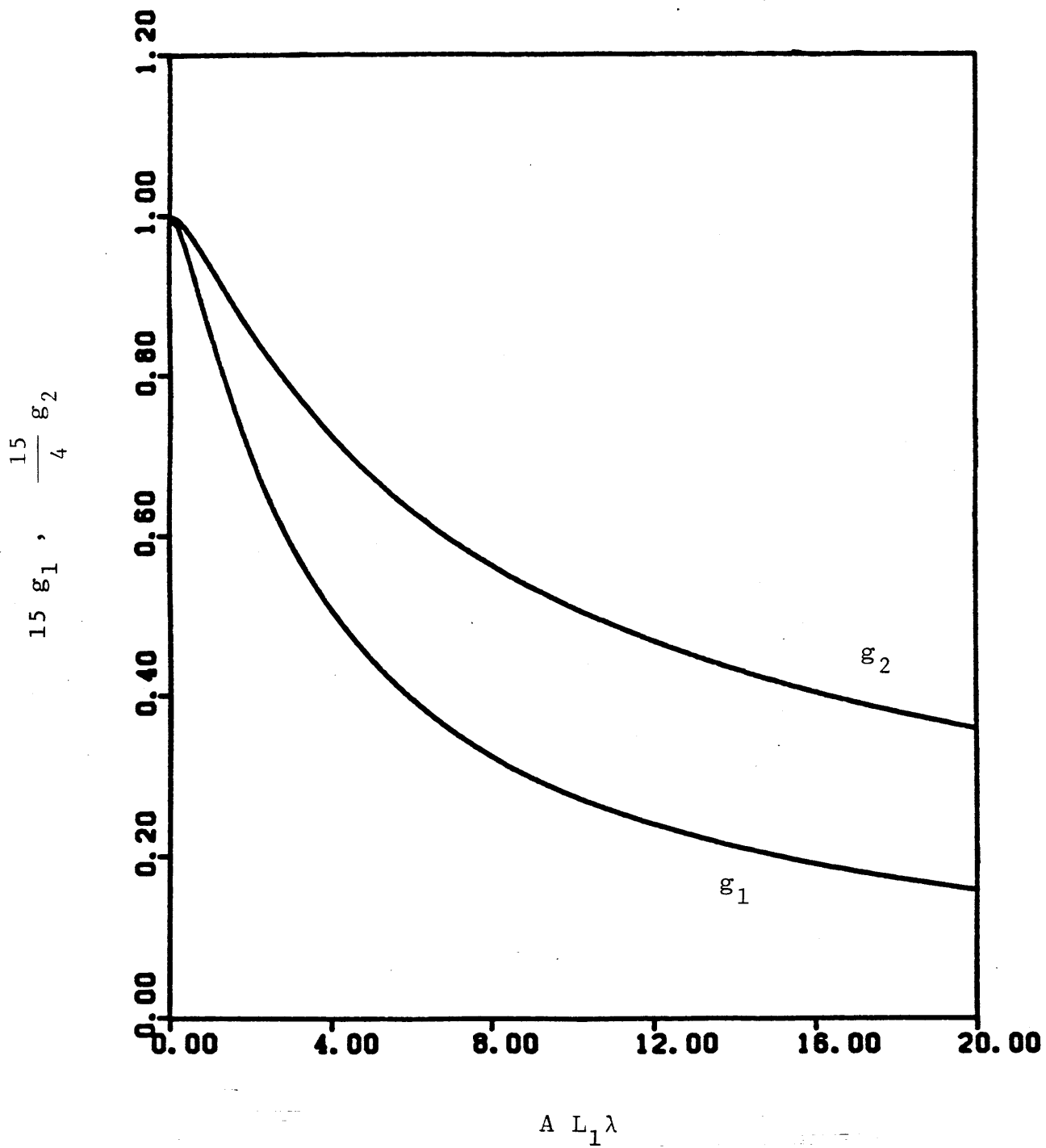
Figure 5.1   Functions g_1, g_2, defined by Equations (5.16), versus $AL_1\lambda$.

and x = $AL_1\lambda_1$. Function g(x) is plotted in Figure 5.2. Note that

for x = $AL_1\lambda_1 \to 0$, $g \to 1/6$. It is possible to use the exponential

modification of the effective hydraulic conductivity discussed in Chapter

4. This modification is physically justified in the stratified soil

case. We preferred not to use this generalization in the isotropic case,

since no physical justification for using such generalization in the

isotropic case exists. Substituting (5.18) Equation (5.17) gives

$$\gamma = \frac{1}{\beta} + g\sigma_f^2\beta \tag{5.20}$$

where β is given by (5.3) or (5.4). Using (5.10), (5.15) and (5.20) it

is now possible to evaluate the macrodispersivities A_{ij}. Section 5.3

gives examples for the dependence of A_{ij} on H and q for the Panoche

clay loam and the Maddock sandy loam soils.

5.2.2 Statistically Anisotropic Soil with the Mean Flow Perpendicular to

       Stratification

This section evaluates the macrodispersivities A_{ij} in the case of

a stratified soil and mean flow perpendicular to stratification. The

case of horizontal stratification with isotropy in the plane of

stratification, zero lateral mean hydraulic gradients and unity vertical

gradient are examined. This case corresponds to steady vertical mean

infiltration where gravity forces dominate. Since a lateral gradient does

not exist the mean specific discharge q is oriented in the downward

vertical direction x_1, and the angle ϕ of Figure 3.1 is zero (see
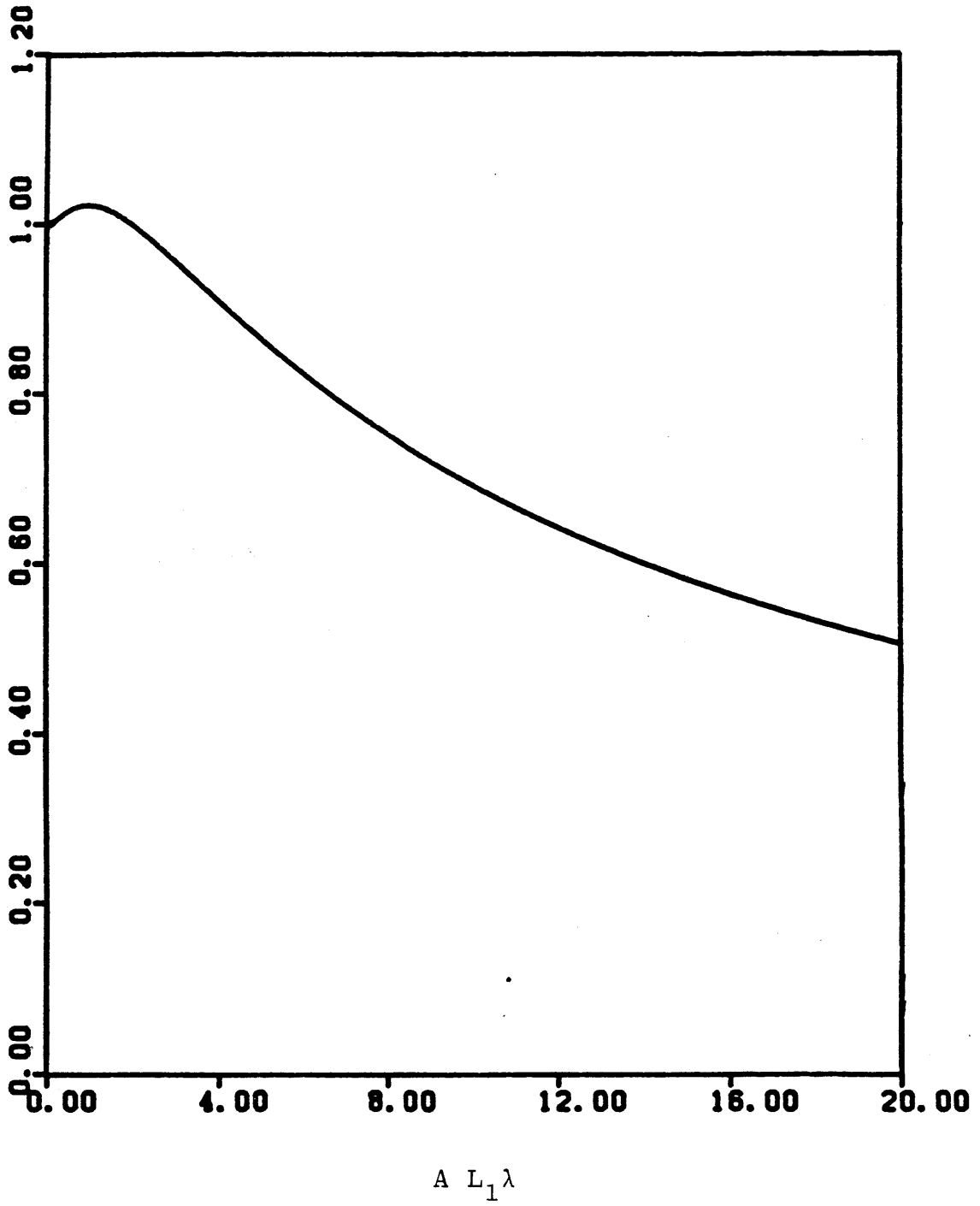
Figure 5.2   Function g, defined by Equation (5.19), versus $AL_1\lambda$.

Section 3.3.3).

Similarly to Section 5.2, the macrodispersivity A_{ij}, in the case of $\partial H/\partial x_j = 0$, is given by (5.4). For axes x_1, x_2, x_3 being oriented in the principal directions of statistical anisotropy, the spectral density function $S(\underline{k})$ in (5.4) is even with respect to k_1, k_2, k_3. Following the discussion in Section 5.2, (5.4) gives $A_{ij} = 0$ for $i \neq j$, while A_{11}, A_{22} are given by (5.5), (5.11), and γ^2 is defined by (5.6). Using the transformation $u_1 = \lambda_1 k_1$, $u_2 = \lambda k_2$, $u_3 = \lambda k_3$, where λ_1 and λ are the correlation lengths in directions perpendicular and parallel to stratification, (5.5) and (5.10) give

$$A_{11} = \frac{\sigma_f^2}{\pi^2 \gamma^2} \delta^4 \lambda_1 \iiint_{-\infty}^{\infty} \frac{(u_2^2 + u_3^2)^2}{[u_1^2 + \delta^2(u_2^2 + u_3^2)]^2 + A^2 L_1^2 \lambda_1^2 u_1^2}$$

$$\cdot \frac{\varepsilon[u_1^2 + \mu\delta^2(u_2^2 + u_3^2)]}{u_1^2 + \varepsilon^2[u_1^2 + \mu\delta^2(u_2^2 + u_2^2)]^2} \frac{1}{(1 + u^2)^2} du_1 du_2 du_3 \qquad (5.21)$$

and

$$A_{22} = \frac{\sigma_f^2}{\pi^2 \gamma^2} \delta^2 \alpha_L \iiint_{-\infty}^{\infty} \frac{u_1^2 u_2^2}{[u_1^2 + \delta^2(u_2^2 + u_3^2)]^2 + A^2 L_1^2 \lambda_1^2 u_1^2}$$

$$\cdot \frac{u_1^2 + \mu\delta^2(u_2^2 + u_3^2)}{u_1^2 + \varepsilon^2[u_1^2 + \mu\delta^2(u_2^2 + u_3^2)]^2} \frac{1}{(1 + u^2)} du_1 du_2 du_3 \qquad (5.22)$$

where $\delta = \lambda_1/\lambda$, $\varepsilon = \alpha_L/\lambda_1$, $\mu = \alpha_T/\alpha_L$.

It is generally impossible to analytically evaluate the integrals in (5.21), (5.22). Using the fact that $\varepsilon \ll 1$, these integrals are further simplified, and it is possible to evaluate analytically. Two cases are examined: (i) $\delta \gg \varepsilon \approx 0$ (mild stratification) and (ii) $\delta \approx 0$ (strong stratification).

Let $\delta \gg \varepsilon$. This implies that the anisotropy ratio $\delta = \lambda_1/\lambda$ cannot be assumed to be zero. Integrals (5.21), (5.22) in this case can be evaluated similarly to the isotropic case using the fact that $\varepsilon \ll 1$. Let $u_1 = \varepsilon v$. Equation (5.21) then gives

$$A_{11} = \frac{\sigma_f^2}{\pi^2 \gamma^2} \delta^4 \lambda_1 \iiint_{-\infty}^{\infty} \frac{(u_2^2 + u_3^2)^2}{[\varepsilon^2 v^2 + \delta^2(u_2^2 + u_3^2)]^2 + A^2 L_1^2 \alpha_L^2 v^2}$$

$$\cdot \frac{\varepsilon^2 v^2 + \mu \delta^2(u_2^2 + u_3^2)}{v^2 + [\varepsilon^2 v^2 + \mu \delta^2(u_2^2 + u_3^2)]^2} \cdot \frac{1}{(1 + \varepsilon^2 v^2 + u_2^2 + u_3^2)^2} \, dv \, du_2 \, du_3. \quad (5.23)$$

Taking the limit for $\varepsilon \to 0$ gives

$$A_{11} = \frac{\sigma_f^2}{\pi^2 \gamma^2} \delta^6 \lambda_1 \mu \iiint_{-\infty}^{\infty} \frac{(u_2^2 + u_3^2)^3}{\delta^4(u_2^2 + u_3^2)^2 + A^2 L_1^2 \alpha_L^2 v^2}$$

$$\cdot \frac{1}{v^2 + \mu^2 \delta^4(u_2^2 + u_3^2)^2} \frac{1}{(1 + u_2^2 + u_3^2)^2} \, dv \, du_2 \, du_3 \quad . \quad (5.24)$$

This integral is evaluated in Appendix I. Substituting from Appendix I gives

$$A_{11} = \frac{\sigma_f^2 \lambda_1}{\gamma^2} \frac{1}{1 + AL_1 \alpha_T} \quad . \quad (5.25)$$

This equation is similar to (5.10), which corresponds to a statistically isotropic soil. Note however, that γ^2 in (5.25) is different than γ^2 in (5.10). The longitudinal macrodispersivity A_{11} is convection controlled in this case as well. The transverse macrodispersivity for $\delta \gg 0$ is evaluated as follows. Taking the limit for $\varepsilon \to 0$, (5.22) simplifies to

$$A_{22} = \frac{\sigma_f^2}{\pi^2 \gamma^2} \delta^2 \, \alpha_L \int\!\!\!\int\!\!\!\int_{-\infty}^{\infty} \frac{u_2^2[u_1^2 + \mu\delta^2(u_2^2 + u_3^2)]}{[u_1^2 + \delta^2(u_2^2 + u_3^2)]^2 + A^2 L_1^2 \lambda_1^2 u_1^2}$$

$$\cdot \frac{1}{(1+u^2)^2} \, du_1 du_2 du_3 \quad . \tag{5.26}$$

Substituting $\alpha_L = \varepsilon\lambda_1$, and given that $\varepsilon \ll 1$, the main contribution to the integral comes from $u_1^2 \approx 0$. Substituting $u_1 = \varepsilon v$ gives

$$A_{22} = \frac{\sigma_f^2}{\pi^2 \gamma^2} \delta^2 \, \lambda_1 \varepsilon^2 \int\!\!\!\int\!\!\!\int_{-\infty}^{\infty} \frac{u_2^2[\varepsilon^2 v^2 + \mu\delta^2(u_2^2 + u_3^2)]}{[\varepsilon^2 v^2 + \delta^2(u_2^2 + u_3^2)]^2 + A^2 L_1^2 \lambda_1^2 \varepsilon^2 v^2}$$

$$\cdot \frac{1}{(1 + \varepsilon^2 v^2 + u_2^2 + u_3^2)^2} \, dv \, du_2 du_3 \tag{5.27}$$

or

$$A_{22} = \frac{\sigma_f^2}{\pi^2 \gamma^2} \lambda_1 \, \beta^2 \int\!\!\!\int\!\!\!\int_{-\infty}^{\infty} \frac{u_2^2[\varepsilon^2 v^2 + \mu\delta^2(u_2^2 + u_3^2)]}{[\beta^2 v^2 + (u_2^2 + u_3^2)^2]^2 + A^2 L_1^2 \lambda_1^2 \varepsilon^2 \delta^4 v^2}$$

$$\frac{1}{(1 + \varepsilon^2 v^2 + u_2^2 + u_3^2)^2} \, dv \, du_2 du_3 \tag{5.28}$$

where $\beta = \epsilon/\delta$. Taking the limit of (5.28) for $\epsilon \rightarrow 0$ gives

$$A_{22} = \frac{\sigma_f^2}{\pi^2 \gamma^2} \lambda_1 \beta^2 \mu \delta^2 \iiint\limits_{-\infty}^{\infty} \frac{u_2^2(u_2^2 + u_3^2)}{[\beta^2 v^2 + (u_2^2 + u_3^2)^2]^2}$$

$$\cdot \frac{1}{(1 + u_2^2 + u_3^2)^2} \, dv du_2 du_3 \quad . \tag{5.29}$$

The integral in (5.29) is evaluated in Appendix J. Substituting from Appendix J gives

$$A_{22} = \frac{\pi \sigma_f^2}{8 \gamma^2} \delta \alpha_T \quad . \tag{5.30}$$

The transverse macrodispersivity in this case is not convectively controlled but it is determined by local dispersion.

The macrodispersivities A_{ij} are now evaluated for δ being very small, (i.e. perfectly stratified soil). The longitudinal macrodispersivity A_{11} is evaluated first. Taking the limit of the second term of the integrand in (5.21) for $\delta^2 \rightarrow 0$, and the limit of the denominator of this term for $\epsilon^2 \rightarrow 0$, gives

$$A_{11} = \frac{\sigma_f^2}{\pi^2 \gamma^2} \delta^4 \lambda_1 \epsilon \iiint\limits_{-\infty}^{\infty} \frac{(u_2^2 + u_3^2)^2}{[u_1^2 + \delta^2(u_2^2 + u_3^2)]^2 + A^2 L_1^2 \lambda_1^2 u_1^2}$$

$$\cdot \frac{1}{(1 + u^2)^2} \, du_1 du_2 du_3 \quad . \tag{5.31}$$

209

given that ϵ^2 and $\delta^2 \approx 0$ the main contribution to this integral comes from $u_1^2 \approx 0$. Substituting $u_1 = \epsilon v$ gives

$$A_{11} = \frac{\sigma_f^2}{\pi^2 \gamma^2} \, \alpha_L \int\!\!\int\!\!\int_{-\infty}^{\infty} \frac{(u_2^2 + u_3^2)^2}{[\beta^2 v^2 + (u_2^2 + u_3^2)]^2 + A^2 L_1^2 \lambda^2 \delta^2 \epsilon^2 v^2}$$

$$\cdot \frac{1}{(1 + \epsilon^2 v^2 + u_2^2 + u_3^2)^2} \, dv \, du_2 du_3 \quad . \tag{5.32}$$

where $\beta^2 = \epsilon^2/\delta^2$ and taking the limit of the integrand for $\epsilon \to 0$ produces

$$A_{11} = \frac{\sigma_f^2}{\pi^2 \gamma^2} \, \alpha_L \int\!\!\int\!\!\int_{-\infty}^{\infty} \frac{(u_2^2 + u_3^2)^2}{[\beta^2 v^2 + (u_2^2 + u_3^2)]^2}$$

$$\cdot \frac{1}{(1 + u_2^2 + u_3^2)^2} \, dv du_2 du_3 \quad . \tag{5.33}$$

This integral is evaluated in Appendix K. The longitudinal macrodispersivity in this case is given by

$$A_{11} = \frac{\pi \sigma_f^2}{4\gamma^2} \, \delta \lambda_1 \quad . \tag{5.34}$$

Note that $A_{11} \to 0$ as $\delta \to 0$. The longitudinal macrodispersivity is convection controlled in this case as well. The transverse macrodispersivity A_{22} in the case of δ being small is now evaluated. Taking the limit of the second term of the integrand in (5.22) for $\delta^2 \to 0$, and the limit of the denominator of this term for $\epsilon^2 \to 0$, (5.22) simplifies to

$$A_{22} = \frac{\sigma_f^2}{\pi^2 \gamma^2} \, \delta^2 \alpha_L \int\int\int_{-\infty}^{\infty} \frac{u_1^2 u_2^2}{[u_1^2 + \delta^2(u_2^2 + u_3^2)]^2 + A^2 L_1^2 \lambda_1^2 u_1^2}$$

$$\cdot \, \frac{1}{(1 + u^2)^2} \, du_1 du_2 du_3 \quad .$$

This integral is evaluated in Appendix L. The transverse macrodispersivity for $\delta^2 \rightarrow 0$ is given by

$$A_{22} = \frac{\sigma_f^2}{2\gamma^2} \, \frac{\alpha_L}{AL_1\gamma_1} \, \delta^2 \, \ln(1 + \frac{1}{\delta^2}) \quad . \tag{5.35}$$

Note that $\delta^2 \ln(1 + 1/\delta^2) \rightarrow 0$ as $\delta^2 \rightarrow 0$. The transverse macrodispersivity is controlled by local dispersion in this case.

Parameter γ^2, in the case of a stratified soil, is evaluated as follows. Using (5.17) and substituting $\hat{K}_{11}$ given by (4.120), which corresponds to the steady state case, yields

$$\gamma = \frac{\exp\left[-\frac{\sigma_f^2}{2} \, \frac{\beta}{1 + AL_1\lambda_1}\right]}{\beta} \tag{5.36}$$

where β is given by (5.3) or (5.4). Section 5.3 gives examples for the dependence of A_{ij} on H and q in the case of a Pannoche clay loam and a Maddock sandy loam soil.

5.2.3 Statistically Anisotropic Soil with Arbitrary Orientation of Mean Flow

This section evaluates the macrodispersivities A_{ij} in the general case when a lateral gradient exists and the mean flow is not

perpendicular to stratification (see Figure 3.1). In this general case,
A_{ij} is given by (3.92), where $S_{q_j q_i}$ are given by (3.87), (3.88)
and (3.89), q is given by (3.94), and the directional cosines a_{ij} are
given by (3.95) and (3.96). This section evaluates A_{ij} in the
particular case of a horizontally stratified soil and $\partial H/\partial x_j$ being
relatively small. The assumption $\partial H/\partial x_j$ small implies small lateral
gradients. In a statistically anisotropic formation however, due to the
large lateral hydraulic conductivities, even small lateral gradients may
produce significant lateral flow (see Chapter 4). We may then conclude
that in this case, the mean specific discharge vector $\vec{q}$ is not oriented
towards the vertical direction x_1' but it is inclined to the vertical
direction with an angle ϕ (see Figure 3.1). Note that the mean flow
model (3.17) predicts the components J_1', J_2', J_3' of the mean
gradient vector $\vec{J}$ in the principal axes of statistical anisotropy. In
order to evaluate A_{ij} (from 3.92) and be able to use the mean transport
model (3.71), the magnitude and direction of $\vec{q}$ must be determined as a
function of J_1', J_2', J_3'. In this section, A_{ij} is evaluated in
two steps. First, A_{ij} is evaluated assuming that $\vec{q}$ is known. Then
vector $\vec{q}$ is evaluated in terms of the gradients J_1', J_2', J_3'.

Assuming that $\partial H/\partial x_j$ is small, it holds that $L_j \approx J_j$ and J_j
$\partial H/\partial x_j \approx 0$. Equations (3.87), (3.88) and (3.89) then simplify to

$$dZ_{q_i} = K_m \frac{J_j(\delta_{ij}k^2 - k_i k_j)}{k^2 + jAL_j k_j} (dZ_f - H\, dZ_a) \quad . \tag{5.37}$$

Using the spectral representation property (3.51), the cross-spectral

212

density function $S_{q_j q_i}$ is evaluated

$$S_{q_j q_i}(\underline{k}) = \frac{1}{d\underline{k}} E[dZ_{q_j} dZ_{q_i}^*)] =$$

$$= K_m^2 \frac{J_m J_n (\delta_{im}k^2 - k_i k_m)(\delta_{jn}k^2 - k_j k_n)}{k^4 + A^2 (L_j k_j)^2} \beta^2 S_{ff}(\underline{k}) \quad (5.38)$$

where β is given by (5.3) or (5.4).

Equation (5.38) is expressed in the system of axes x_1, x_2, x_3 which are not necessarily identical to the principal statistical anisotropy axes x_1', x_2', x_3'. Assuming an exponential covariance function for f and a, and using the transformation $k_i' = a_{ij} k_j$ where a_{ij} are the directional cosines: $a_{ij} = \cos(x_j', x_i)$, $S_{ff}(\underline{k})$ in (5.38) is given by

$$S_{ff}(k_1, k_2, k_3) = \frac{\sigma_f^2 \lambda_1 \lambda_2 \lambda_3}{\pi^2 [1 + \lambda_1^2 (a_{1j}k_j)^2 + \lambda_2^2 (a_{2j}k_j)^2 + \lambda_3^2 (a_{3j}k_j)^2]^2} . \quad (5.39)$$

Substituting (5.38) into (3.92) and noting that the term multiplying jk_1 is odd and therefore has zero contribution to the integral, (3.92) simplifies to

$$A_{ij} = \frac{K_m^2 \beta^2}{q^2} \iiint\limits_{-\infty}^{\infty} \frac{J_m J_n (\delta_{im}k^2 - k_i k_m)(\delta_{jn}k^2 - k_j k_n)}{k^4 + A^2 (L_j k_j)^2}$$

$$\cdot \frac{\alpha_L k_1^2 + \alpha_T (k_2^2 + k_3^2)}{k_1^2 + [\alpha_L k_1^2 + \alpha_T (k_2^2 + k_3^2)]^2} S_{ff}(\underline{k}) \, d\underline{k} . \quad (5.40)$$

213

Expanding the product in the numerator of the first term, the above equation is written as

$$A_{ij} = \frac{1}{\gamma^2 J_1^2} \left[J_i J_j P - J_j J_n Q_{in} - J_m J_i Q_{jm} + J_m J_n R_{ijmn} \right] \qquad (5.41)$$

where γ^2 is given by (5.6) and

$$P = \iiint\limits_{-\infty}^{\infty} \frac{k^4}{k^4 + A^2(L_j k_j)^2} \frac{\alpha_L k_1^2 + \alpha_T(k_2^2 + k_3^2)}{k_1^2 + [\alpha_L k_1^2 + \alpha_T(k_2^2 + k_3^2)]^2} S_{ff}(\underline{k}) \, d\underline{k}$$

$$Q_{ij} = \iiint\limits_{-\infty}^{\infty} \frac{k^2 k_i k_j}{k^4 + A^2(L_j k_j)^2} \frac{\alpha_L k_1^2 + \alpha_T(k_2^2 + k_3^2)}{k_1^2 + [\alpha_L k_1^2 + \alpha_T(k_2^2 + k_3^2)]^2} S_{ff}(\underline{k}) \, d\underline{k} \qquad (5.42)$$

$$R_{ijmn} = \iiint\limits_{-\infty}^{\infty} \frac{k_i k_j k_m k_n}{k^4 + A^2(L_j k_j)^2} \frac{\alpha_L k_1^2 + \alpha_T(k_2^2 + k_3^2)}{k_1^2 + [\alpha_L k_1^2 + \alpha_T(k_2^2 + k_3^2)]^2} S_{ff}(\underline{k}) \, d\underline{k} \quad .$$

Integrals (5.42) are all of the folowing general form

$$I = \iiint\limits_{-\infty}^{\infty} \frac{C(\underline{k})}{k^4 + A^2(L_j k_j)^2} \frac{\alpha_L k_1^2 + \alpha_T(k_2^2 + k_3^2)}{k_1^2 + [\alpha_L k_1^2 + \alpha_T(k_2^2 + k_3^2)]^2} S_{ff}(\underline{k}) \, d\underline{k} \qquad (5.43)$$

where $C(\underline{k})$ is obtained by comparison to (5.42). Using the fact that $\varepsilon = \alpha_L/\lambda_1 \ll 1$, the above integrals can be further simplified. Using the transformation $u_1 = \lambda_1 k_1$ (5.43) becomes

214

$$I = \iiint\limits_{-\infty}^{\infty} \frac{C\left(\frac{u_1}{\lambda_1}, k_2, k_3\right)}{\left(\frac{u_1^2}{\lambda_1^2} + k_2^2 + k_3^2\right)^2 + A^2\left(\frac{L_1 u_1}{\lambda_1} + L_2 k_2\right)^2}$$

$$\cdot \frac{\varepsilon\left[u_1^2 + \mu\lambda_1^2(k_2^2 + k_3^2)\right]}{u_1^2 + \varepsilon^2\left[u_1^2 + \mu\lambda_1^2(k_2^2 + k_3^2)\right]^2} S_{ff}\left(\frac{u_1}{\lambda_1}, k_2, k_3\right) du_1 dk_2 dk_3 \qquad (5.44)$$

where it is assumed that $L_3 = J_3 = 0$. For $u_1^2 \neq 0$ the integrand in (5.44) is proportional to ε and has a negligible contribution. The main contribution comes from $u_1^2 \approx 0$. Let $u_1 = \varepsilon v$. Equation (5.44) then is written as

$$I = \iiint\limits_{-\infty}^{\infty} \frac{C\left(\frac{\varepsilon v}{\lambda_1}, k_2, k_3\right)}{\left(\frac{\varepsilon^2 v^2}{\lambda_1^2} + k_2^2 + k_3^2\right)^2 + A^2\left(\frac{L_1 \varepsilon v}{\lambda_1} + L_2 k_2\right)^2} \cdot$$

$$\cdot \frac{\varepsilon^2 v^2 + \mu\lambda_1^2(k_2^2 + k_3^2)}{v^2 + \left[\varepsilon^2 v^2 + \mu\lambda_1^2(k_2^2 + k_3^2)\right]^2} S_{ff}\left(\frac{\varepsilon v}{\lambda_1}, k_2, k_3\right) dv dk_2 dk_3 \qquad (5.45)$$

and taking the limit for $\varepsilon \to 0$

$$I = \iiint\limits_{-\infty}^{\infty} \frac{C(0, k_2, k_3)}{(k_2^2 + k_3^2)^2 + A^2 L_2^2 k_2^2} \frac{\rho}{v^2 + \rho^2} S(0, k_2, k_3) dv dk_2 dk_3 \qquad (5.46)$$

where

$$\rho = \mu\lambda_1^2(k_2^2 + k_3^2) \quad . \quad \text{Using}$$

215

$$\int_{-\infty}^{\infty} \frac{\rho}{v^2 + \rho^2} \, dv = \pi \tag{5.47}$$

Equation (5.46) simplifies to

$$I = \pi \iint_{-\infty}^{\infty} \frac{C(0,k_2,k_3)}{(k_2^2 + k_3^2)^2 + A^2 L^2 k_2^2} \, S(0,k_2,k_3) \, dk_2 dk_3 \quad . \tag{5.48}$$

The spectral density function $S(0,k_2,k_3)$ is given by (5.39) where now $k_1 = 0$. Using (3.96), (5.48) is written as

$$I = \frac{\sigma_f^2 \lambda_1^2 \lambda^2}{\pi} \iint_{-\infty}^{\infty} \frac{C(0,k_2,k_3)}{(k_2^2 + k_3^2)^2 + A^2 L_2^2 k_3^2}$$

$$\cdot \frac{1}{[1 + \lambda_1^2 \sin^2\phi k_2^2 + \lambda^2 \cos^2\phi k_2^2 + \lambda^2 k_3^2]^2} \, dk_2 dk_3 =$$

$$\tag{5.49}$$

$$= \frac{\sigma_f^2 \lambda_1^2 \lambda^2}{\pi} \iint_{-\infty}^{\infty} \frac{C(0,k_2,k_3)}{(k_2^2 + k_3^2)^2 + A^2 L_2^2 k_2^2} \frac{1}{(1 + b^2 k_2^2 + \lambda^2 k_3^2)^2} \, dk_2 dk_3$$

where

$$b^2 = \lambda_1^2 \sin^2\phi + \lambda^2 \cos^2\phi \tag{5.50}$$

and ϕ is the angle between axes x_1' and x_1 (see Figure 3.1). Using the transformation $u_2 = bk_2$, $u_3 = \lambda k_3$ the above integral is expressed as

$$I = \frac{\sigma_f^2 \lambda_1 \lambda}{\pi b} \iint_{-\infty}^{\infty} \frac{b^4 C(0, \frac{u_2}{b}, \frac{u_3}{\lambda})}{(u_2^2 + \xi^2 u_3^2)^2 + A^2 L_2^2 b^2 u_2^2} \frac{1}{(1 + u^2)^2} \, du_2 du_3 \tag{5.51}$$

216

where

$$\xi^2 = \frac{b^2}{\lambda^2} = \frac{\lambda_1^2}{\lambda^2} \sin^2\phi + \cos^2\phi \quad . \tag{5.52}$$

Note that in general ξ^2 and $A^2 L_2^2 b^2$ are not zero. Using (5.41) and (5.51) the macrodispersivities A_{ij} are evaluated as follows:

$$A_{11} = \frac{\sigma_f^2 \lambda_1 \lambda}{\pi \gamma^2 b} (T_{22} + 2\xi^2 T_{23} + \xi^4 T_{33})$$

$$A_{22} = \frac{\sigma_f^2 \lambda_1 \lambda}{\pi \gamma^2 b} \frac{J_2^2}{J_1^2} \xi^4 T_{33}$$

$$A_{33} = \frac{\sigma_f^2 \lambda_1 \lambda}{\pi \gamma^2 b} \frac{J_2}{J_1^2} \xi^4 T_{23} \tag{5.53}$$

$$A_{12} = \frac{\sigma_f^2 \lambda_1 \lambda}{\pi \gamma^2 b} \frac{J_2}{J_1} \xi^2 (T_{23} + \xi^2 T_{33})$$

and $A_{21} = A_{12}$, $A_{13} = A_{31} = A_{23} = A_{32} = 0$, where

$$T_{22} = \iint\limits_{-\infty}^{\infty} \frac{u_2^4}{(u_2^2 + \xi^2 u_3^2)^2 + A^2 L_2^2 b^2 u_2^2} \frac{1}{(1+u^2)^2} du_2 du_3$$

$$T_{23} = \iint\limits_{-\infty}^{\infty} \frac{u_2^2 u_3^2}{(u_2^2 + \xi^2 u_3^2)^2 + A^2 L_2^2 b^2 u_2^2} \frac{1}{(1+u^2)^2} du_2 du_3 \tag{5.54}$$

$$T_{33} = \iint\limits_{-\infty}^{\infty} \frac{u_3^4}{(u_2^2 + \xi^2 u_3^2)^2 + A^2 L_2^2 b^2 u_2^2} \frac{1}{(1+u^2)^2} du_2 du_3$$

217

In Appendix M, integrals T_{22}, T_{23}, T_{33} are reduced to one dimensional integrals, which require further numerical integration. Note that the mean flow (3.17), predicts the components of the gradient $\vec{J}$ in the axes of statistical anisotropy x_1', x_2', x_3'. In order to be able to use Equations (5.53) and the mean transport model (3.71), parameters γ, ξ and the components of $\hat{J}$ on axes x_1, x_2, x_3 must be evaluated. This requires evaluation of the direction and magnitude of the mean flow vector $\vec{q}$.

Using Equation (3.13), the mean flow in the direction of the axes x_1' and x_2' can be expressed as follows

$$\bar{q}_i' = \hat{K}_{ii} \bar{J}_i' \tag{5.55}$$

where $\hat{K}_{ii}$ must be evaluated for J_1', J_2', J_3'. Assuming that $J_1' \approx 1$, $J_2' \approx 0$ and $J_3' = 0$, it is possible to approximate these effective hydraulic conductivities to the effective hydraulic conductivities corresponding to $J_1' = 1$, $J_2' = 0$ and $J_3' = 0$. The effective hydraulic conductivities in the case of a stratified soil have been evaluated in Section 3.4. Using (4.120), which corresponds to the steady state and substituting β, given by (5.3) or (5.4) we obtain

$$\bar{q}_1 = K_m \exp\left\{ -\frac{\sigma_f^2}{2} \frac{\beta^2}{1+AL_1\lambda_1} \right\} J_1' = K_m \rho_1 J_1'$$

$$\tag{5.56}$$

$$\bar{q}_2 = K_m \exp\left\{ \frac{\sigma_f^2}{2} \frac{\beta^2}{1+AL_1\lambda_1} \right\} J_2' = K_m \rho_2 J_2'$$

where the definition of ρ_1, ρ_2 in (5.56) is obvious. The mean specific discharge then is given by

$$q = K_m \left(\rho_1^2 J_1'^2 + \rho_2^2 J_2'^2 \right)^{1/2} \qquad (5.57)$$

while the directional angle ϕ, between axes x_1, x_1' (see Figure 3.1) is given by

$$\phi = \text{arctg} \left(\frac{\bar{q}_2}{\bar{q}_1} \right) = \text{argtg} \left\{ \exp \left[\sigma_f^2 \frac{\beta^2}{1 + AL_1 \lambda_1} \right] \frac{J_2'}{J_1'} \right\} = \text{arctg} \left[\frac{\rho_2}{\rho_1} \frac{J_2'}{J_1'} \right] . \quad (5.58)$$

Given the values of ϕ and J_1', J_2', the components of $\vec{J}$ in the axes x_1, x_2, x_3 can be evaluated using $J_i = a_{ji} J_j'$, or

$$J_1 = J_1' \cos \phi + J_2' \sin \phi$$

$$J_2 = -J_1' \sin \phi + J_2' \cos \phi \qquad . \qquad\qquad (5.59)$$

Substituting (5.57) and (5.59), (5.6) gives

$$\gamma^2 = \frac{\rho_1^2 J_1'^2 + \rho_2^2 J_2'^2}{\beta^2 (J_1 \cos \phi + J_2 \sin \phi)^2} \qquad . \qquad (5.60)$$

Parameter ξ is given by (5.52). In conclusion, if J_1', J_2' and H are known, the effective macrodispersivities A_{ij} are evaluated from (5.52) where parameters ξ, γ^2, J_1, J_2 are given by (5.52), (5.60), (5.59) and q and ϕ are given by (5.57) and (5.58).

In the case of $J_2' \to 0$, it holds $q = \bar{q}_1$, and $\phi = 0$. Equation (5.52) then yields $A_{11} = \sigma_f^2 \lambda_1 / \gamma^2$ and $A_{22} = A_{33} = A_{12} = 0$. A similar result was derived in Section 5.3 (see Equation 5.25). Note that in the general case of $J_2' \neq 0$, the lateral macro-

dispersivities A_{22}, A_{33}, A_{12}, evaluated using (5.52), are non

zero. We conclude that in this case the transverse hydraulic gradient

J_2' may cause a relatively large convectively controlled transverse

dispersion.

5.3   Applications, Discussion and Comparisons to Field Observations

This section gives examples of application of the stochastic theory, and compares the results to field observations.   Section 5.3.1 evaluates the macrodispersivities corresponding to the Panoche clay loam and the Maddock sandy loam soil using the theory developed in Section 5.2, and gives an interpretation of these results.   Section 5.3.2 discusses and analyzes several field observations and compares them to the predictions of the stochastic theory.

5.3.1   Applications and Discussion of Results

The macrodispersivities A_{ij} and the bulk macrodispersion coefficient $\hat{E}_{ij}$, are evaluated as a function of the mean capillary tension head and the mean specific discharge for the Panoche clay loam and a Maddock sandy loam soil (see Chapter 2).   The cases of a statistically isotropic and a stratified soil, with flow perpendicular to bedding, are examined.   It is assumed that the soil property fluctuations f and a are uncorrelated.

Figure 5.3 plots the longitudinal macrodispersivity A_{11} as a function of the mean capillary tension head H using (5.11), (5.20) and (5.3), assuming that $\alpha_L = \alpha_T = 1$ cm, and $\lambda = 100$ cm.   Figure 5.4 plots the transverse macrodispersivity A_{22} as a function of H using (5.15), (5.16), (5.20) and (5.3).   These plots correspond to an isotropic soil formation.   These figures show that as H increases, (i.e., soil desaturates), A_{11} and A_{22} initially increase.   After reaching a maximum value, A_{11} and A_{22} start to monotonically decrease for increasing H.   This behavior can be explained as follows.

Figure 5.3   Longitudinal macrodispersivities A_{11} versus mean capillary
tension head H for an isotropic soil with λ = 100 cm and
$\alpha_L = \alpha_T$ = 1 cm.

Figure 5.4   Transverse macrodispersivities A_{22} versus mean capillary
              tension head H for an isotropic soil with $\lambda = 100$ cm and
              $\alpha_L = \alpha_T = 1$ cm.

223

Assume that the soil matrix is initially saturated (H = 0). When H increases, the coarser volumes of the soil start to desaturate and the flow goes around them through the finer soil paths. In this case, flow has to follow a more tortuous path than the one in the saturated case. This results in an A_{ii} which initially increases as H increases. As the soil matrix continues to desaturate however, the finer soil volumes begin to desaturate. It is then possible that the continuity of the flow paths is interrupted, i.e. volumes of fine soil may contain stagnant water masses which cannot move since they are impeded by a relatively coarse soil. It is expected then that, at large H, the macro-dispersivities A_{ii} decrease for increasing H. Wilson (1974), predicted a similar type of dependence of A_{ii} on the soil moisture content using a microscopic statistical pore scale model. The dependence of A_{ij} on H, in our model, is due to spatial variability and not to pore scale effects, since such effects were not considered. We may then conclude (similarly to Chapter 4) that spatial variability and microscopic (pore scale) variability produce similar effects.

Figure 5.3 shows that for H small, the longitudinal macro-dispersivity for the Maddock soil is larger than the one for Panoche soil. This is probably due to the larger variability of the saturated hydraulic conductivity in the Maddock soil. As H increases however, A_{11} in the Maddock soil drops relatively fast while the A_{11} corresponding to the Pannoche soil remains more constant. This is probably due to the fact that the Maddock soil has a larger variety of textures than the Panoche soil. Because of this, it is expected that as the Maddock soil desaturates the coarser volumes of soil empty quickly.

This generates immobile water masses in the finer soil volumes. This may explain the fast decrease of A_{ii} for increasing H in this soil. In the relatively uniform Panoche soil however, the soil desaturates almost uniformly throughout the soil formation and immobile soil water volumes are not generated. This could explain the insensitivity of A_{ii} on H, shown in Figures 5.3, 5.4.

Comparison of Figure 5.3 to 5.4 shows that the longitudinal macrodispersivity A_{ii} is much larger than the transverse macrodispersivity A_{22}. As (5.11) shows, A_{11} is proportional to λ_1 and it is governed by convective flow. The transverse macrodispersivity A_{22} however, given by (5.15), is proportional to the local dispersivities. This implies that the transverse macrodispersivity in this case, is governed by local dispersion. This explains the fact that A_{11} is significantly larger than A_{22}.

In the one-dimensional steady state infiltration case examined in Sections 5.2.2, 5.2.3, there is a one to one dependence of the mean specific discharge $q = \hat{K}_{11}$ to the mean capillary tension head H. It is of interest to evaluate the dependence of the macrodispersivities A_{ii} to the mean specific discharge q. For the set of values of H shown in Figure 5.3, 5.4, A_{ii} are evaluated from (5.18), (5.11) and (5.15). Figure 5.5 and 5.6 plot the longitudinal and transverse macrodispersivities as a function of q. These figures show that at large q, A_{ii} are practically independent of q. For q small however, A_{ii} depend on q. To further illustrate a point, Figures 5.7 and 5.8 plot the bulk macrodispersion coefficients $\hat{E}_{ii} = A_{ii}q$ as a function of q. These curves resemble a linear dependence of $\hat{E}_{ii}$ on q. Note
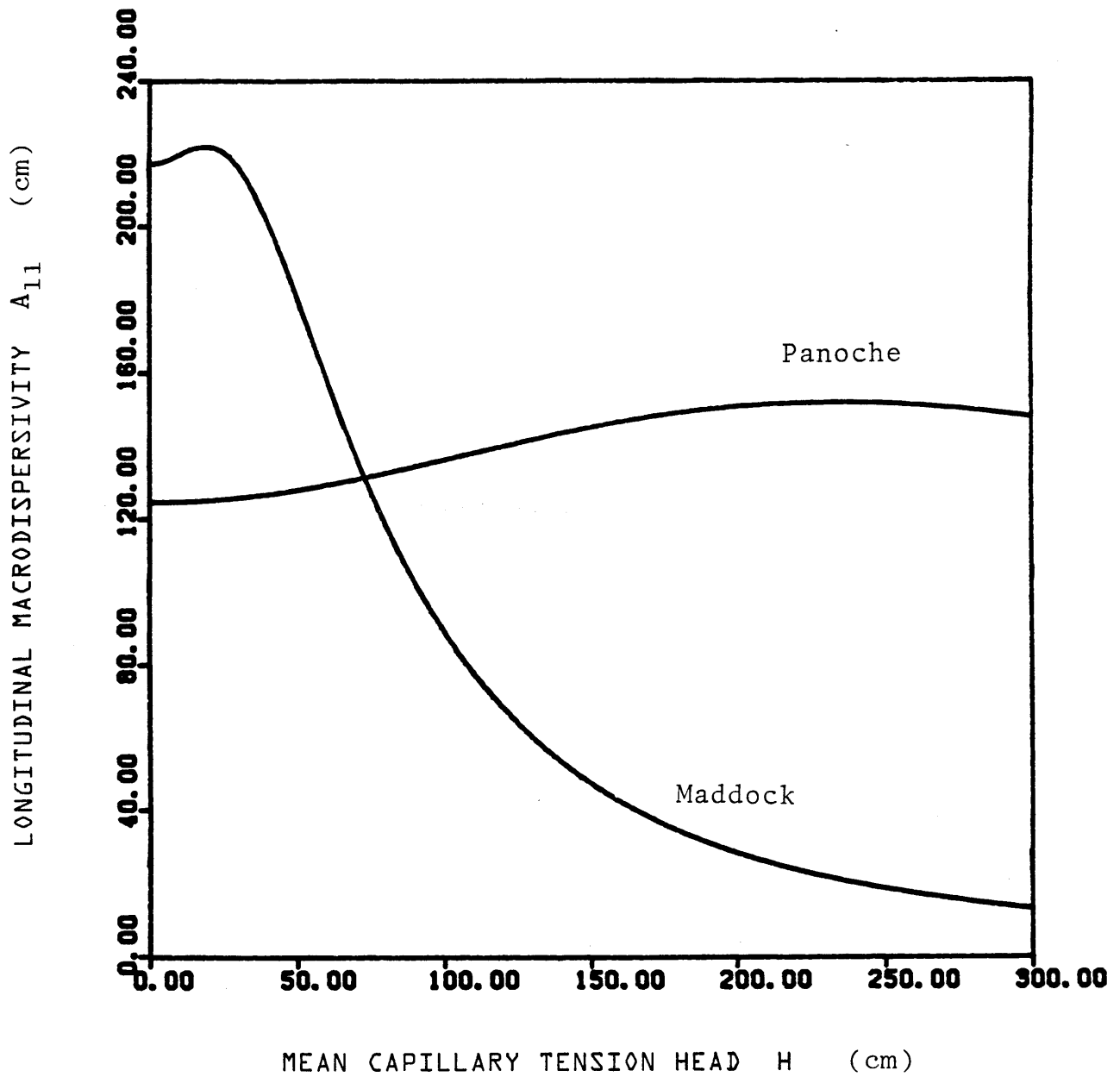
225
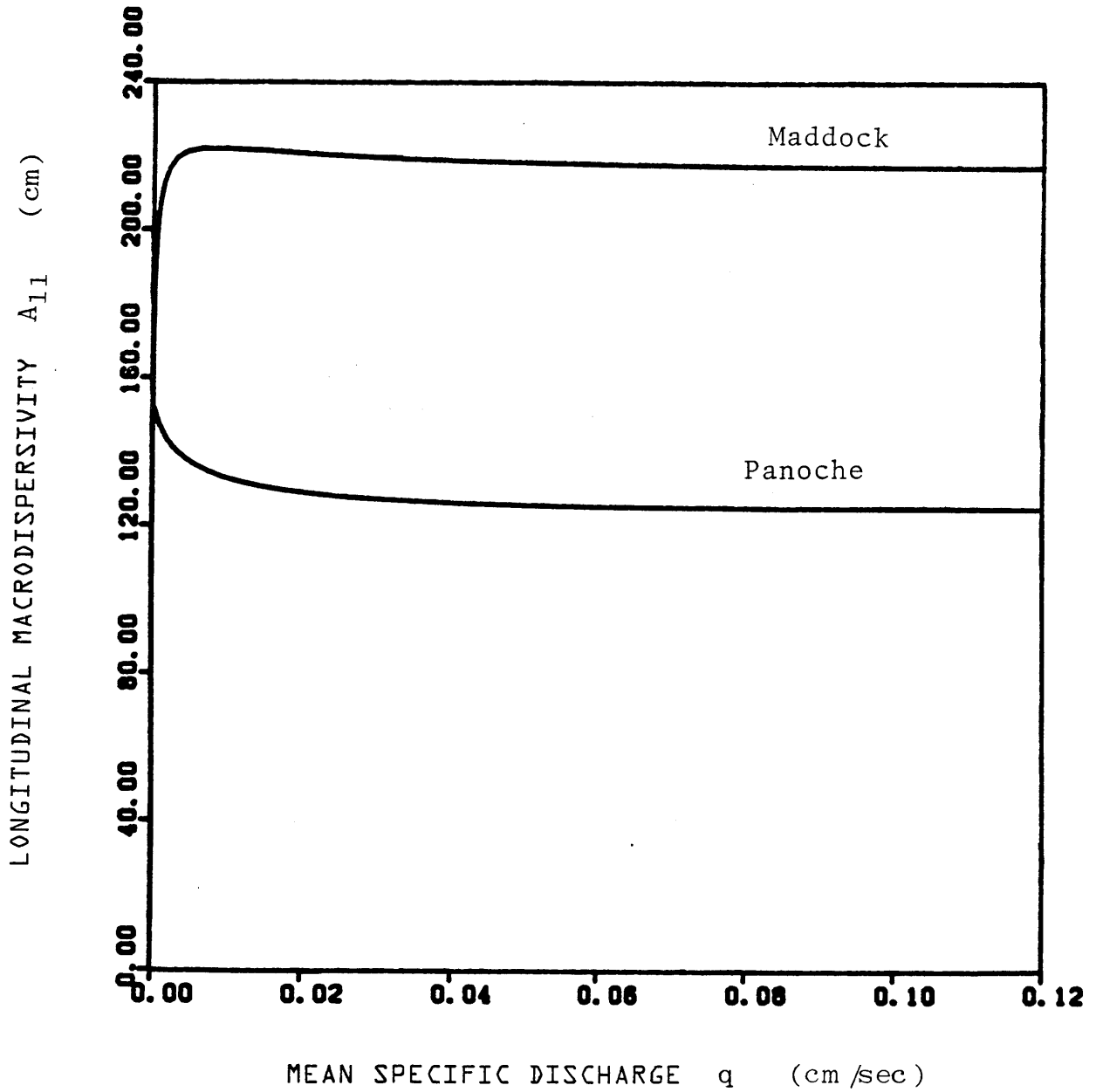
Figure 5.5 Longitudinal macrodispersivities A_{11} versus mean specific
discharge q for an isotropic soil with λ = 100 cm and
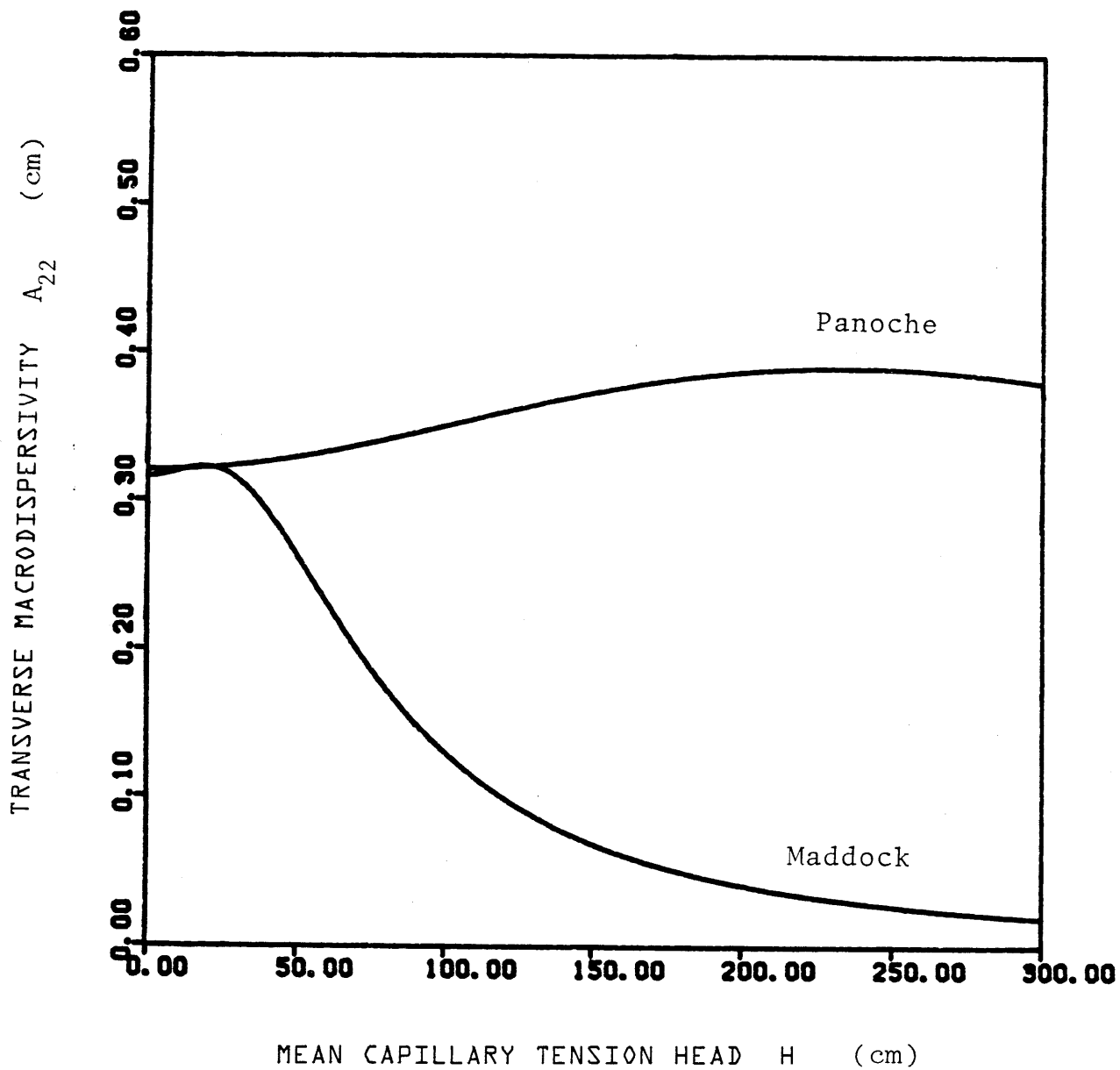$\alpha_L = \alpha_T = 1$ cm.
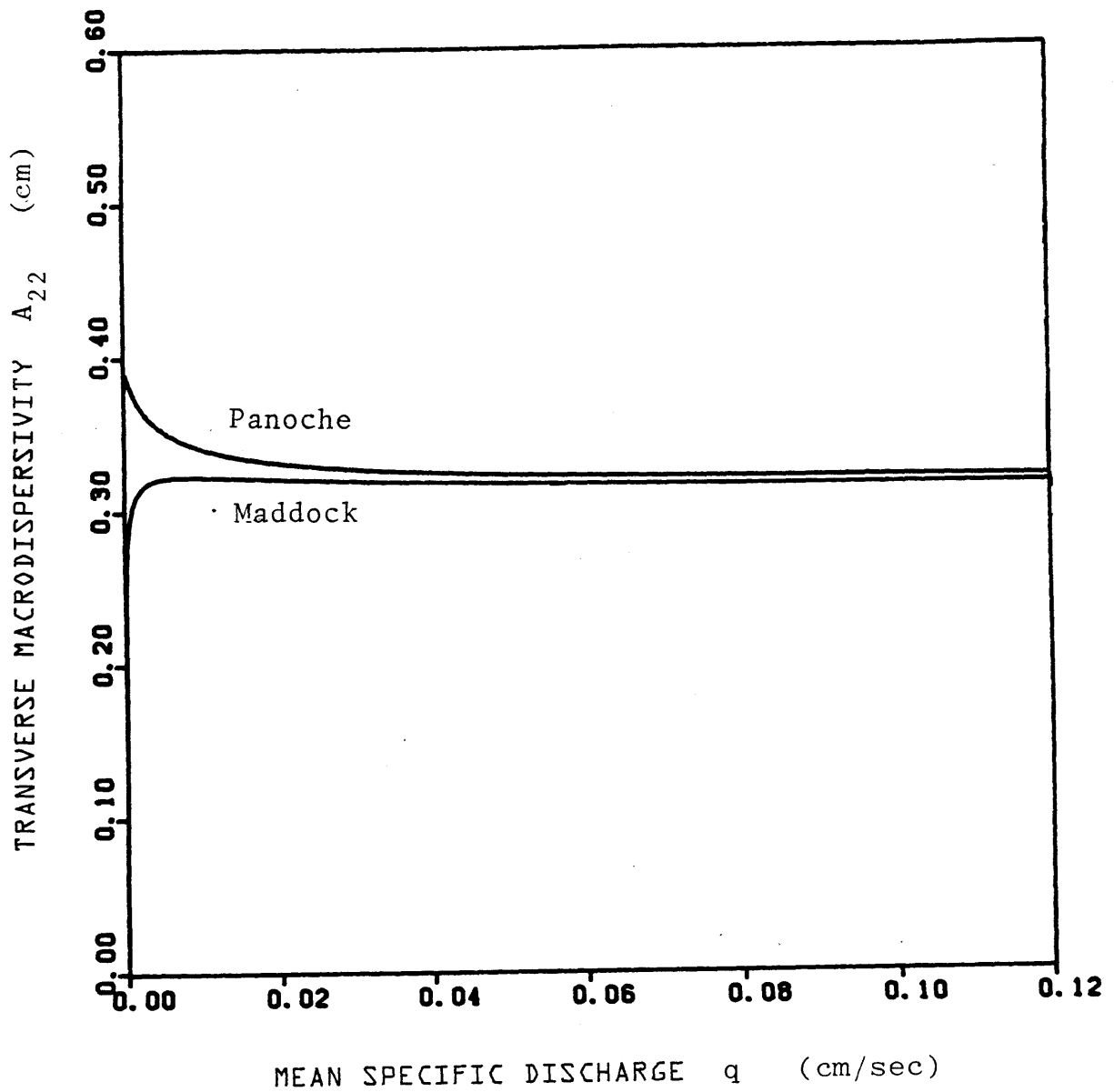
Figure 5.6   Transverse macrodispersivities A_{22} versus mean specific
discharge q for an isotropic soil with λ = 100 cm and
$\alpha_L = \alpha_T$ = 1 cm.
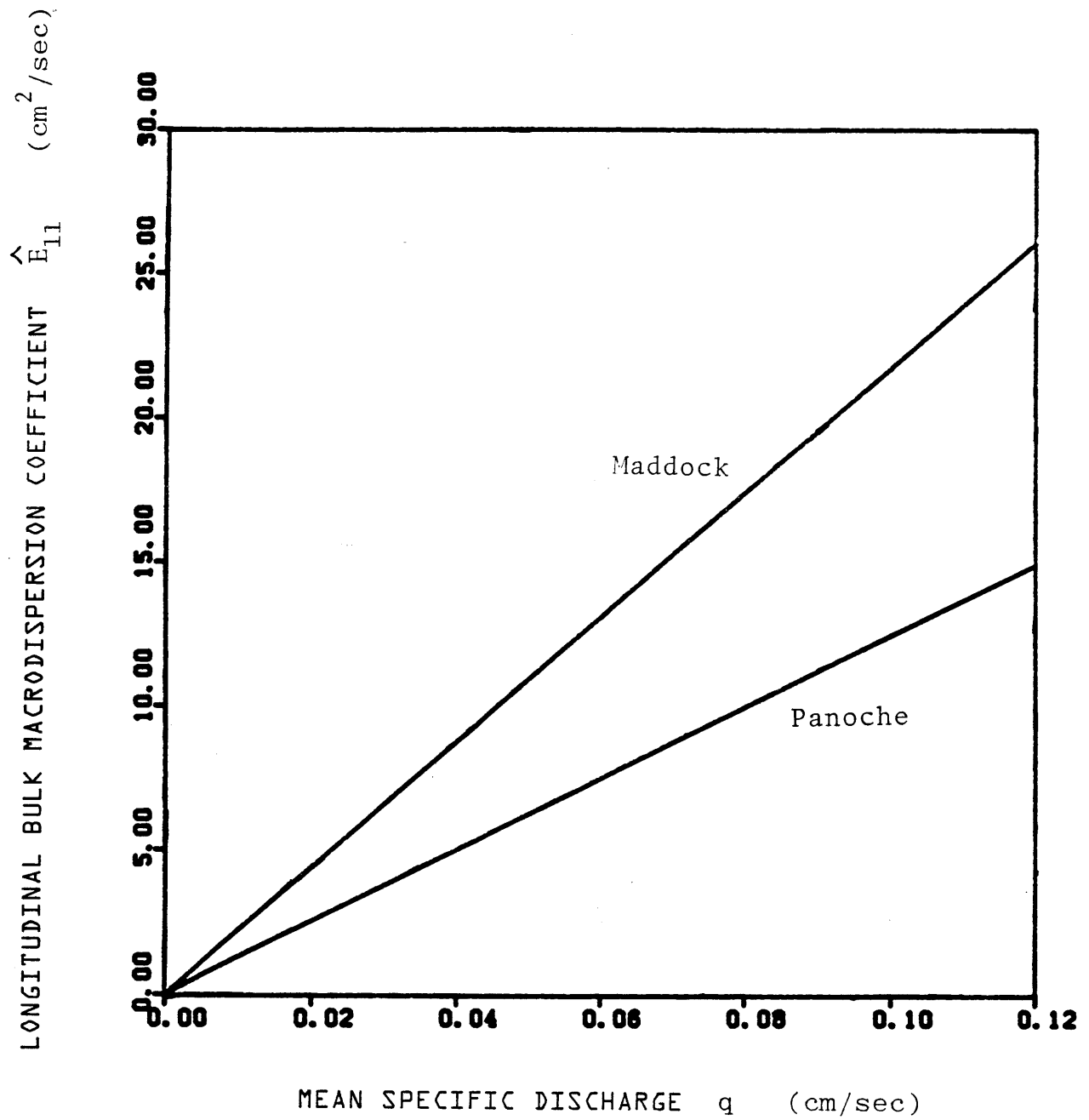
Figure 5.7 Longitudinal bulk macrodispersion coefficients $\hat{E}_{11}$ versus
mean specific discharge q for an isotropic soil with
λ = 100cm and α_L = α_T = 1cm.
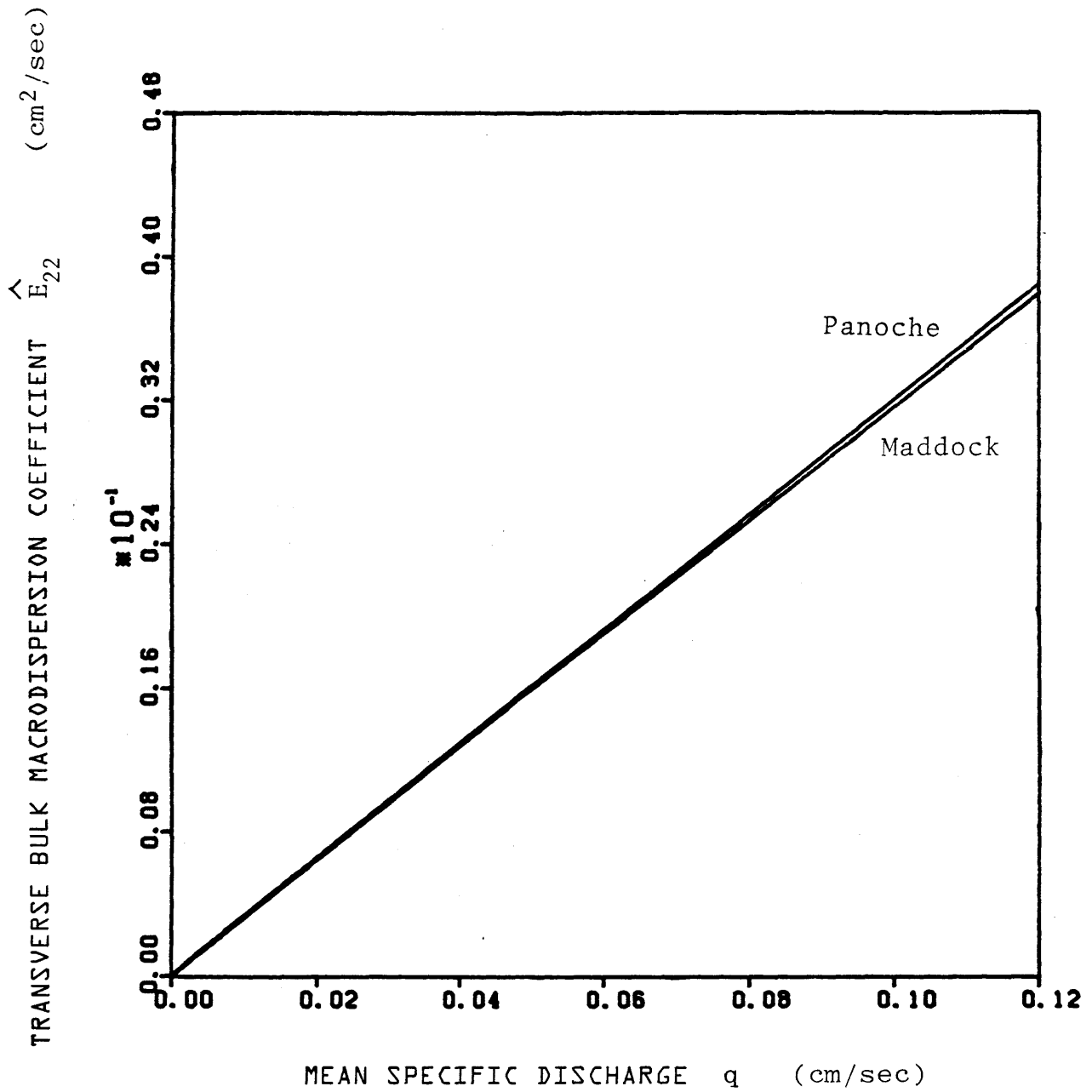
Figure 5.8   Transverse bulk macrodispersion coefficients $\hat{E}_{22}$ versus mean specific discharge for an isotropic soil with $\lambda = 100$ cm and $\alpha_L = \alpha_T = 1$ cm.

229

that the slope of these curves for q being relatively small depends on q, (see also Figure 5.5, 5.6). The $\hat{E}_{ii}$ corresponding to such small values of q however, is relatively small and it may be possible to assume that $\hat{E}_{ii}$ is proportional to q without a significant overall error. We may then conclude that the bulk macrodispersion coefficient is given by

$$\hat{E}_{ii} = A_{ii} \, q \qquad\qquad (5.61)$$

where the macrodispersivities A_{ii} are practically independent of the specific discharge q.

Figure 5.9 plots the longitudinal macrodispersivity A_{11} using Equations (5.25), (5.36) and (5.3). This case corresponds to a statistically anisotropic soil formation with the mean flow perpendicular to stratification and $\delta \gg \varepsilon$. These figures show that A_{11} increases monotonically for increasing H. This is because as H increases $\gamma \to 0$ (see (5.36)). This result may not be very realistic since evaluation of $S_{q_j q_i}$ in (3.92) required expansion of the exponential in (3.81), (3.82), which for H relatively large may not be appropriate. Figures 5.10 and 5.11 plot A_{11} and $\hat{E}_{11}$ as a function of q in this case. Figure 5.10 shows that A_{11} depends on q at small q (large H). Figure 5.11 however, suggests that $\hat{E}_{11}$ is approximately proportional to q.

The transverse macrodispersivity A_{22} in this case ($\delta \gg 0$) is given by Equation (5.30). Comparison to (5.25) shows that $A_{22} \approx 0.004$
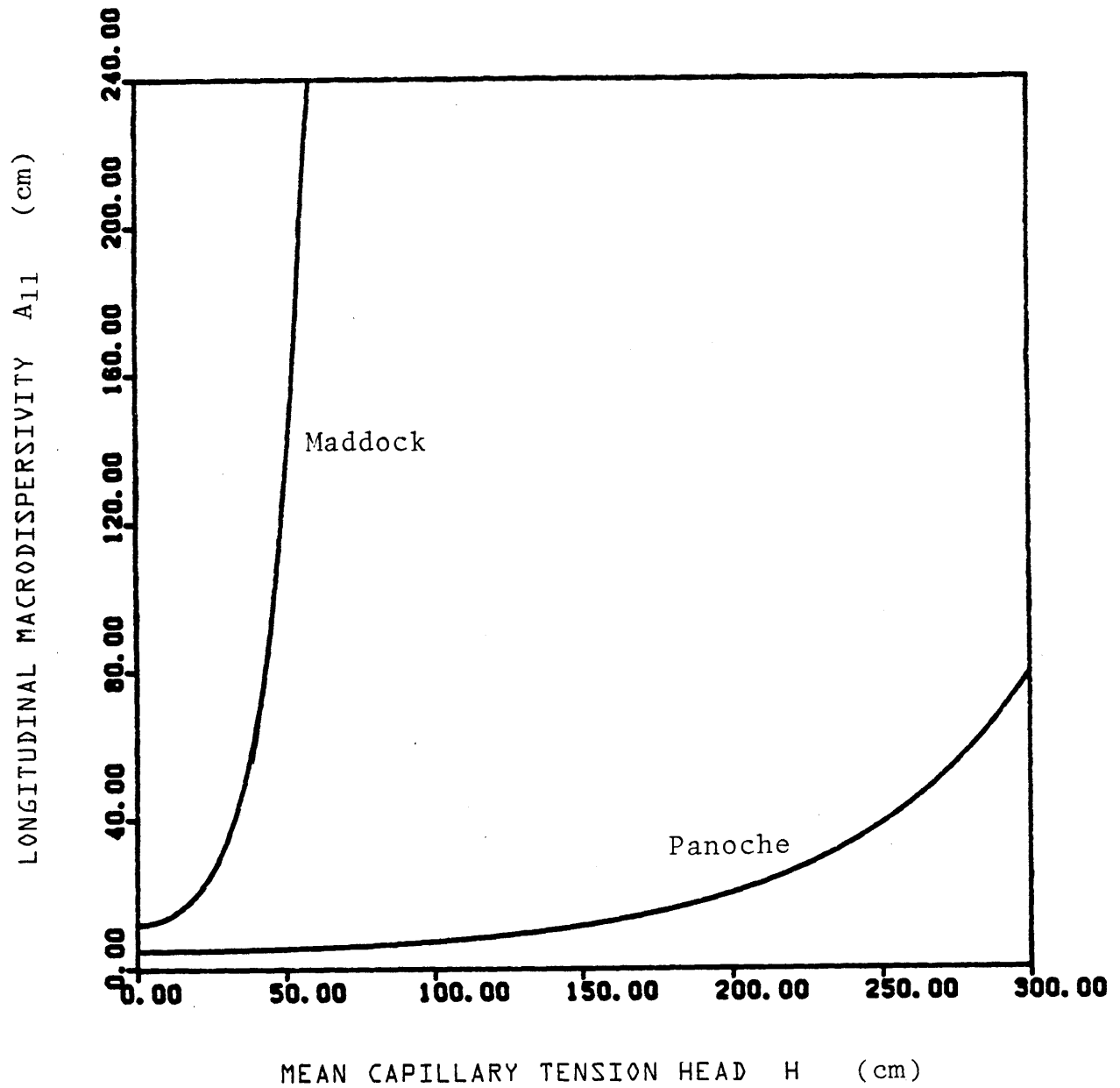
Figure 5.9   Longitudinal macrodispersivities A_{11} versus mean capillary tension head H for a statistically anisotropic soil with $\lambda_1 = 100$ cm, $\lambda_2 = \lambda_3 = 1000$ cm and $\alpha_L = \alpha_T = 1$ cm.
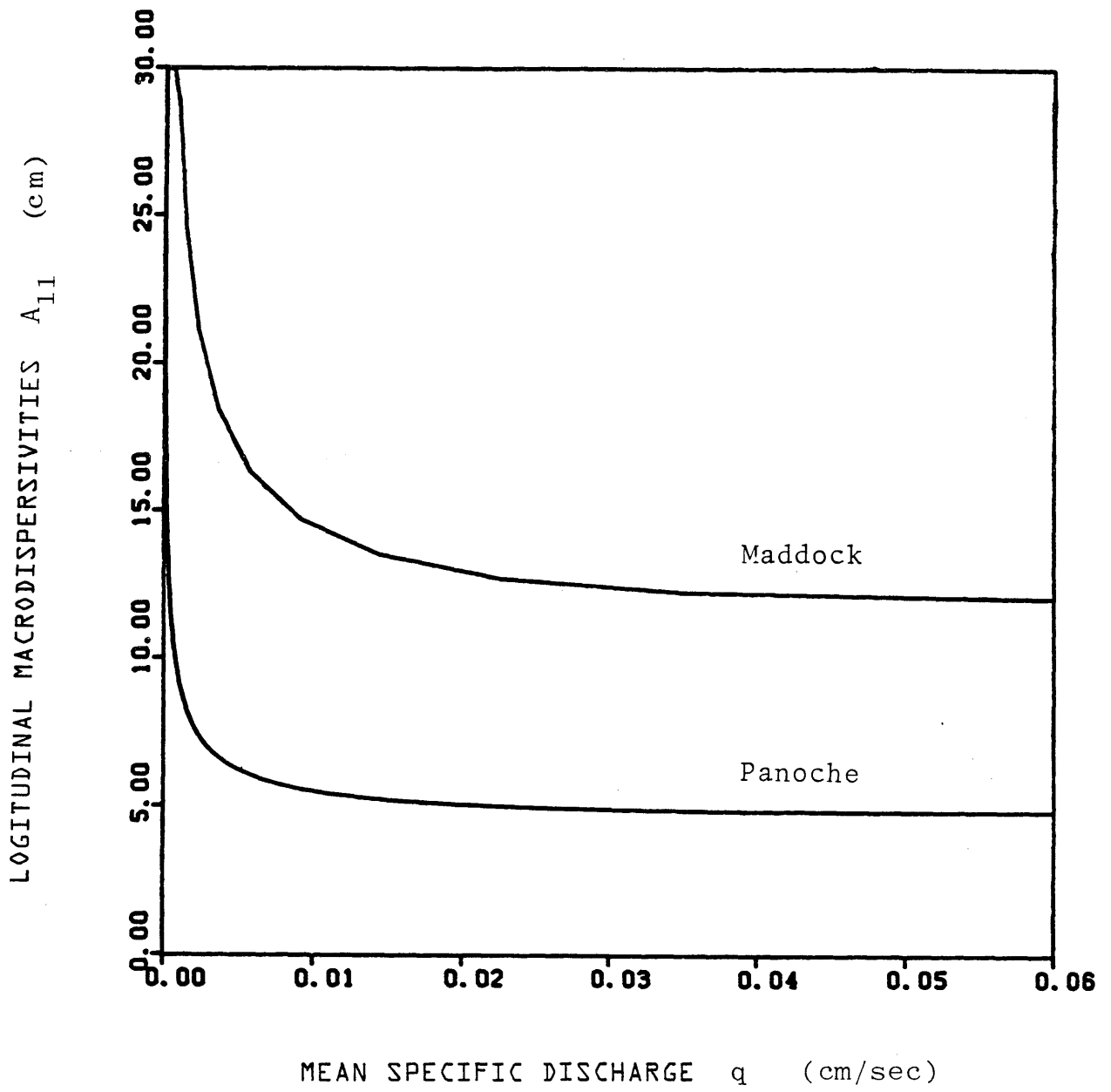
Figure 5.10   Longitudinal macrodispersivities A_{11} versus mean specific discharge q for a statistically anisotropic soil with λ_1 = 100 cm, λ_2 = λ_3 = 1000 cm and α_L = α_T = 1 cm.
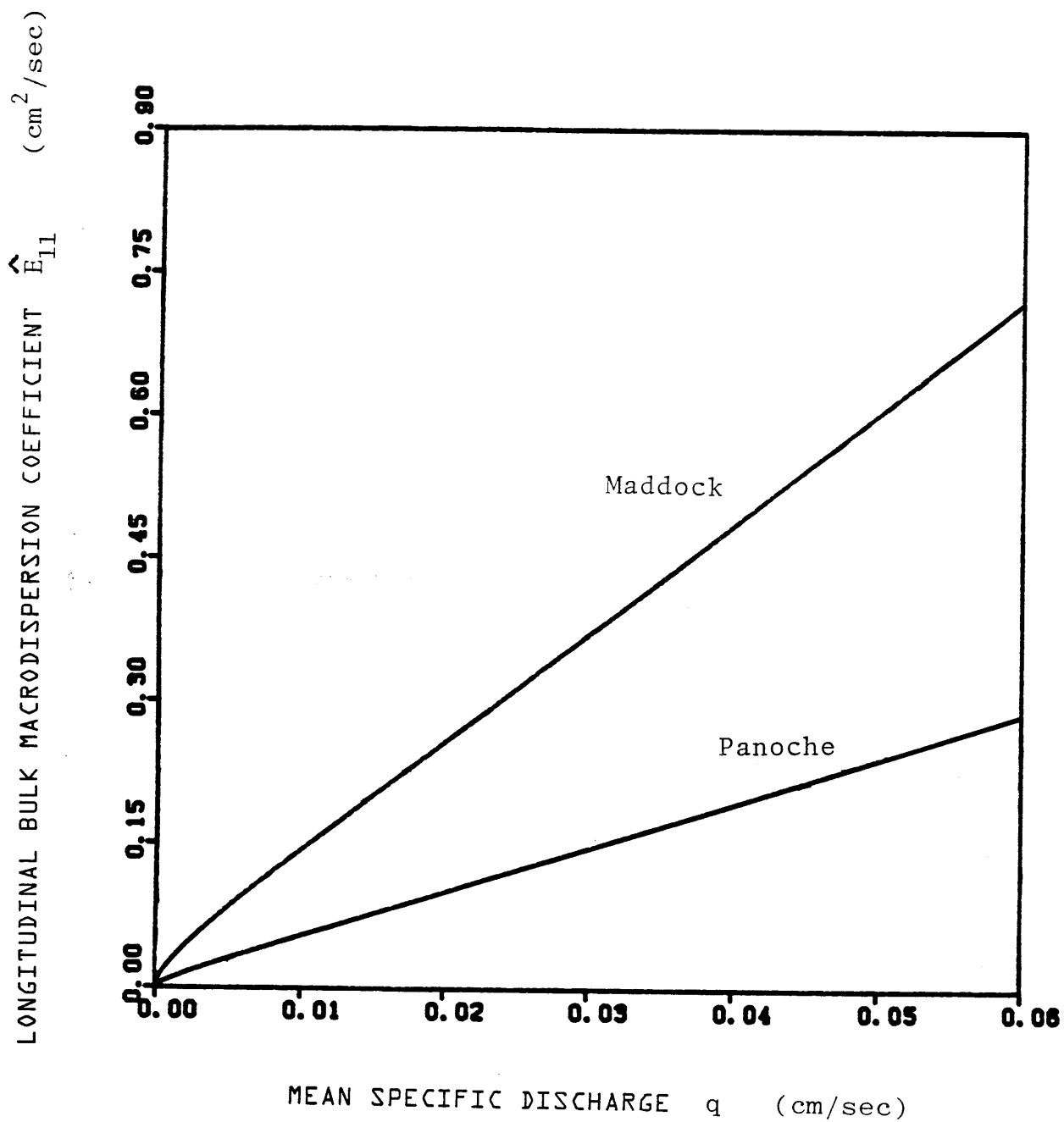
Figure 5.11   Longitudinal bulk macrodispersion coefficients $\hat{E}_{11}$ versus mean specific discharge q for a statistically anisotropic soil with λ_1 = 100 cm, λ_2 = λ_3 = 1000 cm and α_L = α_T = 1 cm.

233

δA_{11}. For $\delta = 0.1$ for example, $A_{22} = 0.0004\ A_{11}$, where A_{11} is plotted in Figures 5.9, 5.10.

The longitudinal and transverse macrodispersivities A_{11}', A_{22}', in the case of $\delta \rightarrow 0$, are given by (5.34) and (5.35). Comparing (5.34) and (5.35) to (5.25) gives: $A_{11}' = 0.78\delta\ A_{11}$ in either soil, while $A_{22}' = 0.0017\ \delta^2\ \ln(1+1/\delta^2)\ A_{11}$ in the Panoche soil and $A_{22}' = 0.00034\ \delta^2\ \ln(1+1/\delta^2)\ A_{11}$ in the Maddock soil.

Table 5.1 summarizes the values of macrodispersivities A_{ii} when q is large. This table shows that for decreasing $\delta = \lambda_1/\lambda$, the macro-dispersivities A_{ii} decrease. It is also seen that generally $A_{22} << A_{11}$. This is because the longitudinal macrodispersivity A_{11} is governed by convective flow while the transverse macrodispersivity A_{22} is determined by local dispersion. Note however, that in the more general case discussed in Section 5.2.3, when lateral flow in a stratified soil exists, the transverse macrodispersivity could be significant due to convective transport.

5.3.2 Discussion of Field Observations and Methods of Analysis

Unfortunately, only a few field scale macrodispersivities have been reported and the analytical methods used in their derivation are often questionable. Nevertheless, it may be useful to analyze reported parameters and compare them to the ones predicted by the stochastic theory. This section reviews several pertinent field observations and discusses the methods used for analysis of the observations.

TABLE 5.1

Macrodispersivities A_{11} (cm)

Soil Type	Panoche soil		Maddock soil	
	Longitudinal A_{11}	Transverse A_{22}	Longitudinal A_{11}	Transverse A_{22}
Isotropic $\lambda = 100$ cm	123.0	0.32	218.0	0.33
Statistically anisotropic δ large ($\delta = 0.1$)	5.0	0.002	12.0	0.005
Statistically anisotropic δ small ($\delta = 0.01$)	0.039	1.6×10^{-6}	0.093	3.0×10^{-7}

Biggar and Nielsen (1976) described experiments conducted in an agricultural setting. Breakthrough curves were obtained at six depths at the centers of twenty 6.5 m-square plots, following a pulse of Cl and NO_3 solution. Then, a simple one-dimensional transport model with constant parameters, an apparent diffusion coefficient, D, and an apparent pore water velocity, v_s, was fitted to each breakthrough curve. A possible criticism of such parameter estimation procedure is that since the parameters D and v_s have been assumed to be uniform over depth they should be fitted simultaneously with the breakthrough curves at all depths (at each location). Fitting a model with different D and v_s at each depth, contradicts the assumption of constant D and v_s. The paper suggests that fitted values of D and v_s follow a lognormal distribution. D is correlated with v_s through an almost linear relationship ($D = 0.6 + 2.93 \, v_s^{1.11}$; D in cm^2/day, v_s in cm/day). Using the data of their Figure 7, we determined an average value of $A_{11} = 5$ cm for the longitudinal macrodispersivity. The paper further discussed the number of samples required in order to obtain a reliable estimate for the mean values of D and v_s. This is another weak point of the paper since it implies that the mean values of D and v_s are the effective parameters that should be used in the mean models for estimation of mean concentrations. Such an assumption does not seem to be justified since the system is nonlinear in the parameters, and local variability has a large-scale effect.

The experiments and methods for calibrating for D and v_s reported in Van de Pol, et al. (1977) and Kies (1982), are similar to Biggar and Nielsen (1976). Thus the criticism on the fitting for D and v_s also

236

applies. The fitted values again seem to follow a lognormal distribution. Kies' data also show that D is related to v_s through an almost linear relationship. The data of Van de Pol, et al. (1977) suggest a value of the longitudinal macrodispersivity A_{11} = 9.41 cm, while the data of Kies (1982) suggest a value A_{11} = 16.8 cm. These papers also imply that the mean values of D and v_s should be used in models predicting the mean concentration. Again, this assumption does not seem justified. Kies' data show an increase in the mean values of D with depth below the soil surface. He also observed that the average solute velocities, v_s, calculated by fitting v_s to the breakthrough curves, is larger than the mean pore water velocities v_m. This is probably due to the fact that most of the water may be moving in larger structures with higher velocities than the average pore water velocity (calculated by dividing the average infiltration rate by the average soil moisture content). He also observed that the ratio v_s/v_m increases with depth, and that Cl travels faster and disperses more than NO_3.

Warrick, et al. (1971) reported on a field experiment in a 6.1 m by 6.1 m plot in the Panoche clay loam soil. A solute pulse was applied on the surface of the soil and was observed as it moved through the soil profile. Experimental data and a numerical soil moisture flow model showed that the infiltration rate approached steady state in a relatively short time. A one-dimensional governing equation for the solute concentration was solved analytically. Using this solution and value of the velocity found from the infiltration rate, the maximum concentration was determined as a function of time and dispersion coefficient D. Comparing this model to experimental data, a value of D = 0.07 cm^2/min

237

(A_{11} = 2.7 cm) gave the best fit. They observed that a value of D close to 0.05 cm^2/min better described the data at small times, whereas D = 0.1 cm^2/min was more nearly correct at large times. This suggests that D may increase with the time or distance the solute has travelled. The approach used in this paper for evaluating D is fundamentally different than the one used in Biggar and Nielsen (1976), Van de Pol, et al. (1977) and Kies (1981). The velocity here is estimated from infiltration data, and the parameter D is fitted to the maximum observed concentrations only, and not to the whole breakthrough curves. A possible criticism of this approach is that information available regarding the shape of the breakthrough curves is not used in the estimation procedure, so the estimated parameters are possibly not optimal.

Warrick, et al. (1971) observed that the calculated distribution curves do not penetrate the soil profile as deeply as the measured ones. A similar phenomenon was observed in Kies (1982). This may be a reflection of preferential flow paths with most of the water moving through the larger water-filled pore sequences. Warrick et al. also observed that solute was not present in the advancing moisture front but lagged behind nearer the soil surface. This phenomenon has been observed elsewhere (e.g., see Andersen and Sevel, 1968). It is called the solute-lag effect (Gelhar, 1977). A probable explanation is that a pressure wave generates displacement of old capillary water at successively increasing depths. Simple calculations (Gelhar, 1977) show that the moisture front travels with speed $v_w \simeq dK/d\theta$ while the solute travels with speed $v_s \simeq K/\theta$. For typical soils, then $v_w \gg v_s$

(e.g. $v_w \approx 20v_s$)..

Foster (1975) and Oakes (1977) present another possible explanation of the solute-lag effect in the English Chalk, based on fracture flow with matrix diffusion. For the data of Young, et al. (1976), Oakes (1977) reports a dispersivity value of 20 cm.

The paper of Andersen and Sevel (1968) is interesting since they made an effort to evaluate an effective dispersion coefficient on a large scale (20 m deep) system. Environmental tritium data was taken in a group of four boreholes which had been augered at time intervals of about two years. Soil moisture profiles had been measured regularly by the neutron method in the boreholes. A simple displacement with dispersion model, assuming constant travel velocity, constant dispersion coefficient and constant soil-moisture content throughout the profile, was tested. A dispersion coefficient of $D = 10^{-7}$ m^2/sec yielded a good fit for the tritium profiles. This corresponds to a longitudinal dispersivity A_{11} = $D/v \simeq 70$ cm. Soil moisture profiles indicated a propagation velocity of the moisture front of about 3 to 3.5 m/month. The actual flow velocity estimated by environmental tritium profiles however, seems to be only 4.5m year. This solute lag effect is similar to the one observed by Warrick, et al. (1971) and discussed above.

Jury, et al. (1982) describe a series of field experiments made in order to test a transfer function model. This model may be criticized in that it does not use any physics about the processes involved; it is a black-box model. Its parameters do not correspond to any physical quantities and must be calibrated based on available data for the particular setting under consideration. Extrapolation of the predictions

239

of such a model to depths, settings or conditions other than the ones
from which it was derived, is not possible. The data presented in the
paper in order to validate the model clearly demonstrates our point. For
example, Figure 5.12 presents measured breakthrough curves and predicted
ones, obtained from the transfer function model of Jury, et al. (1982).
Comparison between these curves indicates that the model overestimates
the solute concentrations near the surface, yields a good fit at 90 cm,
and underestimates them at larger depths. It appears that the model was
calibrated so that it fits the data at the 90 cm depth. The differences
between theory and experiment are statistically significant; the model
predictions fall above the 95 percent confidence interval of the data at
30 cm and below it at 180 cm.

The reason for this discrepancy, we believe, is that the transfer
function model, or any other one-dimensional convective transport model,
yields predictions that correspond to a linear increase of dispersivity
with depth. It is possible that at small depths the dispersivity
increases with the depth but it could approach a constant value as the
depth increases. In that case, the predicted breakthrough curves of
Figure 5.14 would show less spread and greater maximum values at larger
depths, i.e., they would trend toward agreement with the measured data.
Gelhar et al., (1984), evaluated a value of the longitudinal
macrodispersivity $A_{11} = 9.45$ cm, using the data reported by Jury et
al., (1982), and spatial moment methods.

Table 5.2 summarizes the values of the longitudinal
macrodispersivities discussed above along with the longitudinal scale of
the experiment. Some laboratory observations are also included for

240
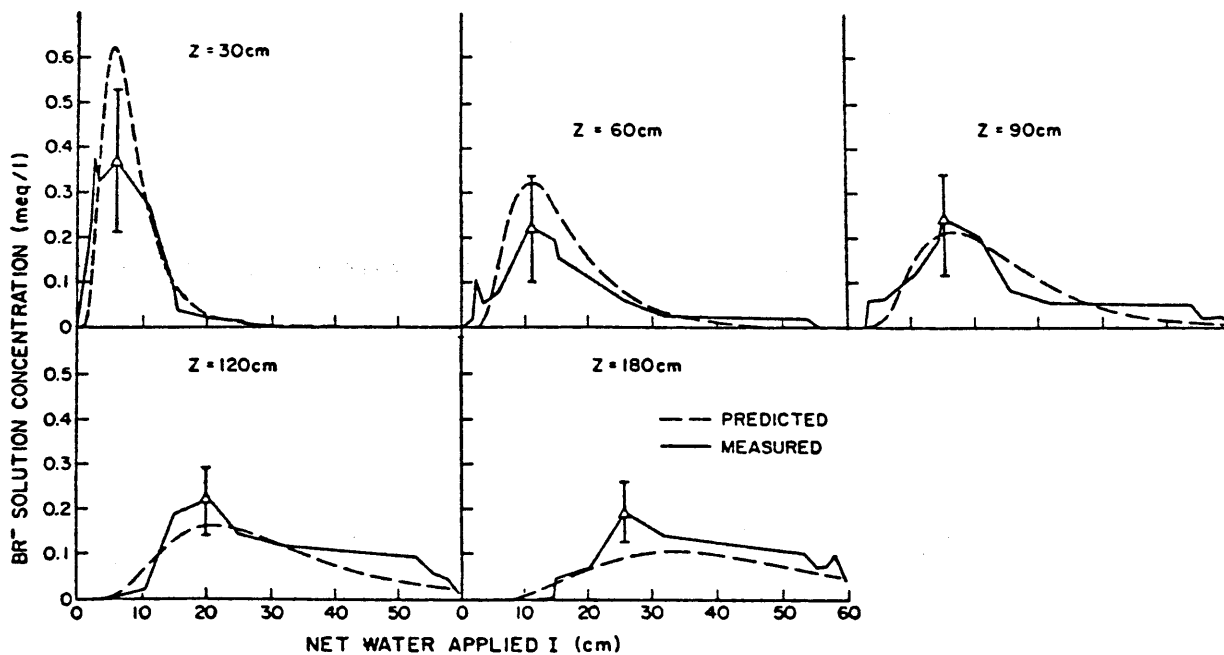
Figure 5.12 Predicted and measured average solute breakthrough curve at
30, 60, 90, 120 and 180 cm. Error bars represent 95%
confidence of measured data (from Jury et al., 1982).

TABLE 5.2

FIELD DISPERSIVITIES, A_{11}

Author	Type of Experiment	Vertical scales of experiment (m).	Longitudinal dispersivity A_{11}(m)
Yule and Gardner, (1978)	Laboratory	0.23	0.0022
Hildebrand and Himmelblau, (1977)	Laboratory	0.79	0.0018
Kirda, et al., (1973)	Laboratory	0.60	0.004
Gaudet, et al., (1977)	Laboratory	0.94	0.01
Brissaud, et al. (1983)	Field	1.00	0.0011, 0.002
Warrick, et al. (1971)	Field	1.20	0.027
Van de Pol, et al. (1977)	Field	1.50	0.0941
Biggar and Nielsen, (1976)	Field	1.83	0.05
Kies, (1981)	Field	2.00	0.168
Jury, et al. (1982)	Field	2.00	0.0945
Andersen, et al. (1968)	Field	20.00	0.70
Oakes, (1977)	Field	20.00	0.20

comparison. In order to quantitatively compare the observed macrodispersivities to the ones predicted by the stochastic theory, the statistical properties of soil variability, the mean flow conditions, etc., should be known in the particular settings where A_{ij} were observed. Since such parameters are not known we must restrict ourselves to qualitative comparisons only. Comparison of Table 5.2 to Table 5.1 shows that the longitudinal macrodispersivities predicted by the stochastic theory are of the same order of magnitude as the observed ones at large scales of observation.

In the case of saturated flow, it has been observed that dispersivity shows an apparent increase as the scale of the experiment increases, (see Gelhar et al., 1983). A possible theoretical explanation of this behavior is given in Gelhar et al. (1979). Figure (5.13) plots the unsaturated longitudinal macrodispersivities, given in Table 5.2, as a function of the scale of the experiment. Although the data at larger scales are limited, the few existing data points show an increase of A_{11} with the scale of the experiment, in analogy to the saturated flow case. The stochastic theory predicts that the longitudinal dispersivity may depend on other factors, such as soil type, soil heterogeneity and moisture content; however, it is not possible to recognize any dependence of A_{11} on these factors, due to the dearth of data.
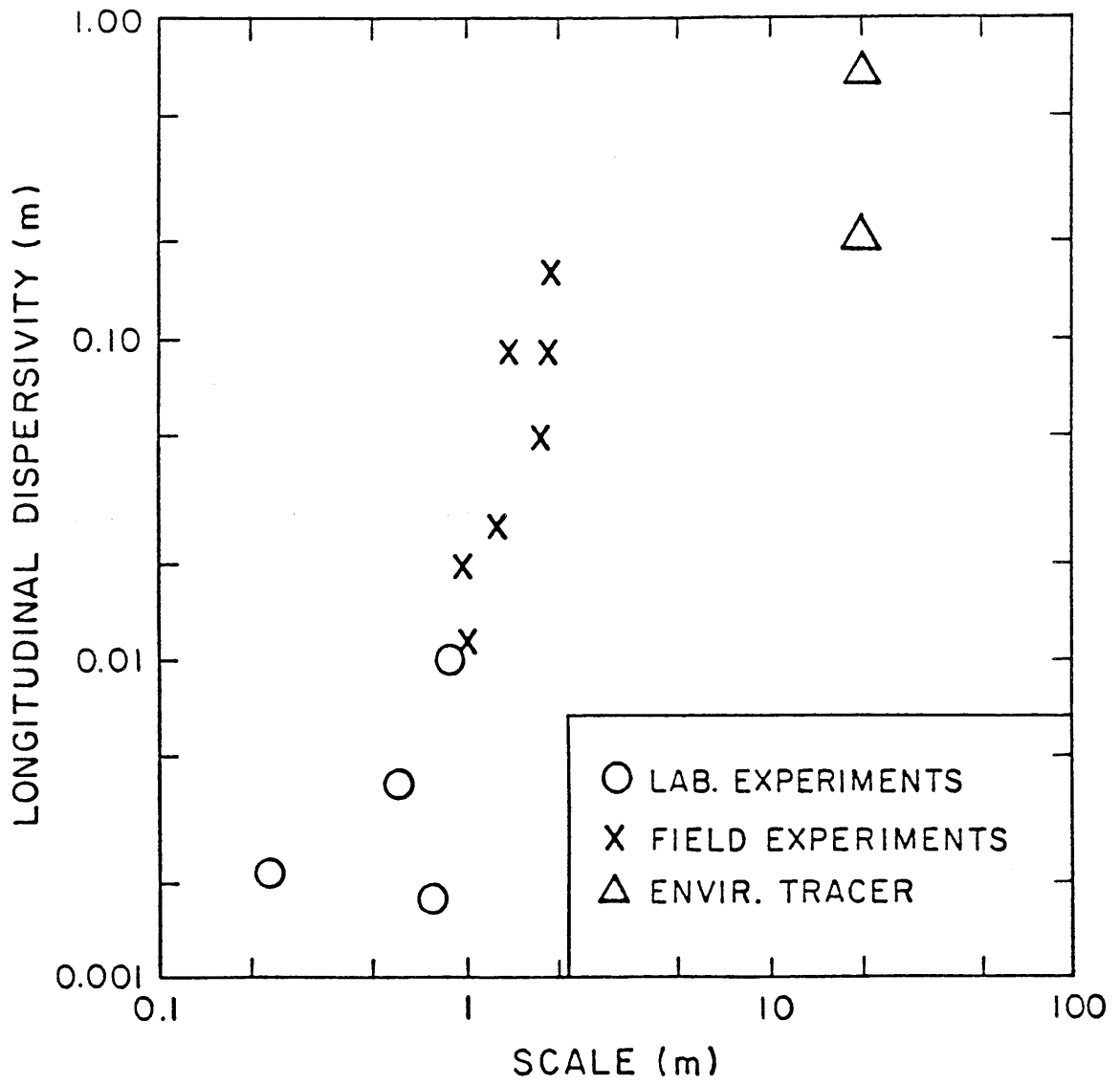
Figure 5.13 Longitudinal dispersivity versus scale of experiment, from Table 5.2.

5.4 Summary and Conclusion

This chapter evaluated effective macrodispersivities in unsaturated soils, using the general theory developed in Chapter 3. Certain simplifications allowed analytical evaluation of the corresponding three-dimensional integrals.

Section 5.2 derived expressions for the macrodispersivities in terms of the local dispersivities, the soil property, and the mean flow characteristics. Section 5.2.1 examined the case of a statistically isotropic soil formation. Using the fact that $\varepsilon = \alpha_L/\lambda \ll 1$, the corresponding integrals were simplified and were analytically evaluated. It was found that the longitudinal macrodispersivity is proportional to the correlation length λ_1, i.e. longitudinal dispersion process is controlled by convective transport. However, the transverse macrodispersivity is proportional to the local dispersivities and independent of the correlation scale, i.e. in this case the transverse dispersion is governed by local dispersion.

Section 5.2.2 examined the case of a statistically anisotropic soil when the mean flow is perpendicular to stratification. Two cases were examined: (i) $\delta = \lambda_1/\lambda$ being relatively large (mild stratification) and (ii) $\delta \approx 0$, (strong stratification). Similarly to the isotropic case, longitudinal dispersion is governed by convective transport while transverse dispersion is governed by local dispersion. Note that in the case of mild stratification, A_{11} is independent of δ but A_{22} is proportional to δ, i.e. A_{22} decreases as the degree of stratification increases. In the case of strong stratification however, A_{11} and A_{22} depend on δ, A_{11} is proportional to δ, while A_{22} is proportional to

$\delta^2 \ln(1+1/\delta^2) \approx \delta^2$. This implies that in the case of strong

stratification, A_{11} and A_{22} decrease as stratification increases.

For $\delta \rightarrow 0$ (perfectly stratified soil), A_{11}, $A_{22} \rightarrow 0$, i.e. in this

case only local dispersion exists.

Section 5.2.3 discussed the more general case of macrodispersion in

a stratified soil formation when a lateral flow gradient exists. In this

case, even a small lateral gradient can produce significant lateral

flow. This flow may generate a significant convectively controlled

transverse dispersion.

Section 5.3 applied the results of the stochastic theory, and

compared these results to field observations. Section 5.3.1 evaluated

the macrodispersivities corresponding to the Panoche clay loam soil and

the Maddock sandy loam soil. It was found that in the case of a

statistically isotropic soil, the macrodispersivities A_{11} and A_{22}

generally depend on the mean capillary tension head H. As soil

desaturates, A_{11} and A_{22} initially increase but after reaching a

maximum value they tend to decrease monotonically. This phenomenon is

probably due to spatial variability of the soil properties. A similar

type of dependence is predicted by the statistical pore scale model of

Wilson (1974). This suggests that spatial variability produces effects

similar to microscopic variability (compare to the hysteresis effect

discussed in Chapter 4). Plotting the bulk macrodispersion coefficient

$\hat{E}_{ii}$ against the mean specific discharge q, showed that $\hat{E}_{ii}$ is

practically proportional to q. This result of the stochastic theory

is in accordance with several field observations discussed in Section

5.3.2. In the case of a statistically anisotropic soil, the stochastic

theory predicted that A_{ii} increases monotonically as H increases. This result could be due to ignoring higher order terms in the stochastic analysis. Plots of $\hat{E}_{ii}$ versus q, showed that $\hat{E}_{ii}$ is practically proportional to q in this case as well.

Section 5.3.2 reviewed a series of reported field observations and discussed the methods used for analysis of the observations in the corresponding publications. It was found that the reported field scale dispersivities are very few and that the analytical methods used in their derivation are often questionable. Nevertheless, qualitative comparisons of these macrodispersivity values to the ones predicted by the stochastic theory showed them to be of the same order of magnitude. The few existing field observations indicated that the longitudinal dispersivity A_{11} may increase with the scale of experiment. Due to the dearth of data it was not possible to recognize any dependence of experimentally observed A_{11} on other factors such as soil type, soil heterogeneity and moisture content.

CHAPTER 6

METHODS FOR TESTING THE VALIDITY OF THE STOCHASTIC THEORY

AND APPLICATION OF LARGE-SCALE MODELS

6.1 Introduction

This chapter discusses methods that could be used for testing the validity of the stochastic theory and applying the large-scale models to real field problems. Section 6.2 suggests a Monte-Carlo approach for testing the validity of the stochastic approach and extends the spectral turning bands method, developed by Mantoglou and Wilson (1982), for digital generation of point values or spatial averages of multiple, cross correlated, statistically anisotropic, stationary random fields. Section 6.3 discusses the important application problem of estimating the parameters required in large-scale models. Statistical inference methods are discussed and a new parameter identification method is developed.

This chapter assumes that numerical codes capable of solving the governing unsaturated flow and transport equations exist. Of course, accuracy and cost may restrict the applicability of such codes. However, it is felt that these problems will soon be solved since computer capabilities are increasing very rapidly today.

6.2 Testing the Validity of the Stochastic Theory Using Monte-Carlo Simulation

In order to obtain analytical expressions for the dependence of the effective parameters on the different soil property and flow characteristics, several assumptions were required in the analysis of the previous chapters (e.g., stationarity, smallness of fluctuations, etc.). It is thus of interest to investigate the validity of the quantitative and qualitative predictions of the stochastic theory in more general cases when the assumptions used in their derivation do not strictly hold. Section 6.2.1 proposes a five step Monte-Carlo procedure for testing the validity of the stochastic theory. This procedure requires computer generation of multiple (vector), three-dimensional statistically anisotropic random fields. Section 6.2.2 extends the spectral turning bands method for generation of such fields. This method may be used for computer generation of realizations of soil property fluctuations, as required by the Monte-Carlo procedure.

6.2.1 Monte-Carlo Procedure

This section proposes a Monte-Carlo procedure that can be used for testing the validity of the stochastic theory. The procedure follows five steps. First a model for the mean and the covariance functions of the local soil properties ℓnK_s, α and C is selected. The selected statistical parameters should take realistic values and should consider the statistical anisotropy (stratification) usually observed in the field.

In the second step, realizations of the cross-correlated soil pro-

perty random fields f, a and γ, that conserve the theoretical statistics selected in the first step, are generated. The spectral turning bands method, developed in the next section, can be used in this step.

In the third step, the flow and concentration outputs ψ and c, corresponding to each soil property realization generated in the second step, are evaluated. This step requires numerical solution of the governing flow and transport equations. Numerical approximation errors and high cost are important considerations in this step.

The fourth step, involves analysis of the output realizations ψ and c. Given the series of realizations of ψ and c obtained in the third step, the ensemble mean H_{MC} and $\bar{c}_{MC}$ are easily evaluated using ensemble averaging. In addition, the effective parameters can be estimated from (3.10), (3.13) and (3.16) where the cross-correlations in these equations can be evaluated using ensemble averaging.

The fifth and last step of the Monte-Carlo procedure involves comparison between the predictions of the stochastic theory and the Monte-Carlo simulation results. Two different types of comparison are suggested. First, given the theoretical statistics of the soil properties, selected in the first step, and the "true" mean H_{MC} and $\bar{c}_{MC}$, the stochastic theory developed in Chapters 3, 4 and 5, is used in order to derive estimates of the effective parameters. These parameters are compared to the "true" effective parameters evaluated in the fourth step using Monte-Carlo simulation. A second comparison consists of "running" a numerical model using the effective parameters estimated by the

250

stochastic theory and comparing these large-scale model outputs $\bar{H}_{ST}$, $\bar{C}_{ST}$, to the "true" mean values $\bar{H}_{MC}$, $\bar{C}_{MC}$ predicted from the Monte-Carlo simulations in the fourth step. Such comparisons involve testing of significance for the errors $\bar{H}_{ST}-\bar{H}_{MC}$ and $\bar{C}_{ST}-\bar{C}_{MC}$.

6.2.2 Extensions of the Spectral Turning Bands Method

The turning bands method for simulation of isotropic random fields was originally proposed by Matheron (1973) and was applied for simulation of certain types of random fields having particular forms of covariance function using a Moving Average unidimensional process generation (see Journel, 1974; Chiles, 1977). Mantoglou and Wilson (1981, 1982), developed a much more flexible spectral turning bands method where the unidimensional processes are simulated using a spectral generator. This method is capable of directly simulating point values or spatial averages of statistically isotropic or anisotropic two dimensional random fields. This section extends the spectral turning bands method for computer generation of multiple, (vector), cross-correlated random fields. The proposed methodology is very general and it can generate point values or spatial averages of two or three-dimensional, isotropic or anisotropic multiple random fields.

Let $Y_i(\underline{x})$; i = 1, k, represent a set of two or three-dimensional, cross-correlated, zero mean, stationary anisotropic random fields, having known cross-covariance and cross-spectral density functions $C_{ij}(\underline{r})$, $S_{ij}(\underline{k})$ where $C_{ij}(\underline{r}) = E[Y_i(\underline{x}) \ Y_j(\underline{x}+\underline{r})]$ and $\underline{x}$, $\underline{r}$ represent spatial and $\underline{k}$ represent wave number coordinates. The objective is to generate

251

(using a digital computer) realizations of random fields $Y_i(\underline{x})$ that preserve the known cross-covariance and cross-spectral density functions $C_{ij}(\underline{r})$, $S_{ij}(\underline{k})$. Functions $C_{ij}(\underline{r})$ and $S_{ij}(\underline{k})$ form a Fourier Transform pair, so that following properties hold.

$$C_{ij}(\underline{r}) = \int_{R^n} e^{j\underline{k}\cdot\underline{r}} S_{ij}(\underline{k}) \, d\underline{k} \tag{6.1}$$

$$S_{ij}(\underline{k}) = \frac{1}{(2\pi)^n} \int_{R^n} e^{-j\underline{k}\cdot\underline{r}} C_{ij}(\underline{r}) \, d\underline{r} \tag{6.2}$$

where n is the dimensionality of the field (n=2 or 3). It is convenient to use a vector-matrix notation in the following developments. Define the vector random field

$$\underline{Z}(\underline{x}) = \begin{bmatrix} Y_1(\underline{x}) \\ Y_2(\underline{x}) \\ \cdots\cdots \\ Y_K(\underline{x}) \end{bmatrix} \tag{6.3}$$

and its cross-covariance function matrix

$$\underline{C}(\underline{r}) = E\left[\underline{Z}(\underline{x})\ \underline{Z}^T(\underline{x}+\underline{r})\right] =$$

$$= \begin{vmatrix} E[Y_1(\underline{x})\ Y_1(\underline{x}+\underline{r})] & E[Y_1(\underline{x})\ Y_2(\underline{x}+\underline{r})] & \cdots & E[Y_1(\underline{x})\ Y_K(\underline{x}+\underline{r})] \\ E[Y_2(\underline{x})\ Y_1(\underline{x}+\underline{r})] & E[Y_2(\underline{x})\ Y_2(\underline{x}+\underline{r})] & \cdots & E[Y_2(\underline{x})\ Y_K(\underline{x}+\underline{r})] \\ \cdots\cdots\cdots\cdots\cdots\cdots\cdots\cdots\cdots\cdots\cdots\cdots\cdots\cdots\cdots\cdots\cdots\cdots \\ E[Y_K(\underline{x})\ Y_1(\underline{x}+\underline{r})] & E[Y_K(\underline{x})\ Y_2(\underline{x}+\underline{r})] & \cdots & E[Y_K(\underline{x})\ Y_K(\underline{x}+\underline{r})] \end{vmatrix}$$

$$= \begin{vmatrix} C_{11}(\underline{r}) & C_{12}(\underline{r}) & C_{1K}(\underline{r}) \\ C_{21}(\underline{r}) & C_{22}(\underline{r}) & C_{2K}(\underline{r}) \\ \cdots\cdots\cdots\cdots\cdots\cdots\cdots\cdots \\ C_{K1}(\underline{r}) & C_{K2}(\underline{r}) & C_{KK}(\underline{r}) \end{vmatrix} \qquad (6.4)$$

where T represents matrix transpose. Define a cross-spectral density function matrix $\underline{\underline{S}}(\underline{k})$ having as elements the cross-spectral density functions $S_{ij}(\underline{k})$. Equations (6.1) and (6.2) then can be expressed in the following matrix form

$$\underline{\underline{C}}(\underline{r}) = \int_{R^n} e^{j\underline{k}\cdot\underline{r}}\underline{\underline{S}}(\underline{k})\ d\underline{k} \qquad (6.5)$$

$$\underline{\underline{S}}(\underline{k}) = \frac{1}{(2\pi)^n} \int_{R^n} e^{-j\underline{k}\cdot\underline{r}}\underline{\underline{C}}(\underline{r})\ d\underline{r} \qquad (6.6)$$

where the integral of a matrix is defined as the matrix of the integrals of its elements.

Instead of generating the three-dimensional field directly, the turning bands method generates unidimensional processes on several lines, using a unidimensional covariance function matrix that corresponds to the known two- or three-dimensional one. Then at each point of the two- or

three-dimensional space a weighted sum of the corresponding values of the one-dimensional processes is assigned.

Assume that we want to generate point values of the two or three-dimensional random field at the discrete nodes (i, j, k) in region $\underline{P}$ of Figure 6.1. Choose an arbitrary origin 0 in the two- or three-dimensional space and generate lines so that their corresponding direction vectors $\underline{u}$ are uniformly distributed on the unit circle or sphere. Along each line i, generate stationary unidimensional discrete processes having zero mean and covariance function matrix $\underline{\underline{C}}_i^{(1)}(\zeta)$ where ζ is the coordinate on line i. The correspondence between $\underline{\underline{C}}_i^{(1)}(\zeta)$ and the given two- or three-dimensional covariance matrix $\underline{\underline{C}}(\underline{r})$ will be derived later. Note that in the general anisotropic case $\underline{\underline{C}}_i^{(1)}(\zeta)$ depends on the direction of line i. Onto line i, orthogonally project the points of the field where we want to generate values, and assign them the corresponding values of the one-dimensional discrete processes. If N(i, j, k) is a point of the region having location vector $\underline{x}$, then the assigned value from line i will be $\underline{Z}_i^{(1)}(\zeta_{N_i})$ where $\zeta_{N_i} =$ $\underline{x}_N \cdot \underline{u}_i$ is the projection of vector $\underline{x}_N$ onto line i (see Figure 6.1), $\underline{u}_i$ is the unit vector on line i, and $\underline{x}_N \cdot \underline{u}_i$ represents the inner product of vectors $\underline{x}_N$ and $\underline{u}_i$. Take L lines as i. For each line generate an independent unidimensional realization using $\underline{\underline{C}}_i^{(1)}(\zeta)$ as covariance function matrix. Then at every point N of the region, there are L assigned values $\underline{Z}_i^{(1)}(\zeta_{N_i}) = \underline{Z}_i^{(1)}(\underline{x}_N \cdot \underline{u}_i)$, where i = 1, ..., L, from the unidimensional simulations. Finally, assign the following value, to point N
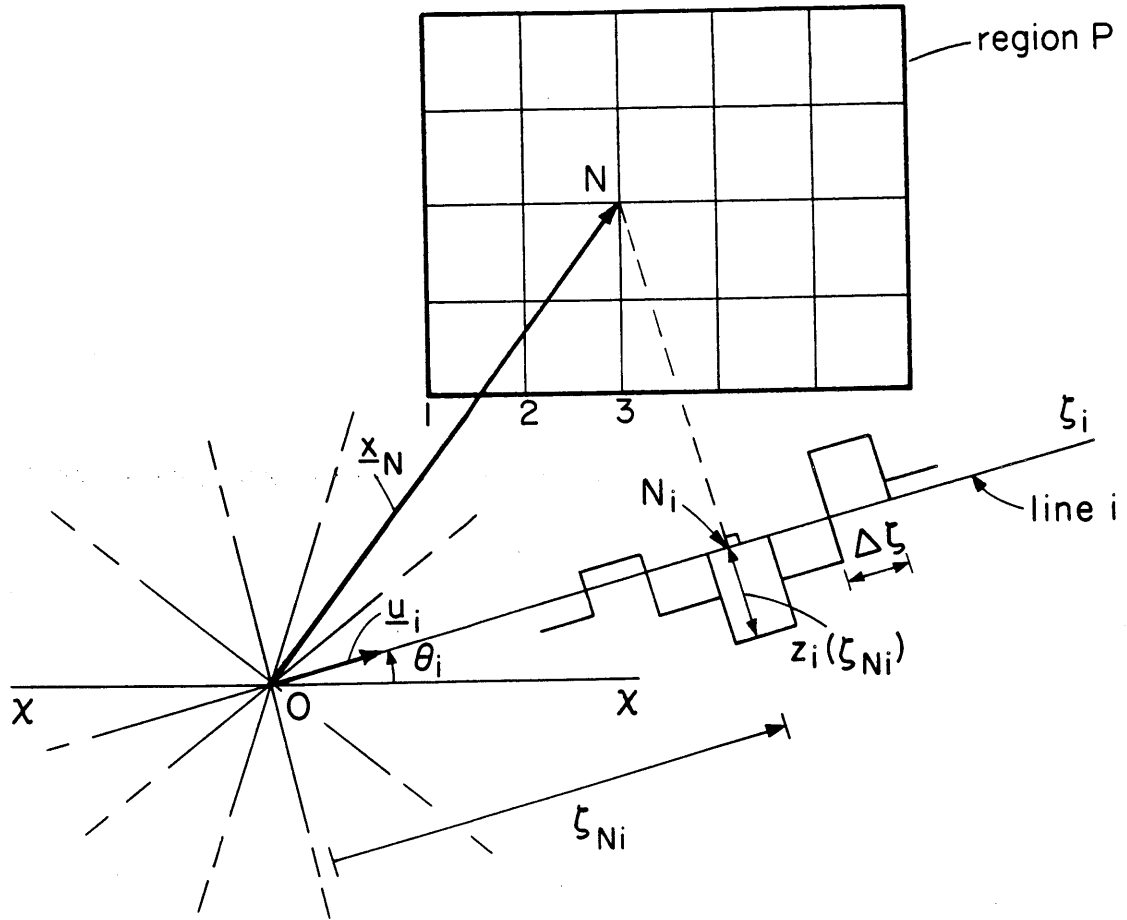
Figure 6.1   Schematic representation of the three-dimensional field P
and the turning bands lines.

$$\underline{Z}_s(\underline{x}_N) = \frac{1}{\sqrt{L}} \sum_{i=1}^{L} \underline{Z}_i^{(1)}(\underline{x}_N \cdot \underline{u}_i) \qquad (6.7)$$

as the realization of the two or three-dimensional random field.

The realizations generated using (6.7) have a zero mean. The objective is to choose a proper unidimensional covariance $\underline{\underline{C}}_i^{(1)}(\zeta)$ (or spectral density function $\underline{\underline{S}}_i^{(1)}(k)$) so that $\underline{Z}_s$ defined in (6.7) has the proper two- or three-dimensional covariance or spectral density function matrix $\underline{\underline{C}}(\underline{r})$, $\underline{\underline{S}}(\underline{k})$. Take two points $\underline{x}_1$, $\underline{x}_2$ in the two- or three-dimensional space. The covariance function matrix of the simulated field is

$$\underline{\underline{C}}_s(\underline{x}_1, \underline{x}_2) = E[\underline{Z}_s(\underline{x}_1) \, \underline{Z}_s^T(\underline{x}_2)]$$

$$= \frac{1}{L} \sum_{i=1}^{L} \sum_{j=1}^{L} E[\underline{Z}_i^{(1)}(\underline{x}_1 \cdot \underline{u}_i) \, \underline{Z}_j^{(1)T}(\underline{x}_2 \cdot \underline{u}_j)] =$$

$$= \frac{1}{L} \sum_{i=1}^{L} E[\underline{Z}_i^{(1)}(\underline{x}_1 \cdot \underline{u}_i) \, \underline{Z}_i^{(1)T}(\underline{x}_2 \cdot \underline{u}_i)] = \frac{1}{L} \sum_{i=1}^{L} \underline{\underline{C}}_i^{(1)}(\underline{r} \cdot \underline{u}_i) \qquad (6.8)$$

where unidimensional processes along two different lines are assumed to be uncorrelated and $\underline{r} = \underline{x}_2 - \underline{x}_1$. The expected value $E[\underline{Z}_i^{(1)}(\underline{x}_i \cdot \underline{u}_i) \, \underline{Z}_i^{(1)T}(\underline{x}_2 \cdot \underline{u}_i)]$ represents the covariance function matrix of the one-dimensional processes on line i between points $\underline{x}_1 \cdot \underline{u}_i$ and $\underline{x}_2 \cdot \underline{u}_i$, which, since unidimensional processes are stationary, is written as $\underline{\underline{C}}_i^{(1)}(\underline{r} \cdot \underline{u}_i)$. For uniformly distributed lines in the two- or three-dimensional space, vector $\underline{u}_i$ is uniformly distributed on the unit circle or on the unit sphere, and the right-hand side of (6.8) is only a function of $\underline{r}$ for large L. This implies that process $\underline{Z}_s$ is stationary and we can write

$$\underline{\underline{C}}_s(\underline{r}) = \frac{1}{L} \sum_{i=1}^{L} \underline{\underline{C}}_i^{(1)}(\underline{r} \cdot \underline{u}_i) \quad . \tag{6.9}$$

For $L \to \infty$, using the law of large numbers Equation (6.9) becomes

$$\underline{\underline{C}}_s(\underline{r}) = \lim_{L \to \infty} \left\{ \frac{1}{L} \sum_{i=1}^{L} \underline{\underline{C}}_i^{(1)}(\underline{r} \cdot \underline{u}_i) \right\} = E[\underline{\underline{C}}_u^{(1)}(\underline{r} \cdot \underline{u})] =$$

$$= \int_C \underline{\underline{C}}_u^{(1)}(\underline{r} \cdot \underline{u}) \, p(\underline{u}) \, d\underline{u} \tag{6.10}$$

where subscript u implies dependence of $\underline{\underline{C}}^{(1)}$ on direction $\underline{u}$, c represents the unit circle or sphere and $p(\underline{u})$ is the probability density function of $\underline{u}$ which becomes $1/2\pi$ or $1/4\pi$ in the two- and three-dimensional cases, respectively and $d\underline{u}$ represents a differential length or area on the unit circle or sphere at the end of vector $\underline{u}$.

The three-dimensional case is examined first. Because of stationarity of the processes, without loss of generality, we define orthogonal x_1, x_2, x_3 axes with origin point $\underline{x}_1$ and with x_3 axis in the direction of vector $\underline{r} = \underline{x}_2 - \underline{x}_1$, as shown in Figure 6.2. The unit sphere where the vector $\underline{u}$ ends is also shown. Using spherical coordinates $\underline{r} \cdot \underline{u} = r \cos\phi$, where $r = |\underline{r}|$ and $d\underline{u} = \sin\phi \, d\phi \, d\theta$. Integral (6.10) then gives

$$\underline{\underline{C}}_s(\underline{r}) = \frac{1}{4\pi} \int_0^{2\pi} \int_0^{\pi} \underline{\underline{C}}_{\phi,\theta}^{(1)} (r \cos\phi) \sin\phi \, d\phi \, d\theta \tag{6.11}$$

(subscripts ϕ, θ of $\underline{\underline{C}}^{(1)}$ imply dependence of $\underline{\underline{C}}^{(1)}$ on direction ϕ, θ). Let $\underline{\underline{S}}_{\phi,\theta}^{(1)}(k)$ the spectral density function matrix corresponding to the
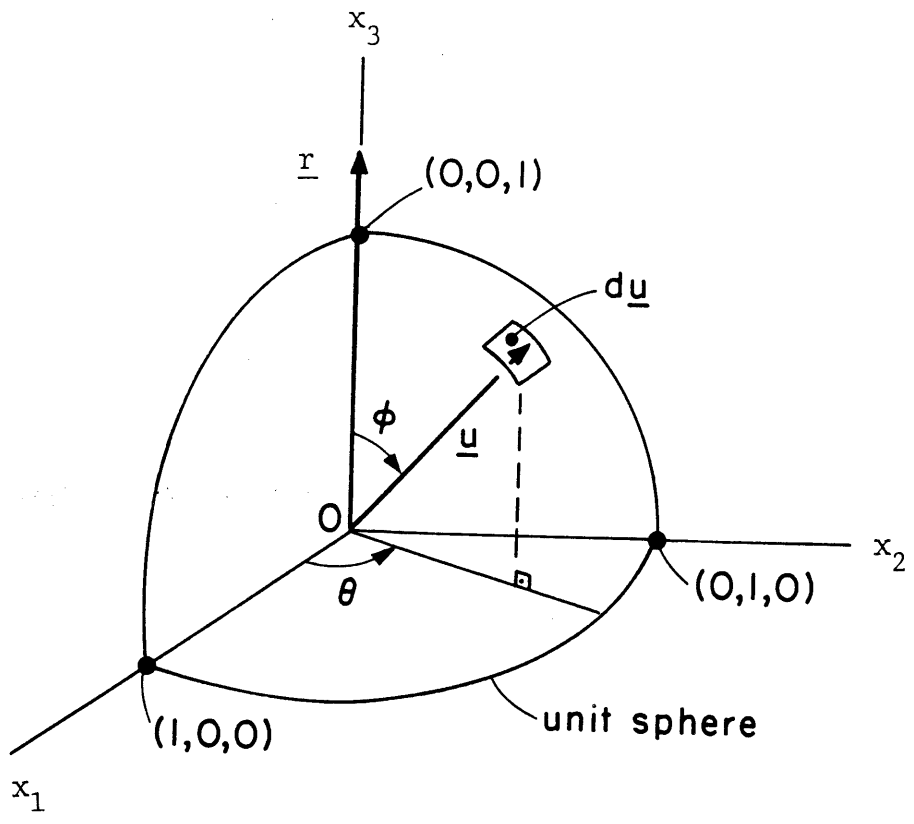
Figure 6.2   Definition sketch for the three-dimensional case, showing
the unit sphere.

covariance function $\underline{\underline{C}}_{\phi,\theta}^{(1)}$. It holds

$$\underline{\underline{C}}_{\phi,\theta}^{(1)} (r \cos\phi) = \int_{-\infty}^{\infty} e^{jk\,r\,\cos\phi} \ \underline{\underline{S}}_{\phi,\theta}^{(1)}(k)dk \quad . \qquad (6.12)$$

Substituting into (6.11) and using the symmetry of the spectral densities yields:

$$\underline{\underline{C}}_s(\underline{r}) = \frac{1}{2\pi} \int_{0}^{2\pi} \int_{0}^{\pi} \int_{0}^{\infty} e^{jk\,r\,\cos\phi} \ \underline{\underline{S}}_{\phi,\theta}^{(1)}(k) \ \sin\phi \ dk \ d\phi \ d\theta \ . \qquad (6.13)$$

Define orthogonal coordinates k_1, k_2, k_3 in the wave number space. The differential volume $dk_1 dk_2 dk_3$ is given in spherical coordinates by: $dk_1 dk_2 dk_3 = k^2 \sin\phi \ dk d\phi d\theta$ where $k = \sqrt{k_1^2 + k_2^2 + k_3^2}$, $k_1 = k \sin\phi \sin\theta$, $k_2 = k \sin\phi \cos\theta$, $k_3 = k \sin\phi$. Note that the limits of the integral in (6.13) cover the whole three-dimensional space R^3. Using orthogonal coordinates (6.13) is expressed as

$$\underline{\underline{C}}_s(\underline{r}) = \iiint_{-\infty}^{\infty} e^{j\underline{k}\cdot\underline{r}} \ \frac{\underline{\underline{S}}_{\phi,\theta}^{(1)}(k)}{2\pi k^2} \ dk_1 \ dk_2 \ dk_3 \quad . \qquad (6.14)$$

To preserve the given three-dimensional covariance function matrix, $\underline{\underline{C}}(\underline{r})$, substitute $\underline{\underline{C}}_s(\underline{r}) \equiv \underline{\underline{C}}(\underline{r})$. Comparing then (6.14) to (6.5) and using the uniqueness of the Fourier transform yields:

$$\underline{\underline{S}}_{\phi,\theta}^{(1)}(k) = 2\pi \ k^2 \ \underline{\underline{S}}(\underline{k})$$

$$= 2\pi \ k^2 \ \underline{\underline{S}}(k \sin\phi \sin\theta, \ k \sin\phi \cos\theta, \ k \sin\phi) \qquad (6.15)$$

This equation relates the spectral density function matrix of the one-

dimensional processes $\underline{Z}^{(1)}$ to the spectral density function matrix of the three-dimensional process. Note that $\underline{\underline{S}}^{(1)}$ depends on the direction ϕ, θ of the corresponding line where the unidimensional process is generated. Since $\underline{\underline{S}}^{(1)}_{\phi,\theta}$ are known, the one-dimensional processes $\underline{Z}^{(1)}$ can now be generated using a one-dimensional generator as will be discussed later.

The two-dimensional case is now investigated. Because of stationarity of the processes, without loss of generality, we define orthogonal axes x_1, x_2 with origin point $\underline{x}_1$ and with x_2 axis in the direction of vector $\underline{r} = \underline{x}_2 - \underline{x}_1$, as shown in Figure 6.3. The unit circle where the vector $\underline{u}$ ends is also shown. Using polar coordinates $\underline{r} \cdot \underline{u} = r \sin\theta$ and $d\underline{u} = d\theta$. Integral (6.10) then gives

$$\underline{\underline{C}}_s(\underline{r}) = \frac{1}{2\pi} \int_0^{2\pi} \underline{\underline{C}}^{(1)}_\theta (r \sin\theta) \, d\theta \tag{6.16}$$

where the subscript θ implies dependence of $\underline{\underline{C}}^{(1)}_\theta$ on θ. Let $\underline{\underline{S}}^{(1)}_\theta(k)$ the spectral density function matrix corresponding to the covariance function matrix $\underline{\underline{C}}^{(1)}_\theta$. It then holds

$$\underline{\underline{C}}^{(1)}_\theta (r \sin\theta) = \int_{-\infty}^{\infty} e^{jk \, r \, \sin\theta} \, \underline{\underline{S}}^{(1)}_\theta (k) dk \quad . \tag{6.17}$$

Substituting into (6.16) and using the symmetry of the spectral densities gives

$$\underline{\underline{C}}_s(\underline{r}) = \frac{1}{\pi} \int_0^{2\pi} \int_0^{\infty} e^{jk \, r \, \sin\theta} \, \underline{\underline{S}}^{(1)}_\theta (k) \, dk \, d\theta \quad . \tag{6.18}$$

Define orthogonal coordinates k_1, k_2 in the wave number space. The differential volume $dk_1 dk_2$ is given by $dk_1 dk_2 = k dk d\theta$ where
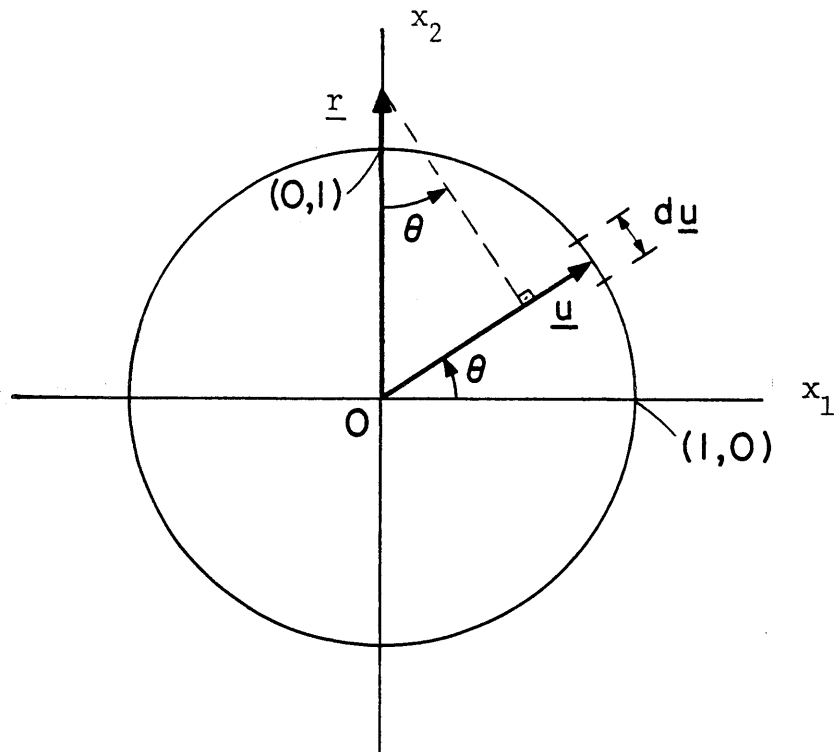
Figure 6.3   Definition sketch for the two-dimensional case, showing the
unit circle.

$k = \sqrt{k_1^2 + k_2^2}$, $k_1 = k_1 \cos\theta$ and $k = k_2 \sin\theta$. Note that the limits of

the integral in (6.18) cover the whole two-dimensional space R^2. Using

orthogonal coordinates (6.18) is expressed as

$$\underline{C}_s(\underline{r}) = \int\limits_{-\infty}^{\infty}\int e^{j\underline{k}\cdot\underline{r}} \frac{\underline{S}_\theta^{(1)}(k)}{\pi k} \, dk_1 \, dk_2 \quad . \tag{6.19}$$

In order to preserve the given two-dimensional covariance function

matrix, substitute $\underline{C}_s(\underline{r}) = \underline{C}(\underline{r})$. Comparing the (6.19) to (6.5) and

using the uniqueness of the Fourier transform gives

$$\underline{S}_\theta^{(1)}(k) = \pi k \, \underline{S}(\underline{k}) =$$
$$= \pi k \, \underline{S}(k \cos\theta, \, k \sin\theta) \quad . \tag{6.20}$$

This equation relates the spectral density function matrix of the one-

dimensional processes $\underline{Z}^{(1)}$ to the spectral density function matrix of

of the two-dimensional process $\underline{S}$. Note that $\underline{S}^{(1)}$ depends on the

direction θ of the corresponding line where the unidimensional process

is generated. Given $\underline{S}_\theta^{(1)}$, the one-dimensional processes can be

generated as will be discussed below.

The method proposed by Shinozuka and Jan (1972) is briefly discus-

sed for generation of the one-dimensional vector processes $\underline{Z}_i^{(1)}(\zeta)$ on

line i of direction θ or ϕ, θ in the two- and three-dimensional case

respectively. Let

$$\underline{Z}_i^{(1)}(\zeta) = 2 \sum_{j=1}^{M} \underline{Q}_i(k_j) \, \Delta k^{1/2} \left| \begin{array}{c} \cos(k_j \zeta + \phi_{j_1}) \\ \cos(k_j \zeta + \phi_{j_2}) \\ \cdots\cdots\cdots\cdots \\ \cos(k_j \zeta + \phi_{j_K}) \end{array} \right| \tag{6.21}$$

where $\underline{Q}_i(k)$ is obtained by decomposition of matrix $\underline{S}_i^{(1)}(k)$, given by (6.15) or (6.20) in the two- and three-dimensional case respectively, i.e.,

$$\underline{Q}_i(k) \cdot \underline{Q}_i^T(k) = \underline{S}_i^{(1)}(k) \quad . \tag{6.22}$$

$\phi_{j\ell}$ are independent random angles uniformly distributed between 0 and 2π, $k_j = (j - 1/2)\,\Delta k$ and $k_j' = k_j + \delta k$ for $j = 1, \ldots, M$. It has been assumed that the spectral density function $\underline{S}_j^{(1)}(k)$ is insignificant outside the region $[-\Omega, +\Omega]$. The discretization frequency Δk is defined as $\Delta k = \Omega/M$, where M is the number of harmonics used. The frequency δk is a small random frequency added in order to avoid periodicities and is uniformly distributed between $-\Delta k'/2$ and $\Delta k'/2$ where $\Delta k'$ is a small frequency $\Delta k' \ll \Delta k$. The magnitude of the errors due to using a finite number of harmonics in the one-dimensional process is discussed in Mantoglou and Wilson, (1982).

Equation (6.10) is obtained in the limit as the number of lines L tends to infinity. Of course only a finite number of lines can be used in application thus an error is introduced (see Mantoglou and Wilson, 1982). The lines in (6.10) are assumed to be randomly oriented on the two- or three-dimensional space. The same TBM equations are also obtained by spacing the lines evenly on the unit sphere or circle with prescribed directions. Mantoglou and Wilson (1982) show that the simulated covariance obtained using the even line spacing approach converges to the theoretical covariance much faster than the random line approach.

Spacing a number of lines evenly on the unit circle is a trivial

problem. However, spacing a number of lines evenly on the unit sphere is only possible for a specific set of number of lines (e.g., 3, 15, ...). In two-dimensions Mantoglou and Wilson (1982) show that a number of 8-16 lines is generally a satisfactory choice. In three-dimensions, experience has shown (Journel and Huijbregts, 1978) that a group of 15 lines, joining the midpoints of the opposite edges of a regular icosahedron, is adequate for practical applications in the isotropic case. In the anisotropic case however, a larger number of lines might be required. Spacing of a number of lines in the unit sphere then could be accomplished by dividing the unit sphere into regions of approximately the same size and shape.

The method developed above is very general and is capable of simulating anisotropic fields having any type of anisotopy. In certain cases (e.g., point processes) it is possible to generate the anisotropic field by generation of an isotropic field followed by a linear transformation of the coordinate system. In other cases however, (e.g., areal average processes) it is not possible to use such transformation and it is necessary to use the general anisotropic method described above.

The problem of direct generation of spatial averages of vector process $\underline{Z}(\underline{x})$ is now discussed. A spatial average process is generally defined as

$$\underline{Z}_A(\underline{x}) = \int_A h(\underline{x}-\underline{s}) \, \underline{Z}(\underline{s}) \, d\underline{s} \qquad (6.23)$$

where A is the support (averaging) region in the two- or three-dimensional space and $h(\underline{x})$ is a weighting function. Using a wave

number representation of (6.23) and the properties of convolution yields

$$dZ_{Z_A}(\underline{k}) = H(\underline{k}) \ dZ_Z(\underline{k}) \qquad (6.24)$$

where $H(\underline{k})$ is the Fourier transform of $h(\underline{x})$. Using the property $\underline{\underline{S}}(k) = E[d\underline{Z}(k) \ d\underline{Z}^*(\underline{k})^T]$ produces

$$\underline{\underline{S}}_A(\underline{k}) = \left| H(\underline{k}) \right|^2 \underline{\underline{S}}(\underline{k}) \quad . \qquad (6.25)$$

For a known spectral density function matrix $\underline{\underline{S}}(k)$ the corresponding spectral density function matrix $\underline{\underline{S}}_A$ of the spatial process $\underline{Z}_A$ can be evaluated from (6.25). Given $\underline{\underline{S}}_A(\underline{k})$ the general TBM developed earlier can be used for direct generation of the areal average process.

The wave number response $H(\underline{k})$ of spatial filter $h(\underline{x})$ is evaluated as follows

$$H(\underline{k}) = \frac{1}{(2\pi)^n} \int_{R^n} e^{-j\underline{h}\cdot\underline{x}} \ h(\underline{x}) \ d\underline{x} \qquad (6.26)$$

In the three-dimensional case and for a rectangular block average process for example it holds

$$h(\underline{x}) = \begin{cases} \dfrac{1}{L_1 L_2 L_3} & ; \quad \underline{x} \text{ inside block} \\[2mm] 0 & ; \quad \underline{x} \text{ outside block} \end{cases} \qquad (6.27)$$

where L_1, L_2, L_3 the block dimensions. Assuming that the block is oriented in the direction of the axes x_1, x_2, x_3, substituting (6.27) and evaluating (6.26) yields

$$H(k) = \frac{8}{L_1 L_2 L_3 k_1 k_2 k_3} \sin\left(\frac{k_1 L_1}{2}\right) \sin\left(\frac{k_2 L_2}{2}\right) \sin\left(\frac{k_3 L_3}{2}\right) \quad . \qquad (6.28)$$

In the two-dimensional case for rectangular areal average process it holds

$$h(\underline{x}) = \begin{cases} \dfrac{1}{L_1 L_2} \; ; & \underline{x} \text{ inside the rectangle} \\[2ex] 0 \; ; & \underline{x} \text{ outside the rectangle} \end{cases} \qquad (6.29)$$

where L_1, L_2 the dimensions of the rectangle in the x_1 and x_2 directions, respectively. Mantoglou and Wilson (1981) evaluate the corresponding two-dimensional wave number response function as

$$H(\underline{k}) = \frac{1}{L_1 L_2 k_1 k_2} \sin\left(\frac{k_1 L_1}{2}\right) \sin\left(\frac{k_2 L_2}{2}\right) \quad . \qquad (6.30)$$

Given (6.28) and (6.30) the spectral density function of the averaged three- or two-dimensional process is evaluated from (6.25). Using (6.15) or (6.20), the spectral density function of the corresponding one-dimensional process is evaluated. The one-dimensional processes are generated using the generator described by (6.21) or any other one-dimensional generator (e.g., by matrix decomposition).

Consider for illustration the case of a single three-dimensional point process (i.e. K = 1) having an exponential covariance function (Equation 2.3). Then from (6.15) the corresponding one-dimensional processes have covariance functions given by

$$S_{\phi,\theta}^{(1)}(k) = \frac{2\sigma^2 k^2 \lambda_1 \lambda_2 \lambda_3}{\pi^2 (1 + \lambda_1^2 k^2 \sin^2\phi \sin^2\theta + \lambda_2^2 k^2 \sin^2\phi \cos^2\theta + \lambda_3^2 k^2 \sin^2\phi)} \quad (6.31)$$

and they can be generated by (6.21), where in the single random field case (k=1), Equation (6.22) gives:

$$Q_{\phi,\theta}(k) = \left(S_{\phi,\theta}^{(1)}(k)\right)^{1/2} \quad .$$

267

6.3 Estimation of Large-Scale Model Parameters Using Statistical Inference and System Identification Methods

The effective parameters derived in the previous chapters depend on the large-scale trends (means) of the soil property variability and on the stochastic properties of local soil property variability (variances, correlation lengths, etc.). In order to be able to use the large-scale flow and transport models in applications, these soil property characteristics should be evaluated using available information. Three types of information can be available depending on the particular application. The first type includes direct observations of the local soil properties at a finite number of observation points. The second type of information includes observations of the local capillary tension head and/or concentration outputs. Such observations will be available only after the real system has been excited with water and tracer inputs. The last type of information includes prior knowledge about the soil variability. Such knowledge may be based on geologic information, an expert's judgment, etc. Although often qualitative, this information can be very important since it could suggest an appropriate parametric model for the mean soil properties (e.g., constant, linear, polynomial trend, etc.) the form of the covariance function for the local soil properties (exponential, etc.) a prior mean and covariance for the unknown parameters, etc.

Section 6.3.1 discusses the problem of estimating the soil parameters, required by the large scale models, when observations of the local soil properties are available. Section 6.3.2 discusses the more general system identification problem when observations of the system output

268

and any other observations or prior information are available, and develops a new identification method.

6.3.1 Statistical Inference Methods

This section discusses the problem of inferring the stochastic parameters of soil property variability, when point measurements of the local soil properties are available. The stochastic parameters include the mean, variances, spectral density functions, etc. and are required for specification of the large-scale models. Since statistical inference is an important topic of the parameter estimation literature, the following presentation is by no means complete. The intention is to discuss some inherent problems and to mention the existence of some new methods that might be useful in this problem.

Estimation of the statistical parameters of a soil property random field is associated with two inherent problems. The first problem comes from the fact that only one realization of the random field can be observed (i.e., the existing realization). As it is impossible to estimate an underlying probability density function of a random variable from a single observation of the variable, it is impossible to estimate the statistical properties of a random field from only one of its realizations. In order to get this theoretical difficulty across two approaches could be followed. In the first approach it might be assumed that similar soil formations (e.g., glaciofluvial deposits at different settings in the New Mexico Desert area) are different realizations of the same underlying random field. This is similar to assuming that the generating power at the time of formation of these sediments did not arbitrarily

269

generate them but generated them according to some probability law, depending on what materials existed in the area, laws of physics, etc. This approach of assuming that similar soil formations are realizations of one random field will be particularly useful in the future when sufficient information characterizing the nature of variability of different types of soil formations has been collected and analyzed.

A second approach for estimating the stochastic properties of a random field from one only realization, requires an ergodic hypothesis. Because this hypothesis often generates conceptual difficulties in the field of hydrology, a simple and intuitive interpretation is given below. The ergodic hypothesis assumes that space averages of a single realization of a random field are equal to the ensemble statistics. In other words, even only one realization carries sufficient information about the statistical properties of the underlying random field. This assumption cannot be proved or disproved, since one realization is available. Nevertheless, this assumption helps in (i) removing large-scale variations that their exact form is of importance in the problem under consideration and we may not want to model them as random and (ii) identifying the properties of a random field that produces realizations that look like the observed reality. The ergodicity assumption is simply a convenient tool of analysis. Its appropriateness in a particular problem depends on whether the final product is useful or not.

A second difficulty associated with the practical problem of estimating the statistical parameters of a random field, is the fact that even the one existing realization of the random field is not known at

each point in space. It is only known at a few sampling locations and the sampling domain is of a finite size.

Despite the above theoretical and practical difficulties, estimation of the statistical parameters of a random field, can be feasible if sufficient data exist and the estimation method is appropriately designed and used. The remainder of this section discusses several approaches that have been proposed for inference of stochastic parameters of random fields. Since the literature on the subject is extensive, the following discussion is brief and by no means complete. The objective is to point out some important aspects that should be considered and give some basic references.

The first step of the statistical inference of random fields problem is to evaluate the mean (trend) of the underlying process. Usually a parametric mean model is assumed (e.g., constant, linear, polynomial, etc.). The form of the mean model selected depends on how the data look, the judgment of the modeler, the type of required application, etc. If a constant mean model is assumed, the mean can be easily evaluated as a spatial average of the local measurements. If a spatially varying mean model is assumed, the model coefficients can be estimated using a least squares or a parameter estimation method (e.g., kriging, see Journel and Huijbregts, 1978; Delfiner, 1976; Chauvet et al., 1982; David, 1977, etc).

The residual process is obtained by subtracting the mean from the local measurements. The residuals are assumed to be zero mean stationary and ergodic. The second and most difficult step of the statistical inference problem is estimation of the stochastic properties of the

residuals (i.e., covariance, spectral density function, etc.). Note that the stochastic theory developed in previous chapters requires evaluation of the spectral density functions of the residuals rather than the covariance function.

Two basic approaches could be followed for estimation of the spectral density functions of the residual processes. The first approach follows three steps. In the first step the local measurements are processed and the sample covariance function $C(r_i)$ at discrete separation distances r_i are obtained. If the measurements are obtained in a regular sampling lattice, estimates of the covariance can be obtained as a spatial average of the products of point measurements lying on same distances, (see, e.g., Davis, 1973). If measurements are irregularly spaced, it is possible to discretize distances in several intervals and take a spatial average of products of measurements that fall into particular intervals, (see, e.g., Journel and Huijbregts, 1978; Agterberg, 1970; David, 1977). The second step of this approach consists of fitting a covariance function model $C(r)$ to the discrete sample values of the covariance function $C(r_i)$ obtained in the first step (see, e.g., Agterberg, 1970). Parametric models having a few parameters (e.g., exponential, spherical, etc., covariance models) are particularly useful and very popular. The third step of the analysis consists of evaluation of the spectral density function $S(k)$ by taking the Fourier transform of the covariance function $C(r)$ estimated in the second step.

The second approach follows two steps only. The first step consists of obtaining estimates of the covariance function $C(r_i)$ at discrete separation distances, similarly to the first approach. The second step

272

consists of direct estimation of the spectral density function $S(\underline{k})$ without intermediate evaluation of the covariance function.

Although both approaches are seemingly similar, the second approach seems more attractive for two reasons. First one usually knows more on the spectrum side than on the covariance side and may take into account such knowledge in the estimation procedure. In our problem for example, we know that different components of the spectrum have different contributions to the output (see, e.g., Equation 3.37), so an appropriate weighting could be chosen for a better estimation of the more important components of the spectrum. When estimating the covariance function however, this is not possible since the effects of the different separation distances of the soil properties on the output are not known. A second property that makes spectral estimation more attractive is that the spectral estimates tend to be uncorrelated while covariance estimates are usually correlated. As a result statistical confidence limits are easily established for spectra but not for the covariance.

The spectral estimation problem is now briefly discussed. There seems to exist a large number of methods and their effectiveness largely depents on the particular application. Fourier transform methods have been extensively used in the past. However, several recent methods such as the maximum likelihood method and the maximum entropy method are gaining increasing interest in the multidimensional case and are the subject of current research activity in this field (McGlellan, 1982). Since some of these methods are very promising and unknown in the field of hydrology, they are briefly discussed below mainly for reference purposes.

273

The Fourier transform methods consist of taking the Fourier transform of the covariance function estimated at a discrete number of separation distances. At small separation distances the covariance function is estimated from a large number of pairs of points. At large separation distances however, only a few number of pairs of points are available and significant errors in the estimated discrete values of the covariance function are expected. In order to make the method more robust, a smoothing (windowing) procedure is usually used (see, e.g., Jenkins and Watts, 1968). There are three problems associated with using these methods in the multidimensional case. First, the sampled data should be available in a uniform grid. Second, in the multidimensional case there are only a few windows to choose from (McClellan, 1982). The third problem is that these methods do not produce a high resolution estimate.

The maximum likelihood method (e.g., Cason, 1969; Larimore, 1977) does not require regular sampling or windowing and yields a high resolution estimate of the spectral density function. The objective of the method is to evaluate the spectral density function by maximizing the probability of occurence of the measurements. The maximum likelihood method is of particular interest since it is relatively simple and very flexible.

The maximum entropy method proposed by Burg (1968), can provide good resolution on lower frequency estimates. In the one-dimensional case this estimate can be computed from a linear autoregressive type equation. The maximum entropy estimate provides a good resolution even when the sampled part of the random field is of a limited size. It seems

274

that this method is particularly suited in our applications, where only a limited part of the realization is observed and high resolution at lower frequencies is important. This method, requires solution of a nonlinear optimization problem which might be computationally involved. The efficiency of this algorithm should be demonstrated using real data.

6.3.2 System Identification

In the context of this study system identification is defined as the derivation of a predictive model of a system using any available information, including observations of the system output. This section discusses the problem of the identification of unsaturated flow systems. The theory of this section can be easily extended to the saturated flow case and to the contaminant transport problem.

Two basic steps of system identification are model structure selection and parameter estimation. Selecting an appropriate model structure is of paramount importance in most problems of identification of complex systems (see, Mantoglou, 1983 and Mantoglou and Schweppe, 1983). Several factors guide the model structure selection process such as model structure validity and accuracy (from a physical perspective),parameter identifiability, requirements of the parameter estimation method in terms of cost and accuracy (i.e., linearizations, iterative minimization, covergence, etc., see, Mantoglou and Schweppe, 1983). Successful identification often depends on selecting an appropriate model structure. Recent identification studies have not realized the importance of this problem and consequently results produced are often questionable.

275

In the unsaturated flow case for example, the model of the system derived using physical arguments (i.e., the local governing flow Equation (3.3)) is theoretically the most valid and accurate model of the system. As was discussed earlier however, this model is not very useful in applications since the model parameters correspond to the highly variable local properties which cannot be estimated from a finite data set. Another more pragmatic approach, which essentially represents current hydrologic practice, is to assume that the local model is valid on a larger scale and that the parameters of such a large-scale model are some smooth estimates (mean) of the local highly variable soil properties. It is possible then to estimate the model parameters from a realistic data set, since these parameters are not the local properties but they are large-scale trends. This approach has been extensively used for identification of aquifer flow systems (see, Townley, 1983; Clifton and Newman, 1982; Cooley, 1982; Newman and Yakowitz, 1979; Shah et al., 1978, etc). The large-scale flow equation (usually selected without justification to be of the same form as the local governing equation) is discretized and the unknown parameter values are evaluated at the numerical discretization nodes or blocks. Since the number of parameters is usually large compared to the available information, additional constraints concerning the variability of the node or block parameters are often imposed (e.g., zonation, parameterization, Bayesian estimation). Since the large-scale model parameters and their relationship to physical characteristics are not well defined in these applications, the imposed constraints are often arbitrary and are usually selected for mathematical convenience.

276

Besides the above critique it is possible that the identification approach discussed above may be well suited for identification of aquifer flow systems since the aquifer flow systems are almost linear in the parameters and it is possible that the small-scale property fluctuations may not have significant large-scale effects (see, Mizel et al., 1980; Dagan, 1982). In the unsaturated flow case however, this approach is definitely not appropriate. The unsaturated flow system is highly non-linear in the parameters and, as was seen earlier, the local soil property variability has important large-scale effects (hysteresis, anisotropy, etc). A valid large-scale model structure of the unsaturated flow system should consider the large-scale effects of local soil property variability.

The stochastic methodology developed in Chapters 3 and 4 provides a means for deriving a valid large-scale model structure that takes into account the large-scale effects of local soil property variability. The large-scale model structure obtained using the stochastic theory, provides a theoretically justified, not an arbitrary, approximation of the large-scale processes involved and should be able to capture these large-scale flow processes. The large-scale model parameters depend on a few variables (large-scale trends, variances, correlation lengths, etc.) which can hopefully be estimated using prior knowledge about soil property variability, measurements of the local soil properties and the system output, etc. Note that the large-scale model predicts large-scale flow characteristics rather than local outputs. Because of this a model error is introduced and the statistical properties of this error should be taken into account in the parameter estimation procedure and during model use.

After the important step of model structure selection, the model parameters must be estimated using available information. A parameter estimation method, based on a maximum likelihood criterion, is developed below. The method is very general and flexible, and it can consider both soil property, capillary tension head measurements, and prior information about the model parameters. In addition the method is physically consistent and can take into account the effects of the model error.

Let $\underline{\beta}$ represent the vector of unknown parameters having elements: F, A, Γ, σ_f^2, σ_a^2, σ_γ^2, λ_1, λ_2, λ_3, etc. Define vectors $\underline{\psi}_1$, $\underline{\psi}_2$, ..., $\underline{\psi}_N$ representing the capillary tension head observations, where $\underline{\psi}_i$ include observations at a set of measurement points distributed throughout the flow domain at times $i = 1$, ..., N. Similarly as above define vectors $\underline{H}_1(\underline{\beta})$, $\underline{H}_2(\underline{\beta})$, ... $\underline{H}_N(\underline{\beta})$ to include the capillary tension head predicted by the large-scale model having parameters $\underline{\beta}$, at the locations where measurements of ψ were obtained at times $i = 1$, ..., N. These model predictions can be obtained using a numerical three-dimensional unsaturated flow code. Vectors $\underline{\psi}_i$ are related to $\underline{H}_i$ through

$$\underline{\psi}_i = \underline{H}_i(\underline{\beta}) + \underline{h}_i \tag{6.32}$$

where $\underline{h}_i$; $i = 1$, ..., N, are the large-scale model errors at the measurement locations and times $i = 1$, ..., N. If measurement errors are present they should be added to $\underline{h}_i$. Defining

$$\underline{\psi} = \begin{vmatrix} \underline{\psi}_1 \\ \underline{\psi}_2 \\ \vdots \\ \underline{\psi}_N \end{vmatrix} \quad ; \quad \underline{H} = \begin{vmatrix} \underline{H}_1 \\ \underline{H}_2 \\ \vdots \\ \underline{H}_N \end{vmatrix} \quad ; \quad \underline{h} = \begin{vmatrix} \underline{h}_1 \\ \underline{h}_2 \\ \vdots \\ \underline{h}_N \end{vmatrix} \qquad (6.33)$$

(6.32) is written as:

$$\underline{\psi} = \underline{H}(\underline{\beta}) + \underline{h} \qquad (6.34)$$

where $\underline{\psi}$ now includes the output measurements at all locations and all times. In the case when direct observations of the local soil properties $\ell n K_s$, α and C exist, define vector $\underline{s}$ to include these observations. Let $\underline{P}$ and $\underline{p}$ represent the mean and fluctuations of the soil properties at M measurement points. Vector $\underline{P}$ depends on the unknown parameter vector $\underline{\beta}$ and in particular on the mean properties F, A and Γ. We may then write

$$\underline{s} = \underline{P}(\underline{\beta}) + \underline{p} \quad . \qquad (6.35)$$

Note that functions $\underline{H}(\underline{\beta})$ and $\underline{P}(\underline{\beta})$ in (3.34) and (3.35) depend on $\underline{\beta}$ directly. The random vectors $\underline{h}$ and $\underline{p}$ however, do not directly depend on $\underline{\beta}$ but their corresponding covariances $\underline{\Sigma}_{hh}$ and $\underline{\Sigma}_{pp}$ depend on $\underline{\beta}$. Let us further assume that prior information about parameters $\underline{\beta}$ is available, in terms of a prior mean $\underline{\beta}$ and a prior covariance $\underline{\Sigma}_{\beta\beta}$. Such information may be available if the type and characteristics of the geologic unit are available, or by using the modeler's judgment, etc. In this case $\underline{\beta}$ can be expressed as follows.

279

$$\underline{B} = \underline{\beta} + \underline{b} \qquad (6.36)$$

where $\underline{B}$ and $\underline{\Sigma}_{bb}$ are the prior mean and prior covariance which are assumed to be known. Combining (6.34), (6.35) and (6.36) yields

$$\underline{z} = \underline{\Phi}(\underline{\beta}) + \underline{v} \qquad (6.37)$$

where

$$\underline{z} = \begin{vmatrix} \underline{\psi} \\ \underline{s} \\ \underline{B} \end{vmatrix} \quad ; \quad \underline{\Phi}(\underline{\beta}) = \begin{vmatrix} \underline{H}(\underline{\beta}) \\ \underline{P}(\underline{\beta}) \\ \underline{\beta} \end{vmatrix} \quad ; \quad \underline{v} = \begin{vmatrix} \underline{h} \\ \underline{p} \\ \underline{b} \end{vmatrix} \quad . \qquad (6.38)$$

The covariance matrix of $\underline{v}$ is given by

$$\underline{\Sigma}_{vv}(\underline{\beta}) = \begin{vmatrix} \underline{\Sigma}_{hh}(\underline{\beta}) & \underline{\Sigma}_{hp}(\underline{\beta}) & 0 \\ \underline{\Sigma}_{ph}(\underline{\beta}) & \underline{\Sigma}_{pp}(\underline{\beta}) & 0 \\ 0 & 0 & \underline{\Sigma}_{bb} \end{vmatrix} \qquad (6.39)$$

where it is assumed that parameters $\underline{\beta}$ (which include F, A, Γ, etc.) are not correlated to the actual local property fluctuations (f, a, γ, etc.).

Equation (6.37) corresponds to a general nonlinear parameter estimation problem. Assuming that $\underline{v}$ is a Gaussian vector the maximum likelihood estimate of $\underline{\beta}$ is obtained by minimizing the following cost functional

$$J(\underline{\beta}) = \ell n \left| \underline{\Sigma}_{vv}(\underline{\beta}) \right| + [\underline{z} - \underline{\Phi}(\underline{\beta})] \, \underline{\Sigma}_{vv}^{-1}(\underline{\beta}) \, [\underline{z} - \underline{\Phi}(\underline{\beta})] \qquad (6.40)$$

280

(see, e.g, Schweppe, 1973). Note that even when $\underline{v}$ is not Gaussian the estimate obtained by minimizing (6.40) is a useful estimate since it has some attractive asymptotic properties (see, e.g., Goodwin and Payne, 1977). Using (6.39), (6.40) simplifies to

$$J(\underline{\beta}) = \ell n \left| \underline{\Sigma}_{yy}(\underline{\beta}) \right| + [\underline{y} - \underline{R}(\underline{\beta})]^T \underline{\Sigma}_{yy}^{-1}(\underline{\beta})[\underline{y} - \underline{R}(\underline{\beta})] +$$
$$+ [\underline{B} - \underline{\beta}]^T \underline{\Sigma}_{bb}^{-1} [\underline{B} - \underline{\beta}] \tag{6.41}$$

where

$$\underline{y} = \left| \begin{array}{c} \underline{\psi} \\ \underline{s} \end{array} \right| \quad ; \quad \underline{R}(\underline{\beta}) = \left| \begin{array}{c} \underline{H}(\underline{\beta}) \\ \underline{P}(\underline{\beta}) \end{array} \right| \tag{6.42}$$

$$\underline{\Sigma}_{yy}(\underline{\beta}) = \left| \begin{array}{cc} \underline{\Sigma}_{hh}(\underline{\beta}) & \underline{\Sigma}_{hp}(\underline{\beta}) \\ \underline{\Sigma}_{ph}(\underline{\beta}) & \underline{\Sigma}_{pp}(\underline{\beta}) \end{array} \right| \tag{6.43}$$

and term $\ell n \left| \underline{\Sigma}_{bb} \right|$ has been dropped from the objective function (6.41), since it is assumed to be a constant.

In order to minimize (6.41) it must be possible to evaluate the corresponding values of $\underline{R}(\underline{\beta})$ and $\underline{\Sigma}_{yy}(\underline{\beta})$ given a value of $\underline{\beta}$. $\underline{R}(\underline{\beta})$ may be obtained by numerical solution of the mean flow equation. The covariance matrix $\underline{\Sigma}_{yy}$ can be evaluated using the stochastic theory developed in Chapters 3 and 4 as follows.

Matrix $\underline{\Sigma}_{yy}$ includes elements of the form $E[h(\underline{x}_i, t_m) h(\underline{x}_j, t_n)]$, $E[h(\underline{x}_i, t_m) f(\underline{x}_j)]$, $E[h(\underline{x}_i, t_m) a(\underline{x}_j)]$, $E[h(\underline{x}_i, t_m) \gamma(\underline{x}_j)]$, where $i, j = 1, \ldots, N$ and $m, n = 1, \ldots, M$ for a given value of $\underline{\beta}$ these cross-correlations can be evaluated using the

general theory developed in Chapter 3. In order to be able to evaluate these cross-correlations, the differential Equation (3.45) must be solved as a function of time (numerical solution seems necessary). In certain cases however, (e.g., dry soils and relatively large times) it may be possible to use the steady state appproximation for dZ_h, discussed in Chapters 3 and 4. This approach is similar to the steady-state Kalman Filter assumption often used in system identification studies.

The value of $\underline{\beta}$ that minimizes $J(\underline{\beta})$ can be obtained by using an iterative minimization algorithm (e.g., a gradient search method). Questions of convergence, accuracy and cost of the iterative procedure are of importance and should be considered (see, Mantoglou, 1983; and Mantoglou and Schweppe, 1983).

The identification method described above is very general and flexible and can be used in a large variety of flow identification problems. The particular cases when prior information and/or measurements of local soil properties are not available can be easily treated using simple modifications of the general method. The case of a spatially variable mean (trend), can also be treated using a parameterization of the mean in terms of a basis function vector (e.g., linear, polynomial, etc.). The identification procedure has been developed in a general format and the suggestions for its application are very general. For each particular application, the method should be modified, simplified, etc., depending on the nature and requirements of the problem. In some cases it may be useful to use other techniques as well, for example, interpolation (using kriging, etc.) of the measurements of ψ between the measurement points, before parameter estimation. In other cases it may be appropriate to

assume a completely unknown or completely known covariance matrix for the model errors instead of trying to evaluate them using a quite involved procedure. Another question, which is important in applications, is whether the assumed parametric model (e.g., constant mean, exponential covariance, etc.) is appropriate. Hypothesis testing methods could be used in order to address such questions.

Figure 6.4 illustrates the steps of the identification method discussed above. The intermediate step, where the effective parameters of the large-scale model structure are evaluated is also shown.

$$\underline{x} = \underline{B} - \underline{\beta}$$

$$\underline{x}\, \underline{\underline{\Sigma}}_{bb}^{-1}\, \underline{x}^T$$

Reality

$$\underline{y}$$

$$\beta$$

$$\underline{x} = \underline{y} - \underline{R}(\beta)$$

$$\underline{x}\, \underline{\underline{\Sigma}}_{vv}^{-1}\, \underline{x}^T$$

$$J_1$$

$$J_2$$

$$J(\underline{\beta})$$

$$\underline{R}(\underline{\beta})$$

$$\underline{\underline{\Sigma}}_{vv}$$

Effective parameter evaluator

Numerical solution

Covariance of model error evaluator
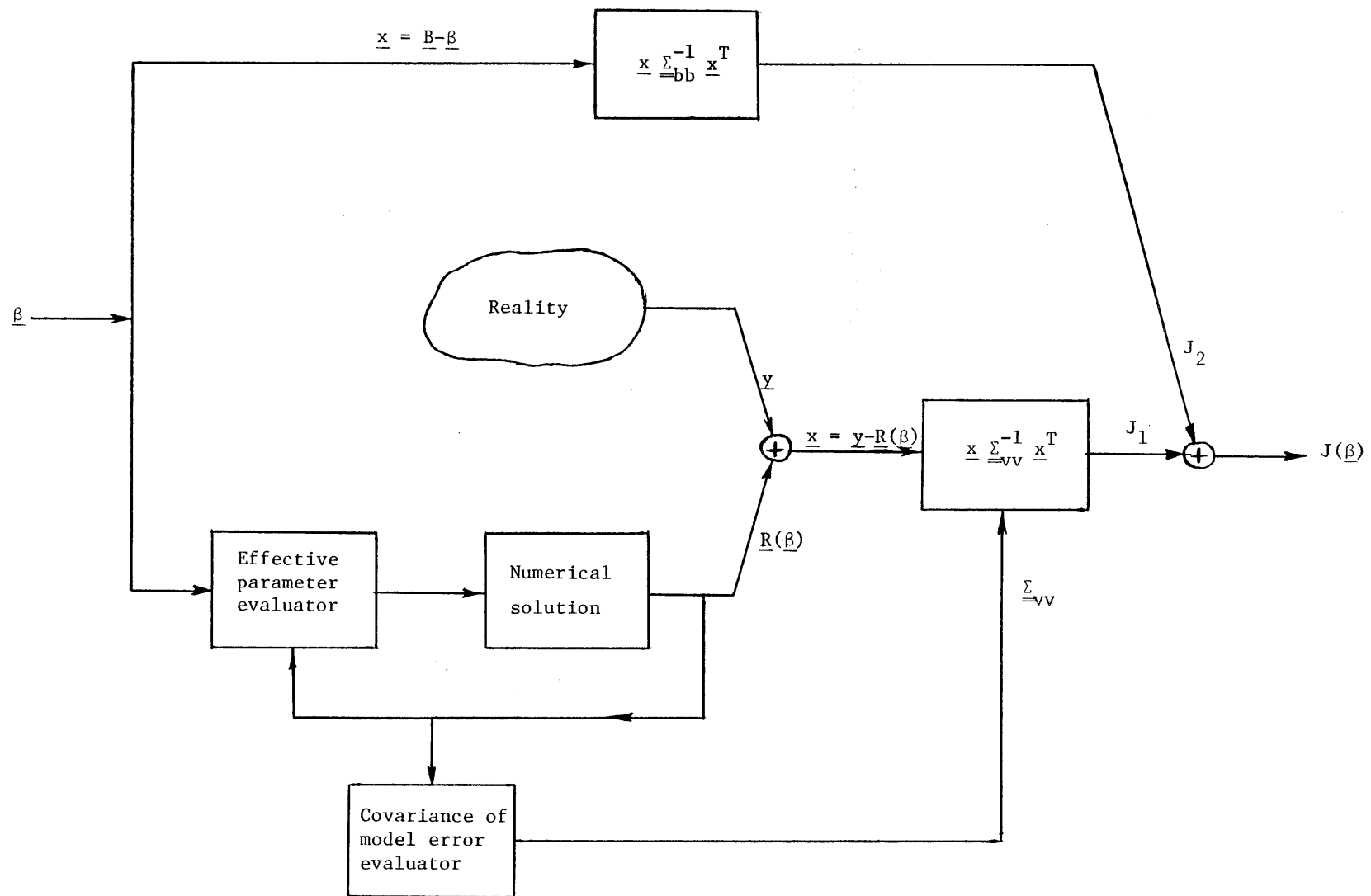
Figure 6.4   Schematic representation of the steps of the identification method. The method involves minimization of cost functional $J(\beta)$ for $\underline{\beta}$ and it involves an intermediate step where the effective parameters are evaluated for a given $\underline{\beta}$.

6.4 Summary and Discussion

This chapter proposed and developed theoretical methods that can be used in order to test the validity of the stochastic theory and apply the large-scale models in real field problems. The suggested methods are very general and can be used directly or with conceptually simple modifications in the saturated flow and transport, oil reservoir modeling and other distributed parameter problems.

Section 6.2 proposed a five step Monte-Carlo procedure for testing the validity of the stochastic method. The spectral turning bands method is extended for digital generation of point values or spatial averages of multiple, cross-correlated stationary random fields. This method is very general, flexible and highly efficient and should have several applications in hydrology and in other fields of geophysics.

Section 6.3 investigated the problem of estimating the parameters required for definition of a large-scale model of the system. The problem of estimating these parameters using the measurements of local soil properties (statistical inference problem) and some inherent problems and methods of analysis are briefly discussed. Then a new identification method is proposed. This method suggests selecting for identification a large-scale model structure of the form derived in previous chapters. It was discussed that this structure is physically justified because it takes into account the large-scale effects of local soil variability (such as hysteresis, anisotropy etc.) and it has a few parameters only that can be hopefully estimated from a limited data set. It is expected that such large-scale model structure describes the large-scale processes better than traditional models which ignore the existence and effects of

spatial soil variability. In addition, since the unknown parameters are relatively few, it is expected that these parameters will be identifiable if sufficient information is available and it is properly used. Past approaches, used in the unsaturated flow case, are based on the assumption that the large-scale model structure is of the same form as the local governing equations where the model parameters are smooth functions of space. This approach does not take into account the large-scale effects of local soil variability and it is not recommended for the unsaturated flow case where such effects (e.g., hysteresis, anisotropy etc.) are important. Note also that if a very dense discretization, which can take into account the local soil variability details, was used, the number of unknown parameters would be extremely large and not identifiable.

Next, Section 6.3 outlined a very general and flexible parameter estimation methodology that can take into account local capillary tension head and soil property measurements as well as prior information about the unknown model parameters. The methodology is based on a maximum likelihood criterion which considers the statistical properties of the model error. The proposed methodology can be easily extended to the saturated flow and the contaminant transport case.

CHAPTER 7

SUMMARY CONCLUSIONS AND RECOMMENDATIONS

7.1 Summary and Conclusions

This study developed a new framework for modeling large-scale, naturally heterogeneous unsaturated flow and transport systems. Due to natural soil variability the large-scale system behavior cannot be adequately described by the local physical models. A general methodology was developed for derivation of realistic large-scale models which are capable of predicting the behavior of real unsaturated flow and transport systems. These models consider the effects of spatial variability of the hydraulic soil properties and have relatively few and identifiable parameters that can be estimated from a realistic data set. A stochastic approach was followed. It was assumed that the local hydraulic soil properties are realizations of three-dimensional, stationary random fields. The local governing flow and transport equations were averaged over the ensemble of realizations of the underlying soil property random fields. The stochastic methodology considers the three-dimensionality of the local flow and transport processes and the nonlinear dependence of the local capillary tension head and concentration outputs on the local soil properties. The so derived large-scale models thus account for the large-scale effects of spatial soil variability.

Chapter 2 discussed the problem of spatial variability of the hydraulic properties of natural soil formations and proposed a representation of such variability in terms of three-dimensional

stationary random fields.

Chapter 3 developed a general stochastic methodology for derivation of large-scale models of unsaturated flow and transport and evaluation of effective parameters for these models. The stochastic approach used the following three steps. First, the local governing flow and transport equations were averaged over the ensemble of the soil property realizations and the form of the large-scale models was constructed. In the second step, the local fluctuations of the capillary tension head or concentration ouputs were related to the local fluctuations of the hydraulic soil properties through a set of linearized stochastic partial differential equations. In the last step of the stochastic methodology, the effective large-scale parameters were evaluated using the linearized fluctuation equations derived in the second step and a spectral representation of stationary processes. The large-scale models derived using this methodology, are expressed in a partial differential equation form and are capable of predicting the mean capillary tension head and the mean concentration outputs. The effective model parameters depend on the mean soil properties and the statistical properties of soil property fluctuations (variances, correlation lengths), but they also depend on the mean capillary tension head and its spatial and time derivatives.

In Chapter 4 the general stochastic theory of Chapter 3 was used to evaluate the effective unsaturated flow parameters in the case of transient flow in stratified soil formations. It was found that the effective hydraulic conductivity, the mean soil moisture content and the effective specific soil moisture capacity show significant hysteresis. It was also found that the effective hydraulic conductivity is

anisotropic with a degree of anisotropy depending on the mean capillary tension head and the mean flow conditions. In the case of wetting, the degree of anisotropy is large, while in the case of drying it is relatively small. These effects are due to the spatial variability of soil properties rather than to pore scale effects, since the latter were not considered in the analysis. This chapter also gave a physical interpretation of the results of the stochastic theory, examined a series of field observations that are in agreement with these results and discussed the implications of the stochastic theory results on practical applications such as waste disposal control.

In Chapter 5 the macrodispersivities were evaluated in the cases of a statistically isotropic and a statistically anisotropic (stratified) soil formation, using the general theory developed in Chapter 3. It was found that the effective macrodispersivity depends on the mean capillary tension head. This phenomenon is probably due to the fact that the spatial variability of the soil properties may introduce a dependence of tortuosity of the unsaturated flow paths on the soil moisture content. The results of this chapter indicated that longitudinal macrodispersion is generally governed by convective transport. In the cases of an isotropic soil or a stratified soil with mean flow perpendicular to stratification, transverse macrodispersion is governed by local dispersion and it is relatively small. However, in the case of a stratified soil with mean flow at an angle to stratification (Section 5.2.3) transverse macrodispersion is convectively controlled and could be significant. Chapter 5 also discussed a series of field observations and compared them to the predictions of the stochastic theory.

Chapters 4 and 5 derived relatively simple generic relationships showing the dependence of the effective large-scale parameters on the different soil property and flow characteristics. Such relationships are extremely useful because of the generality, simplicity and insight they provide. In order to make analytical evaluations possible, several assumptions were required (e.g. stationarity, smallness of fluctuations, etc.). These assumptions may restrict the validity of the results of the stochastic theory in the cases where the assumptions are strictly valid. It is expected however, that these results will be at least qualitatively valid in a wider variety of situations. For example, it is expected that the effective unsaturated flow parameters will show hysteresis and anisotropy in finite domain problems as well, even though the stationarity assumptions required by the stochastic theory are not strictly valid in such cases. Since large-scale behavior of unsaturated flow and transport is presently highly unknown, we believe that even qualitative information is important since it may indicate important characteristics of the problem, thereby suggesting directions that future research should follow.

The validity of the stochastic theory developed in this thesis should be tested with appropriately designed experiments in order to gain confidence in using it in applications such as waste disposal management. Chapter 6 suggested testing the stochastic theory using a Monte-Carlo simulation method. The spectral Turning Band Method was developed for direct synthetic generation of point values or block averages of multiple, statistically anisotropic, two or three-dimensional, stationary random fields. This method is very general and has other geophysical

applications as well. Chapter 6 also discussed the practical problem of estimating the stochastic parameters required by the large-scale unsaturated flow and transport models. Statistical inference methods were briefly discussed and a new identification method was proposed. The main idea of the identification method is to use the large-scale model structure, derived using the stochastic approach, rather than the physical model structure. It is expected that the large-scale model structure will be capable of capturing the basic large-scale flow and transport characteristics and will be suitable in applications because this model requires only a few parameters that can be estimated systematically from a realistic data set.

The results of the stochastic theory developed herein have important implications on practical problems such as waste disposal control. For example, the stochastic theory predicts that, in relatively dry soils, a contamination plume tends to spread laterally while vertical movement is relatively slow. As a result, contamination may arrive at the water table much later than predicted by classical one dimensional models and the horizontal extent of contamination may be much larger than traditionally predicted (see Chapter 4). Such effects should be considered in future modeling studies of large-scale unsaturated flow and transport systems.

The general modeling framework proposed in this thesis is new and is not only applicable to unsaturated flow and contaminated transport but also to other distributed parameter problems (e.g. saturated flow and contaminant transport, oil, geothermal reservoir modeling, etc.).

7.2 Recommendations for Further Research

The most important conclusion of this study is that, due to the spatial variability and parametric nonlinearity of local governing flow and transport equations, unsaturated flow and transport in field settings behave differently than was previously thought. Thus an important recommendation is that future research on this topic, regardless of the methods used, should not ignore the large-scale effects of spatial variability.

Other more specific recommendations are related to validation, application and extensions of the stochastic theory developed in here. Chapter 6 provides several detailed recommendations in these directions. It is also of interest to use a numerical solution for dZ_h in the case of a wet soil and to investigate whether flow in such cases is of a diffusion type. Other possible extensions of this work include treating the unsteady transport case, and evaluation of the variance of concentration c. It also seems promising to try to extend the general ideas to other distributed parameter systems such as aquifers or oil reservoirs.

REFERENCES

Agterberg, F.P., Autocorrelation functions in geology, in Geostatistics, edited by D.F. Merriam, Plenum Press, New York, 1970.

Andersen, L.J. and T. Sevel, Environmental tritium profiles in the unsaturated and saturated zones, Gronhoj, Denmark, IAEA Report SM-182/1, 1968.

Andersson, J. and A.M. Shapiro, Stochastic analysis of one-dimensional steady state unsaturated flow: A comparison of Monte Carlo and perturbation methods, Water Resources Research, 19(1), pp. 121-133, 1983.

Bakr, A.A., L.W. Gelhar, A.L. Gutjahr and J.R. MacMillan, Stochastic analysis of spatial variability in subsurface flows, 1, Comparison of one and three dimensional flows, Water Resources Research, 14(2), pp. 263-272, 1978.

Bear, J., Hydraulics of Groundwater, MacGraw-Hill, 1979.

Bear, J., Dynamics of Fluids in Porous Media, American Elsevier Publishing Company, Inc., New York, 1972.

Beven, K. and P. Germann, Macropores and water flow by soils, Water Resources Research, 18(5), 1311-1325, 1982.

Biggar, J.W. and D.R. Nielsen, Spatial varibility of the leaching characteristics of a field soil, Water Resources Research, 12(1), 78-84, 1976.

Bouma, L., Soil morphology and preferential flow along macropores, Agricultural Water Management, 3, 235-250, 1981.

Bresler, E. and G. Dagan, Convective and pore scale dispersive solute transport in unsaturated heterogeneous fields, Water Resources Research, 17(6), pp. 1683-1693, 1981.

Bresler, E. and G. Dagan, Unsaturated flow in spatially variable fields 3. Solute transport models and their application to two fields, Water Resources Resarch, 19(2), pp. 429-435, 1983.

Brissaud, F., A. Pappalarado and Ph. Couchat, Gamma neutron method applied to field measurement of hydrodynamic dispersion, Journal of Hydrology, 63, 331-343, 1983.

Burg, J.P., Maximum entropy spectral analysis, presented at the 37th Int. Meet., Soc. Explor. Geophys., Oklahoma City, OK, 1968.

Carvallo, H.O., D.K. Cassel, J. Hammond and A. Bauer, Spatial variability of in situ unsaturated hydraulic conductivity of Maddock sandy loam, Soil Sci., 121(1), 1-8, 1976.

Capon, J., High resolution frequency-wavenumber spectrum analysis, Proceedings IEEE, 57(8), pp. 1408-1418, 1969.

Chauvet, P. and A. Galli, Universal Kriging, Report No. C-96, Centre de Morphologie Mathematique, Fontainebleau, France, 1982.

Chiles, J.P., Geostatistique des Phenomenes non Stationares in France, These de Docteur- Ingenier, Univ. de Nancy, Nancy, France, 1974.

Clifton, P.M. and S.P. Newman, Effects of kriging and inverse modeling on conditional simulation of the Arva Valley aquifer in southern Arizona, Water Resources Research, 18(4), pp. 1215-1234, 1982.

Cooley, R.L., Incorporation of prior information on parameters into nonlinear regression groundwater flow models, Water Resources Research, 18(1), pp. 965-976, 1982.

Crosby, J.W., D.L. Johnstone, C.H. Drake and R.L. Fenton, Migration of pollutants in a glacial outwash environment, Water Resources Research, 4(5), pp. 1095-1114, 1968.

Crosby, J.W., D.L. Johnstone and R.L. Fenton, Migration of pollutants in a glacial outwash environment 2, Water Resources Research, 7(1), pp. 204-208, 1971.

Dagan, G., Models of groundwater flow in statistically homogeneous porous formations, Water Resources Research, 15, 47-63, 1979.

Dagan, G., Stochastic modeling of groundwater flow by unconditional and conditional probabilities, 1. Conditional simulation and the direct problem, Water Resources Research, 18(4), 813-833, 1982.

Dagan, G., Stochastic modeling of groundwater flow by unconditional and conditional probabilities, 2, The solute transport, Water Resources Research, 18(4), pp. 835-848, 1982.

Dagan, G. and E. Bresler, Solute dispersion in unsaturated heterogeneous soil at field scale: Theory, Soil Sci. Soc. Am. J., 43, pp. 461-467, 1980.

Dagan, G. and E. Bresler, Unsaturated flow in spatially variable fields, 1. Derivation of models of infiltration and redistribution, Water Resources Research, 19(2), pp. 413-420, 1983.

David, M., Geostatistical Ore Reserve Estimation, Elsevier, New York, 1977.

Davis, J.C., Statistics and Data Analysis in Geology, John Wiley, New York, 1973.

Delfiner, P., Linear estimation of nonstationary spatial phenomena, in Advanced Geostatistics in the Mining Industry, M. Guarascio et al. eds., D. Reidel, Dordrecht, pp. 48-68, 1976.

Dettinger, M.D. and J.L. Wilson, First order analysis of uncertainty in numerical models of groundwater flow, 1, Mathematical development, Water Resources Research, 17, pp. 149-161, 1981.

Foster, S.D. and A. Smith-Carrington, The interpretation of tritium in the Chalk unsaturated zone, Journal of Hydrology, 46, pp. 343-364, 1980.

Freeze, R.A., A stochastic-conceptual analysis of one-dimensional groundwater flow in nonuniform homogeneous media, Water Resources Research, 11, pp. 725-741, 1975.

Gaudet, J.P., H. Jegat, G. Vachaud and P. J. Wierenga, Solute transfer with exchange between mobile and stagnant water through unsaturated sand, Soil Sci. Soc. Amer. J., 41(4), pp. 665-671, 1977.

Gelhar, L.W., General report on the session on subsurface water quality, In the Third Fort Collins International Hydrology Symposium, June 27-29, Fort Collins, CO., 1977.

Gelhar, L.W. and C.L. Axness, Three-dimensional stochastic analysis of macrodispersion in aquifers, Water Resources Research, 19(1), pp. 161-180, 1983.

Gelhar, L.W., A. Mantoglou, C. Welty and K.R. Rehfeldt, A review of field scale subsurface solute transport processes under saturated and unsaturated conditions, Electric Power Research Institute, Report No. RP-2485-05, Palo Alto, CA., 1984.

Goodwin, G.C. and R.L. Payne, Dynamic System Identification, Experiment Design and Data Analysis, Academic Press, New York, 1977.

Gradshteyn, I.S. and I.M. Ryzhik, Table of Integrals, Series and Products, Academic Press, New York, 1980.

Hildebrand, M.A. and P.M. Himmelbau, Transport of nitrate ion in unsteady unsaturated flow in porous media, AICHE Journal, 23(3), 326-335, 1977.

Jenkins, G.M. and D.G. Watts, Spectral Analysis and its Applications, Holden-Day, San Francisco, 1968.

Johnston, C.D., D.H. Hurle, D.R. Hudson and M.I. Height, Water movement through preferred paths in lateritic profiles of the Darling Plateau, Western Australia, Groundwater Research Paper No. 1, Commonwealth Scientific and Industrial Research Organization, Australia, 1983.

295

Journel, A.B. and Ch.J. Huijbregts, Mining Geostatistics, Academic, New York, 1978.

Journel, A.G., Geostatistics for conditional simulation of ore bodies, Economic Geology, Vol. 69, 673-687, 1974.

Jury, A.W. and L.H. Stolzy, A field test of the transfer function model for predicting solute transport, Water Resources Research, 18(2), pp. 369-375, 1982.

Kent, B., C.R. Mauldin and M.W. Cooper, Evaluation of subsurface migration from solar ponds, Underground Resource Management Report, Austin, TX., 1982.

Kies, B., Solute transport in unsaturated field soil and in groundwater, Ph.D. Dissertation, Dept. of Agronomy, New Mexico State University, Las Cruces, NM, 1981.

Kirda, C., D.R. Nielsen and J.W. Biggar, Simultaneous transport of chloride and water during infiltration, Soil Sci. Soc. Amer. J., 37(3), 339-345, 1973.

Knoll, K.C. and J.L. Nelson, Radioisotope and moisture distribution beneath a model crib, Hanford Atomic Products Operation, Report HW-71573, Richland, WA., 1962.

Larimore, W.E., Statistical inference of stationary random fields, Proceedings of the IEEE, 65(6), 1977.

Lumley, J.L. and H.A. Panofsky, The Structure of Atmospheric Turbulence, John Wiley, New York, 1974.

Mantoglou, A. and J.L. Wilson, The turning bands method for simulation of random fields using line generation by a spectral method, Water Resources Research, 18(5), pp. 1379-1394, 1982.

Mantoglou, A. and J.L. Wilson, Simulation of Random Fields with the Turning Bands Method, R.M. Parsons Lab., Report No. 264, MIT, Cambridge, MA., 1981.

Mantoglou, A., Nonlinear Model Structures in System Identification, S.M. Thesis, Department of Electrical Engineering and Computer Science, MIT, Cambridge, MA, 1983.

Mantoglou, A. and F.C. Schweppe, Model structures in system identification, Working Paper, Dept. of Electrical Engineering and Computer Science, M.I.T., Cambridge, MA., 1983.

McClellan, J.H., Multidimensional spectral estimation, Proceedings of the IEEE, 70(9), 1982.

Milly, P.C.D., Moisture and heat fluxes across the land surface: Parameterization for atmospheric general circulation models and the effects of spatial variability, Ph.D. Thesis, Dept. of Civil Engineering, M.I.T., Cambridge, MA., 1982.

Mizell, S.A., L.W. Gelhar and A.L. Gutjahr, Stochastic analysis of spatial variability in two-dimensional groundwater flow with implications for observation-well-network design, Report No. H-6, Hydrology Research Program, New Mexico Institute of Mining and Technology, Socorro, NM, 1980.

Newman, S.P. and S. Yakowitz, A statistical approach to the inverse problem of aquifer hydrology, 1, theory, Water Resources Research, 15(4), pp. 845-860, 1979.

Nielsen, D.R., J.W. Biggar and K.T. Erh, Spatial variability of field measured soil-water properties, Hilgardia, 42(7), pp. 215-260, 1973.

Oakes, D.B., The movement of water and solutes through the unsaturated zone of the chalk in the United Kingdom, Third International Hydrology Symposium, Fort Collins, CO, 1977.

Palmquist, W.N. and A.I. Johnson, Vadose flow in layered and nonlayered materials, U.S.G.S. Prof. Paper 450-C, C142-C143, 1962.

Price, S.M., R.B. Kasper, M.K. Additon, R.M. Smith and G.V. Last, Distribution of plutonium and americium beneath the 216-Z-1A crib: A status report, Rockwell International, Repor RHO-ST-17, Richland, WA, 1979.

Prill, R.C., Movement of moisture in the unsaturated zone in a less - mantled area, Southwestern Kansas, U.S.G.S. Prof. Paper 1021, 1977.

Quinsenberry, V.L. and R.E. Phillips, Percolation of surface-applied water in the field, Soil Sci. Soc. Amer. J., 40, pp. 484-489, 1976.

Routson, R.C., W.H. Price, D.J. Brown and K.R. Fecht, High level waste leakage from the 241-T-106 tank at Hanford, Rockwell International, Report RHO-ST-14, Richland, WA., 1979.

Schweppe, F.C., Dynamic Model Structures, Prentice Hall Inc., 1973.

Shah, P.C., G.R. Gavalas and J.H. Seinfeld, Error analysis in history maching: The optimum level of parameterization, SPEJ, June 1978.

Shinozuka, M. and C.-M. Jan, Digital simulation of random processes and its applications, J. Sound Vib., 25(1), 111-128, 1972.

Starr, J.L., H.C. DeRoo, C.R. Frink, and J.-Y. Parlange, Leaching characteristics of a layered field soil, Soil Sci. Soc. Amer. J., 42, pp. 386-391, 1978.

Thomas, G.W. and R.E. Phillips, Consequences of water movement in macropores, J. Environ. Quality, 8(2), pp. 149-152, 1979.

Townley, R.L., Numerical Models of Groundwater Flow: Prediction and Parameter Estimation in the Presence of Uncertainty, Ph.D. Thesis, Dept. of Civil Engineering, M.I.T., Cambridge, MA, April 1983.

Trauntwein, S.J., D.E. Daniel and H.W. Cooper, Case history study of water flow through unsaturated soil, in The Role of the Unsaturated Zone in Radioactive Hazardous Waste Disposal, Mercer et al., eds. Ann Arbor Science, Ann Arbor, MI, 1983.

Van de Pol, R.M., P.J. Wierenga, and D.R. Nielsen, Solute movement in a field soil, Soil Sci. Soc. Amer. J., 41, pp. 10-13, 1977.

Waldrop W.R. L.W. Gelhar, R.P. Betson and D.B. Stephens, Groundwater transport studies, Phase II Design and cost estimates, Report RP2485-05, Tennessee Valley Authority, Tennessee 37828.

Warrick, A.W., J.B. Biggar and D.R. Nielsen, Simultaneous solute and water transfer for an unsaturated soil, Water Resources Research, 7(5), 1216-1225, 1971.

Wierenga, P.J. Solute transport through soils: Mobile-immobile water concepts, Review of Ground-Water Flow and Transport Models in the Unsaturated Zone, Report NUREG/CR-2917, PNL-4427, U.S. Nuclear Regulatory Commission, Washington, D.C., 1982.

Wilson, J.L., Dispersive Mixing in a Partially Saturated Porous Medium, Ph.D. Thesis, Dept. of Civil Engineering, M.I.T., Cambridge, MA, 1977.

Yeh, T.-C., L.W. Gelhar and A.L. Gutjahr, Stochastic analysis of effects of spatial variability on unsaturated flow, Report No. H-11, Hydrology Research Program, New Mexico Institute of Mining and Technology, Socorro, NM, 1982.

Yule D.F. and W.R. Gardner, Longitudinal and transverse dispersion coefficients in unsaturated plainfield sand, Water Resources Research, 14(4), 582-588, 1978.

298

This Appendix evaluates the solution of Equation (3.45), where δ_1, δ_2 are given by (3.46) and $J_t = \partial H/\partial t > 0$. The general solution of (3.45) is given by (3.38) where now

$$g_1(\tau) = \delta_1 + \delta_2(t)$$

$$g(\tau) = AJ_t \tag{A.1}$$

It holds

$$\int_0^t g_1(\tau)d\tau = A J_t t \tag{A.2}$$

$$\int_0^t (\delta_1 + \delta_2 \tau) e^{A J_t \tau} d\tau =$$

$$= \{\frac{\delta_1}{AJ_t} e^{AJ_t t} + \delta_2 e^{AJ_t t} \lfloor \frac{t}{AJ_t} - \frac{1}{(AJ_t)^2} \rfloor - \lfloor \frac{\delta_1}{AJ_t} - \frac{\delta_2}{(AJ_t)^2} \rfloor\} \tag{A.3}$$

Equation (3.38) then gives

$$y(\underline{k}, t) = \{y(\underline{k}, 0) + \frac{\delta_1}{AJ_t} e^{AJ_t t} + \delta_2 e^{AJ_t t} \lfloor \frac{t}{AJ_t} - \frac{1}{(AJ_t)^2} \rfloor -$$

$$- \lfloor \frac{\delta_1}{AJ_t} - \frac{\delta_2}{(AJ_t)^2} \rfloor\} e^{-AJ_t t} \tag{A.4}$$

and using (3.46), A.4 yields

$$y(\underline{k}, t) = \lfloor \frac{dZ_f - H\, dZ_a - \frac{dZ_\gamma}{\Gamma}}{A} + \frac{dZ_a}{A^2} \rfloor +$$

$$+ \lfloor y(\underline{k}, 0) - \frac{\delta_1}{AJ_t} + \frac{\delta_2}{(AJ_t)^2} \rfloor\, e^{-AJ_t\, t} \qquad\qquad (A.5)$$

In this Appendix the integral

$$I_1 = \int_0^\infty \frac{a_1 \, k_1^2 + a_2}{k_1^4 + a_3 \, k_1^2 + a_4} \; \frac{1}{1 + a_5 \, k_1^2} \; dk_1 \qquad (B.1)$$

is evaluated. The above integral is written as

$$I_1 = R_1 + R_2 \qquad (B.2)$$

where

$$R_1 = \int_0^\infty \frac{B_1 \, k_1^2 + B_2}{k_1^4 + a_3 \, k_1^2 + a_4} \; dk_1 \qquad (B.3)$$

$$R_2 = \int_0^\infty \frac{B_3}{1 + a_5 \, k_1^2} \; dk_1 \qquad (B.4)$$

with

$$B_1 = \frac{a_1 - a_2 \, a_5}{1 + a_4 \, a_5^2 - a_3 \, a_5}$$

$$B_2 = a_2 + a_4 \, a_5 \, B_1 \qquad (B.5)$$

$$B_3 = -a_5 \, B_1$$

Integral R_1 is evalutaed first. The type of integration depends on the sign of $\Delta = a_3^2 - 4a_4$. For $\Delta > 0$, the denominator of the integrand in B.3 has two real and negative roots: $\rho_1 = -f$, $\rho_2 = -g$ where f, g are given by

$$f, \; g = \frac{a_3}{2} \pm \frac{1}{2} \sqrt{a_3^2 - 4a_4} \qquad (B.6)$$

and $f, \; g, \; > 0$. Then

$$\frac{B_1 k_1^2 + B_2}{k_1^4 + a_3 k_1^2 + a_4} = \frac{B_1 k_1^2 + B_2}{(k_1^2 + f)(k_1^2 + g)} = \frac{C_1}{k_1^2 + f} + \frac{C_2}{k_1^2 + g} \qquad (B.7)$$

$$C_1 = \frac{B_2 - B_1 f}{g - f}$$

$$\qquad (B.8)$$

$$C_2 = \frac{B_1 g - B_2}{g - f}$$

Integral B.3 is now easily evaluated.

$$R_1 = C_1 \frac{\pi}{2\sqrt{f}} + C_2 \frac{\pi}{2\sqrt{g}} \qquad (B.9)$$

Substituting B.8 and using B.6 yields

$$R_1 = \frac{\pi}{2} \frac{(A\Gamma G) B_1 + B_2}{(A\Gamma G) \sqrt{4A\Gamma G + A^2 L_1^2}} \qquad (B.10)$$

For $\Delta < 0$, the denominator of the integrand in B.3 has no real roots. In this case a different type of integration is required. Since $\Delta = a_3^2 - 4a_4 < 0$ it holds $|a_3|/2 < \sqrt{a_4}$. Let $p = \sqrt{a_4} \; |A\Gamma G|$. It is possible then to express a_3 as $a_3 = 2p \cos\tau$. Using the transformation of variables $t = k_1^2$, B.3 yields

302

$$R_1 = \frac{1}{2} \int_0^\infty \frac{B_1 t^{1/2} + B_2 t^{-1/2}}{t^2 + 2p(\cos\tau)t + p^2} \, dt \qquad (B.11)$$

Using Equation No. 3.252.12 of Gradshteyn and Ryzhik (1980), for $\mu = 3/2$, yields.

$$T_1 = \int_0^\infty \frac{t^{1/2}}{t^2 + 2p(\cos\tau)t + p^2} \, dt =$$

$$= -\pi \, p^{-1/2}(\cosec\tau) \, \cosec(\frac{3\pi}{2}) \, \sin(\frac{\tau}{2}) = \frac{\pi}{\Gamma_p} \, \frac{\sin(\tau/2)}{\sin\tau} \qquad (B.12)$$

Using the identity $\sin\tau = 2\sin(\tau/2)\cos(\tau/2)$ yields

$$T_1 = \frac{\tau}{2\sqrt{p}} \, \frac{1}{\cos(\tau/2)} \qquad (B.13)$$

Substituting

$$\cos(\tau/2) = \sqrt{\frac{1}{2}(1 + \cos\tau)} = \sqrt{\frac{2p + a_3}{4p}} \qquad (B.14)$$

Equation B.13 gives

$$T_1 = \frac{\pi}{\sqrt{2p + a_3}}$$

Note that

$$\Delta = a_3^2 - 4a_4 = (2A\Gamma G + A^2 L_1^2)^2 - 4 A^2 \Gamma^2 G^2 = A^2 L_1^2 (A^2 L_1^2 + 4 A\Gamma G).$$

Since $A^2 L_1^2 > 0$ for $\Delta < 0$ it is $A\Gamma G < 0$, and $|A\Gamma G| = -A\Gamma G$.

Equation B.14 then simplies to

$$T_1 = \frac{\pi}{AL_1}$$

Equation No. 3.252.12 of Gradshteyn and Ryzhik, (1980) for $\mu = 1/2$ yields

$$T_2 = \int_0^\infty \frac{t^{-1/2}}{t^2 + 2_p(\cos\tau) t + p^2}$$

$$- \pi P^{-3/2} (\text{cosec}\tau) \text{cosec}(\frac{\pi}{2}) \sin(-\frac{\tau}{2}) = \frac{\pi}{p\sqrt{p}} \frac{\sin(\tau/2)}{\sin \tau} =$$

$$= \frac{\pi}{2p\sqrt{p}} \frac{1}{\cos(\tau/2)} \qquad (B.16)$$

Substituting B.14 and form ArG and for ArG < 0, Equation B.16 simplifies to

$$T_2 = - \frac{\pi}{(ArG)(AL_1)} \qquad (B.17)$$

Substituting B.15 and B.17, Equation B.11 yields

$$R_1 = \frac{\pi}{2} \frac{(ArG)B_1 - B_2}{(ArG)(AL_1)} \qquad (B.18)$$

Integral R_2 is easily evaluated from Gradshteyn and Ryzhik, (1980)

$$R_2 = \frac{\pi}{2\lambda_1} B_3 \qquad (B.19)$$

Given the above expressions for R_1 and R_2 integral I_1 is evaluated form B.2. For $\Delta > 0$, substituting B.10 and B.19 Equation B.2 gives.

$$I_1 = \frac{\pi}{2} \left[\frac{(A\Gamma G)\, B_1 + B_2}{(A\Gamma G)\, \sqrt{4A\Gamma G + A^2 L_1^2}} + \frac{B_3}{\lambda_1} \right] \qquad (B.20)$$

Substituting B_1, B_2, B_3 from B.5, Equation B.20 yields

$$I_1 = \frac{\pi}{2} \left[\frac{a_1 \sqrt{a_4} + a_1 a_4 a_5 - \sqrt{a_4}\, a_2 a_5 + a_2 - a_2 a_3 a_5}{(A\Gamma G)\, \sqrt{4A\Gamma G + A^2 L_1^2}\, (1 + a_4 a_5^2 - a_3 a_5)} \right. -$$

$$\left. a_5 \frac{a_1 - a_2 a_5}{(1 + a_4 a_5^2 - a_3 a_5)\lambda_1} \right] \qquad (B.21)$$

while for $\Delta < 0$, substituting B.18 and B.19, Equation B.2 gives

$$I_1 = \frac{\pi}{2} \left[\frac{(A\Gamma G)\, B_1 - B_2}{(A\Gamma G)\,(AL_1)} + \frac{B_3}{\lambda_1} \right] \qquad (B.22)$$

Substituting B_1, B_2, B_3 from B.5, Equation B.22 gives

$$I_1 = \frac{\pi}{2} \left[\frac{-a_1 \sqrt{a_4} - a_1 a_4 a_5 + \sqrt{a_4}\, a_2 a_5 - a_2 + a_2 a_3 a_5}{(A\Gamma G)\,(AL_1)\,(1 + a_4 a_5^2 - a_3 a_5)} \right. -$$

$$\left. a_5 \frac{a_1 - a_2 a_5}{(1 + a_4 a_5^2 - a_3 a_5)\lambda_1} \right] \qquad (B.23)$$

305

In this Appendix the integral

$$I_2 = \int_0^\infty \frac{(a_1 k_1^2 + a_2)k_1^2}{k_1^4 + a_3 k_1^2 + a_4} \frac{1}{1 + a_5 k_1^2} \, dk_1 \tag{C.1}$$

is evaluated. This integral is written as

$$I_2 = R_1 + R_2 \tag{C.2}$$

where

$$R_1 = \int_0^\infty \frac{B_1 k_1^2 + B_2}{k_1^4 + a_3 k_1^2 + a_4} \, dk_1 \tag{C.3}$$

$$R_2 = \int_0^\infty \frac{B_3}{1 + a_5 k_1^2} \, dk_1 \tag{C.4}$$

with

$$B_1 = \frac{a_2 + a_1 a_4 a_5 - a_1 a_3}{1 + a_5^2 a_4 - a_3 a_5}$$

$$B_2 = -a_4(a_1 - a_5 B_1) \tag{C.5}$$

$$B_3 = a_1 - a_5 B_1$$

Integrals R_1 and R_2 have been evaluated in Appendix B. Substituting B_1, B_2, B_3 given by C.5 into B.20 of Appendix B gives for $\Delta > 0$

$$I_2 = \frac{\pi}{2} \left[\frac{a_2 \sqrt{a_4} + a_2 a_4 a_5 + a_1 a_4 a_5 \sqrt{a_4} - a_1 a_3 \sqrt{a_4} - a_1 a_4}{(\text{A}\Gamma\text{G}) \sqrt{4\ \text{A}\Gamma\text{G} + A^2 L_1^2}\ (1 + a_4 a_5^2 - a_3 a_5)} + \right.$$

$$\left. + \frac{a_1 - a_2 a_5}{(1 + a_4 a_5^2 - a_3 a_5)\lambda_1} \right] \qquad\qquad (C.6)$$

while B.22 gives for $\Delta < 0$

$$I_2 = \frac{\pi}{2} \left[\frac{-a_2 \sqrt{a_4} - a_2 a_4 a_5 - a_1 a_4 a_5 \sqrt{a_4} + a_1 a_3 \sqrt{a_4} - a_1 a_4}{(\text{A}\Gamma\text{G})\ (\text{A}L_1)\ (1 + a_4 a_5^2 - a_3 a_5)} + \right.$$

$$\left. + \frac{a_1 - a_2 a_5}{(1 + a_4 a_5^2 - a_2 a_5)\ \lambda_1} \right] \qquad\qquad (C.7)$$

APPENDIX D

This Appendix derives an approximate solution to the one dimensional
unsaturated flow equation, when a soil moisture pulse is placed at the
soil surface. This solution is similar to the one given by Wilson (1974)
but here we estimate the mean capillary tension head H rather than the
soil moisture content.

It is assumed that the initial mean capillary tension head H_0 is
constant throughout the soil depth. It is also assumed that the vertical
hydraulic conductivity is given by $\hat{K}_{11} = K_G e^{-AH}$ and that the mean
soil moisture content is given by $\Theta = -\Gamma H + E[\theta_0]$ and it is independent
of the mean flow conditions. The moisture pulse input at the soil
surface generates a soil moisture wave. An approximate solution
predicting the movement of this wave is obtained as follows.

The governing one-dimensional mean flow equation is given by

$$\hat{C}\frac{\partial H}{\partial t} = \frac{\partial}{\partial x_1}\left[\hat{K}_{11}(H)\frac{\partial(H + x_1)}{\partial x_1}\right] = \frac{\partial}{\partial x_1}\left[\hat{K}_{11}(H)\frac{\partial H}{\partial x_1}\right] + \frac{\partial\hat{K}_{11}(H)}{\partial x_1} \tag{D.1}$$

Let

$$H = H_0 + H^* \tag{D.2}$$

where H_0 the initial capillary tension head and H^* the fluctuation of
H around H_0 due to the generated soil moisture wave. If the
fluctuation H^* is relatively small it is possible to approximate $\hat{K}_{11}$
in Equation D.1 by

308

$$\hat{K}_{11}(H) \approx \hat{K}_{11}(H_0) + \frac{\partial \hat{K}_{11}}{\partial H}\bigg|_{H = H_0} (H - H_0) \tag{D.3}$$

Using $\hat{K}_{11} = K_G e^{-AH}$ and D.2, D.3 gives

$$\hat{K}_{11}(H) \approx \hat{K}_{11}(H_0) - A\,\hat{K}_{11}(H_0)\;H^* \tag{D.4}$$

Substituting D.2 and D.4 into D.1 gives

$$\hat{C}\,\frac{\partial H^*}{\partial t} = \hat{K}_{11}(H_0)\,\frac{\partial^2 H^*}{\partial x_1^2} - \frac{A\,\hat{K}_{11}(H_0)}{2}\,\frac{\partial^2 H^{*2}}{\partial x_1^2} - A\,\hat{K}_{11}(H_0)\,\frac{\partial H^*}{\partial x_1} \tag{D.5}$$

Assuming that the square of H^* is relatively small D.5 simplifies to

$$\frac{\partial H^*}{\partial t} + \frac{A\,\hat{K}_{11}(H_0)}{\hat{C}}\,\frac{\partial H^*}{\partial x_1} = \frac{\hat{K}_{11}(H_0)}{\hat{C}}\,\frac{\partial^2 H^*}{\partial x_1^2} \tag{D.6}$$

or

$$\frac{\partial H^*}{\partial t} + v\,\frac{\partial H^*}{\partial x_1} = D\,\frac{\partial^2 H^*}{\partial x_1^2} \tag{D.7}$$

where $v = A\,\hat{K}_{11}(H_0)/\hat{C}$ and $D = \hat{K}_{11}(H_0)/\hat{C}$. This is a simple one dimensional diffusion equation. Solving D.7 for H^* and substituting into D.2 gives the following approximation for the mean capillary tension head,

309

$$H = H_o - \frac{d/\hat{C}}{\sqrt{4\pi Dt}} \exp\left[-\frac{(x_1 - vt)^2}{4\,Dt}\right] \qquad (D.8)$$

where d the depth of water added in the pulse. Equation D.8 predicts H as function of time at a given depth. Taking the time derivative of D.8 with respect to time gives

$$\frac{\partial H}{\partial t} = \frac{d/\hat{C}}{\sqrt{4\pi\,Dt}} \exp\left[-\frac{(x_1 - vt)^2}{4\,Dt}\right]\left[-\frac{1}{2t} + \frac{x_1^2 - v^2 t^2}{4\,Dt^2}\right] \qquad (D.9)$$

The pair of equations D.8, D.9 defines the values of H and J_t as a function of time t at any depth x_1 as the soil moisture pulse moves vertically through the soil matrix past this depth. Equations D.8 and D.9 have been used for generating values H and J_t and the corresponding effective hydraulic conductivities in Figures 4.13, 4.14, 4.15, 4.16.

This appendix evaluates the derivative $\partial y/\partial t$ of Equation (4.10). In this evaluation it is assumed for simplicity that the second order derivatives $\partial^2 H/\partial t^2$ and $\partial^2 H/\partial x_i \partial t$ are relatively small. It is also assumed that the squares $\lfloor \partial H/\partial t\rfloor^2$ and $\lfloor \exp(-AH)\rfloor^2$ are relatively small. Substituting the expression for G given by (3.31), Equation (4.10) is written as

$$y = \frac{\lfloor jJ_1(dZ_f - HdZ_a) k_1 - J_i \frac{\partial H}{\partial x_i} dZ_a\rfloor K_G}{K_G(k_1^2 + jAL_1k_1)e^{-AH} + Ar\frac{\partial H}{\partial t}} e^{-AH} +$$

$$+ \frac{(r\, dZ_f - r\, HdZ_a - dZ_\gamma)}{K_G(k_1^2 + j\, AL_1k_1)e^{-AH} + Ar\frac{\partial H}{\partial t}} \frac{\partial H}{\partial t} \qquad (E.1)$$

Let $y = p_1 + p_2$ where p_1 and p_2 the first and second terms of E.1. Taking the derivative of p_1 with respect to t gives

$$\frac{\partial p_1}{\partial t} = \frac{-j\, J_1 \frac{\partial H}{\partial t} dZ_a k_1}{K_G(k_1^2 + j\, AL_1k_1)e^{-AH} + Ar\frac{\partial H}{\partial t}} k_G e^{-AH} +$$

$$\lfloor j\, J_1(dZ_f - HdZ_a) k_1 - (J_{i\frac{\partial H}{\partial x_i}}) dZ_a\rfloor K_G \cdot$$

$$\left\{\frac{-Ae^{-AH}\lfloor K_G(k_1^2 + jL_1k_1)e^{-AH} + Ar\frac{\partial H}{\partial t}\rfloor - e^{-AH}\lfloor -AK_G(k_1^2 + jAL_1k_1)e^{-AH} + Ar\frac{\partial^2 H}{\partial t^2}\rfloor}{\lfloor K_G(k_1^2 + j\, AL_1k_1)e^{-AH} + Ar\frac{\partial H}{\partial t}\rfloor^2}\right\}\frac{\partial H}{\partial t}$$

$$(E.2)$$

Using the assumption $\partial^2 H/\partial t^2 \approx 0$ and $[\exp(-AH)]^2 \approx 0$, E.2 simplifies to

$$\frac{\partial p_1}{\partial t} = \frac{j\, J_1 k_1(dZ_a + AdZ_f - AH\, dZ_a) - A(J_i\frac{\partial H}{i\partial x_i})dZ_a}{K_G(k_1^2 + j\, AL_1 k_1)e^{-AH} + A\Gamma\frac{\partial H}{\partial t}}\, K_G e^{-AH}\frac{\partial H}{\partial t} \qquad (E.3)$$

Dividing the numerator and denominator of E.3 by $K_G\, e^{-AH}$ gives

$$\frac{\partial p_1}{\partial t} = -\frac{j\, J_1 k_1(dZ_a + AdZ_f - HAdZ_a) - A(J_i\frac{\partial H}{i\partial x_i})\, dZ_a}{(k_1^2 + j\, AL_1 k_1) + A\Gamma G}\, \frac{\partial H}{\partial t} \qquad (E.4)$$

The second term of E.1 yields

$$\frac{\partial p_2}{\partial t} = -\frac{\Gamma\frac{\partial H}{\partial t}dZ_a}{K_G(k_1^2 + j\, AL_1 k_1)e^{-AH} + A\Gamma\frac{\partial H}{\partial t}}\, \frac{\partial H}{\partial t} +$$

$$+(\Gamma dZ_f - \Gamma H\, dZ_a - dZ_\gamma)\frac{\partial H}{\partial t}\left\{-\frac{-AK_G(k_1^2 + j\, AL_1 k_1)e^{-AH} + A\Gamma\frac{\partial H^2}{\partial t^2}}{[K_G(k_1^2 + j\, AL_1 k_1)e^{-AH} + A\Gamma\frac{\partial H}{\partial t}]^2}\, \frac{\partial H}{\partial t}\right\} \qquad (E.5)$$

Assuming that $\partial^2 H/\partial t^2 \approx 0$ and dividing numerator and denominator by $K_G\, e^{-AH}$, E.5 gives

$$\frac{\partial p_2}{\partial t} = -\frac{\Gamma G\, dZ_a}{(k_1^2 + j\, AL_1 k_1) + A\Gamma G}\, \frac{\partial H}{\partial t} + \frac{A(\Gamma\, dZ_f - \Gamma H\, dZ_a - dZ_\gamma)(k_1^2 + j\, AL_1 k_1)}{[(k_1^2 + j\, AL_1 k_1) + A\Gamma G]^2}\, (\frac{\partial H}{\partial t})^2$$

$$(E.6)$$

Assuming that the square $(\partial H/\partial t)^2 \approx 0$, this equation simplifies to

$$\frac{\partial p_2}{\partial t} = - \frac{\Gamma G \, dZ_a}{(k_1^2 + j \, AL_1 k_1) + A\Gamma G} \frac{\partial H}{\partial t} \qquad (E.7)$$

The derivative $\partial y/\partial t$ is given by

$$\frac{\partial y}{\partial t} = \frac{\partial p_1}{\partial t} + \frac{\partial p_2}{\partial t} \quad . \qquad (E.8)$$

This appendix evaluates the integral

$$I = \iiint\limits_{-\infty}^{\infty} \frac{(u_2^2 + u_3^2)^3}{(u_2^2 + u_3^2)^2 + A^2 L_1^2 \alpha_L^2 v^2} \frac{1}{v^2 + \mu^2 (u_2^2 + u_3^2)^2} \frac{1}{(1 + u_2^2 + u_3^2)^2} dv \, du_2 \, du_3$$

(F.1)

Using cylindrical coordinates

$$\begin{aligned} v &= v \\ u_2 &= r \cos \theta \\ u_3 &= r \sin \theta \end{aligned}$$

(F.2)

and integrating with respect to θ gives

$$I = 4\pi \int\limits_0^\infty \int\limits_0^\infty \frac{r^7}{r^4 + A^2 L_1^2 \alpha_L^2 v^2} \frac{1}{v^2 + \mu^2 r^4} \frac{1}{(1 + r^2)^2} dr \, dv$$

(F.3)

Let

$$I_1 = \int\limits_0^\infty \frac{1}{r^4 + A^2 L_1^2 \alpha_L^2 v^2} \frac{1}{v^2 + \mu^2 r^4} dv$$

(F.4)

using Equation (3.264.2) of Gradshteyn and Ryzhik (1980), for $\mu = 1$ gives

$$I_1 = \frac{\pi}{2} \frac{1}{\mu r^6 (1 + A L_1 \alpha_L \mu)}$$

(F.5)

Substituting into F.3 gives

$$I = \frac{2\pi^2}{\mu} \frac{1}{1 + A L_1 \alpha_T} \int\limits_0^\infty \frac{r}{(1 + r^2)^2} dr = \frac{\pi^2}{\mu} \frac{1}{1 + A L_1 \alpha_T}$$

(F.6)

This appendix evaluates the integral

$$I = \int\limits_{-\infty}^{\infty}\int\int \frac{u_2^2[u_1^2 + \mu(u_2^2 + u_3^2)]}{u^4 + A^2 L_1^2 \lambda^2 u_1^2} \; \frac{1}{(1 + u^2)^2} \; du_1 \; du_2 \; du_3 \qquad (G.1)$$

Using spherical coordinates

$$
\begin{aligned}
u_1 &= u \cos\phi \\
u_2 &= u \sin\phi \sin\theta \\
u_3 &= u \sin\phi \cos\theta
\end{aligned}
\qquad (G.2)
$$

and integrating with respect to θ, G.1 becomes

$$I = \pi \int\limits_{0}^{\pi}\int\limits_{0}^{\infty} \frac{u^4 \sin^3\phi(\cos^2\phi + \mu \sin^2\phi)}{u^2 + A^2 L_1^2 \lambda^2 \cos^2\phi} \; \frac{1}{(1 + u^2)^2} \; du \; d\phi \qquad (G.3)$$

Let

$$I_1 = \int\limits_{0}^{\infty} \frac{u^4}{u^2 + A^2 L_1^2 \lambda^2 \cos^2\phi} \; \frac{1}{(1 + u^2)^2} \; du \qquad (G.4)$$

and using Equation B.2 of Yeh (1982), G.4 gives

$$I_1 = \frac{\pi}{4} \; \frac{1 + 2 A L_1 \lambda \cos\phi}{(1 + A L_1 \lambda \cos\phi)^2} \qquad (G.5)$$

Substituting into G.3 gives

$$I = \frac{\pi^2}{2} \int_0^{\pi/2} \frac{(1 + 2\, AL_1\lambda\, \cos\phi)\,(\cos^2\phi + \mu\,\sin^2\phi)}{(1 + AL_1\lambda\, \cos\phi)^2}\, \sin^3\phi \; d\phi$$

(G.6)

Let $\cos\phi = t$ then: $-\sin\phi\, d\phi = dt$. Then

$$I = \frac{\pi^2}{2} \int_0^1 \frac{(1 + 2\, AL_1\lambda\, t)\left[t^2 + \mu(1 - t^2)\right](1-t^2)}{(1 + AL_1\lambda\, t)^2}\, dt =$$

$$= \frac{\pi^2}{2} \int_0^1 \left[\frac{2}{1 + AL_1\lambda\, t} - \frac{1}{(1 + AL_1\lambda\, t)^2}\right]\left[(\mu-1)t^4 + (1-2\mu)t^2 + \mu\right] dt$$

(G.7)

Expanding the product in G.7 gives

$$I = \frac{\pi^2}{2}\left[2(\mu-1)\, T_3 + 2(1-2\mu)\, T_2 + 2\mu\, T_1 - (\mu-1)\, P_3 - (1-2\mu)\, P_2 - \mu\, P_1\right] =$$

$$= \frac{\pi^2}{2}\left[(-2\, T_3 + 2\, T_2 - P_3 - P_2) + (2\, T_3 - 4\, T_2 + T_1 - P_3 + 2\, P_2 - P_1)\mu\right]$$

(G.8)

where

$$T_1 = \int_0^1 \frac{1}{1 + xt}\, dt = \frac{1}{x}\ln(1 + x)$$

$$T_2 = \int_0^1 \frac{t^2}{1 + xt}\, dt = \frac{1}{2x} - \frac{1}{x^2} + \frac{1}{x^3}\ln(1 + x)$$

$$T_3 = \int_0^1 \frac{t^4}{1+xt}\, dt = \frac{1}{4x} - \frac{1}{3x^2} + \frac{1}{2x^3} - \frac{1}{x^4} + \frac{1}{x^5} \ln(1+x)$$

$$\text{(G.9)}$$

$$P_1 = \int_0^1 \frac{1}{(1+xt)^2}\, dt = \frac{1}{1+x}$$

$$P_2 = \int_0^1 \frac{t^2}{(1+xt)^2}\, dt = \frac{1}{x} + \frac{2}{x^2} - \frac{1}{1+x} - \frac{2}{x^3} \ln(1+x)$$

$$P_3 = \int_0^1 \frac{t^4}{(1+xt)^2}\, dt = \frac{1}{1+x} - \frac{1}{x} + \frac{4}{3\,x^2} - \frac{2}{x^3} + \frac{4}{x^4} - \frac{4}{x^5} \ln(1+x)$$

and $x = AL_1\lambda$. The above integrals were evaluated using the recursive formulas (2.111.2) and (2.111.3) of Gradshteyn and Ryzhik (1980). Substituting these expressions, G.8 gives

$$I = \pi^2 \left[g_2 + g_2\mu \right] \qquad\qquad \text{(G.10)}$$

where

$$g_1 = \frac{1}{x} - \frac{4}{x^2} - \frac{6}{x^3} + \frac{12}{x^4} + \left(-\frac{12}{x^5} + \frac{8}{x^3} \right) \ln(1+x)$$

$$\text{(G.11)}$$

$$g_2 = -\frac{5}{x} + \frac{12}{x^2} + \frac{6}{x^3} - \frac{12}{x^4} + \left(\frac{12}{x^5} - \frac{16}{x^3} + \frac{4}{x} \right) \ln(1+x)$$

Note that for $x \to 0$, $\ln(1+x) \to 0$ and g_1, g_2 tend to $g_1 = 1/15$, and $g_2 = 4/15$.

This appendix evaluates the integral

$$I = \iiint\limits_{-\infty}^{\infty} \frac{(u_2^2 + u_3^2)^2}{\delta^4(u_2^2 + u_3^2)^2 + A^2 L_1^2 \alpha_L^2 v^2}$$

$$\frac{1}{v^2 + \mu^2 \delta^4(u_2^2 + u_3^2)} \; \frac{1}{(1 + u_2^2 + u_3^2)^2} \; dv \; du_2 \; du_3 \qquad \text{(H.1)}$$

using cylindrical coordinates, as in F.2, and integrating with respect to θ gives

$$I = 4\pi \int\limits_{0}^{\infty} \int\limits_{0}^{\infty} \frac{r^7}{\delta^4 r^4 + A^2 L_1^2 \alpha_L^2 v^2} \; \frac{1}{v^2 + \mu^2 \delta^4 r^4} \; \frac{1}{(1 + r^2)^2} \; dr \; dv \quad \text{(H.2)}$$

Let $\quad I_1 = \dfrac{1}{A^2 L_1^2 \alpha_L^2} \displaystyle\int\limits_{0}^{\infty} \dfrac{1}{v^2 + \dfrac{\delta^4 r^4}{A^2 L_1^2 \alpha_L^2}} \; \dfrac{1}{v^2 + \mu^2 \delta^4 r^4} \; dv$

using Equation (3.264.2) of Gradshteyn and Ryzhik (1980) for $\mu = 1$ gives

$$I_1 = \frac{\pi}{2} \; \frac{1}{\mu \delta^6 r^6 (1 + A L_1 \alpha_L \mu)} \qquad\qquad \text{(H.3)}$$

Substituting into H.2 and integrating with respect to r, gives

$$I = \frac{\pi^2}{\mu \delta^6} \; \frac{1}{1 + A L_1 \alpha_T} \qquad\qquad \text{(H.4)}$$

This appendix evaluates the integral

$$I = \int\!\!\int\!\!\int_{-\infty}^{\infty} \frac{u_2^2(u_2^2 + u_3^2)}{[\beta^2 v^2 + (u_2^2 + u_3^2)]^2} \; \frac{1}{(1 + u_2^2 + u_3^2)^2} \; du\, du_2\, du_3 \qquad (I.1)$$

Using cylindrical coordinates, as in F.2, and integrating with respect to θ gives

$$I = 2\pi \int_0^{\infty}\!\!\int_0^{\infty} \frac{r^5}{[\beta^2 v^2 + r^2]^2} \; \frac{1}{(1 + r^2)^2} \; dr\, dv \qquad (I.2)$$

Let

$$I_1 = \int_0^{\infty} \frac{1}{(\beta^2 v^2 + r^2)^2} \; dv \; = \; \frac{\pi}{4} \; \frac{1}{\beta r^3} \qquad (I.3)$$

Substituting into I.2 and integrating with respect to r yields

$$I = \frac{\pi^3}{8} \; \frac{1}{\beta} \qquad (I.4)$$

This appendix evaluates the integral

$$I = \iiint\limits_{-\infty}^{\infty} \frac{(u_2^2 + u_3^2)^2}{[\beta^2 v^2 + (u_2^2 + u_3^2)^2]^2} \; \frac{1}{(1 + u_2^2 + u_3^2)^2} \; dv \; du_2 \; du_3 \qquad (J.1)$$

Using cylindrical coordinates, as in F.2, and integrating with respect to θ gives

$$I = 4\pi \int\limits_0^{\infty} \int\limits_0^{\infty} \frac{r^5}{[\beta^2 v^2 + r^4]^2} \; \frac{1}{(1 + r^2)^2} \; dv \; dr \qquad (J.2)$$

Let

$$I_1 = \int\limits_0^{\infty} \frac{1}{(\beta^2 v^2 + r^4)^2} \; dv = \frac{\pi}{4} \frac{1}{\beta r^3} \qquad (J.3)$$

Substituting into J.2 and integrating with respect to r gives

$$I = \frac{\pi^3}{4} \frac{1}{\beta} \qquad (J.4)$$

APPENDIX K

This appendix evaluates the integral

$$I = \iiint\limits_{-\infty}^{\infty} \frac{u_1^2 u_2^2}{[u_1^2 + \delta_1^2(u_2^2 + u_3^2)]^2 + A^2\lambda_1^2 u_1^2} \frac{1}{(1 + u^2)^2} \, du_1 \, du_2 \, du_3 \quad (K.1)$$

Using spherical coordinates k, ϕ and θ and integrating with respect to θ, K.1 gives

$$I = 2\pi \int_0^{\pi/2} \int_0^{\infty} \frac{u^4 \cos^2\phi(1-\cos^2\phi) \sin\phi}{u^2[\cos^2\phi + \delta^2(1-\cos^2\phi)]^2 + A^2 L_1^2 \lambda_1^2 \cos^2\phi} \frac{1}{(1 + u^2)^2} \, d\phi \, du$$

$$(K.2)$$

Using the transformation $t = \cos\phi$, K.2 becomes

$$I = 2\pi \int_0^1 \int_0^{\infty} \frac{u^4 t^2(1 - t^2)}{u^2[t^2 + \delta^2(1 - t^2)]^2 + A^2 L_1^2 \lambda_1^2 t^2} \frac{1}{(1 + u^2)^2} \, dt \, du \quad (K.3)$$

Let

$$I_1 = \int_0^{\infty} \frac{u^4}{u^2[t^2 + \delta^2(1-t^2)]^2 + A^2 L_1^2 \lambda_1^2 t^2} \frac{1}{(1 + u^2)^2} \, du \quad (K.4)$$

Using Equation B.2 of Yeh (1982), K.4 gives

$$I_1 = \frac{\pi}{4} \frac{t^2 + \delta^2(1-t^2) + 2 A L_1 \lambda_1 t}{[t^2 + \delta^2(1-t^2)][t^2 + \delta^2(1-t^2) + A L_1 \lambda_1]^2} \quad (K.5)$$

Substituting into K.3 gives

$$I = \frac{\pi^2}{2} \int_0^1 \frac{[(1-\delta^2)t^2 + \delta^2 + 2\,AL_1\lambda_1 t]\;t^2(1-t^2)}{[(1-\delta^2)t^2 + \delta^2][(1-\delta^2)t^2 + \delta^2 + AL_1\lambda_1 t]^2}\,dt \qquad (K.6)$$

For $\delta^2 \to 0$ this equation simplifies to

$$I = \frac{\pi^2}{2} \int_0^1 \frac{(t + 2AL_1\lambda_1)\,t\,(1 - t^2)}{(t^2 + \delta^2)(t + AL_1\lambda_1)^2}\,dt \qquad (K.7)$$

Writing

$$\frac{(t + 2\,AL_1\lambda_1)\,t\,(1 - t^2)}{(t^2 + \delta^2)(t + AL_1\lambda_1)^2} = B_0 + \frac{B_1 t + B_2}{t^2 + \delta^2} + \frac{B_3}{t + AL_1\lambda_1} + \frac{B_4}{(t + AL_1\lambda_1)^2}$$

$$(K.8)$$

where (after a few calculations)

$$B_0 = -1$$

$$B_1 = \frac{2a^3(1 + \delta^2)}{(a^2 + \delta^2)^2}$$

$$B_2 = \frac{\delta^2(1 + \delta^2)(\delta^2 + 3a^2)}{(a^2 + \delta^2)^2}$$

$$(K.9)$$

$$B_3 = \frac{2a^3(1 + \delta^2)}{(a^2 + \delta^2)^2}$$

$$B_4 = \frac{a^2(a^2 - 1)}{(a^2 + \delta^2)}$$

322

where $a = AL_1\lambda_1$. It is

$$I = \frac{\pi^2}{2} \left(B_0 T_0 + B_1 T_1 + B_2 T_2 + B_3 T_3 + B_4 T_4 \right) \tag{K.10}$$

where

$$T_0 = \int_0^1 dt = 1$$

$$T_1 = \int_0^1 \frac{t}{t^2 + \delta^2} \, dt = \frac{1}{2} \ln\left(1 + \frac{1}{\delta_1^2}\right)$$

$$T_2 = \int_0^1 \frac{1}{t^2 + \delta^2} \, dx = \frac{1}{\delta} \operatorname{arctg}\left(\frac{1}{\delta}\right) \approx \frac{\pi}{2\delta}$$

$$T_3 = \int_0^1 \frac{1}{t + AL_1\lambda_1} \, dt = \ln\frac{1 + AL_1\lambda_1}{AL_1\lambda_1}$$

$$\tag{K.11}$$

$$T_4 = \int_0^1 \frac{1}{(t + AL_1\lambda_1)^2} \, dt = \frac{1}{AL_1\lambda_1(1 + AL_1\lambda_1)}$$

Substituting the above expression into K.11 and taking the limit for $\delta \to 0$ gives

$$I = \frac{\pi^2}{2} \frac{1}{AL_1\lambda_1} \ln\left(1 + \frac{1}{\delta^2}\right) \tag{K.12}$$

This appendix reduces the two-dimensional integrals (5.54) to one dimensional integrals. Take, for example integral T_{22}. Using cylindrical coordinates it holds

$$T_{22} = 4 \int_0^{\pi/2} \int_0^\infty \frac{r^3 \cos^4 \phi}{r^2(\cos^2 \phi + \delta^2 \sin^2 \phi)^2 + A^2 L_2^2 b^2 \cos^2 \phi} \frac{1}{(1 + r)^2} \, dr \, d\phi$$

<div align="right">(L.1)</div>

Let

$$I = \int_0^\infty \frac{r^3}{a^2 r^2 + d^2} \frac{1}{(1 + r^2)^2} \, dr$$

<div align="right">(L.2)</div>

where $\quad a^2 = \cos^2 \phi + \delta^2 \sin^2 \phi, \quad d^2 = A^2 L_2^2 b^2 \cos^2 \phi.$

<div align="right">(L.3)</div>

Using $r^2 = x$ gives

$$I = \frac{1}{2} \int_0^\infty \frac{x}{a^2 x + d^2} \frac{1}{(1 + x)^2} \, dx$$

<div align="right">(L.4)</div>

Let

$$\frac{x}{a^2 x + d^2} \frac{1}{(1 + x)} = \frac{B_1}{a^2 x + d^2} + \frac{B_2}{1 + x}$$

<div align="right">(L.5)</div>

where

$$B_1 = \frac{-d^2}{a^2 - d^2}$$

<div align="right">(L.6)</div>

$$B_2 = \frac{1}{a^2 - d^2}$$

then

$$I = \frac{1}{2}(B_1 I_1 + B_2 I_2) \qquad (L.7)$$

where

$$I_1 = \int_0^\infty \frac{1}{(a^2 x + d^2)(1 + x)}\, dx$$

and

$$(L.8)$$

$$I_2 = \int_0^\infty \frac{1}{(1 + x)^2}\, dx$$

Using Equation (3.223.1) of Gradshteyn and Ryzhik, (1980) for $\mu = 1$ gives

$$I_1 = \frac{\pi}{a^2 - d^2} \frac{\left(\frac{d^2}{a^2}\right)^{\mu-1} - 1}{\sin(\mu\pi)} \qquad (L.9)$$

Note that for $\mu \to 1$, the numerator and denominator of the above equation tends to zero. Then

$$I_1 = \frac{\pi}{a^2 - d^2} \lim_{\mu \to 1} \frac{\frac{\partial}{\partial \mu}\left[(d^2/a^2)^{\mu-1} - 1\right]}{\frac{\partial}{\partial \mu}(\sin \mu\pi)} = \frac{\ell n(d^2/a^2)}{a^2 - d^2} \qquad (L.10)$$

and

$$I_2 = \frac{\pi}{4} \qquad (L.11)$$

Equation L.6 then gives

$$I = \frac{1}{8(a^2 - d^2)}\left[\pi - \frac{8d^2}{a^2 - d^2} \ell n(d^2/a^2)\right] \qquad (L.12)$$

where a^2, d^2 are given by L.3. Substituting into L.1 gives

$$T_{22} = 4 \int_0^{\pi/2} I(\phi) \cos^4\phi \, d\phi \qquad (L.13)$$

where $I(\phi)$ is given by L.12 and L.3. Integral L.13 cannot be analytically evaluated and it requires numerical evaluation.